Aerosol Size Distribution Modeling for the Pacific Northwest

Robert A. Elleman

A dissertation submitted in partial fulfillment of the
requirements for the degree of

Doctor of Philosophy

University of Washington

2007

Program Authorized to Offer Degree: Atmospheric Sciences

University of Washington
Graduate School

This is to certify that I have examined this copy of a doctoral dissertation by

Robert A. Elleman

and have found that it is complete and satisfactory in all respects,
and that any and all revisions required by the final
examining committee have been made.

Chair of the Supervisory Committee:

_____

David S. Covert

Reading Committee:

_____

David S. Covert

_____

Clifford F. Mass

_____

Jeffrey R. Arnold

Date:_____

In presenting this dissertation in partial fulfillment of the requirements for the Doctoral degree at the University of Washington, I agree that the Library shall make its copies freely available for inspection. I further agree that extensive copying of the dissertation is allowable only for scholarly purposes, consistent with “fair use” as prescribed in the U.S. Copyright Law. Requests for copying or reproduction of this dissertation may be referred to Proquest Information and Learning, 300 North Zeeb Road, Ann Arbor, MI 48106-1346, 1-800-521-0600, to whom the author has granted “the right to reproduce and sell (a) copies of the manuscript in microform and/or (b) printed copies of the manuscript made from microform.”

Signature _____

Date _____

University of Washington

Abstract

Aerosol Size Distribution Modeling
for the Pacific Northwest

Robert A. Elleman

Chairperson of the Supervisory Committee:
Professor David S. Covert
Department of Atmospheric Sciences

The goal of this project is to more accurately model the aerosol size distribution with the Community Multiscale Air Quality modeling system (CMAQ). The approach is to compare its performance to observations in the Pacific Northwest and to make improvements to the model science.

The official CMAQ v4.4 underpredicts the total particle number concentration by 1-2 orders of magnitude. The bias is consistent throughout the day and across the urban-influenced region. It becomes progressively worse for smaller sizes and is not associated with any particular chemical species, emissions source, or air mass aging. Errors in total aerosol loading, meteorology, and gaseous aerosol precursors do not show a pattern consistent with the number underprediction. Of all the aerosol processes that create and destroy particles in the urban environment, the nucleation of new particles and the emission size distributions in the official CMAQ v4.4 attract attention for their scientific deficiencies and their tendency to produce the observed errors.

The latest mechanisms for ternary NH_3-H_2SO_4-H_2O nucleation and nucleation mode scavenging and growth are added to CMAQ, and the emission size distribution is updated to reflect modern mesoscale measurements. Modeled particle concentrations increase substantially, but they are still underpredicted by up to an order of magnitude. Nucleation changes are responsible for most of the increase but are also responsible for spatially inconsistent performance. Emissions updates increase the number of particles smoothly

across urban-influenced areas by a factor of 2-4. The modeled size distributions, especially in the ultrafine range, are a better match to observations, although errors in the accumulation mode remain. The fact that these changes make a noticeable improvement in results adds weight to the premise that regional nucleation occurs regularly during the Puget Sound summer and that emissions of Aitken mode particles are an important component to the ambient aerosol size distribution. Although the updates to CMAQ represent only our incomplete understanding of aerosol pollution, they are able to reduce the underprediction of aerosol number concentrations and produce size distributions with the appropriate major features.

Table of Contents

List of Figures

Figure Number Page

List of Tables

Acknowledgements

I express my gratitude to everyone who helped me complete this endeavor.

To my primary advisor, Dave Covert, for being patient, thorough, and respectful. He is a model scientist and teaches by example. To my secondary advisor, Cliff Mass, for being more of an air quality advisor than he admits to being qualified for. To committee member Tim Larson for thoughtful comments, and to GSR Alison Cullen for volunteering her time.

To committee member / mentor / coworker Jeff Arnold for his enthusiasm in all of these roles. To Brian Lamb for treating me like one of his own, and to two of his own, Jack Chen and Susan O'Neill, for modeling support. To the UW PM Center, to NW-AIRQUEST, and to the CMAQ development team for scientific and financial support. To the "Godfather of Air Quality in the Northwest", Rob Wilson, for doing what godfathers do – well, at least the law-abiding and benevolent government manager sorts of godfathers.

To all the friends and family who have been absolutely instrumental to my sanity and happiness in graduate school. You are too many to list, and that fact alone attests to your role. Special mention goes to Mom and Dad who blindly supported my decision to divert my career to something they had never heard of, to Jen Kay for an infinite well of understanding, and to Kevin Rennert for his generous spirit.

1. Introduction

Atmospheric aerosol pollution negatively impacts human health, reduces atmospheric visibility, and perturbs the Earth's energy balance. Regulations in the United States focus on particles smaller than 2.5 μm primarily for their deleterious health consequences, but current research suggests that a majority of this effect may be triggered by particles smaller than 100 nm (Oberdörster et al., 2005). Aerosol properties, especially for the very smallest particles, vary in space across an urban area and in time throughout the day. A full characterization requires sophisticated instrumentation that is impractical to deploy in enough places to capture these variations. Numerical models of meteorology and air quality can serve a role in characterizing the concentration and properties of aerosol throughout an urban area. They are also useful tools to explore control strategies, provide short-term forecasts, test our understanding of the science, and explore new theories about air pollution science. The objectives of this study are to test a widely-used air quality model for its ability to represent aerosols in the Pacific Northwest and to make improvements to the model science that will be useful for all simulations in urban-dominated environments.

1.1. Properties of Aerosols

The strict definition of an aerosol is a solid or a liquid suspended in a gas. In the atmospheric science community, only the solids and hydrated solids from atmospheric pollution – and not the atmosphere suspending them – are referred to as "aerosols". Aerosols are also called particulate matter or sometimes just particles. These latter two

terms connote a solid, but it is important to remember that these atmospheric aerosols may be liquid or at least contain liquid water at common lower tropospheric temperatures and relative humidities.

Anthropogenic aerosols are generated by combustion, smelting, and mechanical friction. Combustion of fossil fuels and biofuels produces hot gases, unburned fuel oil, solid metals, and solid carbon clusters. Many of the gases transfer to the aerosol phase when the exhaust dilutes with cooler ambient air and when chemical reactions in the exhaust create less volatile species. Combustion aerosol is comprised of organic carbon, elemental carbon, sulfate, liquid water, and metals. Mechanical friction of two materials can remove small bits from one or both and inject them into the atmosphere. Most particles generated in this fashion are large and quickly fall to the surface, but atmospheric turbulence can suspend the smaller ones long enough to be an important source of atmospheric aerosol. The composition of mechanically derived aerosols depends on the source material. Examples are carbon from automobile tires and mineral dust from agricultural fields. Mechanically derived aerosols have diameters equivalent to spheres between 1 μm and 40 μm, while combustion aerosols have diameters of 1 nm to 1 μm. Both survive in the atmosphere for days to weeks on average, but the full range is a few seconds for large particles close to the ground and many months for aerosol lofted into the stratosphere.

The natural earth system also produces aerosols. Natural combustion aerosols include those from forest fires and volcanoes whose plumes can buoyantly rise high into the troposphere or into the stratosphere. Mechanically derived natural aerosols come from multiple sources. Sea-salt is produced through evaporation of suspended ocean water droplets. Fragments of plant and animal matter can also be suspended in the atmosphere, while pollen is designed to float on the winds as an aerosol. Strong winds pick up dust from the surface in arid regions, and volcanoes eject large amounts of pulverized rock.

This natural background is a complication to studying the effect of anthropogenic aerosols, but it is only one of the challenges.

Aerosols are not inert after entering the atmosphere. Before their eventual return to the earth's surface through dry and wet deposition, they are modified by coagulation, condensation, evaporation, fragmentation, nucleation, dissolution, efflorescence, and cloud droplet activation. Particles have natural Brownian motion that causes them to collide and potentially stick with other particles. Supersaturated gases such as sulfuric acid, nitric acid, and heavy organic compounds condense onto existing particles in proportion to the available surface area. When conditions change, the condensable compounds may evaporate back to the atmosphere and shrink the particle. Particles may fragment into two or more smaller pieces when polar, semi-volatile gases have evaporated to leave a brittle core. Supersaturated gases form new particles from the gas-phase when condensation to existing particles is not fast enough and when the new particles are able to quickly grow by condensation to larger, more stable sizes. Depending on ambient meteorology and aerosol composition, most aerosols are hygroscopic and, at a high enough relative humidity, will condense water vapor on their surface and even dissolve in the aerosol water. As the relative humidity reaches 100%, the aerosol continues to condense water vapor and may even activate to become a cloud droplet. Cloud water chemistry is very effective at adding sulfate and organic carbon to the droplet. If the droplet then evaporates, the aerosol is returned to the atmosphere, often much more massive then before its experience as a droplet nucleus. If it instead forms precipitation, the aerosol components will be lost to the earth's surface. Aerosols are also lost by dry deposition when they settle and impact on surface features. All of these complicated aerosol processes depend on the gas-phase concentration of pollutants and water vapor, on meteorological variables such as temperature and actinic flux, and on pre-existing aerosol properties.

The size distribution of particles is an important component of aerosol dynamics and chemistry. The simplest designation of aerosol with respect to size is "total suspended

particles" (TSP). It is defined as all particles trapped on an ambient filter. The particle sizes it captures will depend on the how the filter is deployed relative to very local sources of large particles. The upper diameter limit is generally considered to be 40 μm because larger particles settle too quickly to be captured on the filter face. More specific designations of aerosol size attempt to isolate particles with a particular chemistry, formation mechanism, and interaction with the human airway. PM_{10} is defined to be the mass concentration of particles with aerodynamic diameters less than 10 μm. The hydrated particle diameter is used even though the dry mass is measured because the inlet impactor that determines the size cut is at ambient conditions. PM_{10} includes all combustion aerosol and most mechanically derived aerosol. It is called the inhalable fraction because it can be inhaled past the mouth and nostrils. $PM_{2.5}$ and PM_1, both sometimes referred to as the fine mode or fine fraction, are the same concept as PM_{10} but with cuts at 2.5 μm and 1.0 μm, respectively. $PM_{2.5}$ is also called the respirable fraction because it penetrates to the lung passages. PM_1 more rigorously isolates combustion aerosol. The difference between PM_{10} and $PM_{2.5}$, labeled $PM_{10\text{-}2.5}$ or the coarse fraction, isolates particles with aerodynamic diameters between 2.5 μm and 10 μm that are usually mechanically derived. Ultrafine particles have a diameter smaller than 100 nm. Their diameter is a dry, mobility diameter since instruments usually determine the size of particles in this range with a differential mobility analyzer. Ultrafine particles, especially those around 20 nm in diameter, have the highest probability of traveling all the way through the human respiratory system to the alveolar sacs (Oberdörster et al., 2005).

A detailed mathematical description of the particle size distribution can be represented by an analytical model or a discrete increment model. The latter, often called a sectional model, reports the number of particles in typically 5-50 bins. The log of the diameters that divide the bins are usually equally spaced so that there are more at smaller diameters. Common analytical models for the size distribution are lognormal, power-law, or modified gamma distributions.

Atmospheric processing and the mechanical generation of aerosol tend to create distinct lognormal modes (Whitby, 1978). The mass-based coarse mode peaks at around 5-8 μm for mechanically derived aerosol. Combustion aerosol produces an Aitken number mode centered near 20 nm. These particles grow over time into the accumulation mode, whose number peaks around 100 nm. Nucleation mode particles are between 1 and 15 nm, but in practice are between 3 and 15 nm or between 8 and 15 nm depending on the instrument's lower detection limit. Because these particles are so new, they have undergone little atmospheric processing and are not likely to result in a lognormal mode. Another twist on the lognormal mode structure occurs when clouds activate just a portion of the accumulation mode. When these particles later evaporate, they are much larger due to aqueous chemical processes and form a distinct droplet mode from the rest of the un-activated accumulation mode. However, it is very common to observe three lognormal modes. Chemical subsets of the aerosol population are distributed differently but often by modes that can be similarly modeled.

The overlapping lognormal modes can be separated and each represented mathematically as a function of size:

$$\frac{dN}{d\ln D_p} = \frac{N}{(2\pi)^{1/2}\ln\sigma_g}\exp\left(-\frac{\left(\ln D_p - \ln D_g\right)^2}{2\ln^2\sigma_g}\right) \qquad (1.1)$$

where N is the total number of particles in the mode, D_p is the particle diameter, D_g is the modal median diameter, and σ_g is the modal standard deviation. The number and mass distributions have the same standard deviation but with median diameters related by:

$$\ln D_{gv} = \ln D_g + 3\ln^2\sigma_g \qquad (1.2)$$

where D_{gv} is the mass-based median diameter. It is convenient to express observed distributions as the sum of three or more lognormal modes because the size distribution can be quickly summarized by each mode's total number, median diameter, and standard deviation or by each mode's number, surface area, and mass. It is also convenient from a modeling standpoint because, instead of the number in each bin, only nine parameters –

three parameters per mode – are needed to represent the entire distribution of three overlapping lognormal modes.

All of the aerosol dynamical and chemical processes depend on the sizes of the particles in the aerosol population. For a given amount of aerosol mass in a cubic meter, the number of particles increases as the mean diameter decreases since each particle will weigh less. At the same time the total surface area will increase since the surface area to volume ratio scales inversely with the particle diameter. This has physical importance because aerosol processes depend on the number of particles, their surface area, their mass, and their surface area to mass ratio. As particles become smaller, they sweep out a narrower track in proportion to the diameter, but this track is much longer per unit time because the Brownian motion of each particle is inversely proportional to the diameter cubed. The net effect is that coagulation increases with smaller particles. The surface area to volume ratio is important for several processes. Gaseous diffusion is limited by the amount of surface in contact with the atmosphere; for particle fall speed, the surface is key for the aerodynamic drag, and the volume or mass is important for the gravitational force. Smaller particles have a higher surface area to volume ratio, favoring condensation and reducing dry deposition. Smaller particles are less likely to condense water vapor, serve as cloud condensation nuclei, be involved in cloud chemistry, and be removed by wet deposition. However, the higher coagulation rate for the smallest particles makes them more likely to attach to cloud droplets and become involved in cloud processing. Knowing the size of the particles and not just the overall mass is important for understanding the evolution of the aerosol population as well as for modeling and predicting its transformation.

1.2. Importance of Aerosols

Aerosols are important environmentally for climate, visibility, ecological health, and human health. Aerosols both scatter and absorb incoming solar radiation, and their net effect depends on their single scattering albedo relative to the albedo of the clouds and

the land surface. The direct, top-of-atmosphere forcing by aerosols is estimated between -0.07 and -1.24 W/m^2 (Houghton et al., 2001). The middle point of this range is ¼ of the magnitude of the well-mixed greenhouse gas forcing. More elaborate feedbacks – collectively called aerosol indirect effects – arise due to the interaction of aerosols with other radiatively important parameters such as cloud albedo and cloud lifetime.

On a regional scale, the interaction of particles with incoming solar radiation obscures visibility of scenic vistas. Anthropogenic aerosol pollution is the main contributor to visibility degradation in national parks and other protected natural areas (Watson, 2002), and this fact has prompted United States Environmental Protection Agency (U.S. EPA) regulations to reduce regional haze (U.S. EPA, 1999). Sulfur and nitrogen compounds in aerosol are also responsible for acidification of soils, and wet and dry deposition of particulate mercury is an important pathway into alpine ecosystems (Schroeder and Munthe, 1998). Regulations also address these pollution issues (U.S. EPA, 2007a; U.S. EPA, 2005), but most regulations for particulate matter in the atmosphere are designed to protect human health.

Dozens of studies have linked fine mode particulate matter to respiratory and cardiovascular morbidity and mortality. In general, cardiovascular and respiratory mortality reportedly increases by 1-18% for every 10 μg/m^3 increase in long-term exposure to $PM_{2.5}$ (Dockery et al., 1993; Pope et al., 1995; Pope et al., 2002; Pope et al., 2004; Miller et al., 2007). Particulate matter has also been associated with a long list of morbidity impacts, many of which carry risk of imminent or future mortality. This includes hospital admissions for respiratory and cardiovascular ailments (e.g., Delfino et al., 1997), infant birth weight (e.g., Parker et al., 2005), decreased lung development in adolescents (Gauderman et al., 2004), and aggravation of asthma symptoms (e.g., Sheppard et al., 1999). Aerosols may even induce inheritable genetic mutations (Samet et al., 2004). There is no evidence of a threshold below which aerosol concentrations are no longer harmful (Pope, 2004). There are also few conclusions about which chemical

components or physical characteristics are responsible for the health effects despite many promising hypotheses about pathways (Davidson et al., 2005).

For all of the distinct areas of aerosol relevance, the actual size of the particle, not merely $PM_{2.5}$, is critical to understanding its effect. Light scattering in visible wavelengths peaks for particles with diameters around 500 nm and is a strong function of diameter on either side of this peak (van de Hulst, 1981). Inclusion of particles in acid rain depends on the activation diameter of the cloud droplets. Smaller particles make it farther through the respiratory tract with a maximum penetration at 20 nm diameter. Smaller than 20 nm, particles have more Brownian motion and are progressively more likely to impact in the nasopharyngeal region. There is significant evidence that ultrafine particles may be more toxic per unit mass than $PM_{2.5}$. This may be because smaller particles have a higher surface area to volume ratio, or it may be due to the smaller particle's ability to deposit efficiency in the alveolar regions of the lungs, evade natural clearance mechanisms, breach the lung boundary, interact with neurons (Oberdörster et al., 2005), or penetrate red blood cells (Rothen-Rutishauser et al., 2006).

While the entire aerosol size distribution is important for multiple applications, it is highly variable within an urban region. $PM_{2.5}$ and PM_1 can vary substantially in total mass and in chemical composition in an urban area (Freiman et al., 2006), but the concentration of particles in the ultrafine range can have a characteristic spatial scale of just a few hundred meters (Zhu et al., 2002a, 2002b). It is impossible to observe aerosol size distributions on this scale for an entire urban region. The task is easier for more integral quantities like $PM_{2.5}$ and light scattering. Continuous, automated $PM_{2.5}$ samplers such as the Tapered Element Oscillation Microbalance (TEOM) are inexpensive enough for university researchers and many local air pollution agencies to purchase several, and basic nephelometers to measure light scattering (and estimate mass) are less expensive still. To measure the entire size distribution or simply the number of ultrafine particles, it is necessary to invest in expensive equipment that requires frequent attention by skilled technicians. It is usually impractical to deploy more than a small number in an urban

area. So, measurement techniques are not capable of measuring all aerosol sizes in enough locations to adequately characterize ambient concentrations.

1.3. Modeling Strategies

Modeling techniques can fill in the gaps where measurements are impractical. The major difficulty is to trust the modeled aerosol concentrations. A model is only as good as its inputs, its underlying physical theory, and its numerical implementation of that theory. Emissions are notoriously difficult to estimate properly, especially within residential areas. Wood smoke emissions are highly dependent on the particular stove technology in each residence, for example. Even if a house-by-house inventory could be accomplished, the emissions are just as dependent on the less-than-rational behavior of the residents. Emissions from light industry change rapidly as thousands of sources appear and disappear. Even information about large, well-regulated sources is not well transmitted to those in charge of the emissions inventory (Clint Bowman, personal communication). As anyone who follows weather reports knows, meteorological models frequently have errors resulting in forecasts that are uncertain to some degree. These errors and uncertainties come from many sources, including systematic errors in model physics, in our understanding of the atmosphere, and in our ability to simulate what we understand with existing computer resources. Air quality models have similar issues but with the added complication of incorporating emission and meteorological models (and their associated uncertainties) as inputs. Thus, aerosol models, while they characterize aerosol physics and chemistry in space and time, have an uncertainty about the predicted values. This uncertainty is seldom quantified, but a thorough comparison to available observations can help characterize and reduce model error and bias.

Despite their inherent error, models can serve several useful purposes. Even with its limitations a sophisticated and well-understood model can estimate aerosol size distributions in locations where there are not observations, as long as the model error has been carefully characterized against detailed observational data. It can provide input to

indoor/outdoor, human exposure, and health effects models to advance our understanding of air pollution and health. Air quality models are linked to weather forecast models to make short-term forecasts of air pollution (Vaughan et al., 2004; Otte et al., 2005). These forecasts bring media attention to potential air pollution episodes, warn susceptible populations about the danger, and provide the public an opportunity to modify emission behavior and prevent a potential air pollution health risk. Governments and local air pollution control districts rely heavily on air pollution models for testing different control scenarios for criteria pollutants and for atmospheric visibility. Probably the most under-appreciated service of air quality models is to bring attention to deficiencies in our understanding of the science, provide a laboratory for testing solutions, and even substantiate observations with model simulations based on accepted theory.

There are a large number of air quality models, but only a few can simulate aerosols realistically. The most sophisticated for urban to regional applications are the Comprehensive Air quality Model with extensions (CAMx) (ENVIRON, 2006), the Gas, Aerosol, Transport, and Radiation model (GATOR) (Jacobson, 1997a; Jacobson, 1997b), and the Community Multiscale Air Quality modeling system (CMAQ) (Byun and Schere, 2006; Byun and Ching, 1999). All are three-dimensional, Eulerian models capable of capturing important aerosol size and compositional features. Among them CMAQ has a sophisticated aerosol treatment especially for size distributions, effectively balances speed with completeness, has the largest user community, and is well supported by the air quality community in the Pacific Northwest. There are variations of CMAQ that treat aerosols differently (CMAQ-MADRID and CMAQ-UCD) (Y. Zhang et al., 2004; K. M. Zhang, 2005), but the standard release manages aerosols in a manner that is more likely to be used widely by other investigators. Thus, this study investigates CMAQ for modeling aerosol size distributions in the Pacific Northwest.

1.4. Goal and Approach of This Study

The goal of this study is to more accurately model aerosol size distributions in the Pacific Northwest. The methodology is to evaluate a current state-of-the-art model, make a decision about the model's applicability, decide what improvements are necessary, and update the model in the most scientifically defensible manner. When this study was initiated in 2002, there were no published applications of a sophisticated regional air quality model for $PM_{2.5}$ in this region, nor was there a published analysis of performance for the entire size distribution at any location. Since then, Yin et al. (2004) examined 24-hour average organic and total $PM_{2.5}$ at two sites in the Lower Fraser Valley for the period 1 to 7 August 1993; O'Neill et al. (2006) investigated 24-hour total and speciated $PM_{2.5}$ performance in Washington, Oregon, and Idaho for half of July 1996; and Smyth et al. (2006) compared CMAQ results to hourly $PM_{2.5}$ at five sites in the Lower Fraser Valley and compared to speciated $PM_{2.5}$ at the Pacific 2001 sites (Li, 2004). In terms of ultrafine particles, Roth et al. (2003) tested various particle nucleation algorithms in the Lower Fraser Valley but did not compare to observations nor investigate the entire size distribution. Y. Zhang et al. (2006b) evaluated size distribution performance in Atlanta for 11 days and tested the sensitivity to the specified emission size distribution. Park et al. (2006) extended this Atlanta analysis to cover 1.5 years and examined sensitivity to a different emission size distribution. Fan et al. (2006) explored the effect of organic carbon particle nucleation on the modeled size distributions in Houston. These articles tread closely to the goal and structure of this study. While they highlight the importance of the problem, they also do not directly address size distribution performance in the Pacific Northwest, nor investigate model performance throughout the boundary layer, nor propose the same aerosol dynamics modifications to the CMAQ model as this in study.

This dissertation examines CMAQ's size distribution performance both aloft and at the surface for the PNW2001 (Jobson et al., 2002) and Pacific 2001 (Li, 2004) field campaigns and at routine ground stations. Chapters 2 and 3 describe the CMAQ model, the PNW2001 and Pacific 2001 experiments, and the evaluation of the meteorological

modeling for this project. Chapter 4 then scrutinizes CMAQ v4.4 in its ability to reproduce the observed aerosol characteristics and gas-phase species concentrations. Chapters 5, 6, and 7 discuss the background, application, and results for improvements to CMAQ's nucleation algorithm, emission size distribution, and the combination of the nucleation and emissions improvements. Chapter 8 summarizes the results and provides perspective to the study.

2. CMAQ Modeling System

2.1. CMAQ v4.4 Overview

The Community Multiscale Air Quality (CMAQ) modeling system v4.4 is a comprehensive, three-dimensional Eulerian model of gaseous and aerosol air pollution (Byun and Schere, 2006; Byun and Ching, 1999). It models spatial scales from the urban level (Seattle) to the continental level (US and Canada) and temporal scales of a couple days to multiple years. With emissions and meteorological data as input, it continuously emits gases and particles into the domain. These emissions advect and mix throughout the domain, undergo chemical transformations, deposit on the land surface, and interact with clouds. The result is a three-dimensional, hourly concentration map of dozens of gaseous and aerosol species. Aerosol concentrations are reported in the Aitken and accumulation modes for sulfate, ammonium, nitrate, organic and elemental carbon, and water, and are reported in the coarse modes for soil and sea salt. Aerosol extinction and modal properties are also output in separate files. This discussion of CMAQ applies to version 4.4, which was the most current publically-available version at the time of this study (Pleim et al., 2004). A summary of more recent official releases, as well as of other variations of CMAQ, is provided in sections 2.3 and 2.4.

An emissions inventory provides CMAQ with input gaseous and aerosol concentrations from typically hundreds of source categories. Anthropogenic emissions are represented as area, line, and point sources. Area sources such as home heating and light industry are given as the total amount of emissions of a chemical species in a

county. Line sources are highway emissions given as the vehicle miles traveled on a road segment multiplied by vehicle dependent emission factors. Point sources such as power plants and oil refineries emit large, concentrated plumes. An emissions processor such as the Sparse Matrix Operator Kernel Emissions (SMOKE) (Houyoux et al., 2002) converts the emissions inventory into gridded, three-dimensional, hourly emissions. Each source category has a temporal and chemical profile. Together they take the yearly or daily totals of emissions from the source and allocate them to particular hours and to the specific chemical species in CMAQ. The temporal emission factor can vary by hour, day of the week including holidays, week of the month, and month of the year, but special events are not accounted for. County-wide area and nonroad mobile emissions are distributed in the CMAQ grid based on spatial surrogates appropriate for the source. A version of MOBILE6 (U.S. EPA, 2003) within SMOKE computes gridded, hourly mobile source emissions based on traffic data and on ground temperature from the meteorology model. Point source emissions are allocated temporally and placed into one or more vertical levels depending on atmospheric stability, the temperature of the plume, and plume exit velocity. Biogenic sources are distributed according to land use characteristics and meteorological conditions. All the source types are merged into one emissions dataset specific to the time and meteorology of the simulation.

CMAQ uses the results from a meteorological model to characterize the atmosphere during the period of interest. The Meteorology-Chemistry Interface Processor (MCIP) (Byun and Schere, 2006; Byun et al., 1999a) in CMAQ is responsible for processing meteorological data. It has been widely applied to the Penn State / National Center for Atmospheric Research (NCAR) mesoscale model version 5 (MM5) (Dudia et al., 2001). A separate but similar processor called PREMAQ has been developed to process Eta model output from the National Center for Environmental Prediction (NCEP) for a real-time version of CMAQ (Otte and Pleim, 2005). PREMAQ has been further updated to handle output from the Nonhydrostatic Mesoscale Model core of the Weather Research

and Forecasting (WRF/NMM) system and has been renamed WCIP (Byun et al., 2006). PREMAQ and WCIP do not apply for this study and will not be discussed in detail.

MCIP inputs meteorological data, regrids it to the CMAQ domain, computes boundary layer parameters needed in CMAQ that were not output by MM5 or WRF, and adjusts the data for mass consistency. Most modelers design their CMAQ domain to match the horizontal resolution and extent of the meteorological domain, but often the meteorological model contains more vertical levels above 850 mb than used in CMAQ. MCIP uses a weighted average to collapse the meteorological model vertical levels to those of the CMAQ simulation. For MM5 data, MCIP recalculates the Monin-Obukhov length, the velocity scale (w_*), and the near-surface temperature and winds based on standard Monin-Obukhov similarity theory (Byun et al., 1999a). The Models-3/CMAQ dry deposition model in MCIP estimates dry deposition velocities for major gaseous species using photosynthetically available radiation, soil moisture, relative humidity, temperature, land use categories, temperature profile, and wind profile from meteorological model output to determine the total atmospheric resistance. The wind and density fields in MM5 are not consistent due to errors propagating from spatial and temporal interpolations, parameterizations for clouds and the Planetary Boundary Layer (PBL), Four-Dimensional Data Assimilation (FDDA), and exchanges at boundaries of domains and within nested domains. Because air quality models track pollutants by their concentration, an error or fluctuation in mass will result in inaccurate concentrations and unrealistic injections and sinks of pollution (Byun, 1999a, Byun, 1999b, and Byun et al., 1999b). Thus MCIP adjusts the wind field to be mass consistent before advection and then re-adjusts the final density field again to account for numerical advection errors.

Decoupling the meteorological and air quality models creates inconsistencies between the models. The most important relates to vertical diffusion parameterizations. MM5 and WRF contain several options for vertical diffusion in the boundary layer. CMAQ v4.4 only includes simple first order K-theory local closure and the Asymmetric Convective Model (ACM1) non-local closure (Pleim and Byun, 2001). It is important for CMAQ to

use the same or similar boundary layer parameterization as the meteorological model if CMAQ is going to use meteorological model output to drive vertical diffusion. MM5 does contain the ACM1 parameterization, but an analysis in Chapter 3 will show that it performs worse than the Medium Range Forecast (MRF) scheme commonly used for regional weather forecasts. In addition, ACM1 in CMAQ is known to overmix the boundary layer, which can result in artificially accelerated chemistry in the model (J. Arnold, personal communication). The modeler is left with a choice between model inconsistency and poor performance in CMAQ.

Ideally the meteorology and chemical transport models would be merged and would provide several sophisticated boundary layer parameterizations. Progress has been made towards these goals but not in time for this study. A new boundary layer parameterization called Asymmetric Convection Model 2 (ACM2) (Pleim, 2006) has a consistent treatment of heat, momentum, and trace gas fluxes that can be used in both meteorological and air quality models. Early results are more promising than for ACM1, but ACM2 has not yet been widely tested and applied with both meteorology and air quality models. The 2007 version of CMAQ will take one step towards a consistent meteorological and air quality simulation by including the feedback of aerosols on photolysis rates. A full coupling of WRF and CMAQ is in development but is far from implementation. It would follow in the footsteps of WRF/Chem, whose most common implementation is an on-line coupling of WRF and an air quality model similar to CMAQ (Grell et al., 2005). For sophisticated aerosol modeling with CMAQ, inconsistencies between the off-line meteorology model and CMAQ remain.

CMAQ introduces the emissions from SMOKE into the domain and advects and diffuses the pollutants using meteorological model output (Byun and Ching, 1999; Pleim et al., 2003; Schere, 2002). The pollutants in each grid cell react chemically, interact with clouds, receive solar actinic flux, and deposit to the surface. Aerosols nucleate, condense, evaporate, coagulate, interact with clouds, and deposit. All of these processes are simultaneous in reality, but Eulerian air quality models split the processes serially for

each time step. CMAQ models each 5-12 minute time step in the following order: emission, vertical diffusion, advection, mass consistency adjustment, horizontal diffusion, cloud processes, gas-phase chemistry, and aerosol processes. The simulation is initialized with background concentrations and is allowed sufficient time (on the order of days) to reduce the influence of the initial conditions and to develop a realistic representation of urban chemistry. Either local k-theory diffusion or the non-local Asymmetric Convection Model drives vertical diffusion. The user can employ the piecewise parabolic or Bott finite-volume methods for advection. The piecewise parabolic method is used nearly exclusively because, although more numerically diffusive than the Bott scheme, it is computationally less intensive and the results from it are practically indistinguishable from those of the Bott solution. Boundary conditions are temporally-static profiles for each side of the outer domain. If there is an inner nest, boundary conditions are fed dynamically from the outer nest to the inner nest in a one-way paradigm. Once emissions and transport have taken place, processes within a cell modify gaseous and aerosol concentrations.

In CMAQ, clouds absorb gases into their droplets, incorporate aerosols through droplet nucleation and impaction, and scavenge gases and aerosols by precipitation (Roselle and Binkowski, 1999; Binkowski and Roselle, 2003; Mueller et al., 2006). MM5 or WRF provides CMAQ with vertically resolved cloud mixing ratios. MCIP diagnoses sub-grid, boundary layer clouds, but this can only be applied to horizontal grid sizes larger than 4 km. In resolved clouds, gases dissolve into droplets based on Henry's Law constants, dissociation constants, and cloud water pH. Accumulation and coarse mode aerosol are assumed to have been cloud condensation nuclei sites and are incorporated into the cloud water. Aitken mode aerosol is slowly incorporated into cloud water to simulate coagulation of aerosol and droplets. Aqueous phase chemistry within the cloud droplet can produce cloud water sulfate. All cloud water species become accumulation mode mass with no change in the number of particles or the modal geometric standard deviation. It is not possible for CMAQ v4.4 to develop a distinct condensation and droplet mode. Wet deposition of aqueous-phase gas and aerosol species is proportional to

the precipitation rate, water content, and thickness of the cloud. The cloud is assumed to form after the advection process and disappear before passing its results to the gas-phase portion of the model.

The gas-phase chemistry module solves for equilibrium gas-phase concentrations. Because of the very large number of gaseous species and reactions in the urban environment, the process is first simplified by lumping similar species into chemical mechanisms. The three incorporated in CMAQ v4.4 are Carbon Bond-IV or CB-IV (Gery et al., 1989), the second generation of the Regional Acid Deposition Model or RADM2 (Stockwell et al., 1990), and the 1999 version of the Statewide Air Pollution Research Center mechanism or SAPRC-99 (Carter, 2000), in order of computational need and mechanism complexity. RADM2 is no longer supported in v4.5 and above, and CB05 is added in v4.6. SAPRC-99 contains a more complete representation of organic chemistry important to the production of secondary organic aerosol and thus is generally used for aerosol applications. Equilibrium concentrations of gas-phase species are numerically solved with a choice of the SMVGEAR, Rosenbrock, and Euler Backward Iterative (EBI) solvers. All solve the incorporated chemical reactions as a set of simultaneous ordinary differential equations, and all attempt to balance stability, accuracy, and speed. SMVGEAR is accurate and stable but slow, while EBI is a good balance between accuracy, stability, and speed. The equilibrium of species depends on temperature and actinic flux in each grid cell as derived from meteorological input. Total concentrations of sulfuric acid and organic species are partitioned into gas and aerosol phases in the aerosol module.

2.2. Aerosol Module in CMAQ v4.4

CMAQ attempts to model all the important processes that affect aerosol concentrations. Particles are emitted, mix into the atmosphere, advect with the winds, nucleate from gases, coagulate, grow by condensation, evaporate, act as cloud condensation nuclei, form from evaporating cloud droplets, and deposit to the earth’s

surface. Emission, transport, and cloud processes are performed external to the core aerosol module in CMAQ. The philosophy of aerosol modes forms the basis of the aerosol module. The size distribution is assumed to be made up of three, log-normal modes: Aitken, accumulation, and coarse. The modes are not tracked by their median diameter and geometric standard deviation but rather by their zeroth (M_0), second (M_2), and third (M_3) moments. They are related to the number, surface area, and volume by a factor of 1, π, and $\pi/6$. The three moments determine the standard deviation and number-based median diameter for each mode (Binkowski and Roselle, 2003):

$$\ln^2 \sigma_g = \frac{1}{3}\ln M_0 + \frac{2}{3}\ln M_3 - M_2 \text{ , and} \tag{2.1}$$

$$D_g^3 = \frac{M_3}{M_0 \exp\left[\frac{9}{2}\ln^2 \sigma_g\right]}. \tag{2.2}$$

Coarse mode aerosols are emitted, transported, and involved in cloud processes. However, because sea salt and soil dust emissions are so uncertain, the coarse mode in CMAQ v4.4 acts more as a tracer and is not involved in any of the aerosol dynamical or thermodynamic processes. Its median diameter can change in the model, but its geometric standard deviation is fixed at 2.2. By tracking aerosols in modes, it is assumed that all aerosols in the mode are spherical and internally mixed.

Aerosol emissions come from the emissions inventory as $PM_{2.5}$ and PM_{10}. SMOKE converts the $PM_{2.5}$ to the mass of emitted sulfate, nitrate, organic carbon, elemental carbon, and unspecified fine mode aerosol, and it converts PM_{10} to $PM_{10\text{-}2.5}$. CMAQ distributes the mass of these species into the Aitken, accumulation, and coarse modes according to Table 2.1 and then converts this to the zeroth, second, and third moments in each mode based on an assumed size distribution of emitted aerosols:

$$M_{0,emission} = \frac{\exp\left[\frac{9}{2}\ln^2 \sigma_g\right]}{D_{gv}^3} E_{mass} \frac{6}{\pi\rho}, \quad (2.3)$$

$$M_{2,emission} = \frac{\exp\left[\frac{1}{2}\ln^2 \sigma_g\right]}{D_{gv}} E_{mass} \frac{6}{\pi\rho}, \text{ and} \quad (2.4)$$

$$M_{3,emission} = E_{mass} \frac{6}{\pi\rho} \quad (2.5)$$

where E_{mass} is the emitted mass of all species in a mode with a density of ρ. Aerosols are emitted at every time step at every grid point and are distributed vertically according to the mixing state of the boundary layer.

CMAQ v4.4 solves for the equilibrium concentration of inorganic aerosols using a variant of ISORROPIA, a relatively fast, thermodynamic model (Nenes et al., 1998; Nenes et al., 1999). It solves for the equilibrium concentration of sulfate, ammonium, nitrate, and water at a given temperature and relative humidity for sulfate poor, sulfate rich, and acidic sulfate rich conditions, depending on whether the ammonium to sulfate ratio is greater than two, between one and two, or less than one. The original ISORROPIA includes sodium and chloride, but CMAQ v4.4 neglects these two species. The dissolution of nitric acid and ammonia is included, and their gas phase concentrations are output from this part of the aerosol module. The water content is determined by the Zdanovskii, Stokes, and Robinson (ZSR) correlation method (Stokes and Robinson, 1966). It weights the molality of each electrolyte in the multicomponent combination by the molality in the case where the electrolyte is the only species in solution. In the original ISORROPIA, only species with a mutual deliquescence RH below the ambient RH are included as aqueous species, and hysteresis is ignored. If the ambient relative humidity is between the mutual deliquescence RH and the deliquescence RH of the most hydroscopic salt, then the aerosol content varies linearly between zero and the water content of the most hydroscopic salt. However, CMAQ v4.4 runs a simplified version of ISORROPIA. It assumes that the aerosol is metastable with respect

to water. This is equivalent to assuming that at one point the aerosol was hydrated at a high relative humidity and that the humidity has not dropped enough for any solid particle to form. Because a liquid solution can dissolve nitric acid, sulfate, and ammonia gas while a solid cannot, the assumption of a metastable aerosol may create too much aerosol mass for cases when the ambient relative humidity drops below the efflorescence relative humidity of the aerosol mixture.

The gas-phase module in CMAQ determines the new sulfate aerosol mass while the aerosol module determines the gas-phase sulfuric acid concentration. The gas-phase module saves the total amount of sulfuric acid created from the reaction:

$$H_2SO_{4(g)} + H_2O + 2OH^{\bullet} + SO_2 \rightarrow H_2SO_{4(g,aq)} + HO_2^{\bullet}. \qquad (2.6)$$

In the aerosol portion of CMAQ, the produced sulfuric acid first nucleates new particles, and the remainder condenses onto existing particles. The gas-phase sulfuric acid concentration is the steady-state amount that results from the production rate in equation (2.6) (Binkowski and Shankar, 1995):

$$C_{ss} = P\tau = \frac{P}{I_{3i} + I_{3j}} \qquad (2.7)$$

where P is the production rate of sulfuric acid, and τ is the condensation time scale and is the reciprocal of the total of the condensation factors from the Aitken (I_{3i}) and accumulation modes (I_{3j}). This steady-state assumption states that the sulfuric acid produced will eventually condense but is limited by the time it takes to diffuse to the existing particles. Nucleation is ignored in this calculation under the assumption that it contributes negligibly to the change in sulfate mass. CMAQ uses the nucleation parameterization by Kulmala et al. (1998) to continuously nucleate binary H_2SO_4-H_2O clusters as a function of the sulfuric acid concentration, relative acidity, relative humidity, and temperature. All new particles are assumed to have a diameter of 2 nm. Kulmala et al. state the parameterization is valid for temperatures between –40 °C and +25 °C, relative humidities between 10 and 100%, and nucleation rates between 10^{-5} and 10^{5} $1/(cm^3 s)$. The produced sulfuric acid that does not nucleate particles must condense onto

existing particles. It is partitioned onto existing Aitken and accumulation mode particles in proportion to the condensation factors for each mode. The condensation factor is a harmonic mean of the free molecular (D_p < 13 nm) and near-continuum (D_p > 130 nm) condensation factors. It determines the relative diffusion rate of sulfuric acid to existing particles as a function of temperature, pressure, and amount of surface area and number of particles in the mode. At the end of the time step, all of the sulfuric acid produced by the gas-phase module has been partitioned into new particles of 2 nm diameter, onto existing Aitken mode particles, and onto existing accumulation mode particles.

The Secondary Organic Aerosol Model (SORGAM) by Schell et al. (2001) solves for the secondary organic aerosol mass. SORGAM builds upon the theory of Pankow (1994) and later expanded by Odum et el. (1996). The premise is that organics in the pre-existing aerosol will form a layer on the particle that will absorb organic gases even when the gases are well below saturation concentrations. The partitioning of organics between the gas and aerosol phases is modeled as a semi-ideal solution. Raoult's Law applies in this case:

$$C_{sat} = XC^*_{sat} \tag{2.8}$$

where C^*_{sat} is the saturation vapor pressure of a given organic species, X is its mole fraction in the aerosol, and C_{sat} is the resulting semi-ideal saturation vapor pressure. Using the assumption that all the organic species have similar molecular weights and interact with each other, the organic aerosol mass of one species is:

$$M_i = \Delta ROG * M_o * \frac{\alpha_i K_{om}}{1 + K_{om} M_o} \tag{2.9}$$

where ΔROG is the change in the precursor (reactive organic gas) to the condensable organic from the gas-phase module, α_i is a stoichiometric conversion factor for the reaction that created the condensable species, K_{om} is the reciprocal of C^*_{sat}, and M_o is all of the absorbing aerosol mass. Equation (2.9) is a quadratic, nonlinear equation to be solved simultaneously for all eight condensable species in the current version of CMAQ: two products each for monoterpene, xylene and toluene and one product for alkane and

cresol. Partitioning coefficients and ΔROG come from smog chamber experiments. Depending on the temperature, pressure, absorbing organic aerosol mass, and production rate of low-volatility organic species, the change in mass of each species could be positive (condensation) or negative (evaporation). The resulting change in aerosol anthropogenic (sum of alkane, cresol, xylenes, and toluenes) and biogenic (sum of monoterpenes) second and third moments is partitioned into a change in Aitken or accumulation mode second and third moments using condensation factors valid for an average low-volatility organic species.

Coagulation in CMAQ is a basic Brownian motion model of spherical Aitken and accumulation mode particles (Jiang and Roth, 2003). The collision frequency function is a harmonic mean of the frequency functions from the free molecular and near continuum regimes (Binkowski and Shankar, 1995). Intracoagulation of Aitken mode particles of diameters D_1 and D_2 results in an Aitken mode particle of size $(D_1^3 + D_2^3)^{1/3}$. Volume is conserved but the surface area is reduced. The same holds for intracoagulation of accumulation mode particles. Intercoagulation of an Aitken mode particle and an accumulation mode particle results in an accumulation mode particle with a slightly larger diameter. Volume is transferred from the Aitken to accumulation mode but is conserved overall, while surface area is transferred from the Aitken to accumulation mode but decreases overall. The coarse mode does not contribute to coagulation in CMAQ.

Once CMAQ has updated the moments and species mass concentrations in the Aitken and accumulation modes, it shifts Aitken mode mass to the accumulation mode if necessary. This process is called “mode merging” (Binkowski and Roselle, 2003) and is done to prevent the Aitken mode from growing into and becoming indistinguishable from the accumulation mode. The Aitken mode must remain a representation of fresh particles. The conditions for mode merging are positive condensation rates for the Aitken and accumulation modes, a larger number of particles in the Aitken mode than in the accumulation mode, and a larger mass condensation rate in the Aitken mode than

accumulation mode. For the zeroth moment, all the Aitken particles with diameters above the intersection of the Aitken and accumulation number distributions are shifted into the accumulation mode. The same process is repeated for the second and third moment distributions. At most half of the moment is shifted in any given time step.

The aerosol module in CMAQ represents state-of-the-art aerosol modeling for the Pacific Northwest. However, as with other meteorology and geophysical models, many opportunities exist to improve CMAQ. Model development has progressed beyond CMAQ v4.4, and the CMAQ community is examining many aspects of aerosol modeling for future enhancements. Several efforts are focused on secondary organics (see e.g., Pleim et al., 2006). This has important implications in the Pacific Northwest where organics comprise up to 50% of the $PM_{2.5}$ (Malm et al., 2004). Others have looked into the issue of nucleation (Park et al., 2006; Fan et al., 2006; Y. Zhang et al., 2006a), the emission size distribution (Park et al., 2006), and sectional aerosol representations (K. M. Zhang, 2005; Y. Zhang et al., 2004). Even with recent attention paid to the entire aerosol size distribution and more detailed properties, there is an opportunity for a more rigorously scientific treatment of aerosols in CMAQ and for a study of CMAQ's aerosol properties in the Pacific Northwest. Only a few reported studies have compared CMAQ to observations of aerosol mass in the Pacific Northwest (Smyth et al., 2006; Jiang et al., 2006; O'Neill et al., 2006). Smyth et al. (2006) explored $PM_{2.5}$ performance for Pacific 2001 but did not investigate model performance for number concentrations or for the size distribution in the ultrafine size range. Pacific Northwest 2001 (PNW2001) and Pacific 2001 provide an excellent dataset to explore detailed CMAQ aerosol performance for the Pacific Northwest.

2.3. Overview of More Recent CMAQ Versions

Since the release of CMAQ v4.4 in September 2004, three versions of CMAQ have been disseminated. They represent a significant advance in air quality modeling capabilities but are unlikely to change this evaluation for the Pacific Northwest (Chapter

4) or change how the science updates in Chapters 5-7 improve the CMAQ aerosol size distributions.

CMAQ v4.5 (Pleim et al., 2005) includes model changes that have the most potential to affect the results of this study. Several of the changes, including two bug fixes, apply directly to the aerosol module (Bhave et al., 2005). The first bug fix relates to mode merging. In this process, a maximum of one-half of the Aitken mode moment is shifted to the accumulation mode in one time step. When the amount shifted should be capped at 50% of the Aitken moment, v4.4 instead shifts none at all. Mode renaming is nonexistent at exactly when it is most needed. Fixing this bug reduces the frequency when the Aitken mode was larger than the accumulation mode, reduces the median diameter of the Aitken mode, and increases the number of particles. Fine mode mass increases as less aerosol is incorporated into cloud water and deposited as precipitation. The other major CMAQ v4.5 bug fix is a unit conversion error that essentially zeroed out gaseous sulfuric acid emissions. Fixing the bug results in higher aerosol sulfate and water concentrations by up to several $\mu g/m^3$ in areas of high sulfate emissions. Because regions of high sulfate emissions also have a higher frequency and intensity of regional nucleation events, the resulting increase in surface area could affect nucleation and the lifetime of nucleated particles. In Chapter 5, this study implements both bug fixes into CMAQ v4.4 to test their effect on the particle number concentrations.

One other CMAQ v4.5 aerosol change could possibly affect CMAQ's size distributions. CMAQ v4.5 includes condensing aerosol sulfate mass in the ISORROPIA calculation of inorganic aerosol equilibria (Bhave et al., 2005). The greater sulfate mass increases aerosol ammonia and water content as well. The higher condensation rate of sulfate, ammonia, and water shifts mass to the accumulation mode, which increases dry deposition and decreases $PM_{2.5}$ slightly. The shift in mass to the accumulation mode may be important, but it is not tested in CMAQ v4.4 with the two bug fixes described just above. To do so would require a reorder of the subroutines in the aerosol module so that the thermodynamic subroutine comes after the nucleation subroutine. This is not

desirable since nucleation theory and nucleation mode processing are sensitive to the thermodynamic equilibrium of surface area and mass. Therefore, this study retains the CMAQ v4.4 treatment of aerosol sulfate in ISORROPIA.

The other important changes to the aerosol module are less likely to materially affect the CMAQ v4.4 size distributions. Changes to the aerosol dry deposition theory increases accumulation mode deposition by a factor of 10 and are shown to decrease sulfate aerosol concentrations by up to 10% in highly concentrated regions (Pleim et al., 2005). A new sea salt module, AERO4, simulates sodium and chloride chemistry. By adding a nitrate condensation pathway in the coarse mode, it could decrease the accumulation mode nitrate close to the Puget Sound and Strait of Juan de Fuca. Elimination of discontinuities and instabilities in ISORROPIA are only very occasionally significant. The dry deposition modification, and to a lesser extent the sea salt addition, may change the details of how CMAQ performs in the Pacific Northwest, but the changes are expected to be small relative to the major conclusions from CMAQ v4.4.

Of the changes to other parts of the CMAQ model in the v4.5 release, modification to the minimum K_z for vertical diffusion has the biggest potential effect on aerosol concentrations and size distributions. Under stable conditions, the minimum K_z in CMAQ v4.4 was previously 1 m^2/s but now it is 0.5 m^2/s for rural areas and 2.0 m^2/s for urban areas. With more mixing in urban areas and less mixing in rural areas at night, nighttime aerosol concentrations are expected to lower in urban areas, and ozone may be more likely titrated in rural areas. Lower urban aerosol concentrations during the morning rush hour allow for more nucleation and a better chance of nucleation mode particle survival. Rural ozone titration at night changes the oxidant concentrations the following morning, which could also modify the amount of condensing aerosol species. Other changes, more tangential to this work, include a new mass conservation scheme and the addition of chemistry for air toxics. While most of the upgrades to CMAQ v4.5 outside of the aerosol module will not affect CMAQ aerosol performance, the change to the minimum vertical diffusion may affect the results from v4.4.

CMAQ v4.5.1 adds important capabilities to CMAQ but less for modeling aerosol size distributions than for $PM_{2.5}$. An update to the ISORROPIA activity coefficients decreases nitrate concentrations in stable, cold boundary layers. Also, CMAQ no longer lumps aerosol species with different molecular weights during cloud processing. The aerosol standard deviation decreases and the aerosol median diameter increases, but the overall effect on aerosol concentrations and properties is minor (CMAS, 2006). Other changes include adding a module for mercury chemistry as well as a new chemistry solver, CB05.

CMAQv4.6 has additional refinements to inorganic aerosol production in humid and cold conditions. Aerosol water is capped at the value for 95% humidity to avoid extraordinarily large amounts of water near 100% humidity. The heterogeneous production of nitric acid from N_2O_5 is turned back on, while the attachment factor of N_2O_5 to existing particles is now temperature and humidity dependent. The ISORROPIA activity coefficients for air below 285 K are updated. In addition, toxic metals and diesel particles are added to the toxics module. None of these model improvements are likely to materially affect results presented here for the Pacific Northwest in late August 2001.

2.4. Other Versions of CMAQ

The air quality modeling community has developed other versions of CMAQ useful for aerosol modeling. The most common uses the Model of Aerosol Dynamics, Reaction, Ionization, and Dissolution (MADRID) (Y. Zhang et al., 2004). All aerosol processes, including cloud processing, are removed from CMAQ and replaced with MADRID. This aerosol module was specifically designed to model secondary organic aerosol. One version (MADRID 1) partitions organics into particle and gas phases based on the same general methodology and underlying experimental data as the SORGAM scheme in CMAQ. MADRID 2 (J. Chen et al., 2006) employs the Model to Predict the Multiphase Partitioning of Organics (MPMPO). MPMPO is similar to SORGAM and MADRID 1

but includes the dissolution of organics into aerosol water, organic acid dimer formation, and updated oxidation mechanisms. It is also linked to the Caltech Atmospheric Chemistry Mechanism (CACM), a gas-phase mechanism specifically tailored for organic chemistry. In both versions of MADRID, aerosol size is represented by a moving-center sectional scheme with typically 2-8 sections. Particle nucleation is derived from sulfuric acid binary nucleation according to McMurry and Friedlander (1979). MADRID 1 and MADRID 2 use two slightly different versions of ISORROPIA for inorganic aerosol species. In the fine mode, ISORROPIA determines the equilibrium gaseous and aerosol concentrations for condensable inorganic species, while the dynamic coarse mode concentrations follow Capaldo et al. (2000). Another enhancement is the use of the Carnegie Mellon University (CMU) bulk aqueous-phase chemical mechanism, which is an updated and enhanced version of RADM2 in CMAQ. Mercury chemistry is an option with MADRID-Hg^{TEAM} (Knipping, 2005). Despite MADRID's advantages for modeling coarse mode chemistry and secondary organics, it is not very useful for modeling the aerosol size distribution because it neglects particle coagulation.

More sophisticated plume-in-grid treatments have been added to CMAQ. CMAQ-APT (Advanced Plume Treatment) (Karamchandani et al., 2002) represents subgrid plumes with the Second-order Closure Integrated puff model (SCIPUFF). It treats turbulence with a second order closure, is able to split and merge puffs, and has no constraints on plume geometry. When CB-IV chemistry is added, it models subgrid gaseous chemistry and is renamed SCICHEM. CMAQ-MADRID-APT (Karamchandani et al., 2006) incorporates the MADRID aerosol module into the subgrid plume. It can be used within CMAQ-MADRID or the standard CMAQ. These sophisticated plume models are only recommended for simulations with a grid resolution of 20 km or larger (Karamchandani et al., 2002). The APT is thus not suitable to represent the subgrid urban environment in a 4-km grid.

CMAQ-UCD substitutes the UC-Davis Aerosol Module into CMAQ (K.M. Zhang, 2005). Similar to the Aerosol Inorganic Model (AIM), the UCD module represents

aerosols with nine discrete size bins between 40 nm and 20 μm. With at most two bins in the ultrafine mode and a small number in the fine mode, the resulting size distributions are unable to reproduce the structure of measured urban distributions. In addition, this module is computationally intensive and is not realistic for most applications.

These alternate versions of CMAQ have sectional representations for aerosols that could in theory represent the aerosol size distribution better than the lognormal modes in CMAQ. Aerosol size distributions are often but not always lognormal. An accurate sectional representation could capture processes that deviate from the lognormal assumption. Unfortunately, this requires a large number of sections. This is especially true close to a source and for freshly nucleated particles. Even the 8 or 9 sections in CMAQ-MADRID (neglecting coagulation) and CMAQ-UCD dramatically slow down the simulation. These sectional models barely represent the Aitken mode and are therefore unlikely to do a better job capturing the Aitken mode than the lognormal version of CMAQ. For modeling aerosol size distributions with a focus on the ultrafine range, it is more useful to the broader community to evaluate and improve the standard lognormal version of CMAQ.

Table 2.1 Partition of emission species into Aitken (i) and accumulation (j) modes and partition of coarse mode emissions into species.

Emission Species	Mode or Component	% Mass
sulfate	i	0
	j	100
nitrate	i	0
	j	100
other fine	i	0
	j	100
organic	i	0.1
	j	99.9
elemental carbon	i	0.1
	j	99.9
coarse	Sea Salt	0
	Soil	90
	General Coarse	10

3. Case Study

3.1. Observational Data

The PNW2001 field campaign was conducted in August 2001 to obtain an airborne and ground based representation of summertime regional pollution in the Puget Sound (Jobson et al., 2002). The objective was to provide data on the south side of the US/Canada border to complement Pacific 2001 (Li, 2004), a major regional air pollution study in the Lower Fraser Valley.

The U.S. Department of Energy Gulfstream-I aircraft was instrumented to measure various gas-phase concentrations, aerosol properties, meteorological variables, and radiation properties. The complete list is given in Table 3.1. Most of the species are reported in one-second intervals even if their measurement timescales are longer. Though not available for every flight, formaldehyde, methanol, acetone, benzene, and toluene were output every 15 or 90 seconds. Three Condensation Particle Counters, one Ultrafine Condensation Particle Counter, one Passive Cavity Aerosol Spectrometer Probe, and one Forward Scattering Spectrometer Probe work together to measure the aerosol size distribution. A TSI nephelometer and a Particle Soot Absorption Photometer (PSAP) provide aerosol scattering and absorption. A rotating drum preserved size-segregated aerosols on filters for later chemical analysis by x-ray fluorescence, but these results are not available. A Multi-Filter Radiometer (MFR) and a Eppley radiometer supply spectral upwelling and downwelling UV-near infrared radiation at six wavelengths and total broadband upwelling and downwelling UV and IR radiation. The goal of these measurements is to characterize gaseous and aerosol pollution in Puget Sound.

The Gulfstream aircraft sampled regional pollution on 20 (Monday), 26 (Sunday), and 27 (Monday) August. Table 3.2 and Figures 3.1-3.3 summarize the flights and meteorology. Although meteorological conditions did not produce high pollution levels, conditions were representative of weak on-shore flow which frequently occurs in the summer. Morning and afternoon flights were conducted on 20 and 27 August, while only an afternoon flight was conducted on 26 August. Flight altitudes were typically 500 m in the boundary layer west of the Cascades and 1800 m over the Cascade crest. For the morning flights of 20 and 27 August, the aircraft departed the Tri-Cities Airport at 8 AM PST, flew west over the crest of the Cascades between Gilbert Peak and Mount Adams and reached the Cowlitz Valley at 8:30 AM PST. It flew down the valley to Centralia, along the foothills to Enumclaw, and into Boeing Field for a touch-and-go urban profile. The aircraft continued north to make a triangle trip between Everett, Bellingham, and Port Angeles, with touch down at Paine Field in Everett after noon. On the morning of 20 August but not 27 August, the Gulfstream spiraled to the top of the boundary layer over the San Juan Islands. On the afternoons of 20 and 27 August, the Gulfstream took off from Paine Field at 2 PM PST and completed two counter-clockwise circuits in the boundary layer around the Puget Sound. During the first Puget Sound circuit, a profile of the boundary layer was obtained over Mud Mountain Dam. It returned to Pasco over Stampede Pass and Cle Elum on 20 August and over the Alpine Lakes Wilderness and Cle Elum on 27 August. On the afternoon of 26 August, the aircraft departed from Pasco, crossed the Cascades over the Alpine Lakes Wilderness, dropped into the boundary layer near Duvall, performed two circuits and a profile at Mud Mountain Dam, and returned to Pasco over Stampede Pass. The five flights provide the most complete field campaign aloft of Puget Sound gaseous and aerosol air pollution.

The University of Washington-Bothell Beechcraft airplane also collected data in August 2001 as part of PNW2001 (Snow et al., 2002 and Table 3.1). The aircraft measured ozone and aerosol light scattering on 10, 16, and 20 August at 500 m in a clockwise circle around the Puget Sound metropolitan area from Everett to Enumclaw,

northwest to the Hood Canal, and back to Everett. Spirals through the boundary layer were conducted over Enumclaw. Although a more limited dataset than that from the Gulfstream, the Beechcraft dataset has the advantage of collecting data during a smog episode on 10 August and during transport from western U.S. forest fires on 16 August.

As part of PNW2001, ground measurements of NO_x (nitric oxide (NO) plus nitrogen dioxide (NO_2)), carbon monoxide (CO), volatile organic compounds (VOCs), and carbonyls at Lynwood and Mud Mountain Dam were obtained. In addition, five ozonesondes were launched from Enumclaw to roughly coincide with profiles from the Gulfstream aircraft: two on 15 August and one each at 12 PM PST on 20 August, 3 PM PST on 26 August, and 3 PM PST on 27 August. These measurements are intended to complement measurements aboard the research aircraft.

Pacific 2001, a comprehensive air quality study of the Lower Fraser Valley, was conducted at the same time as PNW2001 (Li, 2004; Vingarzan and Li, 2006; Environment Canada, 2002). Measurements were obtained at various times between 10 August and 2 September 2001. Five sites spread along the Fraser Valley capture various aspects of regional air pollution (Figure 3.4). The Cassier Tunnel site at the ends of the tunnel represents fresh emissions from mobile traffic. Because of its spatial scale, this site is not appropriate for comparison to an air quality model with 4 km horizontal resolution. The Slocan Park site characterizes the transition from urban to suburban chemistry and is representative of an urban area. The Langley Ecole site is situated where the aging urban plume interacts with agricultural emissions. The Sumas Mountain site measures the aged urban plume as modified by the agricultural region. The Golden Ears Park site, outside the urban plume trajectory, represents a region of high biogenic emissions. Although not all the data were available for this study, the ground sites measured a comprehensive suite of gaseous and aerosol components and properties: inorganic gases, organic gases, air toxics, isotope chemistry, size-segregated aerosol chemistry, aerosol mass loading, aerosol optical properties, aerosol size distributions, and meteorological and radiation variables. Two aircraft, a Cessna 188 and a Convair 580, sampled the airmass in the

Lower Fraser Valley. The available Cessna data includes particle size distributions, ozone concentrations, and VOC concentrations. The Cessna flew 20 flights on ten days but not during the period of the PNW2001 study. Although not all of the field campaign data are available for 26-28 August, Pacific 2001 significantly aids this CMAQ evaluation.

In addition to the special observations from the field campaigns, routine surface observations add an important 24-hour view of model performance. In the summer of 2001, Washington Department of Ecology was managing 126 sites that measure various criteria pollutants and other species on an hourly basis: NO, NO_2, NO_x, sulfur dioxide (SO_2), CO, ozone (O_3), aerosol scattering, aerosol absorption, PM_{10}, and $PM_{2.5}$. Between one and 20 sites (Table 3.3) measured each pollutant across the state, but not all of the monitors were inside the modeling domain and not all had valid data for every hour. Typical precision and accuracy for most criteria pollutants is also listed in Table 3.3 (Stan Ruhl of Washington Department of Ecology, personal communication; and Washington Department of Ecology, 2004). Several sites monitored $PM_{2.5}$ both with a TEOM and with a nephelometer. In this case, the two measurements were averaged to obtain one representative measurement for the location. Aerosol chemical composition is available from the U.S. EPA Speciated Trends Network (STN) once per week and from the Interagency Monitoring of Protected Visual Environments (IMPROVE) network twice per week. The STN network had four sites in Portland and Seattle that measured several metals as well as ammonium, nitrate, sulfate, soil dust, and total carbon contained in $PM_{2.5}$. The IMPROVE network had nine sites in the Cascades Mountains, Olympic Mountains, and Seattle. It measured major inorganic species but also included a breakdown of total carbon into organic and elemental fractions. Continuous 10-minute averages of aerosol size distributions from 20 nm to 5 μm are also available for most of August at Beacon Hill. The routine ground measurements are the only nighttime observations in the Puget Sound region for comparison against CMAQ.

3.2. CMAQ Case Study Design

To evaluate CMAQ using the PNW2001 dataset, CMAQ v4.4 (Pleim et al., 2004) was run at 4 km grid spacing for the Pacific Northwest. The CMAQ domain (Figure 3.5) has 123 columns and 183 rows, and it covers the entire region that would significantly impact the Puget Sound / Lower Fraser Valley -- from Eugene to the British Columbia Coast Range and from the Pacific Ocean to Moses Lake. There are 22 vertical sigma levels (21 layers) in the model. The lowest layer is ~30 meters above the surface and 14 levels are between the surface and 800 mb. The latest aerosol module with cloud chemistry at the time of the study was employed in conjunction with the SAPRC-99 chemical mechanism and EBI solver for gas-phase concentrations. The simulation used the piecewise parabolic scheme for advection and local k-theory for vertical diffusion. The Models-3/ CMAQ dry deposition model estimated the deposition velocities of gases and aerosols.

The focus of this simulation was 26 and 27 August when PNW2001 included three Gulfstream flights during warm and dry weather conditions. To start the simulation, CMAQ initialized at 00 UTC 24 August with background concentrations from the GEOS-CHEM model (Bey et al., 2001). When CMAQ reached 00 UTC 26 August, the results for this hour were used to restart the model at 00 UTC 24 August. CMAQ then ran again until 00 UTC 26 August. These 96 hours of model runs represent the spin-up from background conditions to an urban airmass. The simulation continued from 00 UTC 26 August until 00 UTC 29 August for 72 hours of valid simulation.

Boundary conditions came from the GEOS-CHEM model valid for 26-28 August 2001 and from typical coastal observations. GEOS-CHEM is a three-dimensional global atmospheric chemistry model that captures the synoptic-scale movement of gaseous tropospheric pollutants. Qing Liang and Lyatt Jaeglé of the University of Washington Department of Atmospheric Sciences supplied 4° latitude by 5° longitude GEOS-CHEM results for August 2001. This dataset became boundary conditions for the 4 km CMAQ grid. When used in this way, CMAQ requires the boundary conditions to be one time-

independent profile per side of the CMAQ domain. The GEOS-CHEM input was temporally averaged for 26-28 August, interpolated to the CMAQ vertical levels, and averaged along each side of the CMAQ domain. Aerosol boundary conditions came from representative measurements at Cheeka Peak on the Olympic Peninsula (Anderson et al., 1999) because this site represents background conditions upwind of the Pacific Northwest pollution sources. All are constant vertically except for sea salt, which is a strong function of height (Figure 3.6). Sulfur dioxide and sulfate were not represented in GEOS-CHEM, so their boundary conditions are representative values from other global transport models for the eastern Pacific Ocean. The jet stream over the Pacific was generally zonal for the week before the period of interest and well north of China and Japan. In conjunction with the clean conditions modeled by GEOS-CHEM, this suggests transport from Asia is not a concern for this simulation.

NW-AIRQUEST, a consortium of air pollution agencies in the Pacific Northwest, provided emissions for all major sources of pollution in the CMAQ domain. The emission inventory is a compilation of information supplied by the Washington State Department of Ecology, Oregon Department of Environmental Quality, Idaho Department of Environmental Quality, Washington State University, the Western Regional Air Partnership, and Environment Canada. In most cases, an emissions inventory for a particular source type is conducted every few years and is valid in the compiled inventory for a year between 1996 and 2003. The disparity between the inventory date and the time of simulation would likely only be an issue for the point sources, which have been updated to 2001 emissions for Washington and Oregon. In addition to the normal surrogate-based area sources, area emissions include soil and livestock ammonia mapped to agricultural land use categories, and include fireplace and woodstove emissions mapped to population density. MOBILE6 produced on-road and off-road mobile emissions. Other mobile sources such as railroad and commercial marine traffic were also represented. The Biogenic Emissions Inventory System (BEIS-3) (U.S. EPA, 2007b) modeled biogenic emissions using the 1 km BELD3 land use database and meteorological input. Jack Chen at Washington State University used SMOKE to merge

all the emission source data and applied MM5 meteorology to obtain hourly, three-dimensional, gridded emissions for this simulation domain.

MM5 was run at 36, 12, and 4 km horizontal grid spacing as meteorological input to CMAQ. The domains focus on the Pacific Northwest (Figure 3.7). The simulation was initialized with 40 km ETA analyses (ETA-221), while 100 km ETA forecasts (ETA-104) provided 3-hourly boundary conditions. Analysis nudging (Stauffer and Seaman, 1990; Seaman et al., 1995) towards the 12-hourly ETA-221 analyses controlled the solution over the multi-day simulation. MM5 was initialized at 00 UTC 01 August with the default land temperature and moisture. The entire month of August was simulated at 36 and 12 km, with restarts every 3-5 days to prevent excessive drift. Other model specifications include 38 sigma levels, simple ice microphysics, Kain-Fritsch cumulus parameterization, no shallow cumulus parameterization, and one-way nesting of the domains. No cumulus parameterization was used at 4 km resolution. Special attention was given to runs initialized at 12 UTC 19 August (ending 00 UTC 23 August) and at 12 UTC 25 August (ending 00 UTC 29 August) because intensive aircraft sampling from PNW2001 is available for 20, 26, and 27 August. 4 km simulations have only been performed for these two periods.

3.3. MM5 Evaluation

For these two simulation periods, sensitivity to analysis and observation nudging (Seaman et al., 1995) and to boundary layer parameterizations was investigated for the 36 and 12 km domains. MM5 was run with analysis nudging at 36 and 12 km, nudging only at 36 km, and no nudging in either domain. All three use the Pleim-Xiu Land Surface Model and Asymmetric Convective Model (PX/ACM) configuration (Pleim and Chang, 1992; Xiu and Pleim, 2001). Nudging adds an extra, non-physical term in the governing equations that is a function of the difference between the current state of the simulation and the temporally closest analysis. It is intended to guide a simulation towards the analyzed solution. Nudging here was done for horizontal winds, temperature, and moisture above the boundary layer, and for winds only in the boundary layer. In addition,

MM5 at 36 and 12 km (with analysis nudging on both domains) was tested with the more conventional Five-Layer Soil Model and MRF (Slab/MRF) boundary layer scheme (Hong and Pan, 1996). When Pleim-Xiu is used, land temperature, land moisture, and canopy moisture parameters are carried over from one run to the next. When MRF is used, soil moisture is represented by moisture availability, which is only a function of season and land use characteristics. Pleim-Xiu responds to the temperature and precipitation patterns of past model runs, while the Five-Layer Soil Model is ignorant of recent droughts or rain events.

The various 12 km runs were assessed against: wind, temperature, relative humidity, and sea level pressure measurements at 200 surface sites in Western Washington, Northwest Oregon, and Southwest British Columbia; satellite observations of clouds; three-dimensional wind fields from the Sand Point profiler; and the vertical structure of temperature and moisture measured by the Gulfstream aircraft during PNW2001. Objective measures such as bias and gross error were balanced with other considerations such as consistency across time and performance during PNW2001 intensive sampling. Using the best performing model configuration at 36 and 12 km, MM5 was run at 4 km with and without nudging to winds observed at 27 hand-picked stations representative of the area. Observation nudging was evaluated through comparison of modeled surface winds to observations at 40 withheld stations. The sensitivity studies attempted to find the most accurate representation of meteorology so as to limit errors in the subsequent CMAQ simulation.

Sensitivity tests on the 36 and 12 km domains show that analysis nudging is effective for this simulation. Table 3.4 ranks each 12 km run for various types of observations. Although not uniform for all metrics, nudging both the 36 and 12 km domains performed the best overall, especially when more focus is given to the boundary layer. Often nudging only the 36 km domain performed worse than not nudging at all. Nudging outer domains to a coarse analysis reduces MM5's sensitivity to errors in initialization and model physics.

The Slab/MRF boundary layer outperforms PX/ACM. Table 3.5 ranks the two runs against observational metrics. Slab/MRF fares worse with respect to the production of boundary layer clouds because it overpredicts morning stratus and underpredicts cumulus on the afternoon of 20 August. However, it fares better in most other respects, especially in its representation of boundary layer temperature, moisture, and height. The PX/ACM configuration produces mixing heights higher than the MRF PBL in all four profiles, and it produces higher than the observed mixing height in the three cases where it can be determined. Figure 3.8 shows the observed profile from the Gulfstream aircraft over Puget Sound at 18 UTC 20 August. Meteorological conditions at this time were dominated by moist, cool flow from the Pacific Ocean and patchy marine stratus clouds. The most important feature of the observed profile is the stable layer below 950 mb. The MRF scheme captures the temperature inversion reasonably well but gives no indication of dry air above the inversion, while the PX/ACM parameterization misses the inversion entirely. Model fits on the afternoon of 27 August (59-hour forecast valid 23 UTC) over Mud Mountain Dam (Figure 3.9) are better than over the Sound on 20 August. Weak, moist, westerly flow and high clouds from a weather system in British Columbia characterize the conditions at the time. Both boundary layer schemes model an inversion that is too high, but the MRF PBL comes closer to the observed inversion height. In general for all four profiles, PX/ACM produced a boundary layer that is too warm, too dry, and too deep. MM5 with the MRF PBL also had problems with a deep boundary layer but yielded a better representation than PX/ACM. Based on the analysis nudging and boundary layer sensitivity tests, analysis nudging and Slab/MRF were chosen for the outer domains to nest down to the 4 km domain.

Observation nudging on the 4 km domain does little to improve MM5's representation of atmospheric conditions during PNW2001. Observation nudging is only done for surface winds. When compared to withheld stations, observation nudging did not significantly improve wind speed or wind direction statistics (Table 3.6). The wind direction mean gross error is as much as 45-55° for all model configurations. There is

often a diurnal cycle to the gross error peaking at ~80° in the early morning when winds were very light and variable and bottoming at 40° for much of the day (Figure 3.10). Both the observations and MM5 are highly inaccurate for wind speeds less than 5 knots as measured overnight during this period. However, even at midday observational nudging has little effect on performance. This could be attributed to the lower than standard radius of influence (25 km vs. 30-50 km) chosen for the Puget Sound's spatially variable summertime wind patterns. One major critique of observational nudging is that it upsets the dynamical balance achieved in the model. Recognizing this along with the ineffectiveness of observational nudging for this case, the 4 km simulation without observation nudging (using Slab/MRF) was selected to provide meteorological input to CMAQ.

Accuracy of the 4 km MM5 simulation can have major effects on CMAQ performance. Errors in wind fields can shift a plume away or towards a monitor and greatly misrepresent pollutant concentrations (for a Pacific Northwest example, see Barna and Lamb, 2000). Errors in temperature affect emission rates, reaction rates, and gas/particle partitioning. Errors in relative humidity propagate to biogenic emissions, aerosol nucleation rates, and aerosol thermodynamics. Accurate cloud fields are important for actinic flux calculations, aqueous phase chemistry, and precipitation scavenging. The entire structure of boundary layer stability and moisture affects the mixing of surface pollutants and affects the volume of air available for pollutant dilution.

For the period between 00 UTC 26 August and 00 UTC 29 August, 2 meter temperature is biased high by 0-5 K (Figure 3.11) west of the Cascades from the Willamette Valley north to Vancouver, BC. The positive bias is greatest 25 and 49 hours after initialization at 12 UTC 25 August. This corresponds to early morning (5 AM PST) when the surface temperature and boundary layer depth are at a minimum. Such a large domain-wide bias may be explained by the tendency of MM5 to not collapse the boundary layer and the tendency of the MRF boundary layer scheme to overestimate vertical diffusion. The temperature bias propagates to relative humidity, which is biased

low by up to 20% in the early morning but is still generally underpredicted by up to 10% throughout the simulation. Despite this error, the extent of the morning stratus cover is well predicted in the Puget Sound region. Mixing heights are overestimated over Mud Mountain Dam at 23 UTC (3 PM PST) on 26 and 27 August by 1500 feet and 500-1000 feet, respectively (Figure 3.12). This increases the mixing volume by approximately 40% and 20%. The wind direction error above 2 km at Sand Point is 10° or less for much of the simulation. Taken together, these meteorological errors might lead to an overprediction of ozone and underprediction of dry aerosol mass at night, and an underprediction of pollutant concentrations in the afternoon.

Table 3.1 List of measurements during PNW2001.

Aircraft	Measurement Type	Measurement	Aerosol Technique
Gulfstream	Gas	VOC	
		formaldehyde	
		SO2	
		NO/NOy	
		O3	
		CO	
	Aerosol	particle composition	SEM / EDAX
		mass	SEM / EDAX
		multi-elemental segregation	SEM / EDAX
		#	UCPC, CPC, & PCASP
		ultrafine and fine size distribution	UCPC, CPC, & PCASP
		scattering	Nephelometer (TSI)
		absorption	PSAP
	Meteorology	temperature	
		dewpoint	
		winds	
	Radiation	UV	
		shortwave	
		longwave	
Beachcraft	Gas	O3	
	Aerosol	light scattering	Nephelometer (Radiance Research)
Ground-Based	Gas	NOx	
		CO	
		VOC	
		carbonyl	
		ozonesonde	
		DoE routine sampling	
	Aerosol	Beacon Hill size distribution	Continuous DMA / CPC and APS
		DoE routine sampling	Impactor PM2.5 and PM10
		IMPROVE	Impactor PM2.5 and PM10

Table 3.2 Summary of PNW2001 flights and meteorological conditions.

Gulfstream Flight	Highlights	Weather
Morning 8/20	US/Canadian transport	Cool with marine stratocumulus buring off around noon
	Vertical profile over San Juan Islands	
	Seattle / Boeing Field touch-and-go	
Afternoon 8/20	Aged urban plume	Afternoon cumulus, humid, on-shore winds
	Vertical profile in aged plume	
Afternoon 8/26	Aged urban plume and background	sunny and warm (80's) after isolated morning stratus
	Vertical profile in aged plume	
Morning 8/27	US/Canadian transport	marine stratus and stratocumulus burning off late morning
	Seattle / Boeing Field touch-and-go	
	Urban plume	
Afternoon 8/27	Aged urban plume and background	cooler (70's), cirrus and altocumulus sagging south from Canada
	Vertical profile in aged plume	

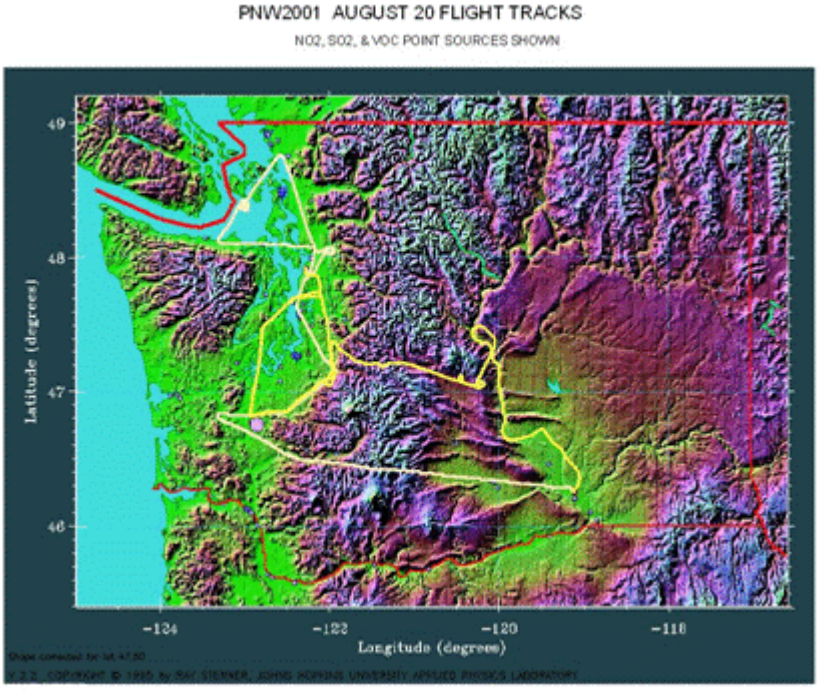

Figure 3.1 PNW2001 flight track for 20 August.

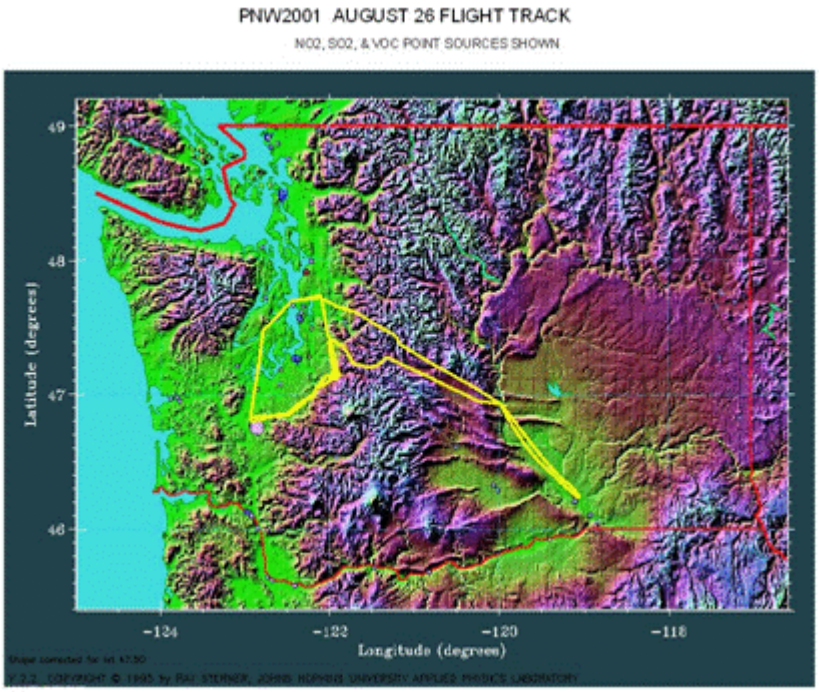

Figure 3.2 PNW2001 flight track for 26 August.

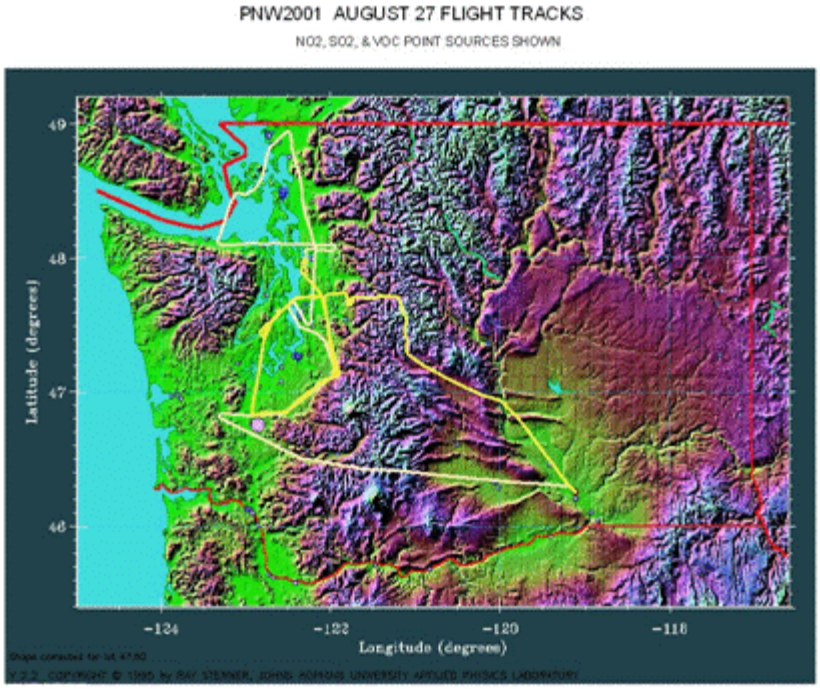

Figure 3.3 PNW2001 flight track for 27 August.

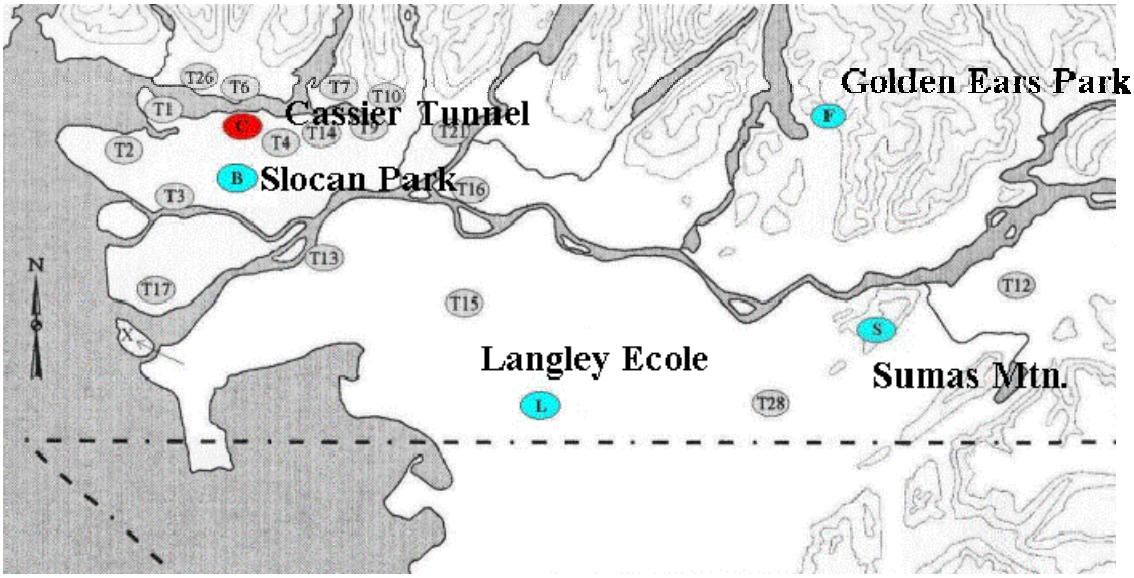

Figure 3.4 Location of Pacific 2001 ground sites (adapted from http://www.msc.ec.gc.ca/projects/pacific2001/study_sites_e.html).

Table 3.3 Washington Department of Ecology ground sites and STN/IMPROVE Pacific Northwest sites.

Pollutant	Technique	# Sites	Site Names	Precision	Accuracy
O3	Dasibi 1008PC	10	Custer, Enumclaw, Issaquah, North Bend, Pack Forest, Paradise, Beacon Hill, Vancouver, Wishram, Yelm	+- 5%	+- 5%
NO	Thermo 42C	1	Beacon Hill		
NO	Thermo 42C	1	Beacon Hill	-3 to 7%	-2 to 10%
NOx	Thermo 42C	1	Beacon Hill		
SO2	Thermo 43C	1	Beacon Hill	0 to 5%	+- 5%
CO	Thermo 48C	10	Bellevue NE 8th/108th, Everett, Lynwood, Seattle 4th/Pike, Beacon Hill, U District, Northgate, Tacoma Pacific Ave., Vancouver, Yakima	+- 5%	+- 10%
aerosol scattering	Radiance Research Nephelometer	16	Bellingham, Kent, Lacey, Lake Forest Park, Lynwood, Marysville, Puyallup, Paradise, Beacon Hill, Duwamish, Queen Anne, South Park, South Mountain, Tacoma Alexander Ave., Tacoma South End, Wishram	+- 5%	
aerosol extinction	Radiance Research Nephelometer + PSAP	1	Beacon Hill		
PM10	TEOM	6	Ellensburg, Kent, Bellingham, Duwamish, Wenatchee, Yakima	+- 8%	+- 5%
PM2.5	TEOM or nephelometer	14	Bellevue Aquatics, Kent, Lacey, Lake Forest Park, Lynwood, Marysville, North Bend, Puyallup, Duwamish, Queen Anne, South Park, Tacoma Alexander Ave., Tacoma South End, Vancouver		
Chemical Composition (STN)	ion chromatography for anions, thermal optical transmittance for total carbon	4 (2)	Portland, Beacon Hill all month; Corson Ave and Maple Leaf not available 8/20,8/26		
Chemical Composition (IMPROVE)	ion chromatography for anions, thermal optical reflectance for EC/OC	9	Columbia Gorge (West), Columbia Gorge (Wishram), Mount Hood, Mount Rainier, North Cascades, Olympic, Beacon Hill, Snoqualmie Pass, White Pass		

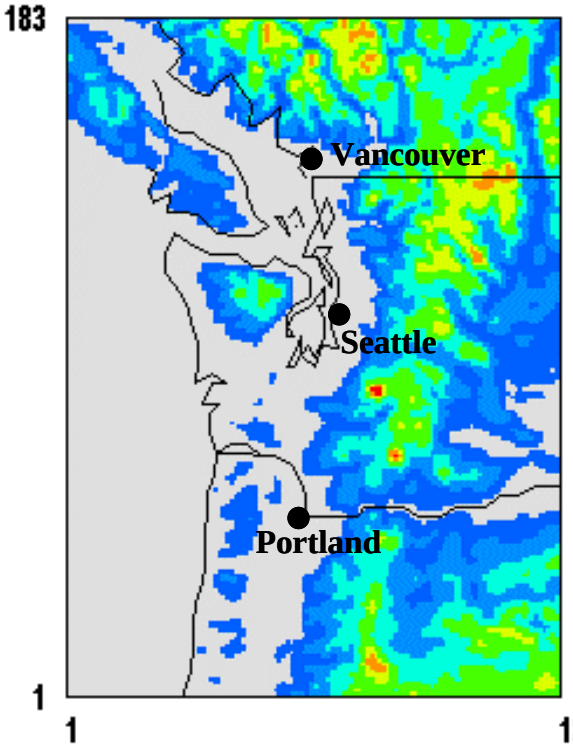

MM5 Level	MM5	CMAQ	CMAQ Level
1	1	1	1
2	0.995	0.995	2
3	0.99	0.99	3
4	0.985	0.985	4
5	0.98	0.98	5
6	0.97	0.97	6
7	0.96	0.96	7
8	0.95		
9	0.94	0.94	8
10	0.93		
11	0.92	0.92	9
12	0.91		
13	0.9	0.9	10
14	0.88	0.88	11
15	0.86	0.86	12
16	0.83	0.83	13
17	0.8	0.8	14
18	0.77		
19	0.74	0.74	15
20	0.71		
21	0.68	0.68	16
22	0.64		
23	0.6	0.6	17
24	0.56		
25	0.52	0.52	18
26	0.48		
27	0.44	0.44	19
28	0.4		
29	0.36	0.36	20
30	0.32		
31	0.28	0.28	21
32	0.24		
33	0.2	0.2	22
34	0.16		
35	0.12		
36	0.08		
37	0.04		
38	0	0	23

Figure 3.5 CMAQ 4 km domain for PNW2001 and vertical sigma levels in MM5 and CMAQ.

(a)

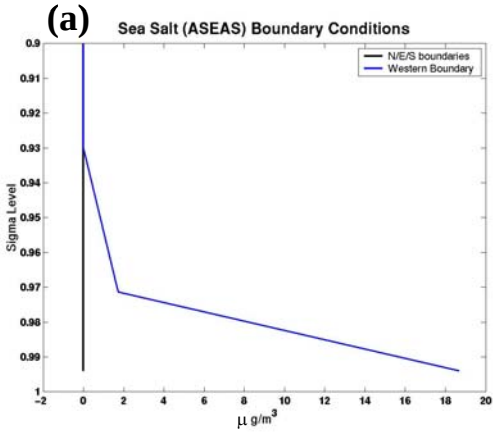

(b)

Aerosol Species	Boundary Conc.	
ASO4J	0.648	μg / m^3
ASO4I	0.292	
ANH4J	0.114	
ANH4I	0.018	
ANO3J	0.063	
AECJ	0.05	
AH2OJ	0.51	
NUMATKN	3.50E+08	# / m^3
NUMACC	8.60E+07	
NUMCOR	5.60E+06	

Figure 3.6 (a) Vertical profile of sea salt boundary conditions. (b) Table of aerosol boundary conditions except sea salt for PNW2001.

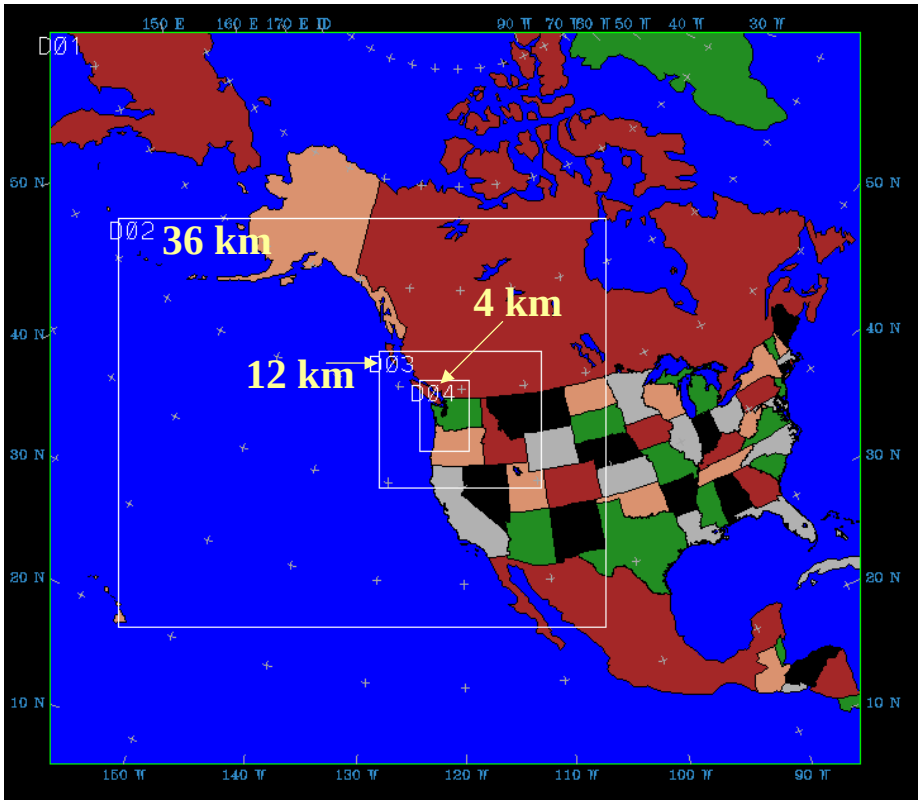

Figure 3.7 MM5 36, 12, and 4 km domains for PNW2001 / Pacific 2001 air quality study.

Table 3.4 Ranking of 12 km domain against meteorological observations for when analysis nudging is used on both 36 and 12 km domains (Nudge 36/12), when analysis nudging is only used on the 36 km domain (Nudge 36), and when no analysis nudging is used (No Nudge).

Parameter	Nudge 36/12	Nudge 36	No Nudge
Surface Obs	1	3	2
Clouds	3	2	1
3-D Winds	1	3	2
PBL Structure	1	3	2
PBL Heights	2	2	2

1 = Best 2 = Second 3 = Worst

Table 3.5 Ranking of 12 km domain against meteorological observations for when PX/ACM and for when Slab/MRF are used to represent the boundary layer.

Parameter	Nudge/PX/ACM	Nudge/Slab/MRF
Surface Obs	2	1
Clouds	1	2
3-D Winds	no major difference	no major difference
PBL Structure	2	1
PBL Heights	2	1

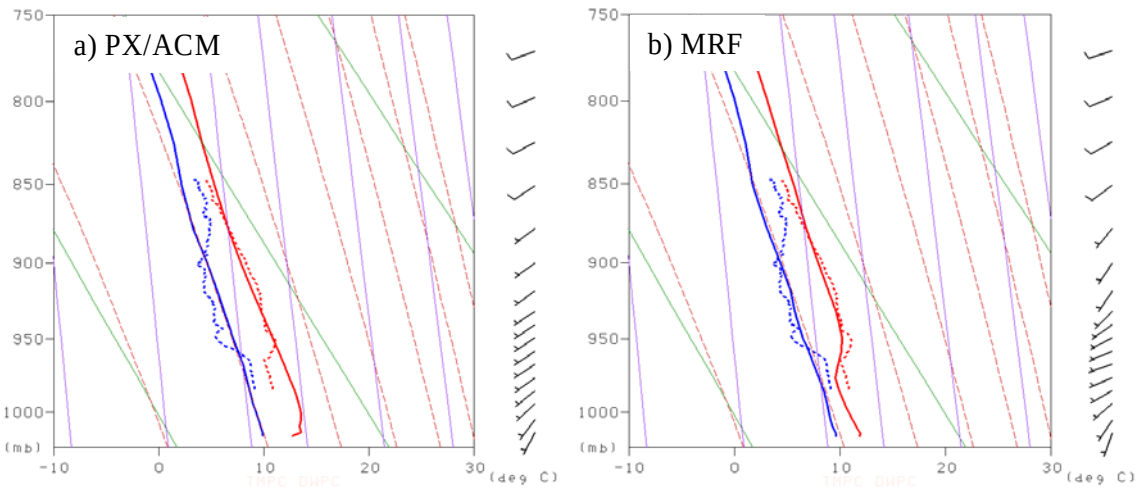

Figure 3.8 Profiles of temperature (red) and dew point (blue) at 1800 UTC 20 August 2001 over Puget Sound, 25 km south of Friday Harbor, WA. The observed profile appears as dotted lines while the solid lines are modeled by 12 km MM5 using the indicated parameterizations.

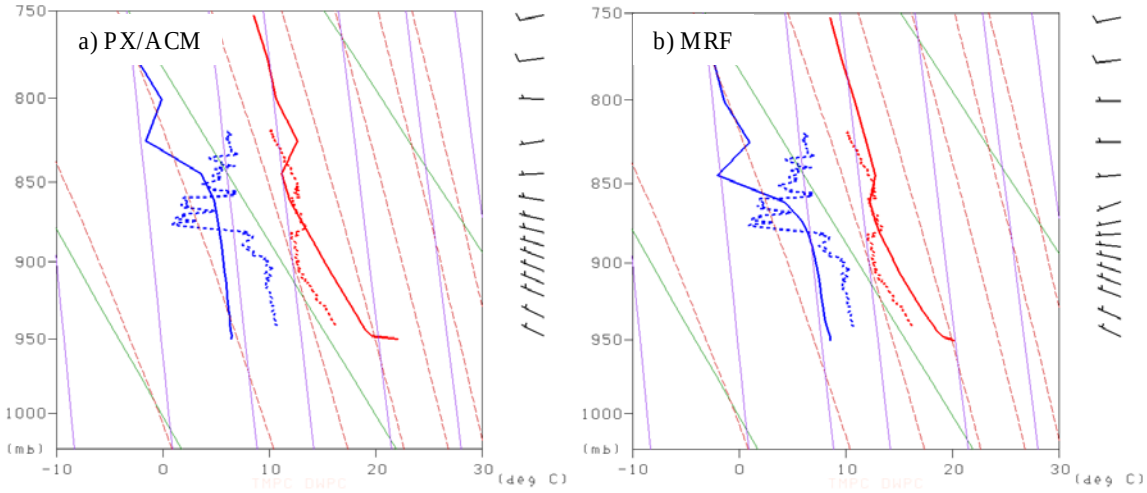

Figure 3.9 Profiles of temperature (red) and dew point (blue) at 2300 UTC 27 August 2001 over Mud Mountain Dam, 50 km east of Tacoma, WA. The observed profile appears as dotted lines while the solid lines are modeled by 12 km MM5 using the indicated boundary layer parameterization.

Table 3.6 Verification statistics for 4 km MM5 when run with observation nudging (Obs Nudge), with no observation nudging (No Nudge), and from the UW real-time forecast system (Real-Time).

Wind Speed for Withheld Stations

Parameter	Case	081912	082512
Bias (m/s)	Obs Nudge	-0.28	-0.26
	No Nudge	-0.28	-0.23
	Real-Time	0.18	0.05
Gross Error (m/s)	Obs Nudge	1.44	1.19
	No Nudge	1.48	1.25
	Real-Time	1.55	1.29

Wind Direction for Withheld Stations

Parameter	Case	081912	082512
Bias (°)	Obs Nudge	9.0	0.7
	No Nudge	7.3	1.1
	Real-Time	2.4	1.7
Gross Error (°)	Obs Nudge	44.0	53.0
	No Nudge	46.4	54.2
	Real-Time	48.1	54.7

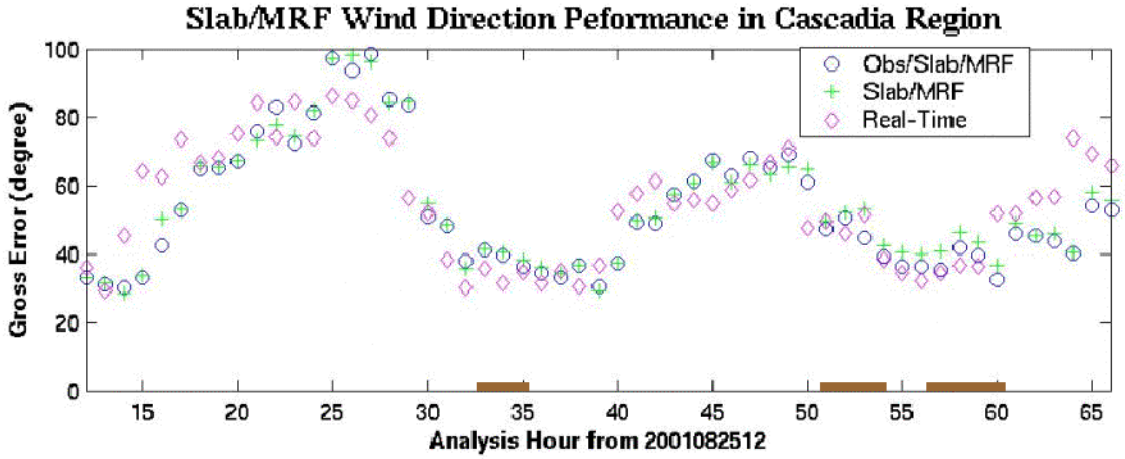

Figure 3.10 Gross error in degrees of surface wind direction for three 4 km MM5 configurations: (1) Five-Layer Soil Model and the MRF boundary layer scheme with observation nudging (Obs/Slab/MRF), (2) Five-Layer Soil Model and the MRF boundary layer scheme without observation nudging (Slab/MRF), and (3) University of Washington operational forecast. Lines along the x-axis denote hours when the Gulfstream obtained airborne measurements on the afternoon of 26 August and on the morning and afternoon of 27 August.

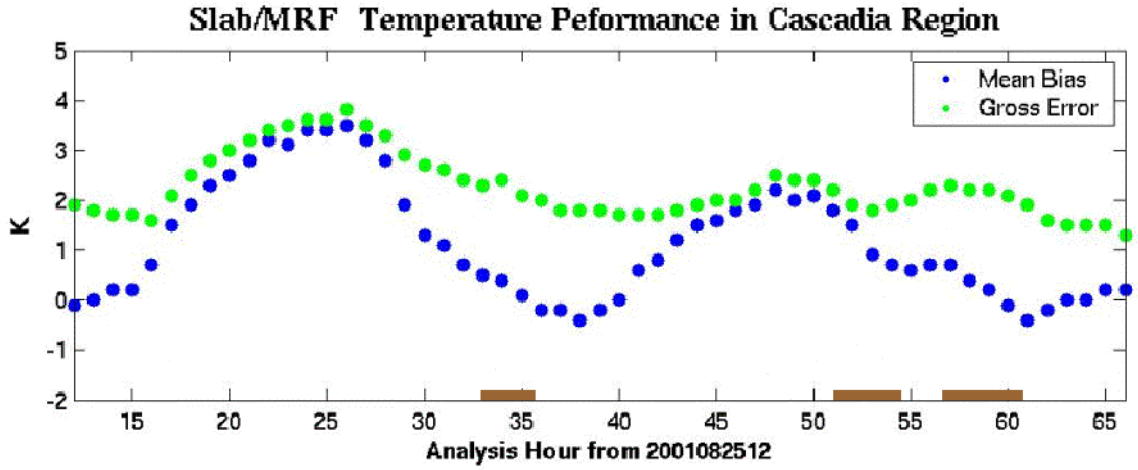

Figure 3.11 Mean bias and gross error in surface temperature for the Slab/MRF 4 km MM5 simulation. The Cascadia region is west of the Cascades between Portland and Vancouver. Lines along the x-axis denote hours when the Gulfstream obtained airborne measurements on the afternoon of 26 August and on the morning and afternoon of 27 August.

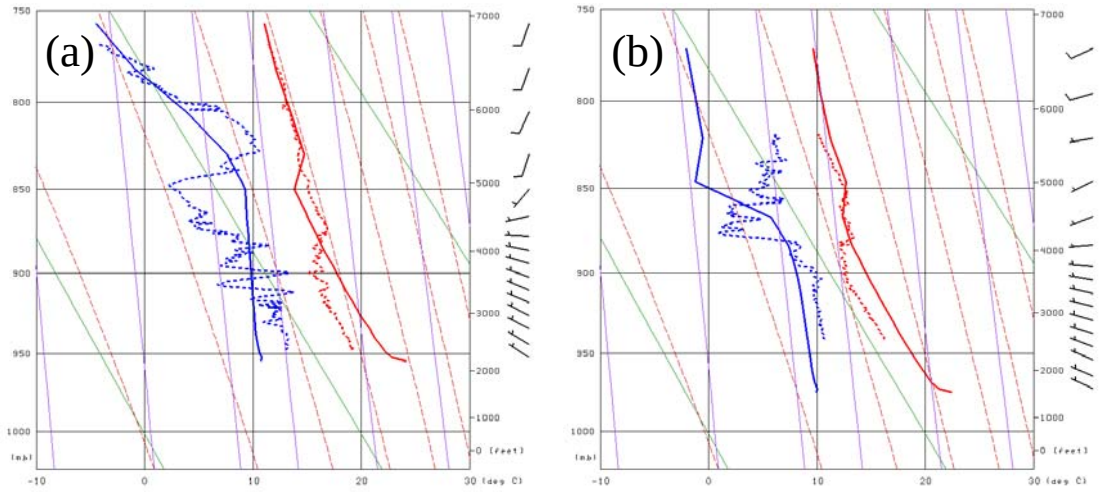

Figure 3.12 Profiles of temperature (red) and dew point (blue) at (a) 2300 UTC 26 August UTC and at (b) 2300 UTC 27 August 2001 over Mud Mountain Dam, 50 km east of Tacoma, WA. The observed profile appears as dotted lines while the solid lines are modeled by MM5 at 4 km resolution using the Five-Layer Soil Model and the MRF boundary layer scheme.

4. Base Case Evaluation

4.1. Comparison of CMAQ to PNW2001 Observations

Results from the CMAQ simulation were compared to gaseous and aerosol observations from PNW2001, Pacific 2001, and routine ground stations. Flight software interpolated the CMAQ output in three spatial dimensions and in time to obtain model concentrations at the time and GPS location of the Gulfstream aircraft. The result is a time-series of CMAQ concentrations valid for each flight track. Performance in different environments was evaluated as the aircraft flew through urban, suburban, rural, and marine air masses. Model performance was assessed as either the difference or quotient between model and observed values. The total number of particles measured by the UCPC primarily tests Aitken mode performance. Since the UCPC can only measure particles with diameters greater than 7 nm (based on a 50% detection limit), the number of modeled CMAQ particles must use this size as a lower cut point:

$$Number_{>7nm} = \frac{N_i}{2}\left[1 + erf\left(\frac{\ln\left(\frac{0.007}{D_{gi}}\right)}{\sqrt{2}\ln\sigma_{gi}}\right)\right] + \frac{N_j}{2}\left[1 + erf\left(\frac{\ln\left(\frac{0.007}{D_{gj}}\right)}{\sqrt{2}\ln\sigma_{gj}}\right)\right] \qquad (4.1)$$

where D_g is in μm and the subscripts i and j denote the Aitken and accumulation modes, respectively. As it measures particles with optical diameters above 110 nm, PCASP excludes many Aitken mode particles and includes a large fraction of the accumulation mode. The total number of particles above 110 nm in CMAQ is called “number of PCASP particles” for this study and is given by equation 4.1 when 0.110 μm is substituted for 0.007 μm. The number of coarse mode particles was ignored since it is

much less than the number in the other two modes. Thus PCASP explores accumulation mode performance with less contamination from the Aitken mode. For clean air, an analysis of CMAQ output showed that up to 50% of the number of modeled PCASP particles can be from the Aitken mode, but it is usually less than 30% of the total in polluted conditions.

The most important result is the underprediction of total number of observable (> 7nm) particles. For all three flights, CMAQ underpredicts number concentrations in urban areas generally by a factor of 10 to 100 (Figures 4.1-4.3). Overprediction is mainly restricted to boundary layer spirals when the aircraft had gone above the actual boundary layer but was still within the modeled boundary layer. Overpredictions in the boundary layer also occur for short periods when the aircraft flew through a sharp clean/polluted air gradient that is blurred by CMAQ's 4 km grid. Examples are at 21.8 UTC 26 August and 23.25 UTC 27 August in Figures 4.1 and 4.3. In background boundary layer conditions west of the Cascades, such as near 17 UTC 27 August (Figure 4.2), the total number concentration is well predicted. This indicates that the boundary condition number concentration is appropriate. Within polluted regions, the underprediction in aerosol number is independent of location in the Puget Sound and independent of aerosol composition (Figure 4.4).

The number of PCASP particles is also generally underpredicted but not to the same extent as the total observable number. Underpredictions are generally a factor of 5-10 for PCASP number concentrations in urban areas. The underprediction persists even when third moment concentrations are compared instead of number concentrations. Overpredictions occur when the airplane was above the actual boundary layer but still in the model boundary layer, and they occur in complex Cascade airflow unresolved by this model grid scale. For as much as the number of PCASP particles varies in the flight path, it is remarkable that the error is so stable in the Puget Sound region. The error is not highly correlated to any particular chemistry (e.g., organic fraction or particle acidity) in

the biogenic-rich forests, ammonia-rich agricultural regions, or automobile-dominated Seattle area (Figure 4.4).

The underprediction occurs even when sulfur dioxide plumes are modeled well. Sulfur dioxide is particularly important in CMAQ since it is the main contributor to particle nucleation and one of the prime contributors to particle growth by condensation. There are certainly cases where plumes are not captured in CMAQ. At 22.75 UTC on 27 August, CMAQ misses a 23-ppbv spike in SO_2 and the corresponding number concentration of 70,000 per cm^3 (Figures 4.5 and 4.3). CMAQ instead models a broad, more dilute plume. However, there are other cases when SO_2 spikes are captured by CMAQ. In the Centralia power plant plumes on the morning of 27 August, CMAQ properly models the spikes in SO_2 and the increase in sulfate aerosol mass (Figure 4.6) at 16.7 and 17.2 UTC, but it underpredicts the number of particles in the aged plume (Figure 4.2). On average for all three flights, SO_2 is underpredicted by more than one ppbv. However, the correlation between errors in SO_2 and errors in total number concentration is 0.34, 0.18, and 0.52 for the three flights, and the correlation between errors in SO_2 and errors in PCASP particles is 0.66, 0.06, and –0.23. Thus errors in SO_2 only explain part of the underprediction in number concentrations.

It is possible that errors in gas-phase precursors and in the oxidizing capacity of CMAQ's urban airmass could propagate to errors in aerosol. Too little hydroxyl could retard sulfuric acid formation and thus new particle production, while the formation of condensable species relies on reactions with ozone, hydroxyl, and nitrate. Some of the errors in gaseous constituents are large and certainly affect the size distribution and mass of aerosol. However, errors in gas-phase constituents vary from flight to flight and often within each flight, and there is no consistent picture from the various comparisons. For example, ozone is overpredicted by up to 60 ppbv on the afternoon of 26 August in the urban-influenced areas east and north of Seattle (Figure 4.7), while it is underpredicted on the 27 August by on average 20 ppbv in the morning and between 0 and 30 ppbv in the afternoon. CMAQ has little bias in NO and NO_y in the background Puget Sound airmass

(Figure 4.8), but it overpredicts both NO and NO_y by up to 40 ppbv near Seattle. Formaldehyde measurements are biased high by 1-3 ppbv on the afternoon of 26 August and low by 0-1 ppbv on the morning of 27 August. Methanol is underpredicted by a factor of 100 on the two flights when it was measured, and acetone was underpredicted by a factor of 1-10 on the afternoon of 26 August when it was measured. The precision of the measurements for formaldehyde, methanol, and acetone is uncertain. From the gas-phase species observed, it cannot be concluded that errors in precursors or the overall chemical environment is responsible for the consistent underprediction of aerosol number.

4.2. Comparison of CMAQ to Pacific 2001 Observations

CMAQ concentrations can be determined at each ground station by using the flight software to interpolate the CMAQ output to the station location or to choose the nearest grid cell. The model values for the lowest layer of CMAQ (~30 meters) are assumed to be valid for the surface. The software also computes a spatial minimum and maximum for each modeled species from the nearest cell and all its neighbors in the lowest and second-to-lowest layers (18 cells in all). This provides a sense of how spatially variable the CMAQ estimate is. A high standard deviation can signal low confidence in the comparison due to slight errors in plume location.

Various statistical techniques can be used to assess CMAQ's accuracy (Table 4.1). Each species has multiple measurements for model comparison and can include hourly observations at one site, one observation at multiple sites, or hourly observations at multiple sites. Each statistic can represent performance as a mean for all stations at all times, a time series averaged for all stations, or a time series for one station. Normalized bias and absolute error aid comparison to other studies, but the normalization method must applied carefully. Normalization before taking the mean emphasizes the error during low observed concentrations. Normalization after the mean eliminates this problem but still de-emphasizes underpredictions because their biases between -100%

and 0 are averaged with overpredictions spread between 0 and +∞. The normalized mean bias and error factors treat underpredictions and overpredictions symmetrically and do not emphasize performace at low observed values. The root mean square error, index of agreement, and correlation coefficient are additional error metrics used. Species with too few observations for statistical power are analyzed qualitatively.

Size distribution measurements from the Pacific 2001 field campaign corroborate the number underprediction observed from the PNW2001 dataset. Aerosol size distributions as measured by the Differential Mobility Analyzer (DMA) are available for the semi-rural Langley and rural Sumas sites (Li, 2004; Mozurkewich et al., 2004). At the Langely site, the number underprediction varies from a factor of eight to a factor of 80 (Figure 4.9; for observations, error bars are the hourly standard deviation, while for CMAQ they are the spatial minimum and maximum from the nearest cell and all its neighbors in the lowest and second-to-lowest layers). Although there is a large gap in the data from 11 PM PST 25 August until 12 PM PST 27 August, the number underprediction appears at all hours of the day. Particle nucleation and secondary condensation could produce errors in particle number, but then the errors would be expected to decrease at night because these processes require daylight and oxidation products. One night of observations is not enough to draw a conclusion, but it does at least suggest that processes independent of daylight, such as primary emissions or coagulation, are the likely cause of the number underpredictions. The worst underprediction comes immediately following the resumption of valid observations at 12 PM PST 27 August. Winds were from the southwest, and trajectories point towards sulfate sources near Bellingham as the culprit (Brook et al., 2004). As revealed in a comparison of particle count, $PM_{2.5}$, and SO_2 (see Figures 4.9, 4.12a, and 4.14a respectively), CMAQ predicts this SO_2-rich plume to reach Langley but does so slowly over a period of several hours rather than the burst shown in the observations. The error in timing and duration likely explains why CMAQ number underpredictions were greater near 12 PM but were smaller a few hours later when CMAQ predicted the arrival of the plume which in reality had already passed the Langley site.

The number underprediction at Langley is worse for smaller particles. Figure 4.10 shows that the underprediction in the nucleation mode (9-20 nm) is generally greater than in the Aitken mode (20-90 nm), which in turn is greater than in the accumulation mode (90-600 nm). The only exception is between 4 PM PST 27 August and 2 AM PST 28 August during the Bellingham plume advection. CMAQ captures the smaller size distribution of this fresh plume but the timing error results in a large underprediciton in nucleation mode number between 12 PM and 4 PM and then a nucleation mode underprediction similar to the other modes between 4 PM and 2 AM. The AMS mass size distribution data (Boudries et al., 2004; Alfarra et al., 2004) also reveal an underprediction at smaller sizes. In Figure 4.11 the mass underprediction is greater by nearly an order of magnitude for the <0.1 μm particles as compared to the 0.1-1 μm particles. Since the underprediction is similar for nitrate, organics, and sulfate, no single aerosol species is obviously responsible for the total number underprediction. All of the size-resolved measurements at Langley indicate that CMAQ's size distributions are shifted to larger sizes than observed for all species.

$PM_{2.5}$ mass performance is not well-correlated to the particle number underprediction. CMAQ surface $PM_{2.5}$ is compared to measurements from both the TEOM (Brook et al., 2004) and traditional gravimetric filters in Figure 4.12. For the first 17 hours of simulation (4 PM PST 25 August to 9 AM PST 26 August), CMAQ overpredicts $PM_{2.5}$ by up to 5 $\mu g/m^3$. Nitrate, organics, and sulfate are all overpredicted during this period, but the large overprediction of nitrate explains CMAQ's $PM_{2.5}$ performance. An over-abundance of fine particulate nitrate is common for CMAQ v4.4 when simulating humid, shallow boundary layers (Bhave et al., 2006). While the observations show a spike in nitrate near hours 4-7 AM PST 26 August due to the advection of pollution from eastern Whatcom County (Brook et al., 2004; Boudries et al., 2004), nitrate in CMAQ increases starting the evening before when the boundary layer collapses and continues increasing constantly throughout the night. This behavior is more indicative of excessive conversion of nitric acid to particulate nitrate than it is of advection. In addition, ammonia (not

shown) is overpredicted for the entire simulation and, through particle neutralization, may promote excess uptake of nitric acid if ammonium nitrate formation is ammonia-limited (Smyth et al., 2006). A similar overprediction of nitrate occurs on the morning of 28 August. On the afternoon of 26 August and morning of 27 August, a sea breeze and land breeze cycle (Snyder and Strawbridge, 2004) produced spikes of more organic and sulfate rich aerosol not captured by CMAQ. The sulfate and SO_2 laden plume near 6 PM 27 August was modeled in CMAQ as a weaker plume arriving a few hours later and persisting longer. While the number underprediction is tied to errors in aerosol mass for this sulfate plume, it persists at other times when the mass is well-modeled and when the mass is overpredicted.

Comparisons at the Sumas Mountain site are complicated by complex terrain. The 4-km resolution in this application of CMAQ is not adequate to resolve the small, steep mountain poking out of the Fraser Valley. Rather, the modeled terrain depicts the mountain as a gradual slope and as part of the Coast Range just north of the Fraser River. While the site is actually on a steep slope 300 meters above sea level, the location in CMAQ is on a graduate slope 70 meters above sea level. As a result, the instruments are often above the nocturnal boundary layer (Strawbridge and Snyder, 2004b; Hayden et al., 2004; Mozurkewich et al., 2004) while CMAQ models them within the nocturnal boundary layer. In reality, nighttime emissions are trapped near the surface, and the observing station records residual pollution from the previous day in which smaller particles have been removed through condensation and coagulation. Fresh emissions do not reach the observing station until 9-10 AM PST the following morning. In CMAQ, emissions continue to reach the site all night long, replenishing the small particles and more reactive gases. One alternative that was attempted in this study was to extract the CMAQ output at 300 m elevation, but then this introduced other complicated errors related to being outside of daytime surface flow effects and related to the timing of boundary layer growth.

At Sumas, particle number is underpredicted by at least a factor of 10 when both the model and observations are within the boundary layer during the afternoon (Figure 4.13a). After the boundary layer collapses and cuts off the observation site from fresh emissions, performance trends towards no bias as CMAQ continues to advect fresh emissions to the location. This is confirmed by examining the number of particles in different size ranges from the DMA (Figure 4.13b). Performance in the nucleation mode is similar to the other modes during the overnight period when CMAQ is erroneously replenishing fresh, smaller particles. In the mixed afternoon boundary layer, the underprediction is greater for smaller sizes as it was at the Langley site on the valley floor. At night, the overprediction in $PM_{2.5}$ at Sumas is 10-30 $\mu g/m^3$ (300-900%), mostly due to an overprediction of nitrate and organics. The only way CMAQ produces enough particles at Sumas is through an error stemming from inadequate topographical resolution.

Discrete size distributions are not available for the urban Slocan site (Li et al., 2004). Twice-daily, 10-hour averages from MOUDI impactors (Anlauf et al., 2006) show an underprediction for elemental carbon, organic carbon, and total mass below 100 nm, but they also show good performance below 100 nm and between 100 nm and 1 μm for ammonium and sulfate. Regardless, the coarse time resolution, small number of measurements in each mode, and large amount of missing data limit confidence in an analysis of available data from the Slocan site.

Precursors to particle nucleation are not an issue for CMAQ in the Lower Fraser Valley. CMAQ could underpredict particle number by producing too little SO_2 or hydroxyl radical to initiate nucleation. Instead, CMAQ generally overpredicts SO_2 and rarely underpredicts it by a significant amount at the valley sites of Slocan and Langley (Figure 4.14). The exception is at the Langley site on the afternoon of 27 August when the sulfur-rich plume from Whatcom County has not yet reached Langley in the model. Sulfur dioxide is underpredicted at Sumas, but it is unclear how topographical errors influence this result. The hydroxyl radical was not measured, but ozone, formaldehyde,

and nitric acid can indirectly indicate the degree of chemical processing. Ozone is overpredicted by up to 30 ppb on the afternoon of the 26 August and underpredicted by 10 ppb on the afternoon of the 27 August (Figure 4.15). The modeled ozone values on 27 August are below 20 ppb, the amount advected in at the western boundary of the domain, which means there is net daytime destruction of ozone in the model that day. When measurements are available, formaldehyde, nitric acid, and PAN are generally overpredicted on the afternoon of 26 August and well-modeled on 27 August. Since the same pattern was exhibited at Slocan Park and Sumas and in the PNW2001 aircraft data in the Puget Sound region, these errors are not due to errors in plume location. CMAQ does not produce an apparent error in SO_2 or photochemistry that can explain the consistent number underprediction.

It would be helpful to understand the major overprediction of ozone on 26 August and underprediction on 27 August in order to assess how this behavior affects $PM_{2.5}$ and aerosol size distribution performance. Nitrogen oxides were often overpredicted in the Fraser Valley as they were in the urban-influenced areas of the Puget Sound, but the overprediction does not vary from 26 to 27 August (Figure 4.16a). The measured organic precursors to ozone (isoprene, ethane, and aromatics) are consistently overpredicted (Figure 4.16b-d). MM5 input to CMAQ overestimated surface temperature by 3 °C and 2 °C on the early mornings of 26 and 27 August, but there was a 1°C positive bias at noon on both days and no temperature bias by the middle of the afternoon. No pattern in precursor gases or temperature can explain the large variation in ozone performance on 26 and 27 August.

Oxidant and ozone production is highly dependent on actinic flux. It would be ideal to compare the actinic flux from CMAQ to that measured at various sites in the domain. Unfortunately, actinic flux in the model is an internal calculation. It is produced for clear sky radiance and then multiplied by a factor dependent on cloud fraction. The cloud fraction itself is not the one from MM5 but is instead rediagnosed within CMAQ from the MM5 humidity and temperature profiles. Therefore, the most direct comparison is

between the CMAQ cloud fraction and satellite imagery (Figure 4.17-4.19). Both show clear skies on 26 August, patchy stratus on the morning of 27 August, and approaching cirrus on the afternoon of 27 August. While there is general agreement, a qualitative view cannot determine if the cloud fraction in CMAQ accurately reflects the cirrus optical depth on 27 August. Surface solar irradiation from the University of Washington (UW) rooftop station (Figure 4.20) and from MM5 output can help gauge the accuracy of CMAQ's cloud fraction. Both observations and model produce a clean sine pattern indicative of sunny skies for 26 August. The MM5 trace is shifted by about 15 minutes, but the overall radiation for the day is positively biased by only 4%. On 27 August, thin cirrus throughout the day reduces the amplitude of the wave, and occasional thicker patches of cloud produce aberrations from a sine wave. Despite neglecting thicker patches of cloud, MM5 captures the impact of the cirrus on surface radiation and produces daily radiation only 3.8% higher than in the observations. Although it is difficult to conclude from these limited and indirect methods, the similar radiation biases on the two days indicate that errors in actinic flux do not explain CMAQ's ozone performance.

It is not known why photochemistry is greatly overpredicted on 26 August and underpredicted on 27 August, but at least meteorology and aerosol precursors are not likely causes. The Pacific 2001 dataset confirms the major results from the PNW2001 comparison, extends the evaluation beyond midday, and adds important information about aerosol size, aerosol composition, and gaseous concentrations. Aerosol number is underpredicted by at least an order of magnitude at all hours of day, is underpredicted more at smaller sizes, and is not obviously due to errors in chemical composition. Model errors in gaseous precursors and meteorology are unlikely to have produced the errors in CMAQ's size distributions.

4.3. Comparison of CMAQ to Washington Surface Observations

Analysis of $PM_{2.5}$ ground measurements show CMAQ aerosol performance over the entire 72-hour simulation. Figure 4.21 illustrates bias and error statistics for the 14 valid

surface stations in Washington. There is a strong positive bias in $PM_{2.5}$ in the first 18 hours of the simulation corresponding to 4 PM PST 25 August until 10 AM PST 26 August. The positive bias increases linearly for the overnight period at urban sites in the lowlands (Figure 4.22) and appears to be related to an increase in model aerosol nitrate (Figure 4.23). From 4 PM PST 26 August until the end of the simulation, CMAQ is biased negatively by 50 to 150%. During the Gulfstream flights (indicated by bars on the abscissa), the $PM_{2.5}$ Normalized Mean Bias Factor is 4%, -56%, and –74%, respectively. $PM_{2.5}$ has periods of overprediction and underprediction, and its performance is not consistent during the PNW2001 flights. There is no consistently large underprediction in $PM_{2.5}$ to explain the negative bias factor of 5-10 in PCASP particle concentration and 10-100 in total particle concentration. Nor is it possible to discredit the results based on poor $PM_{2.5}$ performance since the $PM_{2.5}$ results here are well in line with other CMAQ studies (Table 4.2).

Other hourly ground measurements extend PNW2001 results to the entire simulation period. The Gulfstream flights reveal an overprediction of ozone on 26 August and an underprediction on 27 August. Surface sites (Figure 4.24) show that the overprediction occurrs from 4 PM PST 25 August until 12 AM PST 27 August, and the underprediction lasts from 12 AM until 8 PM 27 August. Ozone overprediction in the early morning is a common feature in CMAQ. The relatively coarse vertical resolution makes it hard for the model to collapse the boundary layer on calm nights and produces a positive surface temperature bias. Without a stable surface layer, nighttime ozone titration does not fully develop. However, in Figure 4.24 the ozone bias by site exhibits no obvious diurnal pattern and demonstrates a relatively constant positive bias for the first 30 hours of simulation. Over all sites and times, the ozone normalized mean bias factor and normalized mean error factor are 28% and 62%. O'Neill and Lamb (2005), O'Neill et al. (2006), and Smyth et al. (2006) have similar biases and errors with CMAQ in the Pacific Northwest, even with longer modeling periods. NO, NO_2, and NO_x measurements at Beacon Hill are overpredicted at almost all hours, consistent with the airborne analysis showing a positive bias near Seattle. Carbon monoxide (not shown) is biased negatively

for the large majority of measurements. Sulfur dioxide at Beacon Hill is accurate to ±5 ppb with little overall bias. The surface measurements show that conditions during airborne flights continued throughout the day and that the surface and airborne measurements measure similar trends on 26 and 27 August.

The only speciated aerosol measurements for CMAQ analysis in Western Washington are 24-hour averages on 26 August from the IMPROVE and STN networks. These measurements merit a cautious interpretation. The actual composition changes throughout the day as wind patterns modify the pollution source and temperature and sunlight changes the amount of condensed species. In addition, most of the sites are located in rural areas away from the majority of anthropogenic sources. Nonetheless, CMAQ overpredicts concentrations as compared to measurements from both networks for aerosol nitrate, which reaches 3 $\mu g/m^3$ at Beacon Hill (Figures 4.25 and 4.26). If every mole of hydrogen accompanying the overpredicted nitrate at Beacon Hill went towards reducing sulfate and increasing ammonium, it would explain ¾ of the underpredicted sulfate (-0.4 $\mu g/m^3$) and overpredicted ammonium (0.93 $\mu g/m^3$). The sulfate underprediction and ammonium overprediction may explain a significant portion of the nitrate overprediction. CMAQ produces 0.8 $\mu g/m^3$ more elemental carbon than measured at Beacon Hill, but this is offset by a similar underprediction in organic carbon. At rural Washington sites, organic carbon is overpredicted by generally 100% (3 $\mu g/m^3$), while sulfate is overpredicted by less than 1 $\mu g/m^3$. Although the sample size is low, the aerosol chemical composition errors from this study are similar to those in the other published studies of CMAQ for the Pacific Northwest (O'Neill et al., 2006; Smyth et al., 2006) and in other CMAQ studies across North America (Table 4.3). Nothing from the comparison to chemical measurements demonstrates a pattern to explain the number concentration errors.

4.4. Discussion of CMAQ Comparisons to Observations

In this study, the errors in number concentrations cannot be easily explained by errors in overall particulate mass or in precursor gases. The correlation between SO_2 errors and number concentration errors suggests that some of the number concentration underprediction can be attributed to misrepresenting the location and intensity of sulfate available for nucleation. Yet errors in SO_2 plumes explain at most 50% of the variance in number concentration errors. Ground observations show that the hours of Gulfstream flights were not anomalous for the period. $PM_{2.5}$ measurements are biased low during the flights on 27 August, but they are not low enough on 27 August nor are they consistent enough across flight days to explain the larger, persistent underpredictions on all three flights. In addition, number concentrations are consistently underpredicted at the Pacific 2001 sites (excluding Sumas at night for issues of resolving the nocturnal boundary layer), and the negative bias cannot be attributed to errors in $PM_{2.5}$ or in chemical composition. Airborne gas-phase, ground gas-phase, and ground aerosol measurements do not produce errors consistent with the errors in number concentration.

The 0–4 K positive temperature bias throughout the period might negatively bias number concentrations. Nucleation of new particles is a strongly decreasing function of temperature in the range of 280-300 K (Napari et al., 2002a). A large warm bias, as well as the resulting decrease in relative humidity, would underestimate new particle production especially in the early morning when the temperature bias is high (Figure 3.11). While the temperature bias is high in the early morning and low in the afternoon, the number bias is similar for both morning and afternoon PNW2001 flights and does not show a diurnal pattern at Langley. The temperature bias may explain part of the number underprediction, but the consistency of the number underprediction points to something more inherent in the aerosol module itself rather than an error specific to this simulation.

Three other published studies have examined CMAQ's number concentrations and size distributions. Y. Zhang et al. (2006b) modeled 1-10 July 1999 at 8 km for the greater Atlanta area. They found number concentrations to be underpredicted by on average 24%

at the Jefferson Street station in the urban center of downtown Atlanta. Park et al. (2006) modeled the same location at 36 km but for 1/1/1999 to 8/31/2000. Number concentrations were underpredicted by on average a factor of 29 despite the dry mass being underpredicted by only 13% (factor of 0.13). The underprediction was worse for smaller sizes and peaks on the lower end of the Aitken mode (10-20 nm). Fan et al. (2006) model an 8-day episode in August 2004 for Houston, TX at 4 km. They also report that CMAQ v4.3 underpredicts total number concentrations by 0.5-1.5 orders of magnitude, and the underprediction becomes progressively worse at particle diameters less than 100 nm. In general, other simulations found similar CMAQ aerosol size distribution performance in different emissions and meteorlogical environments. They support the decision to investigate and improve CMAQ's fundamental aerosol science.

There are several assumptions within CMAQ and the aerosol module that could under-represent the number of particles. These include the treatment of aerosol humidification hysteresis, cloud processing, mode merging, aerosol lognormal modes, binary H_2SO_4-H_2O nucleation, and the size distribution of emitted aerosol.

The assumption of metastable aerosol particles could dissolve gases into the deliquescent particle and thus add mass that would normally remain in the gas phase. The larger particles would favor sulfate condensation over sulfate nucleation. In addition, the larger accumulation mode particles would more efficiently coalesce with Aitken mode particles and artificially reduce the overall number. If this occurs, $PM_{2.5}$ mass would be overpredicted at relative humidities below ~40% when the modeled metastable particle should have effluoresced. Although some accumulation mode mass persists in an airmass from one day to the next, the number concentration error would be greater in the afternoon. This is not the case for the flights examined here.

Cloud processing parameterizations could introduce number biases. CMAQ assumes all coarse and accumulation mode particles are activated in a cloud. While clouds typically activate 50-90% of the aerosol mass (Seinfeld and Pandis, 1998), measurements

of distinct condensation and droplet modes show that not all accumulation mode particles are activated. Activating too many particles could add extraneous mass in the accumulation mode through dissolution and aqueous phase reactions, suppress particle nucleation, and increase coagulation. Ignoring particle nucleation when clouds evaporate, or nucleation at the edge of a stable cloud, leaves out potential sources of particles. Any error in cloud processing of aerosols would be compounded by errors in MM5 cloud fields. All of the cloud-related issues would produce irregular number concentration errors in the patchy marine stratus on the early mornings of 26 and 27 August, but the observations show a fairly uniform error throughout the Puget Sound region. Cloud processing of aerosols in CMAQ needs attention but is unlikely to be the largest cause of the number underprediction for this case study.

The mode merging process in CMAQ is another potential source for errors in particle size. The conditions for mode merging (faster condensation rate for the Aitken mode than the accumulation mode and more particles in the Aitken mode) and the amounts of merging (for each moment, the amount of Aitken mode above the intersection of the Aitken and accumulation modes but capped at 50%) are reasonable but artificial. It is well-understood that particles grow over time and transition from the Aitken mode to the accumulation mode. But since CMAQ treats the modes generically and not each particle individually, it must have a numerical scheme to handle this transition within CMAQ's lognormal aerosol paradigm rather than develop the most realistic, physically-based parameterization possible. There is little way to know if the method in CMAQ does an adequate job of mimicking reality, and it likely does not accurately reflect the natural transition of particles from the Aitken to accumulation mode. It is not clear how this can be done most accurately or how improvements might change the modeled size distributions. Therefore mode merging is not a target for improvement in this study.

The aerosol processes that are most likely to play a role in the size distribution errors are particle nucleation, the treatment of freshly nucleated particles, and the size distribution of emitted particles. Chapter 5 addresses the issues of particle nucleation and

the nucleation mode and investigates how CMAQ's science and performance can both be improved. Chapter 6 investigates the emissions size distributions in CMAQ, their applicability to mesoscale modeling domains, and their scientific integrity. Based on this examination, alternative emissions size distributions are recommended and tested for PNW2001 and Pacific 2001. Chapter 7 combines the updates to nucleation and emissions. These processes are not the only ones with problems in CMAQ, but they are the most likely culprit for the size distribution errors in this case study, and they are the ones most in need of scientific updates. The modeling community should continue to address other sources of error such as cloud processing and mode merging to improve CMAQ aerosol performance and overall model science.

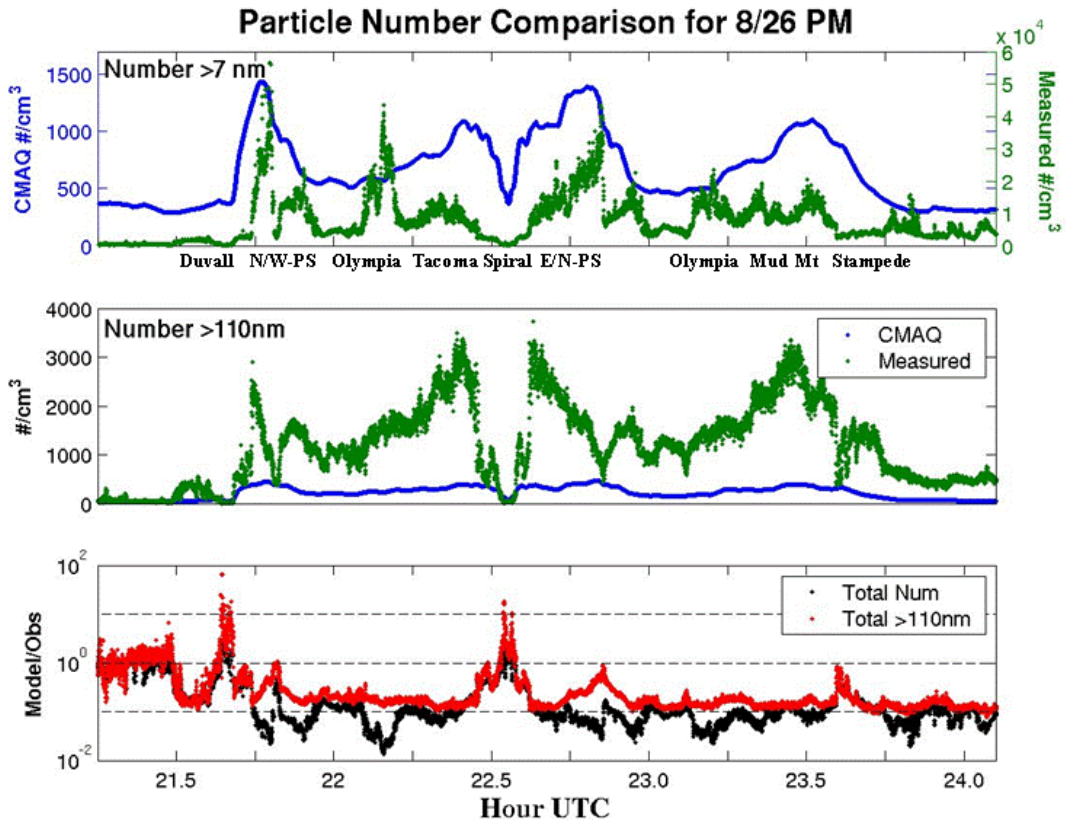

Figure 4.1 Number concentrations from PNW2001 observations and from CMAQ modeling results for the afternoon of 26 August. "N/W-PS", "N-PS", "S-PS", and "E/N-PS" indicate the north and west side of the Puget Sound, WA region, between Seattle and Everett, south of Olympia and Tacoma, and from Enumclaw to Lynwood, respectively.

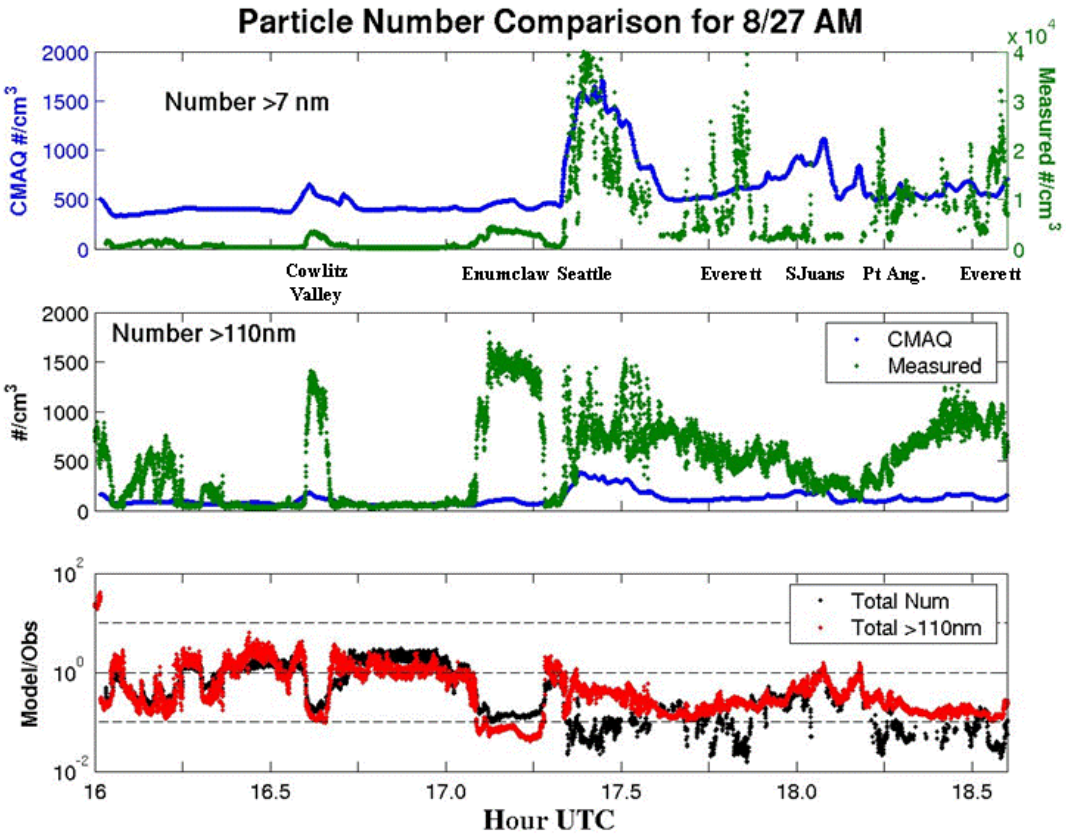

Figure 4.2 Number concentrations from PNW2001 observations and from CMAQ modeling results for the morning of 27 August. "N/W-PS", "N-PS", "S-PS", and "E/N-PS" indicate the north and west side of the Puget Sound, WA region, between Seattle and Everett, south of Olympia and Tacoma, and from Enumclaw to Lynwood, respectively.

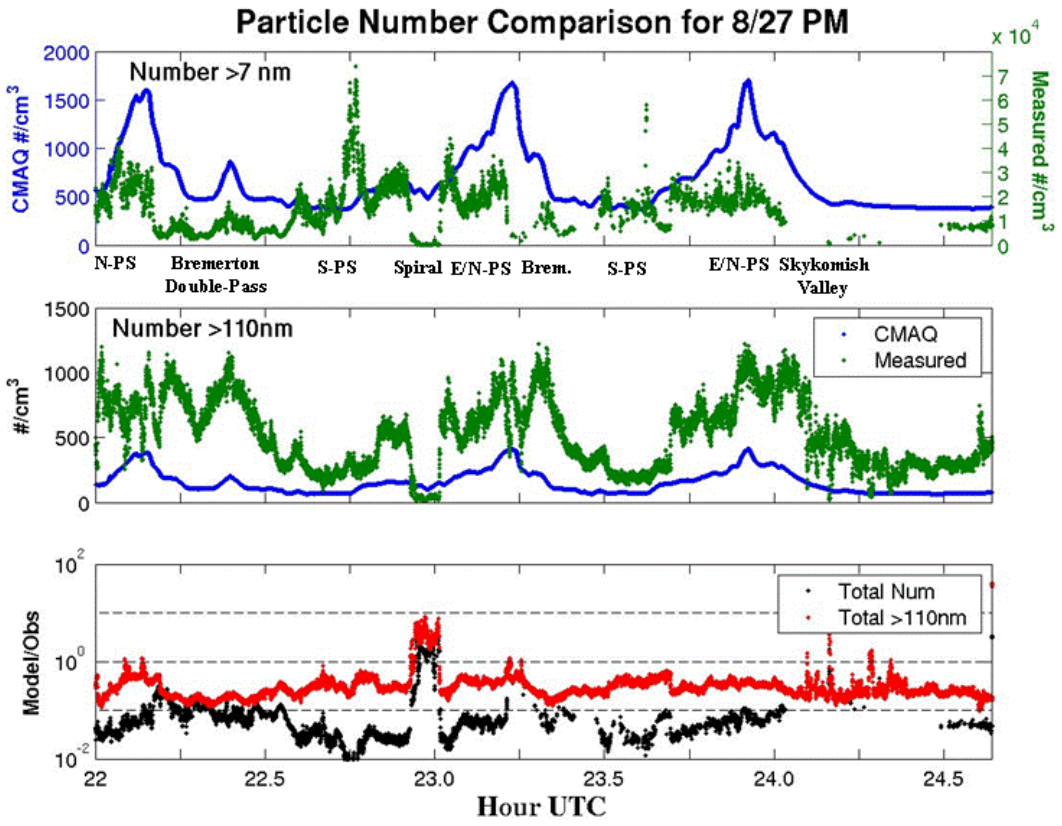

Figure 4.3 Number concentrations from PNW2001 observations and from CMAQ modeling results for the afternoon of 27 August. "N/W-PS", "N-PS", "S-PS", and "E/N-PS" indicate the north and west side of the Puget Sound, WA region, between Seattle and Everett, south of Olympia and Tacoma, and from Enumclaw to Lynwood, respectively.

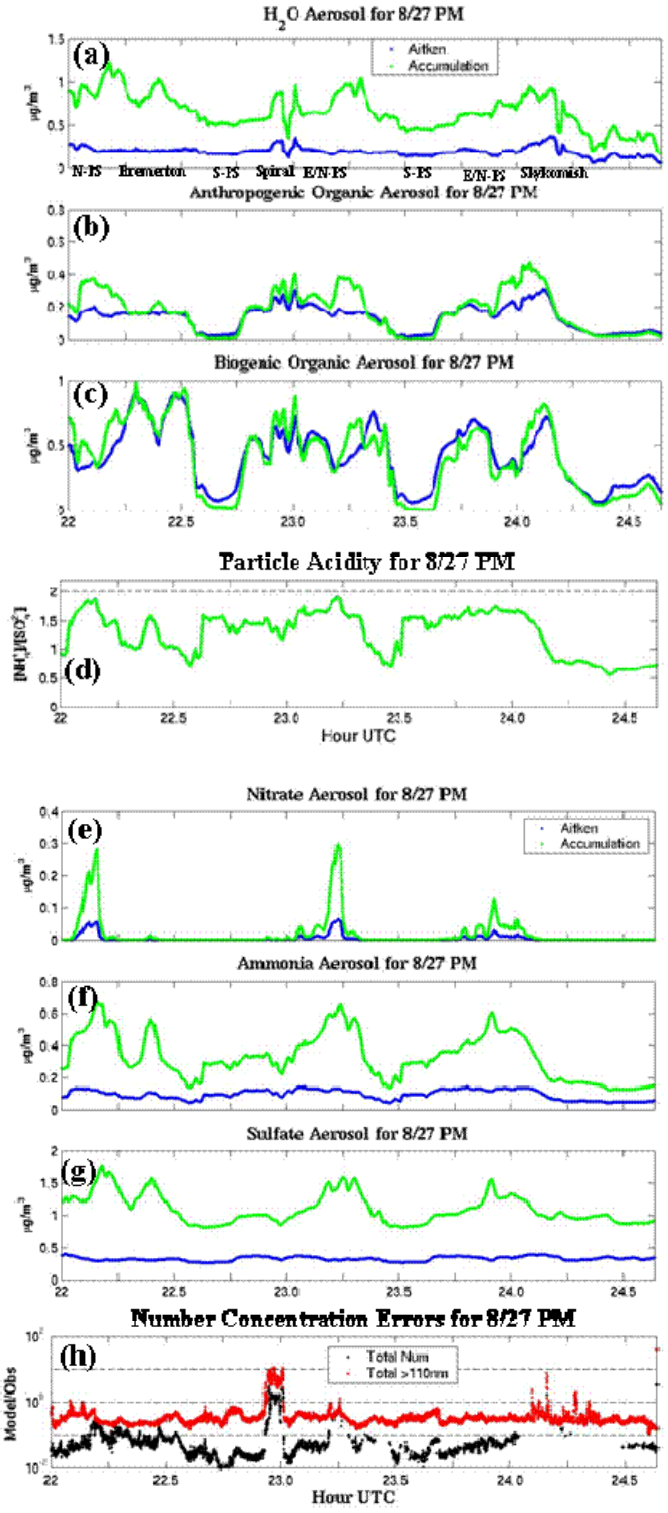

Figure 4.4 CMAQ aerosol concentration during the afternoon flight of 27 August for the components: (a) water, (b) anthropogenic organic, (c) biogenic organic, (e) nitrate, (f) ammonia, and (g) sulfate. Particle acidity is show in (d), and the number concentration error from Figure 4.3 is repeated as (h).

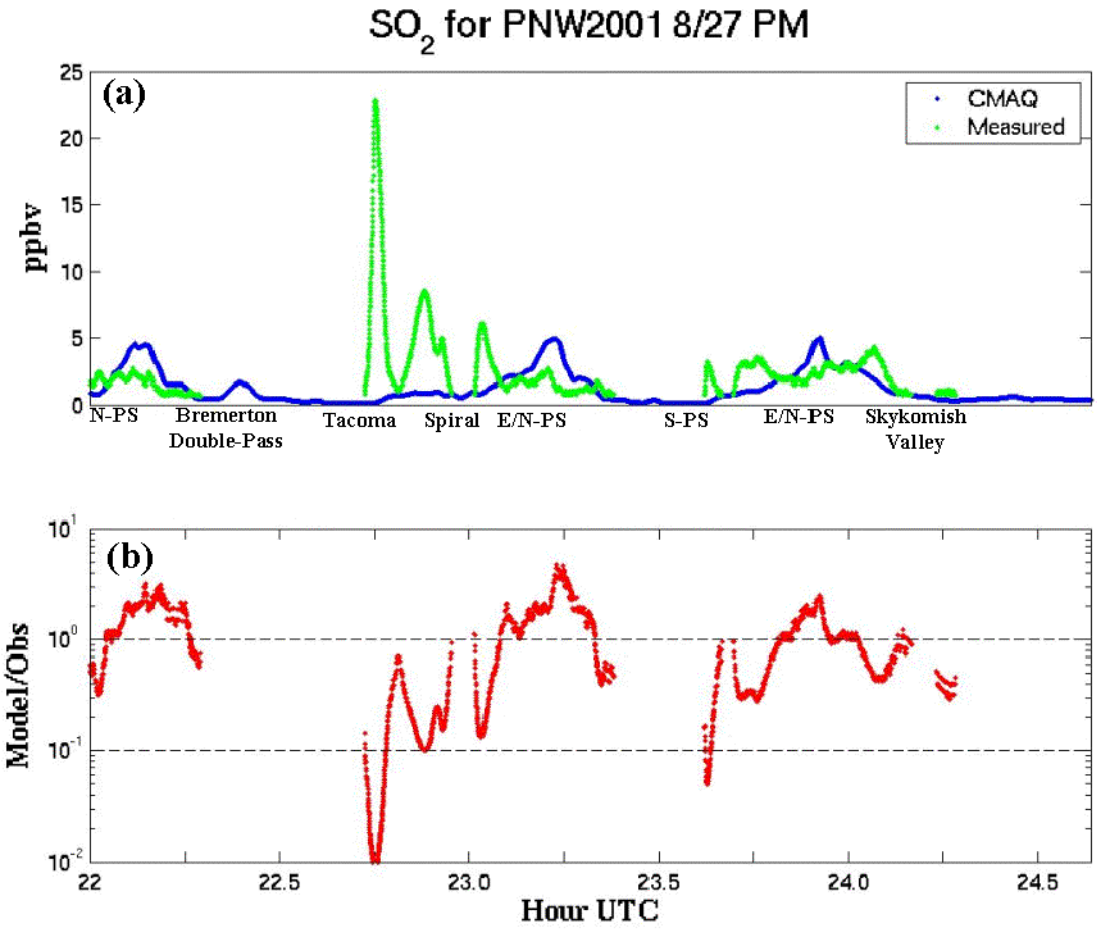

Figure 4.5 (a) PNW2001 sulfur dioxide mixing ratio from the Gulfstream aircraft on the afternoon of 27 August and from CMAQ for the aircraft flight track. (b) Quotient of the modeled and observed values.

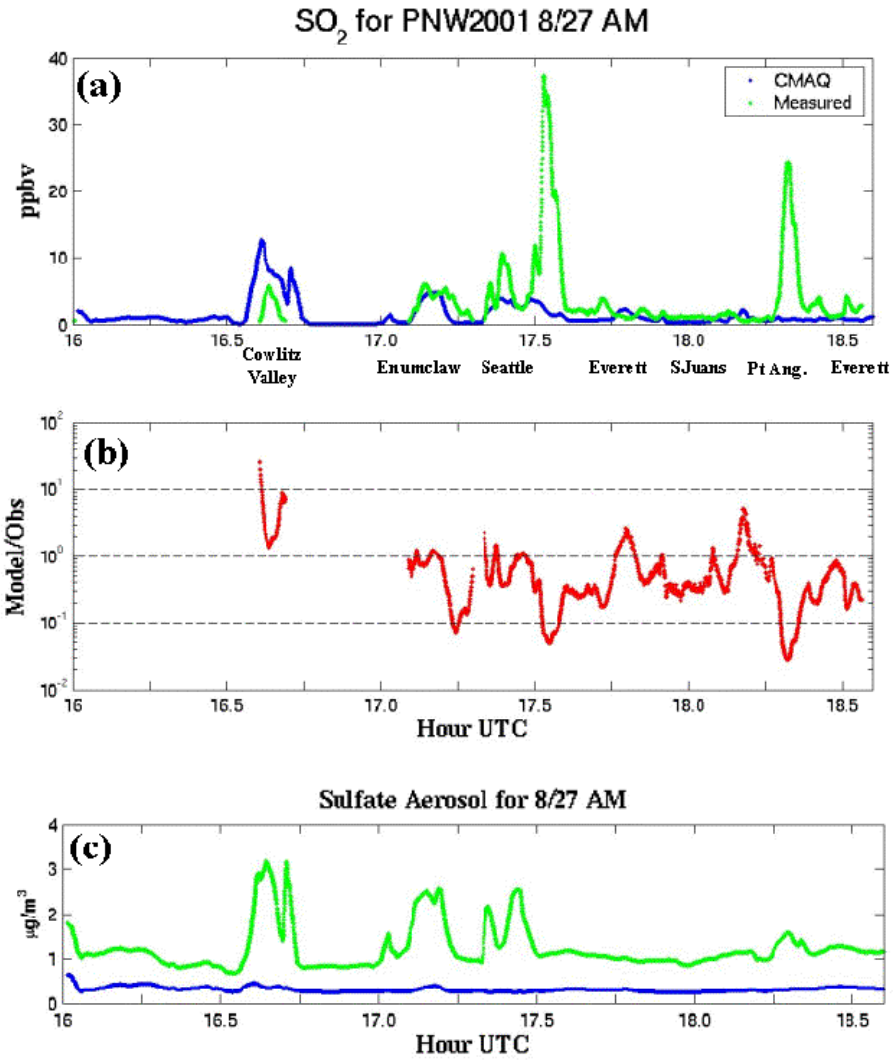

Figure 4.6 (a) PNW2001 sulfur dioxide mixing ratio from the Gulfstream aircraft on the morning of 27 August and from CMAQ for the airplane flight track. (b) Quotient of the modeled and observed values. (c) Sulfate aerosol concentration from CMAQ for the flight track in the Aitken mode (blue) and accumulation mode (green).

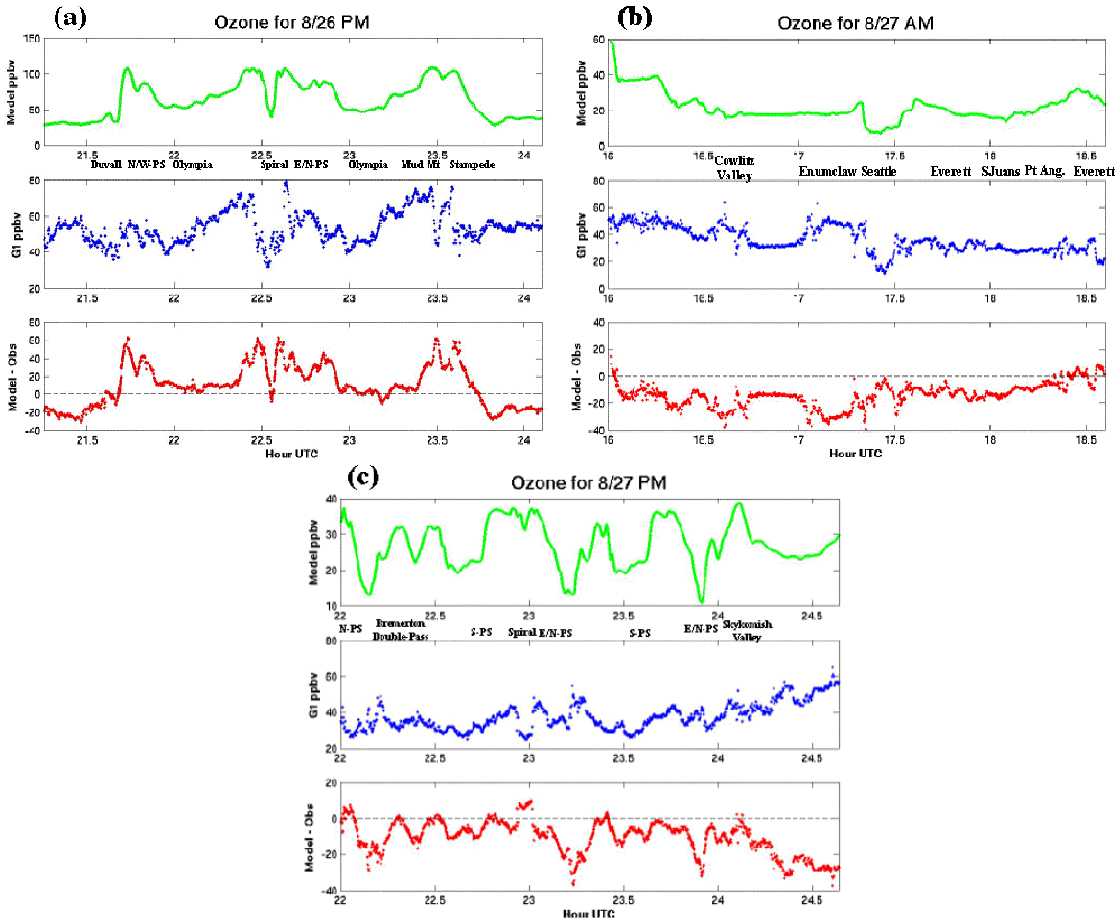

Figure 4.7 Ozone from the Gulfstream during PNW2001, ozone from the CMAQ model for the flight tracks, and the error in ozone for (a) the afternoon of 26 August, (b) the morning of 27 August, and (c) the afternoon of 27 August.

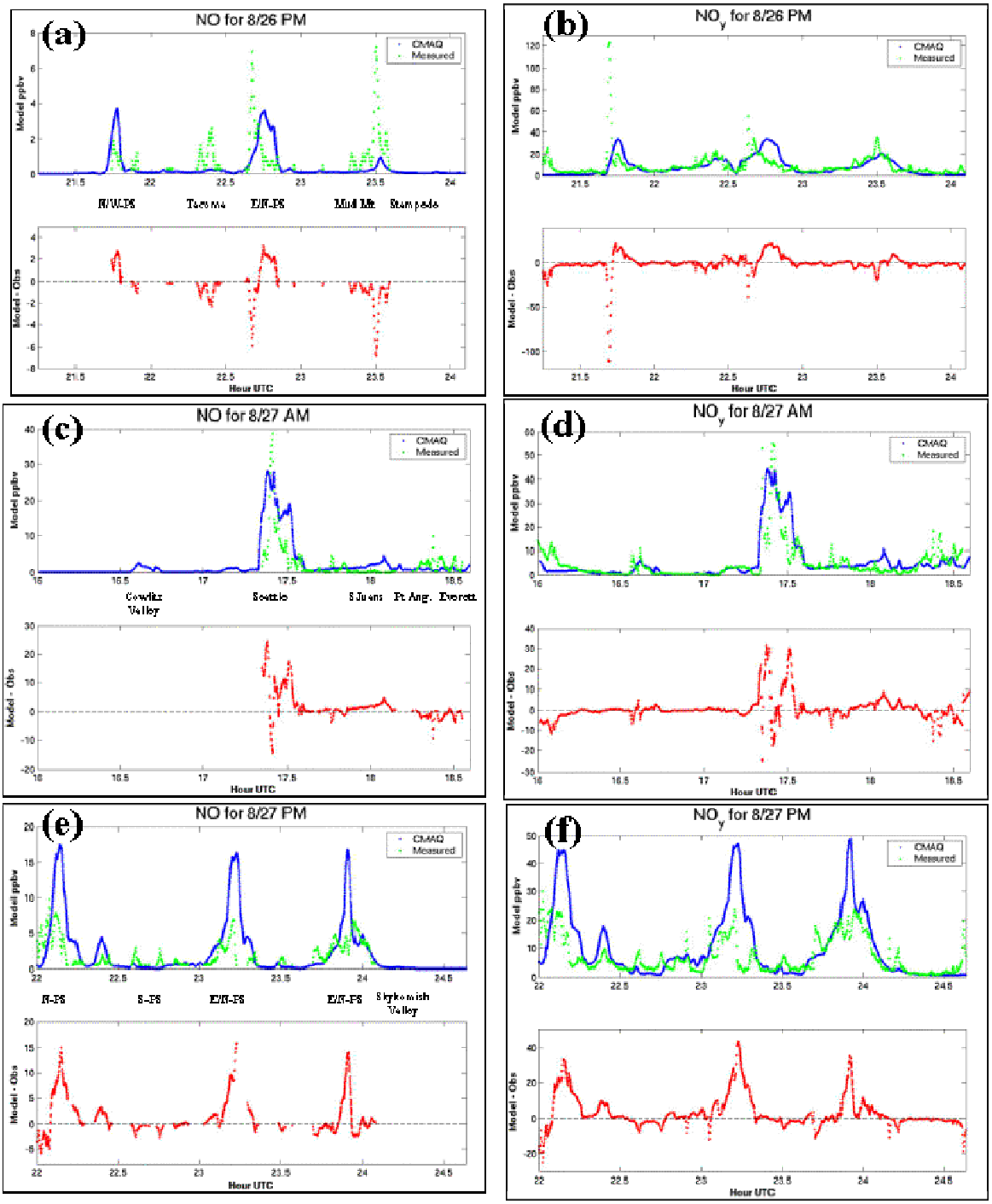

Figure 4.8 NO and NO_y from the Gulfstream during PNW2001, NO and NO_y from the CMAQ model for the flight tracks, and the error in NO and NO_y for (a,b) the afternoon of 26 August, (c,d) the morning of 27 August, and (e,f) the afternoon of 27 August.

Table 4.1 Statistical metrics used for the ground stations.

Metric	**Formula**	**Metric**	**Formula**
Mean Bias	$\frac{1}{N}\sum_{i=1}^{N}\left(M_i - O_i\right)$	Mean Gross Error	$\frac{1}{N}\sum_{i=1}^{N}\left\|M_i - O_i\right\|$
Mean Normalized Bias	$\frac{1}{N}\sum_{i=1}^{N}\left(\frac{M_i - O_i}{O_i}\right)$	Mean Normalized Error	$\frac{1}{N}\sum_{i=1}^{N}\frac{\left\|M_i - O_i\right\|}{O_i}$
Normalized Mean Bias	$\frac{\sum_{i=1}^{N}\left(M_i - O_i\right)}{\sum_{i=1}^{N}O_i}$	Normalized Mean Error	$\frac{\sum_{i=1}^{N}\left\|M_i - O_i\right\|}{\sum_{i=1}^{N}O_i}$
Normalized Mean Bias Factor	if $\overline{M} \geq \overline{O}$, $\frac{\sum_{i=1}^{N}\left(M_i - O_i\right)}{\sum_{i=1}^{N}O_i}$ if $\overline{M} \leq \overline{O}$, $\frac{\sum_{i=1}^{N}\left(M_i - O_i\right)}{\sum_{i=1}^{N}M_i}$	Normalized Mean Error Factor	if $\overline{M} \geq \overline{O}$, $\frac{\sum_{i=1}^{N}\left\|M_i - O_i\right\|}{\sum_{i=1}^{N}O_i}$ if $\overline{M} \leq \overline{O}$, $\frac{\sum_{i=1}^{N}\left\|M_i - O_i\right\|}{\sum_{i=1}^{N}M_i}$
RMSE	$\sqrt{\frac{1}{N}\sum_{i=1}^{N}\left(M_i - O_i\right)^2}$	Index of Agreement	$1 - \frac{\sum\left(M_i - O_i\right)^2}{\sum\left(\left\|M_i - \overline{O}\right\| + \left\|O_i - \overline{O}\right\|\right)^2}$
Correlation Coefficient	$\frac{\sum\left(\left(M_i - \overline{M}\right) * \left(O_i - \overline{O}\right)\right)}{\sqrt{\sum\left(M_i - \overline{M}\right)^2} * \sqrt{\sum\left(O_i - \overline{O}\right)^2}}$		

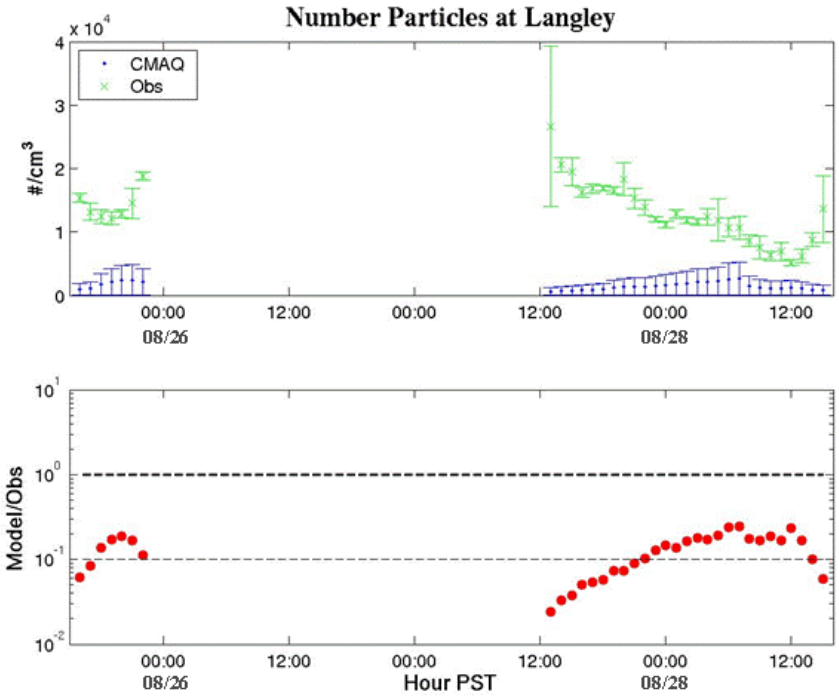

Figure 4.9 Comparison of total number concentrations for Langley DMA observations and CMAQ.

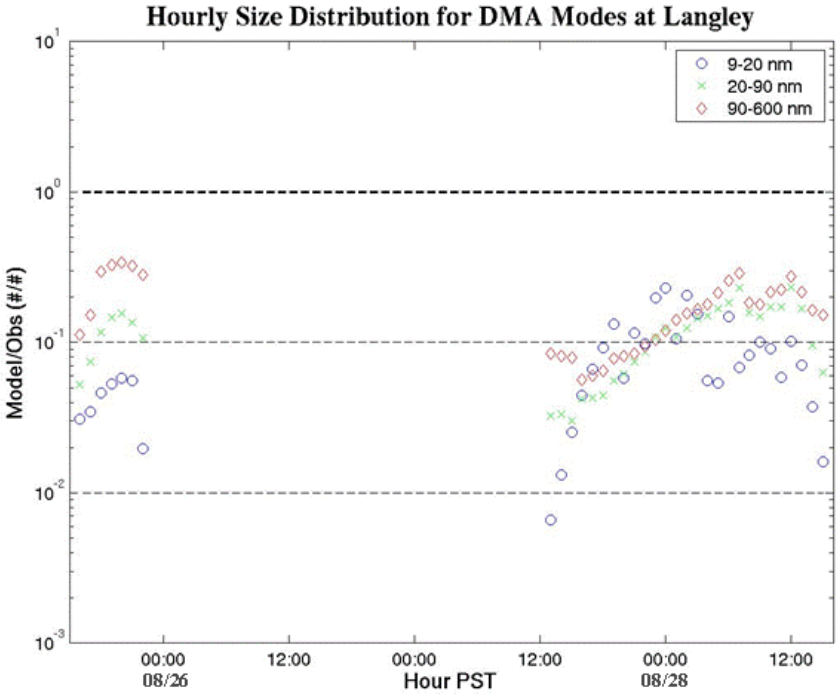

Figure 4.10 Comparison of CMAQ number concentrations at Langely in specific size ranges, or modes, to DMA observations. The data are expressed as a quotient of model number and observed number.

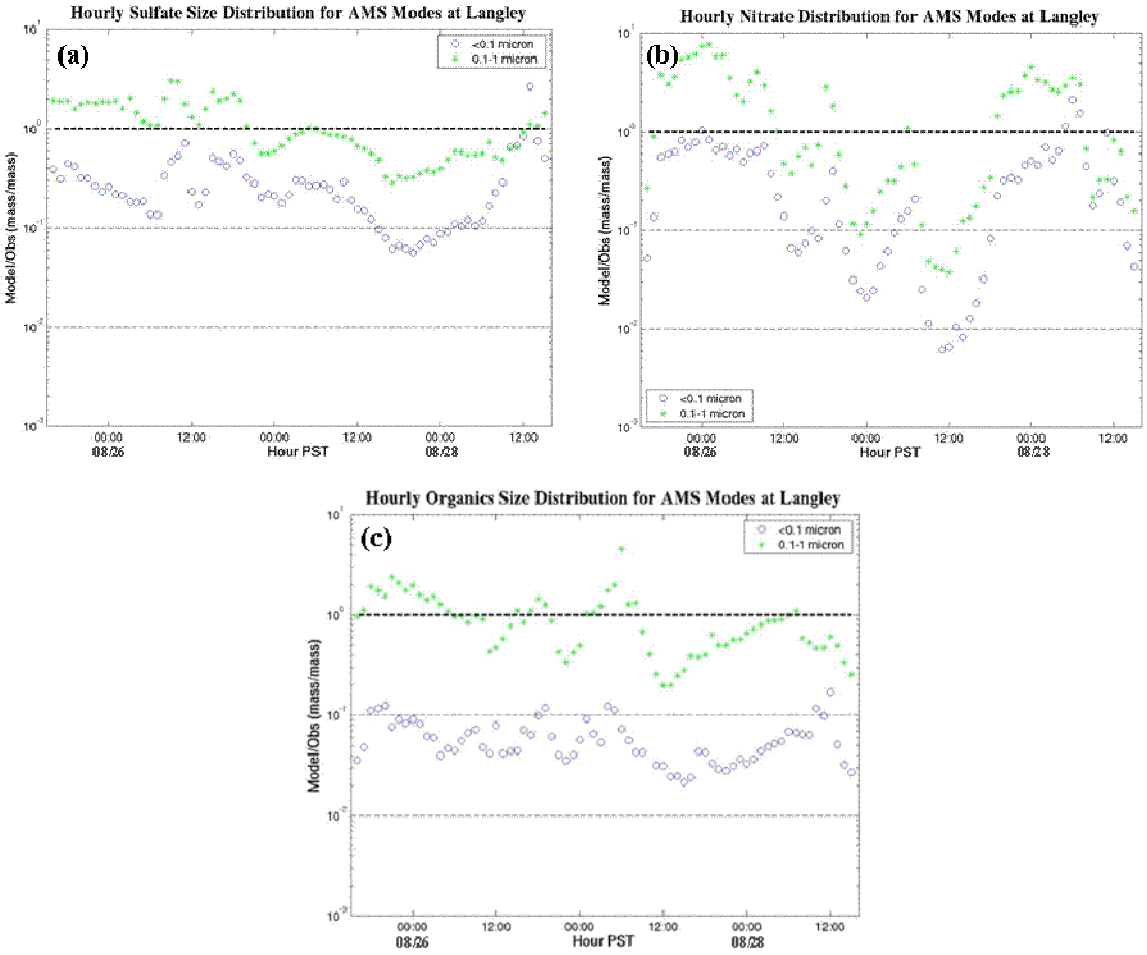

Figure 4.11 Comparison of aerosol mass concentrations by species and by size ranges at Langley. AMS measurements are compared to CMAQ for (a) sulfate, (b) nitrate, and (c) organics.

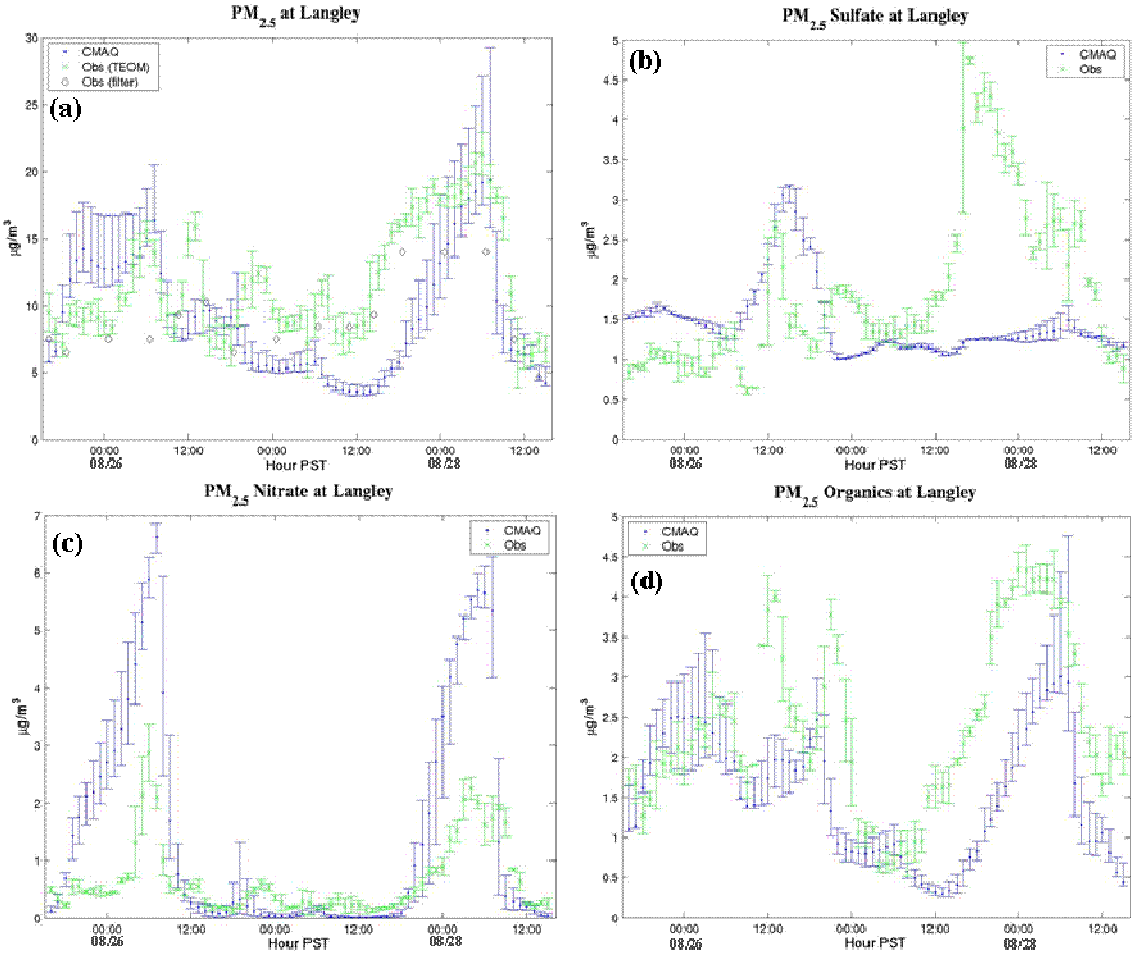

Figure 4.12 Hourly Langley (a) $PM_{2.5}$ from TEOM, gravimetric filters, and CMAQ; and (b) sulfate, (c) nitrate, and (d) organic $PM_{2.5}$ from AMS observations and CMAQ.

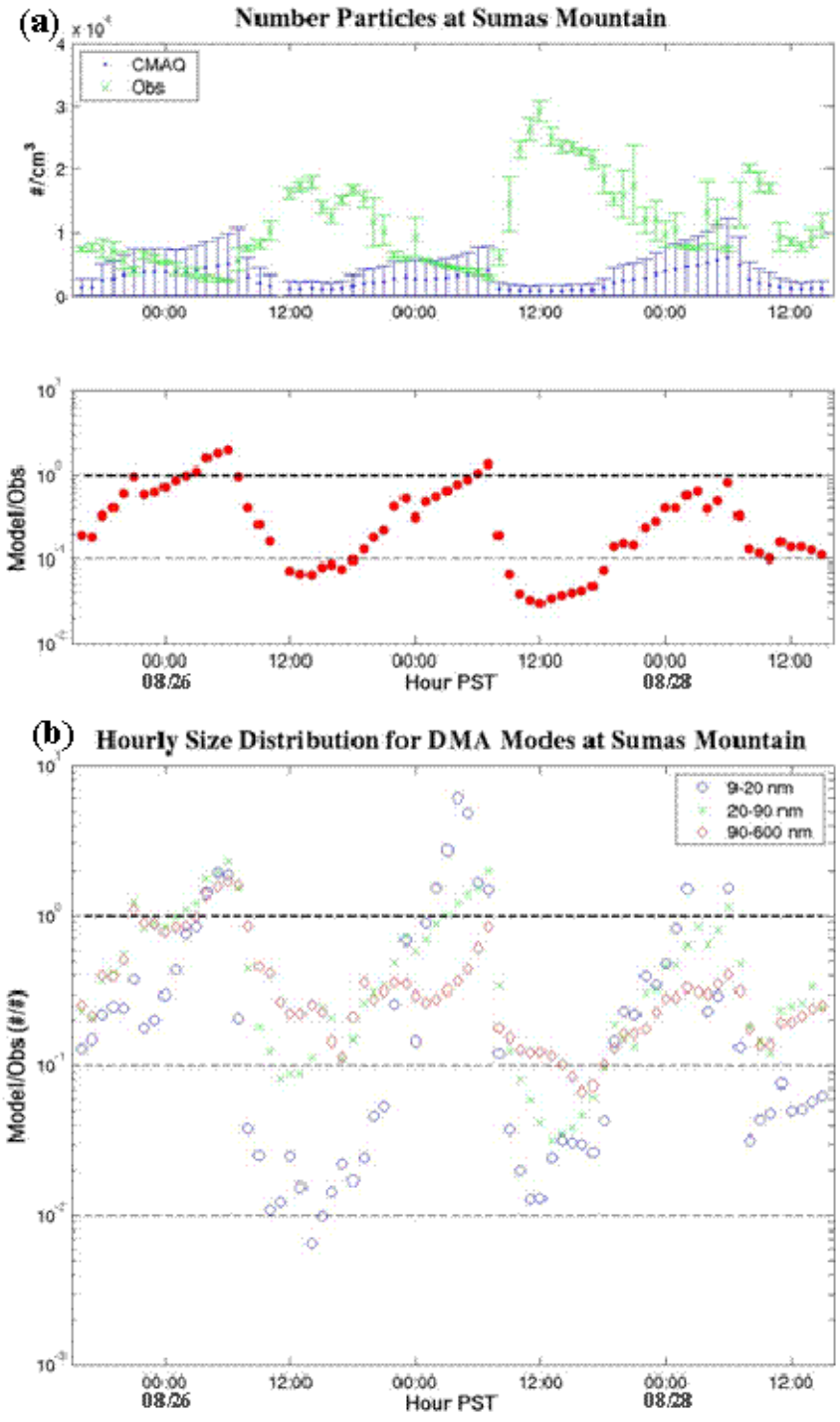

Figure 4.13 (a) Comparison of total number concentrations at Sumas Mountain from DMA and CMAQ, and (b) comparison of number concentrations in size ranges.

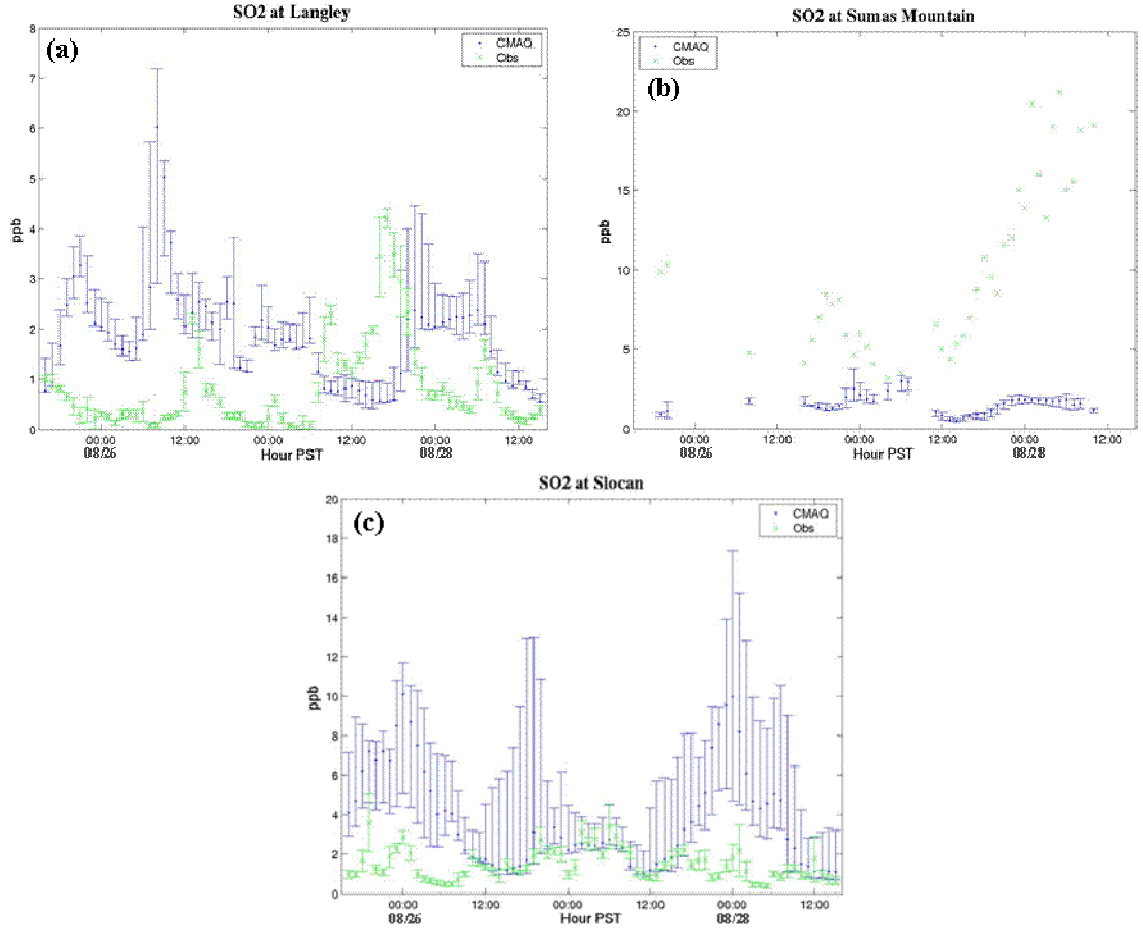

Figure 4.14 SO_2 from observations and CMAQ for (a) Langley, (b) Sumas Mountain, and (c) Slocan.

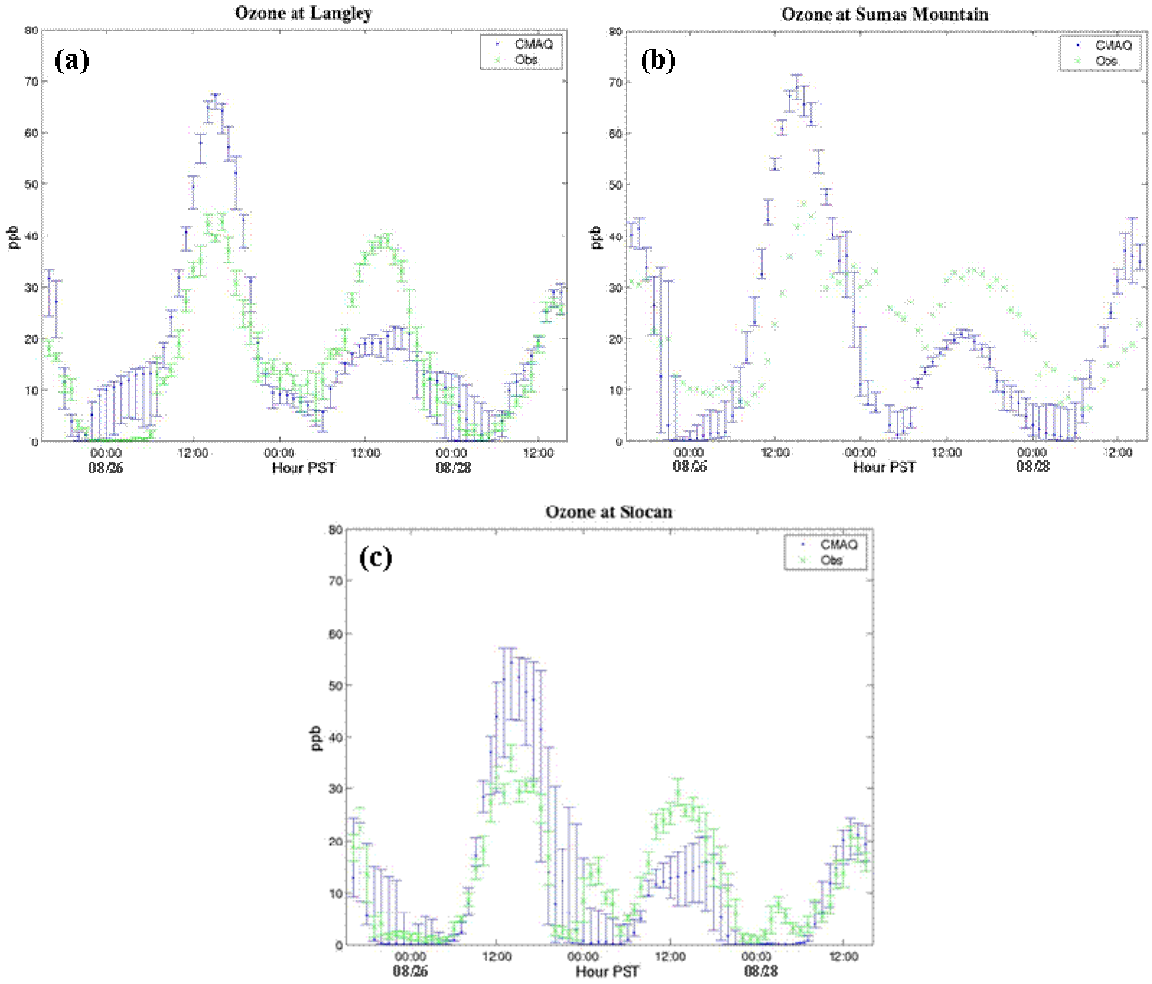

Figure 4.15 Ozone from observations and CMAQ for (a) Langley, (b) Sumas Mountain, and (c) Slocan.

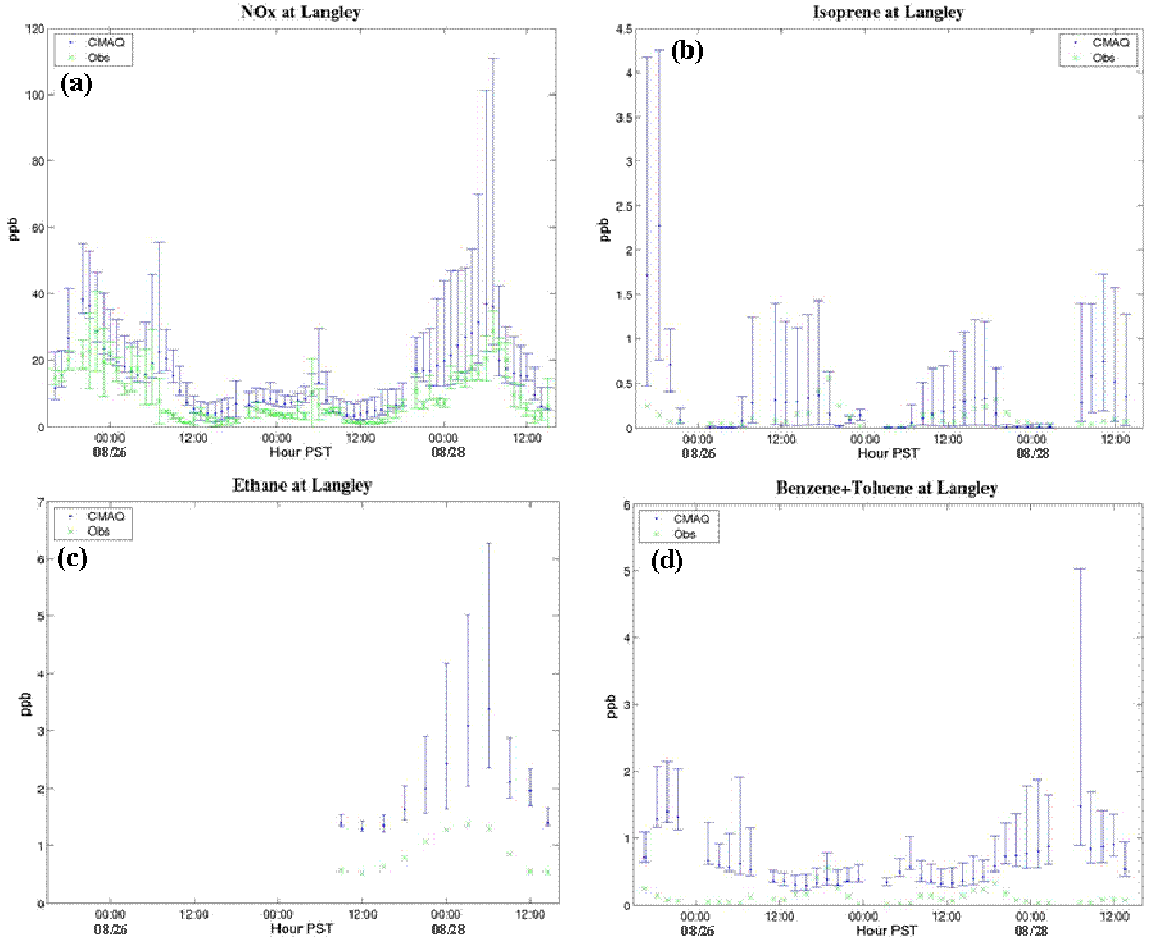

Figure 4.16 Observed and CMAQ mixing ratios at Langley for (a) NO_x, (b) isoprene, (c) ethane, and (d) aromatics.

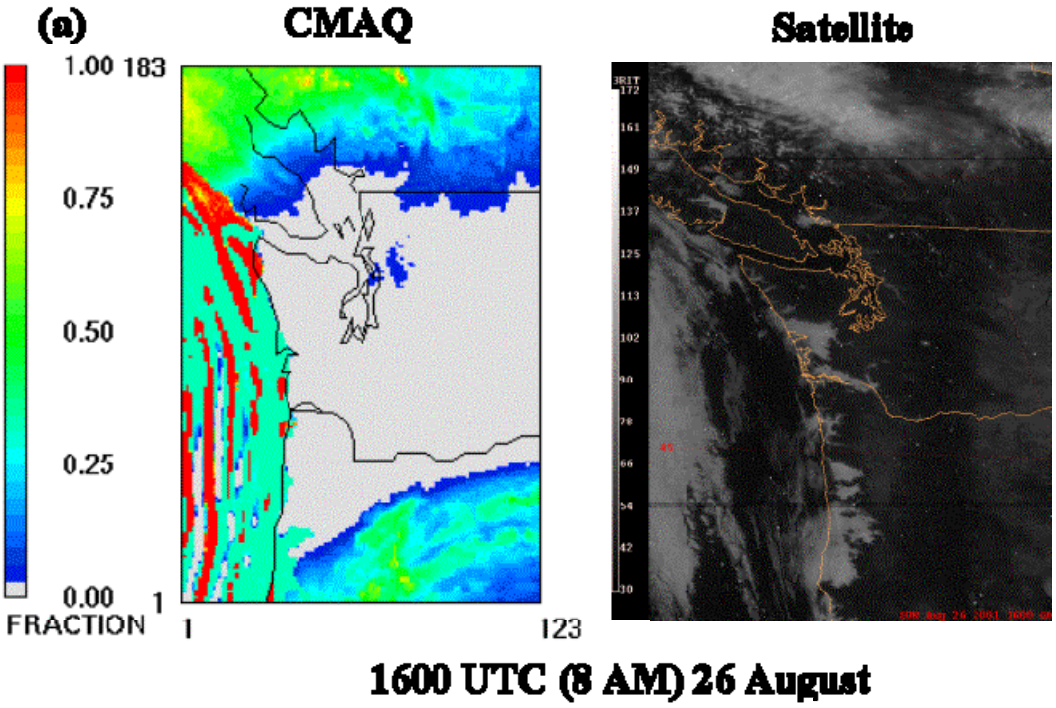

Figure 4.17 CMAQ cloud fraction and GOES-10 visible satellite imagery for the morning 26 August.

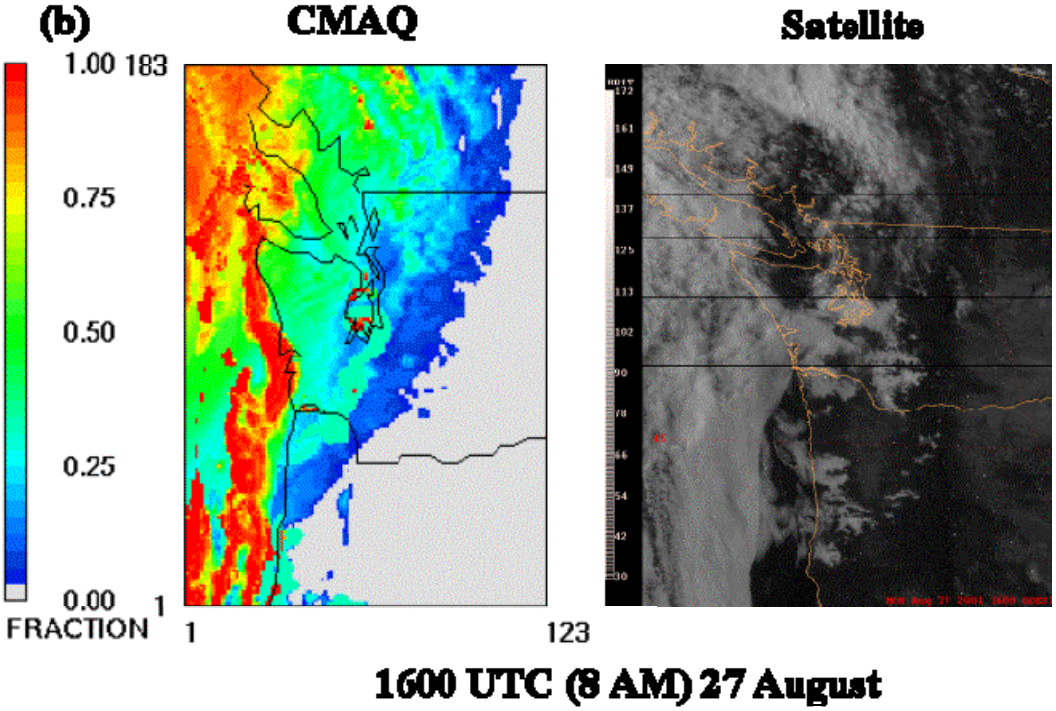

Figure 4.18 CMAQ cloud fraction and GOES-10 visible satellite imagery for the morning 27 August.

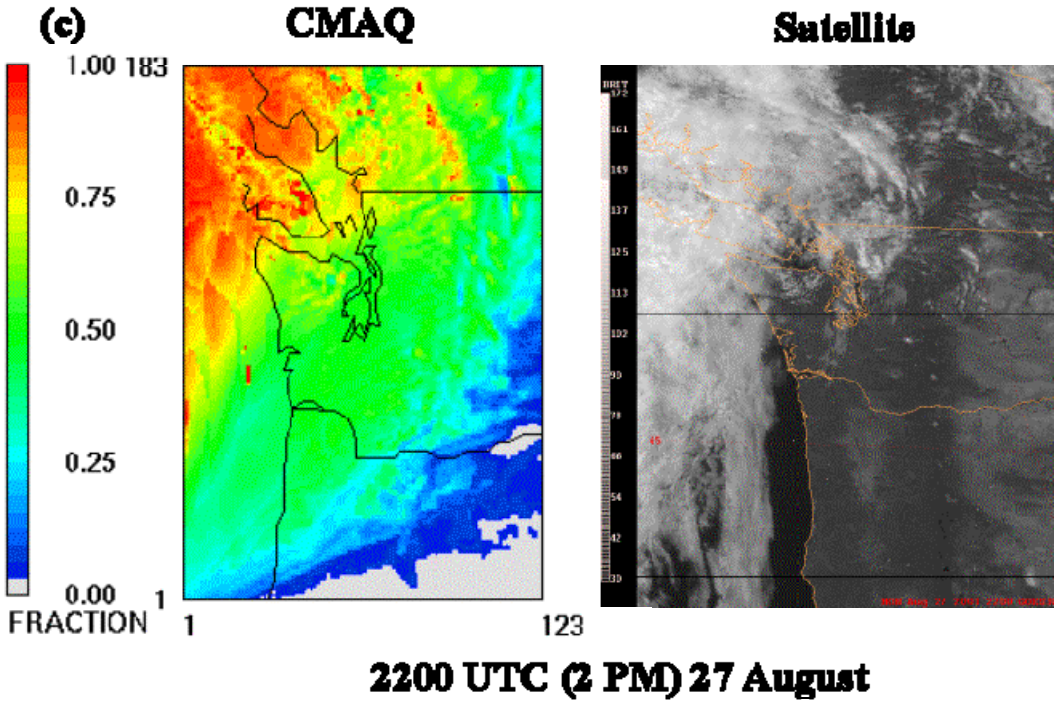

Figure 4.19 CMAQ cloud fraction and GOES-10 visible satellite imagery for the afternoon of 27 August.

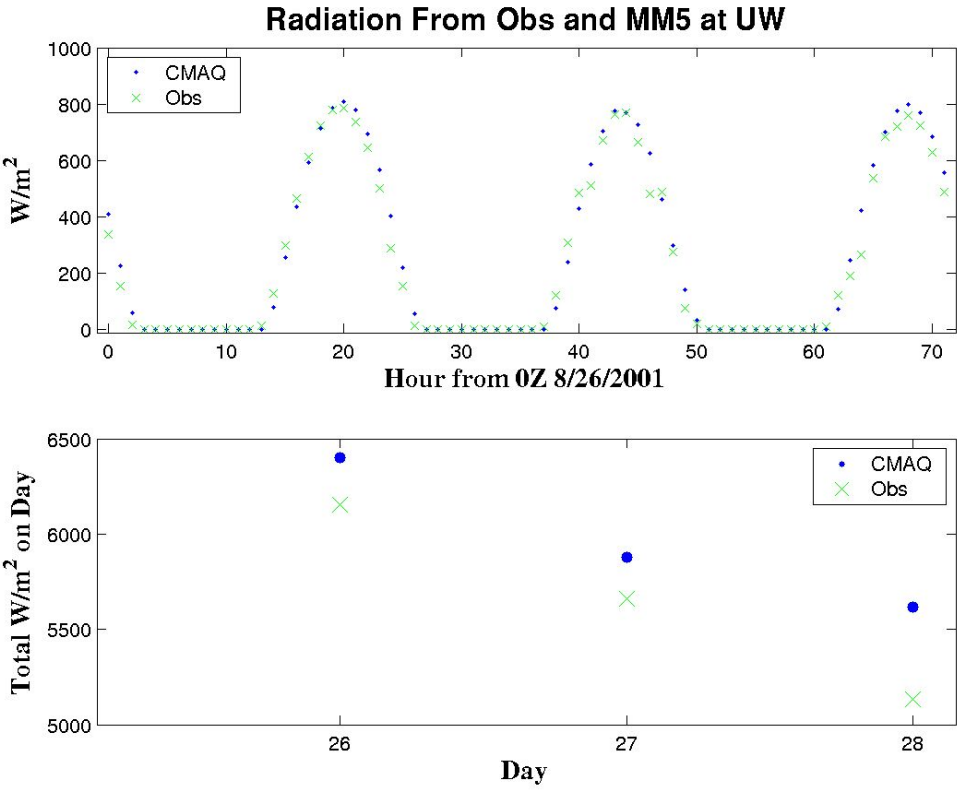

Figure 4.20 Surface radiation as measured on the roof of the UW Atmospheric Sciences Building in Seattle, WA, and radiation as modeled by MM5, the meteorological input to CMAQ. The top panel shows hourly averages. The bottom panel displays daily averages based on Pacific Standard Time.

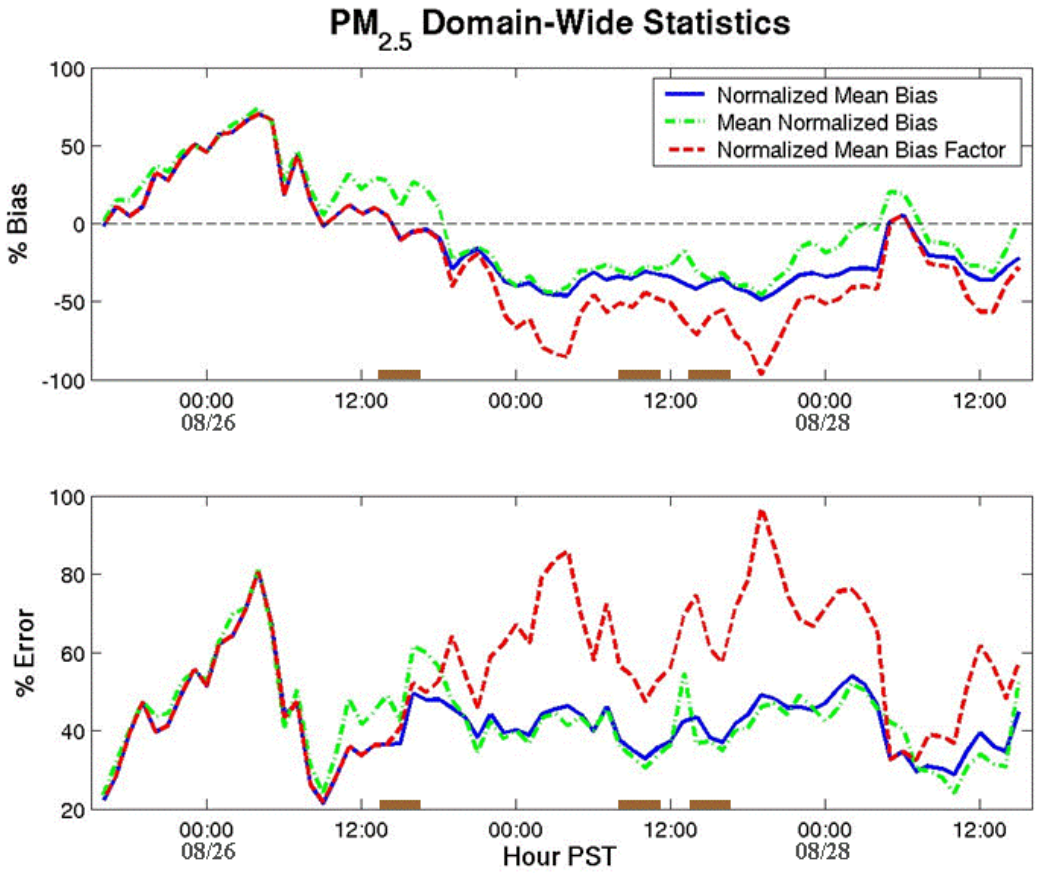

Figure 4.21 Comparison of CMAQ to hourly $PM_{2.5}$ measurements from up to 17 surface TEOM and nephelometer instruments in the Puget Sound. Lines along the abscissa denote hours when the Gulfstream obtained airborne measurements on the afternoon of 26 August and on the morning and afternoon of 27 August.

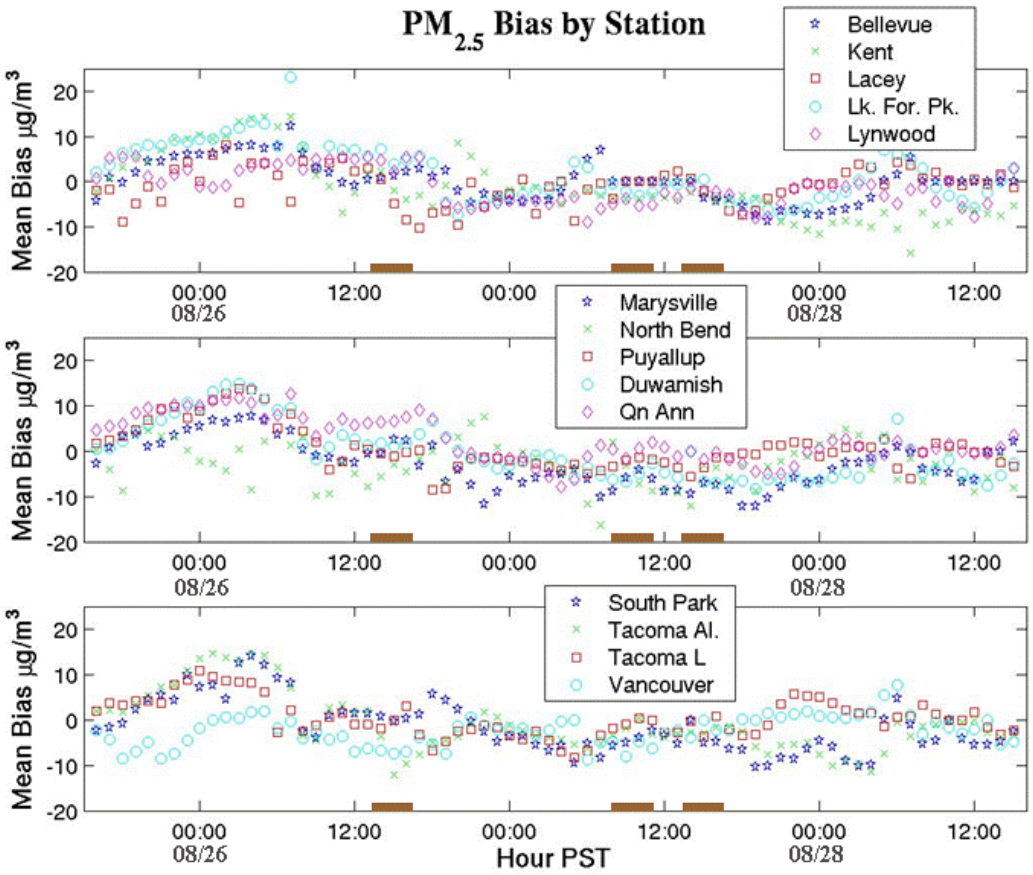

Figure 4.22 CMAQ $PM_{2.5}$ bias relative to observations at 14 ground stations in Western Washington. Lines along the abscissa denote hours when the Gulfstream obtained airborne measurements on the afternoon of 26 August and on the morning and afternoon of 27 August.

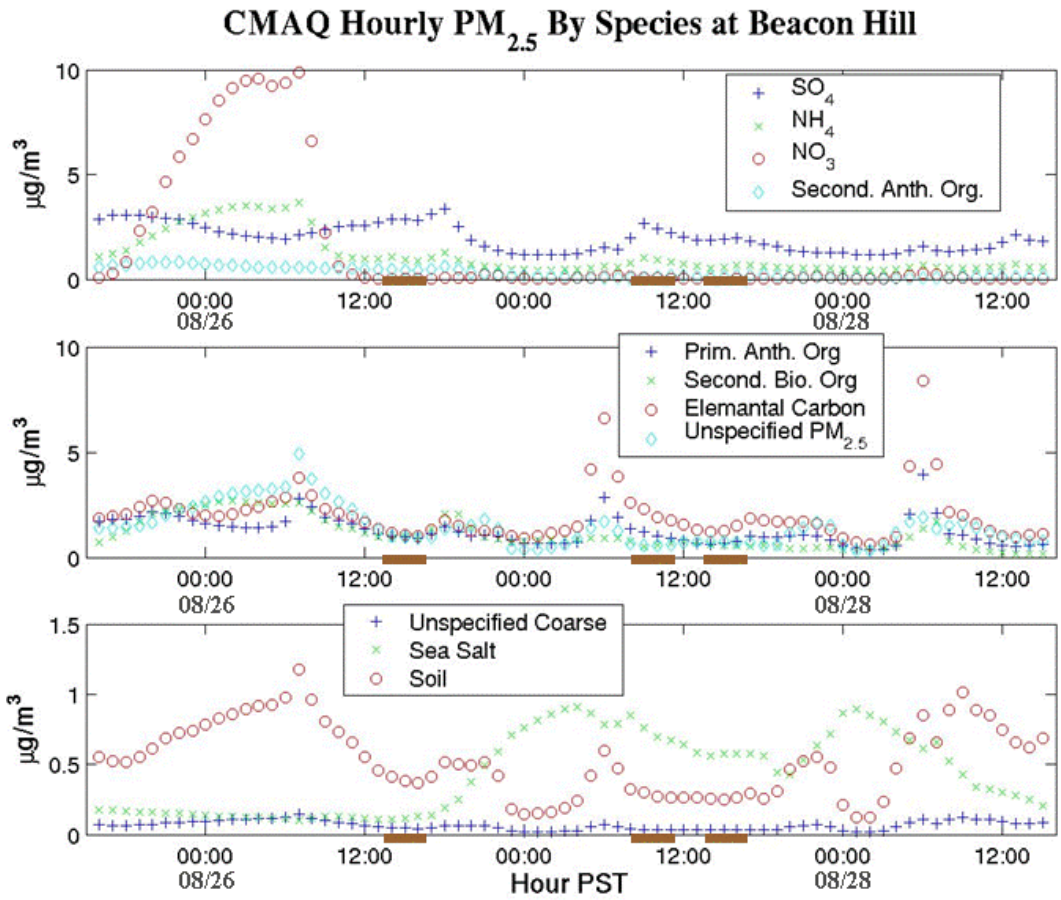

Figure 4.23 CMAQ $PM_{2.5}$ composition at Beacon Hill by species and by hour. Lines along the abscissa denote hours when the Gulfstream obtained airborne measurements on the afternoon of 26 August and on the morning and afternoon of 27 August.

Table 4.2 Comparison of CMAQ $PM_{2.5}$ results to other CMAQ simulations in various geographic regions and model configurations. Mean Bias, Mean Gross Error, and RMSE are in µg/m^3. All normalized metrics are percentages.

	This CMAQ Simulation	O'Neill (2006)	Smyth (2006)	Eder (2006)	Zhang (2006)	Pun (2006)
CMAQ version	v4.4	v4.1	v4.3	v4.4	v4.4	CMAQ-MADRID
Mean Bias	-1.6		3.7	-0.2	-8.5	-0.39
Mean Gross Error	5.2		8.0		9.18	5.0
RMSE	6.3			6.5	11.28	7.1
Mean Normalized Bias	-12				-36	
Mean Normalized Gross Error	50				46	
Normalized Mean Bias	-15%	16%	31%	-3.0%	-45%	16%
Normalized Mean Gross Error	49%	38%	66%	46%	49%	65%
Normalized Mean Bias Factor	-18%				-82%	
Normalized Mean Error Factor	58%				89%	
R^2	0.45				0.33	0.21
Index of Agreement	0.63					

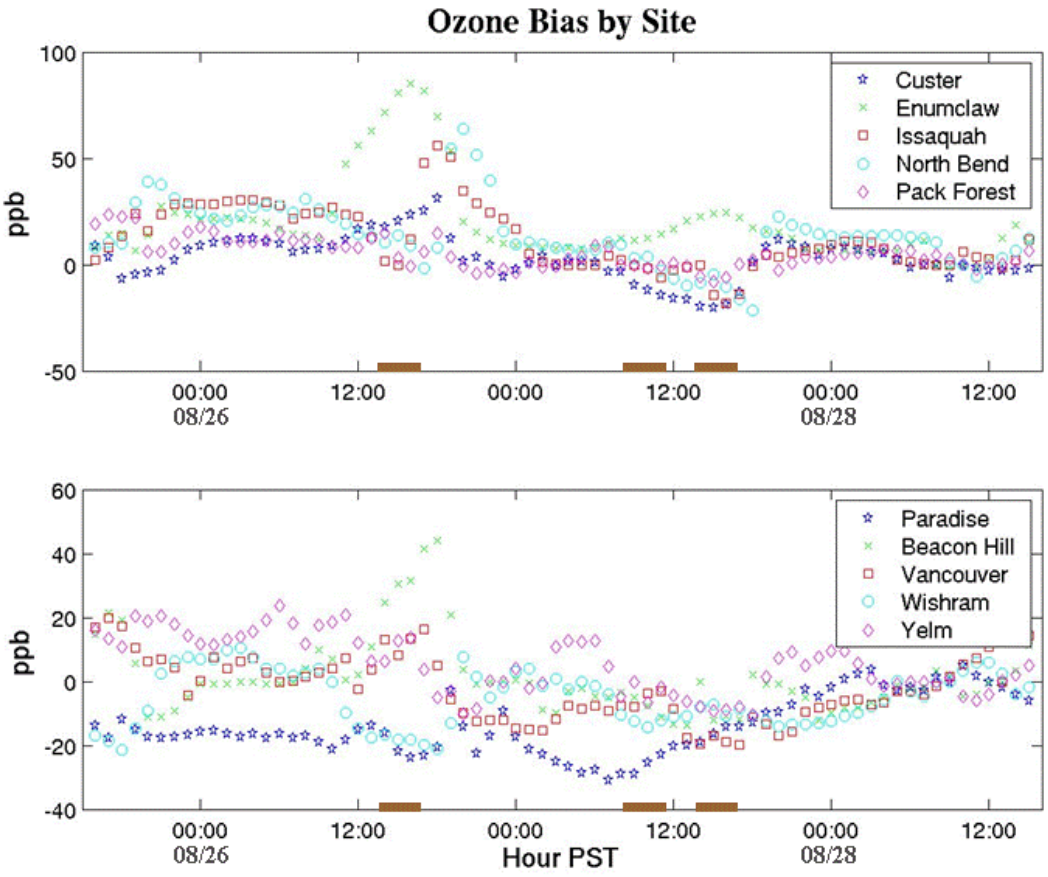

Figure 4.24 CMAQ ozone bias relative to observations at 10 ground stations in Western Washington. Lines along the abscissa denote hours when the Gulfstream obtained airborne measurements on the afternoon of 26 August and on the morning and afternoon of 27 August.

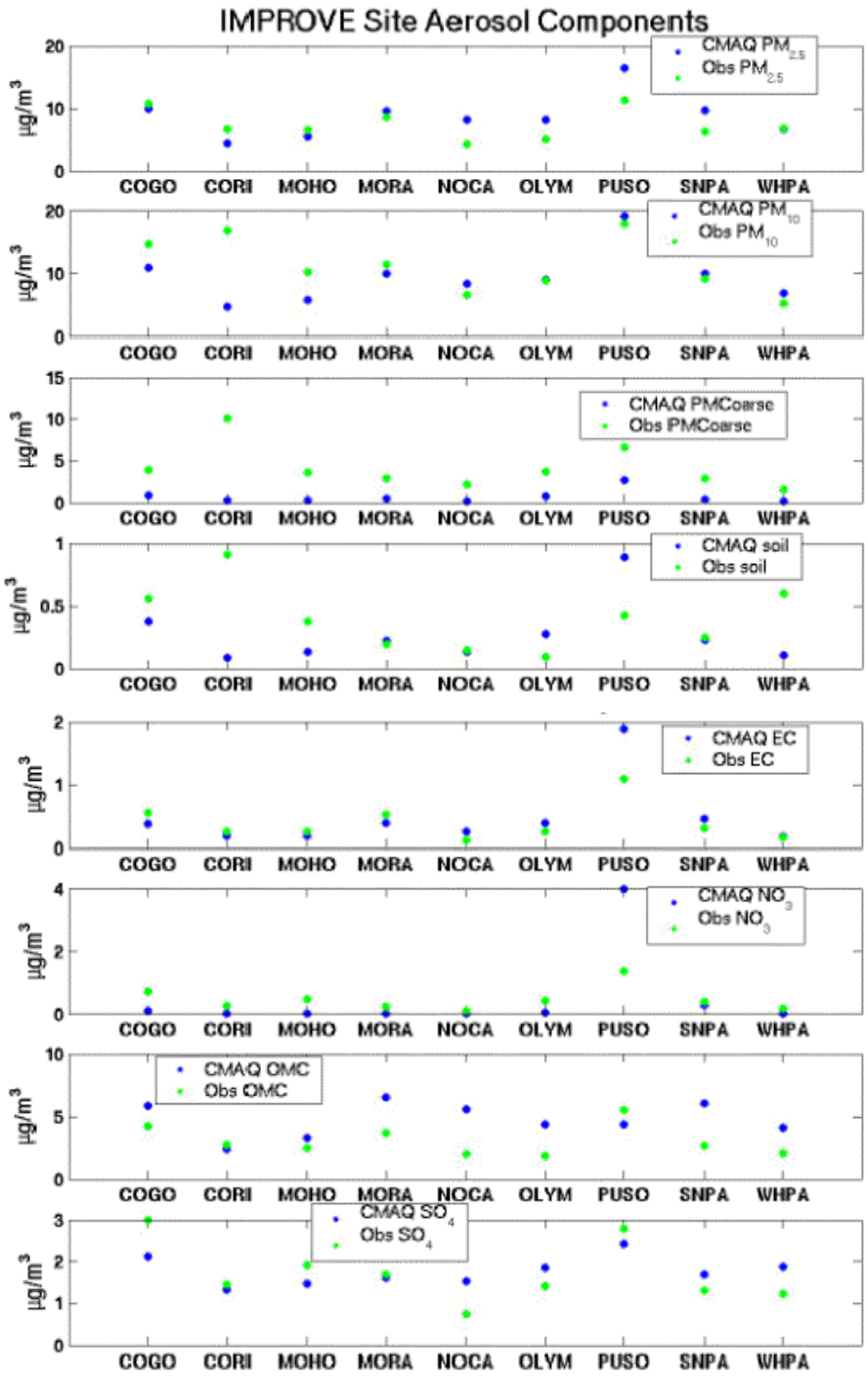

Figure 4.25 Comparison of aerosol species mass from CMAQ and from the IMPROVE network on 26 August at nine sites in the Pacific Northwest. The four-letter codes are translated as: "COGO", western entrance to the Columbia River Gorge; "CORI", Wishram, WA, in the Columbia River Gorge; "MOHO", Government Camp on Mount Hood, OR; "MORA", Ashford, WA, outside Mount Rainier National Park; "NOCA", Ross Dam, WA; "OLYM", Sequim, WA; "PUSO", Beacon Hill, WA; "SNPA", Snoqualmie Pass, WA; and "WHPA", White Pass, WA.

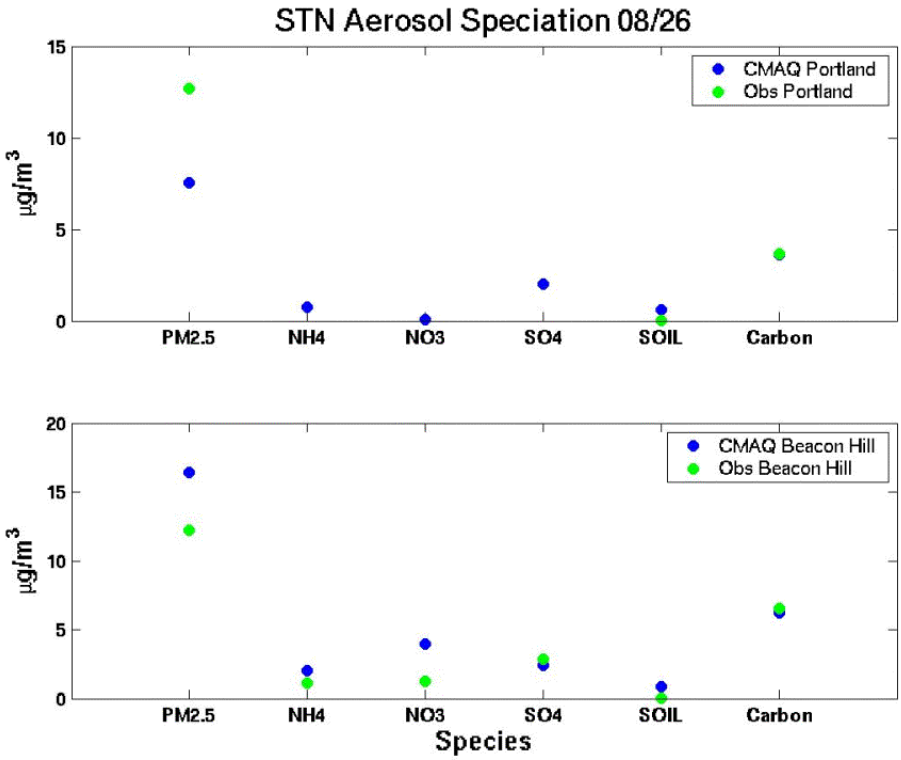

Figure 4.26 Comparison of aerosol species mass from CMAQ and from the STN network on 26 August in Portland, OR on SE Lafayette and in Seattle at Beacon Hill.

Table 4.3 Comparison of CMAQ sulfate, nitrate, elemental carbon, and organic carbon results to other CMAQ simulations in various geographic regions and model configurations. Mean Bias, Mean Gross Error, and RMSE are in μg/m^3. All normalized metrics are percentages. "This Simulation as a mass %" compares the mass percentage of the component instead of the absolute mass of the component.

Sulfate

	This CMAQ Simulation	This Simulation as a mass %	O'Neill (2006)	Smyth (2006)	Eder (2006)	Zhang (2006)	Pun (2006)
CMAQ version	v4.4	v4.4	v4.1	v4.3	v4.4	v4.4	CMAQ-MADRID
Mean Bias	0.045			1.2	-0.12	-0.87	0.87
Mean Gross Error	0.046			1.3		2.5	1.7
RMSE	0.53				-4.9	3.7	2.7
Mean Normalized Bias	16%	-2%				6%	
Mean Normalized Gross Error	33%	25%				45%	
Normalized Mean Bias	3%	-5%	36%	122%	-5%	-15%	37%
Normalized Mean Gross Error	27%	25%	68%	133%	38%	42%	65%
Normalized Mean Bias Factor	3%	-5%				-17%	
Normalized Mean Error Factor	27%	26%				49%	
R^2	0.69	0.08				0.31	0.47
Index of Agreement	0.71	0.45					

Nitrate

	This CMAQ Simulation	This Simulation as a mass %	O'Neill (2006)	Smyth (2006)	Eder (2006)	Zhang (2006)	Pun (2006)
CMAQ version	v4.4	v4.4	v4.1	v4.3	v4.4	v4.4	CMAQ-MADRID
Mean Bias	0.034			4.0	-0.06	-0.73	-0.19
Mean Gross Error	0.055			4.0		0.73	0.2
RMSE	0.93				-1.1	0.78	0.24
Mean Normalized Bias	-55%	-169%				-89%	
Mean Normalized Gross Error	98%	91%				89%	
Normalized Mean Bias	7%	-44%	-67%	1340%	-1%	-90%	-79%
Normalized Mean Gross Error	119%	91%	73%	1340%	87%	90%	96%
Normalized Mean Bias Factor	7%	-78%				-9%	
Normalized Mean Error Factor	119%	162%				9%	
R^2	0.89	0.76				0.2	0.01
Index of Agreement	0.66	0.69					

Elemental Carbon

	This CMAQ Simulation	This Simulation as a mass %	O'Neill (2006)	Smyth (2006)	Eder (2006)	Zhang (2006)	Pun (2006)
CMAQ version	v4.4	v4.4	v4.1	v4.3	v4.4	v4.4	CMAQ-MADRID
Mean Bias	0.085				-0.02	-0.29	-0.03
Mean Gross Error	0.19					0.69	0.12
RMSE	0.29				0.27	0.83	0.20
Mean Normalized Bias	20%	-0.4%				-14%	
Mean Normalized Gross Error	46%	14%				59%	
Normalized Mean Bias	22%	-4%	97%		-6%	-21%	4%
Normalized Mean Gross Error	48%	16%	104%		58%	50%	73%
Normalized Mean Bias Factor	22%	-4%				-27%	
Normalized Mean Error Factor	48%	17%				64%	
R^2	0.91	0.92			0.22	0.44	0.03
Index of Agreement	0.86	0.94					

Organic Carbon

	This CMAQ Simulation	This Simulation as a mass %	O'Neill (2006)	Smyth (2006)	Eder (2006)	Zhang (2006)	Pun (2006)
CMAQ version	v4.4	v4.4	v4.1	v4.3	v4.4	v4.4	CMAQ-MADRID
Mean Bias	1.7			-0.17	0.14	-2.9	-1.1
Mean Gross Error	2			1.4		3	1.2
RMSE	2.3				1.6	3.6	1.6
Mean Normalized Bias	73%	45%				-58%	
Mean Normalized Gross Error	80%	55%				69%	
Normalized Mean Bias	56%	41%	32%	-6%	12%	-68%	-50%
Normalized Mean Gross Error	67%	53%	49%	51%	68%	71%	55%
Normalized Mean Bias Factor	56%	41%				-2%	
Normalized Mean Error Factor	67%	53%				2%	
R^2	0.21	-0.34			0.12	0.06	0.61
Index of Agreement	0.44	0.20					

5. Ternary Nucleation

5.1. Theory

Nucleation of new particles from gas-phase precursors produces, at times, a large fraction of the observed particles in a wide range of atmospheric environments (Kulmala et al., 2004c). These particles, 1 nm in diameter and barely observable, can grow to larger sizes and become important for health effects (Oberdörster et al., 2005; Laden et al., 2006), visibility (McMurry and Friedlander, 1979), and climate (Ramanathan et al., 2001; Laaksonen et al., 2005). Our understanding of how particle nucleation occurs in natural atmospheric conditions is incomplete due to limitations in observing particles in the 1-2 nm range (Kulmala et al., 2004b) and limitations in observing their potential precursors (Ball et al., 1999; Pryor et al., 2004).

Nucleation occurs when a small group of gas molecules collides and sticks for a significant length of time. As long as the cluster's Gibbs free energy is lower than the sum of the individual gas-phase energies, the molecules will remain together to form a new particle, typically having a diameter of about 1 nm. Depending on chemical and thermodynamic conditions, the nascent cluster will preferentially be composed of molecules with high atmospheric concentrations. Otherwise the probability is too low that enough molecules will collide and stick within a very short period of time. The core molecules will also be atmospheric constituents with low vapor pressures, favoring the transition to the solid or aqueous phase. The most commonly invoked nucleation mechanism in the free atmosphere is binary H_2SO_4-H_2O nucleation (Kulmala et al.,

2004c). New particle production has been frequently observed in, or correlated with, SO_2 plumes (e.g., Weber et al., 1997; Weber et al., 2003; O'Dowd et al., 1999; Clarke et al., 1999) and has been reproduced in laboratory experiments (Ball et al., 1999). However, measured sulfuric acid concentrations are not generally high enough to produce the observed nucleation rates (Covert et al., 1992; Weber et al., 2003; Kulmala et al., 2000; Birmili et al., 2000). Binary H_2SO_4-H_2O nucleation is not a complete representation of what occurs in the atmosphere.

Possible additions to the theory are ion-induced nucleation, iodine, and aromatic carboxylic acids. Galactic cosmic rays produce oxygen and nitrogen ions which in turn react with other common constituents like sulfuric acid and water (Yu and Turco, 2001). The process continues as in neutral binary homogeneous nucleation except that the attractive forces of the ions increase the proposed reaction rates by up to an order of magnitude (Yu and Turco, 2000). Support for this theory comes from correlations of changes in cosmic rays with changes in cloud cover (Svensmark and Friis-Christensen, 1997) and limited comparison to observations (Yu et al., 2004). The effect of iodine on particle nucleation has been examined for clean marine air masses where sulfuric acid concentrations are low and iodine concentrations are high (O'Dowd et al., 2002). Aromatic acids from urban pollution such as benzoic acid and toluic acid have been shown in a chamber study to produce more >3 nm particles than sulfuric acid and water vapor alone (R. Zhang et al., 2004). Despite these studies, there is little evidence that these processes occur regularly in urban-influenced environments (Eisele et al., 2006; Q. Zhang et al., 2005).

Ammonia is the most widely recognized species for addition to the nucleation process (Coffman and Hegg, 1995; Korhonen et al., 1999). Ammonia is ubiquitous in the atmosphere, it is the atmosphere's most common base, and it decreases the vapor pressure of a sulfuric acid solution (Marti et al., 1997). Conservatively, ammonia concentrations of 1-10 and 10-100 ppt are necessary for significant nucleation rates in polluted air masses at 278 and at 298 K (Korhonen et al., 1999; Weber et al., 2003).

Typical continental concentrations are between 100 ppt and 10 ppb (Seinfeld and Pandis, 1998). Observations from Pacific 2001 show ammonia concentrations were often above 100 ppt in the Lower Fraser Valley (Pryor et al., 2004) where nucleation events were likely observed (Mozurkewich et al., 2004). Similar ammonia concentrations are reasonable for the Puget Sound where ammonia emissions are lower but still within an order of magnitude. Ammonia is clearly involved in hydrated sulfuric acid cluster formation and is likely involved in new particle production. Ammonia should be considered for modeling number concentrations.

Napari et al. (2002a, 2002b) have developed a NH_3-H_2SO_4-H_2O ternary nucleation model and an accompanying parameterization. Others have published ternary nucleation algorithms but not in a parameterized form appropriate for inclusion in a regional air quality model. The Napari parameterization produces nucleation rates several orders of magnitude higher than both the Vehkamäki et al. (2002) and Kulmala et al. (1998) binary nucleation models at typical atmospheric conditions and concentrations of H_2SO_4 and NH_3 (Korhonen et al., 2003). The model is valid for temperatures between 240 and 300 K, for relative humidities up to 95%, ammonia mixing ratios between 0.1 and 100 ppt, and for a range of sulfuric acid concentrations (10^4 – 10^9 molecules/cm^3) which cover very clean to very polluted environments. The upper temperature bound would be a constraint for extended hot, dry weather in the Pacific Northwest and would be a consistent limit for simulations in much of the rest of the United States. For the PNW2001 / Pacific 2001 simulation, however, it is not an issue since high temperatures were below 300 K in western Washington and southwest British Columbia. The bigger issue for this simulation and likely much of North America is the 100 ppt upper limit on ammonia. The nucleation rate is much less dependent on ammonia concentrations above 100 ppt, but there is a significant difference from the nucleation rate at 100 ppt when ammonia concentrations exceed the limit by several parts per billion. Modelers must be careful about how the algorithm is used in warm and ammonia-rich environments. The Napari algorithm has been implemented into the Modal Aerosol Dynamics model for Europe, MADE (Asmi et al., 2001), and into CMAQ (Y. Zhang et al., 2006a).

Ternary nucleation theory predicts that atmospheric cluster formation easily occurs in the daytime for typical tropospheric pollutant concentrations (Kulmala et al., 2000). This produces a reservoir of thermodynamically stable 1 nm clusters which represents the net flux of forming and evaporating particles. It is difficult to confirm the reservoir's existence because although ion spectrometers have been used to measure charged particles smaller than 1 nm (e.g.: Eisele et al., 2006; Kulmala et al., 2004b; and Vana et al., 2004), for the most part current observational techniques can only measure particles greater than 2.5 nm in diameter (Stolzenburg and McMurry, 1991). Except in extremely clean conditions, there is a very high probability these critical clusters will be scavenged by coagulation with larger particles before they grow to observable sizes (Kerminen et al., 2004b). But since new particle formation events are observed frequently and often on a regional scale (McMurry et al., 2005), clusters do survive to observable and more stable sizes.

Nucleation has historically referred to events where a large number of new particles appears at the instrument's lower detection limit. With the more recent theory that these particles form at sizes well below current measurement capabilities and that most of the particles do not survive to be observed, "nucleation" is refined to refer to new, thermodynamically stable particles, and "new particle production" refers to critical clusters that have survived and grown to sizes which can be observed (McMurry et al., 2005; McMurry and Friedlander, 1979).

The mechanism for a cluster to grow from 1 nm in diameter to 3 or 10 nm is poorly understood. Comparison of theory to observations has revealed that sulfuric acid is often not found in concentrations large enough to grow particles to 3 nm before they are lost via coagulation (Kulmala et al., 2000; Kerminen et al., 2004b). Instead, Kulmala et al. (2000, 2004b, 2004c) proposed a Nano-Köhler theory in which sulfate-based critical clusters provide the nucleus for heterogeneous condensation of water-soluble organic compounds in the same manner as traditional Köhler theory where a 1 μm particle

provides a nucleus for cloud water condensation and growth. Under typical boreal forest chemical environments, the Nano-Köhler effect results in a 3-4 order of magnitude increase in the number of 15 nm particles. Observational evidence for the role of organics comes from field campaigns that found fresh particles to be largely composed of organic species (Mäkelä et al., 2001; O'Dowd et al., 2002). The theory has been extended to include a cascade of organic vapors that are consecutively activated as the particle grows (Kerminen et al., 2004a). Others have proposed that organic vapors react heterogeneously with acidic sulfate hydrate clusters to overcome the large Kelvin effect at such small diameters (Jang et al., 2002; Zhang and Wexler, 2002b). R. Zhang et al. (2004) showed in a laboratory study that the addition of aromatic acid vapors markedly increased the number of observed 3 nm particles. The photochemical by-products of aromatic vapors have a very low vapor pressure, grow the particle through condensation, and lower the surface tension barrier to further growth. These theories are part of a growing body of research suggesting organics play a role in activating critical clusters into stable particles. However, in addition to not yet knowing the relative importance of cluster growth through organic vapor condensation, the specific organic vapors involved and their saturation vapor pressures remain unknown (Kerminen et al., 2004a). Fan et al. (2006) attempted to include secondary condensable organics in CMAQ's nucleation scheme, but they were forced to infer the saturation vapor pressure of the condensable organics from measured nucleation rates. Without basic thermodynamic data, it is not practical to include the role of organics in a regional air quality model.

Although organics have received attention recently, there is still evidence that sulfuric acid plays a major role in the growth of 1 nm nucleated particles into the 20-90 nm Aitken mode size range. Growth rates of nucleation mode particles are proportional to the sulfuric acid concentration (Stolzenburg et al., 2005). Variations in vapor source rates required to explain observed growth rates suggest that sulfuric acid is a major player in urban areas (Kulmala et al., 2005). During the Pittsburgh Air Quality study in the summer of 2002, the calculated sulfuric acid concentration was closely related to observed nucleation events at 3 nm (Stanier et al., 2004b), and sulfate was the first

species to increase its mass in the 18-33 nm size range after a nucleation event had begun (Q. Zhang et al., 2004). During the summer 2002 Aerosol Nucleation and Real Time Characterization Experiment (ANARChE) in Atlanta, particles in the 6-15 nm range were composed primarily of sulfate and ammonium during particle nucleation events (Smith et al., 2005). Hygroscopicity and volatility measurements from a nanometer Tandem Differential Mobility Analyzer revealed that sub-10 nm particles have both the non-volatile and hygroscopic characteristics more closely associated with sulfate than with organics (Sakurai et al., 2005). Furthermore, modeled growth rates due to sulfuric acid condensation and coagulation explained most of the measured growth rates (Stolzenburg et al., 2005). Especially for urban-influenced nucleation, sulfuric acid is a major if not the most important component of particle growth.

It is crucial to understand the growth of 1 nm particles so that nucleation theory can be compared to observations of nucleation events and can be incorporated into existing air quality models. Most air quality models only treat particles larger than 10 or 20 nm. The addition of nucleation and nanoparticle growth requires a new representation of nucleation mode dynamics such as condensation, evaporation, homogeneous nanomode coagulation, and heterogeneous coagulation with other modes. This can be done with a sectional representation of several bins or with a moving bin structure that adds a bin for the particles created at each time step. A sectional representation has been used in a box model (Lehtinen and Kulmala, 2003) and in CMAQ (K. M. Zhang, 2005), and it has been developed for the MADE regional model (Asmi et al., 2005). However, in a comprehensive regional air quality model it is not practical to dedicate the large amount of computer time necessary for a sectional aerosol representation. Instead, it is possible to parameterize the nucleation mode using the most important processes.

The theory of nucleation mode dynamics is based on the original work by McMurry and Friedlander (1979). They related the time scale of gas-phase monomer production to the time scale of diffusion to pre-existing aerosol (McMurry et al., 2005). If the available particulate surface area is large enough, the time scales of diffusion and coagulation are

shorter than the production time scale. Consequently a monomer will be lost to pre-existing aerosol rather than be involved in particle cluster formation. But as long as the critical cluster is undetectable, there is no practical difference in the measurement between direct condensation of the cluster's components onto existing particles and coagulation scavenging of a cluster formed from multiple monomers. The situation is the same for all particles below our detection limit of 3 nm. It is not currently possible to distinguish nucleation and subsequent coagulation from condensation onto pre-existing particles directly from the gas phase. Thus the McMurry and Friedlander concept addresses the competition between scavenging of a saturated gaseous species by a pre-existing aerosol "condensation sink" (Kulmala et al., 2001) and producing either a critical cluster or a particle of a specified size. McMurry and Friedlander applied it to the competition of sulfuric acid condensation versus nucleation of critical clusters. It can equally be applied to the coagulation scavenging of fresh particles by pre-existing aerosol versus the growth of the fresh particles to a larger size. This competition is the major process affecting nucleation mode particles (Kerminen et al., 2004b; Zhang and Wexler, 2002a) and can be used to represent nucleation mode dynamics.

Based on this concept, Kerminen and Kulmala (2002) developed an analytical method to determine the number of 1 nm particles that survive growth to 3-10 nm. The method assumes that coagulation with the Aitken and accumulation modes is the only significant sink for the critical clusters, that the nuclei grow at a constant rate, and that the properties of the pre-existing aerosol remain constant. The survival rate is then a competition between the removal by coagulation and the growth of the particle to a larger and more stable size. The competition is represented by η, defined in units of nm as:

$$\eta = \frac{\gamma * CS}{GR} \tag{5.1}$$

where γ is a proportionality factor in nm^2m^2/h, CS is the condensation sink time scale in $1/m^2$, and GR is the diameter growth rate in nm/h. When η is high, the condensation sink dominates the growth rate and nucleated particles are not likely to survive growth to a stable size; when η is low, particles have a much better survival rate. Gamma varies

weakly with pre-existing aerosol properties, temperature, initial cluster diameter, and final growth diameter such that:

$$\gamma = \gamma_0 \left[\frac{d_{nuc,ini}}{1nm}\right]^{0.2} \left[\frac{d_p}{3nm}\right]^{0.075} \left[\frac{d_{mean}}{150nm}\right]^{0.048} \left[\frac{\rho_{nuc}}{1000kg/m^3}\right]^{-0.33} \left[\frac{T}{293K}\right]^{-0.75} \quad (5.2)$$

where $d_{nuc,ini}$ is the cluster diameter, d_p is the final diameter of interest, d_{mean} is the mean diameter of the existing aerosol population, and ρ_{nuc} is the density of the condensing vapor. In practice, the default value γ_0, 0.23 nm^2m^2/h, is a reasonable approximation. The condensation sink can be calculated as the inverse of the available pre-existing surface area. When multiplied by 4π and the H_2SO_4 vapor diffusion coefficient, the new condensation sink, in units of 1/s, becomes the time scale of fresh particle coagulation to the existing particles. The nanoparticle growth rate can then be approximated as a linear function of the non-volatile condensing species:

$$GR \approx \frac{3.0\times10^{-9}}{\rho_{nuc}} \sum_i \bar{c}_i M_i C_i \quad (5.3)$$

where c_i is the molecular speed of the condensing vapor, M_i is its molecular weight, and C_i is its concentration. Although this applies to any condensing vapor, only sulfuric acid is used in practice because relevant organic saturation vapor pressures are still unknown.

Once η is calculated, the relationship between the number of 1 nm particles and the number of 3 nm particles is:

$$\frac{J_{app}}{J} = \exp\left[\frac{\eta}{d_p} - \frac{\eta}{d_{nuc,ini}}\right]. \quad (5.4)$$

Eta typically varies from a value of 1-5 nm in rural areas to 10 nm or more for urban areas. The production rate of 3 nm particles is typically a factor of 10 lower than the nucleation rate of 1 nm clusters in rural areas (Figure 5.1). For urban regions, the production rate decreases by 3-4 orders of magnitude. The production rate of 10 nm particles is lower than that of 3 nm particles but by less than a factor of 10. These calculations underscore the danger in comparing nucleation rates of critical clusters against observations of >3 or >8 nm particles. The formulae reviewed here provide a link

between the true nucleation rate and the observed new particle production rate as well as provide a parameterization for nucleation mode dynamics.

5.2. Application to CMAQ

To improve the simulation of ultrafine particles and extend the aerosol science of CMAQ, the Napari et al. (2002b) ternary NH_3-H_2SO_4-H_2O nucleation parameterization was implemented into CMAQ v4.4. The inputs to the ternary parameterization are temperature, relative humidity, sulfuric acid concentration, the production rate of sulfuric acid, ammonia concentration, and air density. The last two are the only new inputs compared to the existing binary nucleation routine in CMAQ. Air density is only required for converting the units of the ammonia concentration from $\mu g/m^3$ to ppb. The input sulfuric acid, ammonia, temperature, and RH are forced to remain inside the parameterization limits. For this case study, only the 95% upper RH limit and the 100 ppt ammonia limit are applied. The nucleation rate is also capped at 10^6 $1/(cm^3 s)$ to conform to the parameterization limit, but it was rarely invoked.

The important change to CMAQ and to the ternary parameterization involved the treatment of sulfuric acid concentrations. CMAQ normally solves for the gaseous sulfuric acid concentration, $H_2SO_{4(gas)}$, using the limit of diffusion (Jiang and Roth, 2003). Sulfuric acid is treated as a “non-volatile” compound, but it exists in the gas phase because its gas-to-particle conversion is limited by the time scale of diffusion to available surface area. CMAQ mimics the non-volatility by assuming that the sulfuric acid produced in the gas-phase routine becomes either new nucleated mass or is condensed onto existing particles. CMAQ then calculates a steady-state $H_2SO_{4(gas)}$ using the sulfuric acid production rate and the diffusion time scale. This technique works fairly well when the nucleation rate is low. When it is high, however, the nucleated mass should be removed from the sulfuric acid production rate because it should not be involved in the diffusion-limited $H_2SO_{4(gas)}$. Because the nucleation rate is a function of the steady-state $H_2SO_{4(gas)}$ and the $H_2SO_{4(gas)}$ now depends on the nucleation rate, the nucleation rate and

$H_2SO_{4(gas)}$ are coupled nonlinearly. For this project, a bisection method attempted to iterate the two variables until $H_2SO_{4(gas)}$ varies by less than 10^{-4} $\mu g/m^3$, but the technique unfortunately had difficulties converging to an equilibrium. In any case, the result of this algorithm is fresh 1 nm particles that are immediately added to the Aitken mode. The combination of a monodisperse nucleation mode with a lognormal Aitken mode is a physical inconsistency that is dealt with in the next paragraph. Hereafter, the base Napari ternary nucleation simulation is referred to as "Ternary" for ternary nucleation of 1 nm particles; the standard CMAQ v4.4 as described in Chapter 2 is referred to as "Binary"; and a case without nucleation is "None" (Table 5.1).

Once the nucleation algorithm was updated, the Kerminen and Kulmala parameterization (2002) bridges the gap between the fresh, 1 nm nucleation mode particles and their appearance into CMAQ's Aitken mode. It finds the number of 10 nm particles that will survive the growth process from 1 nm to 10 nm without being lost by coagulation and then immediately adds their number, surface area, and volume into the existing Aitken mode. This step is referred to as "nucleation mode processing", or sometimes just "processing", in this study. Based on measurements in Atlanta and Pittsburgh and on practical limitations as described in the previous section, it is assumed that the 10 nm processed particles are composed entirely of sulfate aerosol. The partitioning of ammonia and water in the new aerosol mass is left for the inorganic thermodynamic equilibrium part of the model, ISORROPIA. The parameter η, which determines the survival of the nanoparticles, is calculated using a linear combination of the condensation sinks from the Aitken and accumulation modes. The condensation sink used in this implementation is consistent with the rest of CMAQ. CMAQ already calculates it elsewhere to determine Aitken and accumulation mode coagulation and condensation rates. The additional parameterization accounts for nucleation mode dynamics and properly adds new Aitken mode particles to the existing Aitken mode.

In reality it would take the 1 nm particles up to 2 hours to go through this growth stage (Kulmala et al., 2004c). The particles would be impacted by varying amounts of

sulfuric acid and other condensable gases during this time. Keeping track of the particle's size and the ambient sulfuric acid concentration at each time step in this process would turn the algorithm into a sectional representation and eliminate the efficiency and simplicity of the Kerminen and Kulmala parameterization. Besides, fresh emissions would typically only travel 40 km in 2 hours and would likely be in the urban-influenced zone the entire time. Immediately growing the particles to 10 nm is a simplification, but the added complexity and inefficiency are not worth the more accurate representation.

To resolve the numerical convergence issues from the "Ternary" implementation, conservation of sulfuric acid was used to constrain the convergence. This has the additional benefit of conserving an important species for air quality models. The total amount of sulfuric acid is given by:

$$S_n = H_2SO_{4(gas),old} + H_2SO_{4(prod)} \tag{5.5}$$

the sum of $H_2SO_{4(gas)}$ from the old time step and $H_2SO_{4(prod)}$, the amount of sulfuric acid produced through gas-phase reactions in the current time step. S_n for this time step is partitioned into:

$$S_n = H_2SO_{4(gas)} + H_2SO_{4(cond)} + H_2SO_{4(nuc)} \tag{5.6}$$

(1) gas-phase sulfuric acid, $H_2SO_{4(gas)}$; (2) sulfuric acid that condenses onto existing particles (including nucleated particles <10 nm that are lost to the Aitken or accumulation mode via coagulation), $H_2SO_{4(cond)}$; (3) and sulfuric acid that nucleates new particle mass and grows into 10 nm particles, $H_2SO_{4(nuc)}$. S_n does not include sulfate mass already in the Aitken and accumulation modes. The gaseous sulfuric acid concentration is still limited by the condensation time scale:

$$H_2SO_{4(gas)} = \frac{H_2SO_{4(cond)}}{\Delta t\left(CS_{ait} + CS_{acc}\right)} \tag{5.7}$$

where CS, the condensation sink time scale (1/s), is applied to the Aitken and accumulation modes and Δt is the CMAQ time step used here to convert $H_2SO_{4(cond)}$ into a condensation rate. The nucleated mass, $H_2SO_{4(nuc)}$, depends on $H_2SO_{4(gas)}$. The subroutine iterates the three components in (5.6) until the total sulfuric acid is conserved to within 2 x 10^{-5} $\mu g/m^3$ (1.2 x10^5 molecules/cm^3) or to within 1%. The bisection

convergence method is used when the current iteration and previous iteration gaseous sulfuric acid concentrations differ by more than 5.0 x 10^{-4} $\mu g/m^3$ (3 x10^6 molecules/cm^3), and the Approximate Newton's Method is used for smaller differences and when the bisection method is inappropriate. This mixture takes advantage of the convergence efficiency of Newton's Method while addressing convergence instability in the governing equations for the first few iterations. The first iteration of the nucleation routine uses first-guess gaseous sulfuric acid concentrations of 4.0 x 10^{-3} and 0 $\mu g/m^3$. For typical conditions of this case study, the procedure converged in 1-4 iterations for evening and nighttime conditions, and 4-7 iterations during the day. This final version of the nucleation routine, called "Ternary w/Processing", added 5% to the total CMAQ runtime compared to the standard binary nucleation case.

CMAQ v4.5, released in September 2005, updated some key aerosol processes that could affect the results of ternary nucleation and nucleation mode processing (Bhave et al., 2005). A conversion error in the emissions subroutine resulted in no gaseous sulfuric acid emissions in v4.4 and earlier versions. Because CMAQ immediately turns these gaseous emissions into primary sulfate aerosol, all simulations underestimate primary sulfate mass. Through inorganic equilibrium it also underestimates aerosol water, ammonium, and nitrate. Bhave et al. estimated the correction increases sulfate by >0.5 $\mu g/m^3$, water by 2.0 $\mu g/m^3$, and other species to a much smaller degree. Additionally, CMAQ v4.5 fixed a bug in the modal merging section of CMAQ that caused too little Aitken mode mass to transfer to the accumulation mode. The fix rarely affected the overall mass simulation but did eliminate the largest occurrences of the Aitken mode diameter becoming larger than the accumulation mode diameter. A third change was to place ISORROPIA after the nucleation algorithm so that the values at the end of the time step are in thermodynamic equilibrium. For testing v4.5 on this case study, the sulfuric acid emission and mode merging fixes were implemented along with ternary nucleation and nucleation mode processing. The ISORROPIA change was not made here because the condensation sink in nucleation mode processing depends critically on the aerosol surface area. ISORROPIA must be run before the nucleation routine to assure the proper

condensation sink and thus nucleation mode processing. It seems likely that having the appropriate condensation sink would be more important for the size distributions than achieving thermodynamic equilibrium at the end of the time step. This run is called "Ternary w/Processing v4.5".

5.3. Results

Switching from binary to ternary nucleation has a large effect on the number of particles produced in CMAQ. Figures 5.2, 5.3, and 5.4 show the number of particles observed by the aircraft for the three flights over Puget Sound during PNW2001 ("obs", green) and as modeled by CMAQ for the aircraft location and time with binary nucleation ("Binary", blue), no nucleation ("None", black), ternary nucleation ("Ternary", red), and ternary nucleation processed to the Aitken mode ("Ternary w/Processing", cyan). In all three figures, the binary nucleation trace is not visible because the no nucleation case is overlain. There is no appreciable difference in the average number of particles between Binary and None (Table 5.2), which means that the Kulmala et al. (1998) binary nucleation scheme generates nearly no new particles for this simulation.

Ternary nucleation, "Ternary", produces daytime particle concentrations in the millions in the urban areas, but most of these particles are below the detection limit of the instruments used in PNW2001 and Pacific 2001. When the CMAQ size distribution is cut at the instrument detection limits of 6.5, 7, and 8.66 nm for Langley ground data, PNW2001 aircraft flights, and Sumas ground data, respectively, the number concentrations are typically between 50,000 and 500,000 per cm^3 for the urban areas and are typically 0-2 orders of magnitude too high. The overprediction is more pronounced for the afternoon of 26 August (Figure 5.2 / 5.5a) than for the morning or afternoon of 27 August (Figures 5.3 / 5.5b and 5.4 / 5.5c). The difference between the days is likely due to more widespread marine air on 27 August, reducing the temperature and actinic flux relative to 26 August. Nucleation is thereby reduced, and its importance for the number concentration diminishes. Performance of the Ternary case on 27 August was the best of the four nucleation options. The Ternary number concentrations have more structure than

the other four nucleation options because the ternary scheme is more sensitive to the pollutant inputs. This is particularly evident on the morning of 27 August, where CMAQ produces three spikes of particles near the foothills of Mount Rainier rather than a broader increase as seen in the observed concentrations. These spikes are located where CMAQ has modeled SO_2 plumes from the Centralia power plant, whereas other modeled number spikes are tied to ammonia plumes. Ternary nucleation produces the most particles of the nucleation options, generally overpredicts the number concentration, and performs the best for the flights on 27 August.

Processing of the nucleation mode produced by ternary nucleation, "Ternary w/Processing", greatly moderates the number of modeled particles (Figures 5.2-5.4, and Figure 5.6). Ternary nucleation produces millions of particles per cm^3, but often only 10-25% survive to 10 nm. Ternary w/Processing overpredicts the number of particles on the afternoon of 26 August but still outperforms the Binary case. Ternary w/Processing performs the best on this day of all four nucleation options. On 27 August, however, Ternary produces the best results and Ternary w/Processing is only slightly better than the Binary case. The lower temperature and actinic flux on 27 August nearly shut down CMAQ production of 10 nm particles for the day. Processing the nucleation mode particles to the Aitken mode eliminates a large fraction of the freshly nucleated particles but sometimes eliminates nearly all of them.

In general, the Ternary w/Processing concentrations follow the pattern of the Ternary case. This indicates that η is nearly constant within the urban areas. Indeed, η remains around 10 nm in urban areas during the daytime hours, and the modeled SO_2, NH_3, and aerosol volume are all correlated with number concentrations for the three PNW2001 flights. There are some excursions, such as on the north part of Puget Sound on the afternoon of 26 August, when the number of particles from the Ternary case increases (hour 21.8 in Figure 5.2) while the number of particles from the Ternary w/Processing case decreases. From the CMAQ aerosol volume for the afternoon of 26 August (Figure 5.7), it is possible to see how the increase in the condensation sink breaks the correlation

between Ternary and Ternary w/Processing. A second example comes on the morning of 27 August. The three spikes in Ternary number concentrations are not present in Ternary w/Processing because the spikes are associated with a very high condensation sink.

The pre-existing aerosol provides a coagulation sink for the nascent particles but also reduces the steady-state $H_2SO_{4(gas)}$ through equation (5.6) and slows the nucleation mode growth rate. Figure 5.8 shows that $H_2SO_{4(gas)}$ is capped at 10^8-10^9 molecules/cm^3 because aerosol volume and SO_2 are often correlated. Whenever there is enough SO_2 to produce large amounts of H_2SO_4, there is enough aerosol volume to accommodate the newly formed $H_2SO_{4(gas)}$ as $H_2SO_{4(cond)}$ in the particle phase. Ternary nucleation produces its largest number concentrations when the sulfuric acid concentrations are near 10^7 molecules/cm^3, and 10^6 molecules/cm^3 can produce anywhere from 10^3 to 10^6 particles. Ternary w/Processing number concentrations have a more well-defined relationship with $H_2SO_{4(gas)}$ than the Ternary case. This can be seen as a lower edge to the data cloud in Figure 5.8b. Because the small particles are lost to coagulation if their growth rate is not fast enough in Ternary w/Processing, there is an effective minimum amount of $H_2SO_{4(gas)}$ required to maintain a certain number concentration. This increases the correlation of number with $H_2SO_{4(gas)}$ and decreases the correlation of number with ammonia. Whereas the binary nucleation case had fairly uniform performance across time and location, the ternary nucleation cases depend more critically on the input parameters and thus show more varied performance.

Number concentration measurements at Langley and Sumas reveal the 24-hour effect of daytime nucleation (Figures 5.9 and 5.10). The Ternary case adds particles during the day relative to the Binary and None cases. Although the number concentration decreases as the particles coagulate slowly over time, the elevated number of particles persists for all hours of the day. This is evident overnight on 25-26 August at Sumas and on 27-28 August at Sumas and Langley. When the ternary nucleation mode is processed, the number concentration is elevated relative to the Binary case in the daytime but only remains slightly elevated overnight. Once the sulfuric acid concentration decreases in the

late afternoon, many of the nascent particles are lost to the condensation sink. Ternary nucleation with no processing produces the best performance for most hours at Langley, while Ternary w/Processing performs the best at Sumas despite its nighttime underprediction.

Adding the v4.5 changes to CMAQ has very little effect on the results. Figure 5.11 shows an example of v4.4 and v4.5 number concentrations for ternary nucleation with processing. There are few hours when the v4.5 changes have an effect on the number concentrations. Even when they do, the effect is on the order of a few thousand particles in a concentration of typically 5000-50,000 per cm^3. The average change for a flight or ground station is at most 1000 particles (Table 5.2). The higher sulfate emissions in v4.5 increase the number and mass of emitted particles near sulfur sources. In urban areas where emissions of organics dominate, the effect of the mode merging fix is more obvious. At night, shifting more mass into the accumulation mode decreases the median diameter of the Aitken mode by 1-4 nm and increases particle concentrations by up to 15%. During the day in some areas on the edge of the urban plume, the increased surface area in the Aitken mode suppresses the effect of regional nucleation and decreases number concentrations relative to Ternary w/Processing in v4.4. The $PM_{2.5}$ mass is increased by 5% at the routine Washington ground stations with the addition of the two v4.5 updates. Overall, these changes are minor, and the results from testing these different versions of nucleation with CMAQ v4.4 can be considered valid for v4.5 as well.

The size distributions from the ground stations reveal the full performance of the None, Binary, Ternary, and Ternary w/Processing cases. The effect of the nucleation scheme has an obvious impact on the time-averaged distributions below 200 nm (Figures 5.12 and 5.13). Adding ternary nucleation increases the prominence of the Aitken mode, but it is the Ternary w/Processing case that best reproduces distinct Aitken and accumulation modes, the peak of the Aitken mode, and the prominence of the Aitken

mode relative to the accumulation mode. Above 200 nm, changes to nucleation have no effect on the size distribution.

The Ternary case produces a very prominent nucleation mode centered on 1.5 nm. Whereas CMAQ normally associates its i-mode with the Aitken mode, the CMAQ i-mode has been transformed into a nucleation mode. The large number of nucleated particles dominates the pre-existing Aitken mode. Because CMAQ is trying to accommodate a nearly monodisperse distribution at 1.5 nm and a lognormal mode at 15-40 nm with just one set of lognormal parameters, there is a significant tail of the distribution above 7 nm. This tail is responsible for the large number of particles in the observable size range in Figures 5.2-5.5 and 5.9-5.10, and it compensates for the underpredicted number in the accumulation and Aitken mode ranges. This explains the apparent paradox that ternary nucleation of 1 nm particles can produce more observable particles than ternary nucleation with processing to an observable size. In a sense, fitting a lognormal distribution has the same effect as applying nucleation mode dynamics to grow the particles to a larger size. This is not surprising given that the lognormal nature of natural aerosols is derived from the atmospheric processing that the Kerminen and Kulmala parameterization attempts to mimic. Ternary nucleation increases the number of particles in the accumulation mode to nearly the observed level, particularly between 70 and 200 nm. The improvement in the traditional Aitken mode range, 20-50 nm, is a by-product of the nucleation mode's large tail. At night, the Ternary treatment still improves performance in the accumulation mode range, but less so since the nucleation mode is less important at night relative to the daytime. In addition to eliminating the Aitken mode, it is clear that ternary nucleation with no processing achieves good number concentrations for the wrong reasons. Ternary nucleation by itself does not solve the problems CMAQ has reproducing the observed size distributions.

When the nucleation mode is processed to the Aitken size range, the result is a distinct Aitken and accumulation mode. The Aitken mode is centered around 10-15 nm and is relatively narrow in the daytime. This is closer to the observed Aitken mode at 20-

30 nm than the other cases. Its narrowness is the result of averaging many hourly size distributions that do not have a dominant Aitken mode with a minority of distributions that have a prominent mode at 10 nm (Figures 5.14 and 5.15). At Langley (Figure 5.12), CMAQ's averaged Aitken mode exceeds the observed Aitken mode in magnitude during the day. The match to observations of the accumulation mode's shape and magnitude are better than for Binary case but worse than for the Ternary case. This appears odd at first since Ternary w/Processing adds mass to the accumulation mode when the 1 nm particles are lost to coagulation. However, this would be difficult to see on the number distributions, and only a hint can be seen above 200 nm. At night the accumulation mode is too weak, but the overall shape is the best of the nucleation options. At Sumas (Figure 5.13), the daytime Aitken mode peaks at a lower diameter than observed and is too pronounced relative to the accumulation mode. The second of these problems lies with the accumulation mode because its concentration is an order of magnitude too low for both ternary nucleation options. At night the shape is good but the concentration is still too low in the accumulation mode. The Ternary w/Processing case produces distinct Aitken and accumulation modes and a better number result than the Binary case, but the size distributions have the best shapes at night when the effect of nucleation is reduced. Adding ternary nucleation and nucleation mode processing does not consistently solve the errors in CMAQ's size distributions.

The choice of nucleation model has a modest effect on aerosol mass and gaseous species. Adding ternary nucleation increases $PM_{2.5}$ by on average 0.5 $\mu g/m^3$ or 6% at the most polluted grid points near Vancouver and Seattle. However, $PM_{2.5}$ changes little on average in the Puget Sound and Lower Fraser Valley because decreases in sulfate mass are offset by increases in nitrate. Processing the ternary nucleation particles to the Aitken mode and conserving sulfur adds 1.3 $\mu g/m^3$ at the ground stations in Washington State and 0.3 $\mu g/m^3$ on average in the Puget Sound and Lower Fraser Valley. This increase is due nearly exclusively to equal increases in sulfate and ammonium mass (0.15 $\mu g/m^3$ or 15-20%). No other species changed appreciably between the Binary case and the Ternary w/Processing case. The mode merging and sulfuric acid emissions fixes in v4.5 increase

$PM_{2.5}$ by 0.1 μg/m^3. No gaseous species concentration is modified by more than 2% except ammonia in the Lower Fraser Valley where it decreases 5% as ammonia is drawn into the new sulfuric acid particles. Overall, the choice of nucleation algorithm increases $PM_{2.5}$ by less than 10% and has almost no effect on gaseous species.

5.4. Conclusions

The binary nucleation theory in the released version of CMAQ v4.4 does not reflect current knowledge of particle formation and processing. Version 4.5 updated some portions of its aerosol science but did not change the nucleation code, and it still produces very few particles during summertime Pacific Northwest conditions. The newer version may perform better in Eastern North America where sulfur emissions are higher, but it will still likely underpredict the number of nucleated particles. It is fortunate that CMAQ produces no particles near 1 nm because it does not have the ability to handle a fourth mode. Simply adding these particles in the Aitken mode would create an unrealistic lognormal mode that is a hybrid of the pre-existing Aitken mode and the fresh, nearly monodisperse nucleation mode. Including nucleation in CMAQ requires both an updated aerosol nucleation theory as well as including nanomode dynamics separate from CMAQ's three mode structure. This would be most successful scientifically with a sectional representation, but the goal here was to create an efficient model that could be widely used by the community for a variety of purposes.

Ternary nucleation of ammonia, water vapor, and sulfuric acid was implemented in CMAQ, and the new particles were processed with vapor condensation and particle coagulation to the model's pre-existing Aitken mode (i-mode). Ternary nucleation on its own produces millions of particles, but only a small fraction in the observable size range (greater than 6-9 nm for this study). When the observable number of particles is compared to actual observations, ternary nucleation with no nanomode processing produces the best overall results for particle number concentrations (Figure 5.16). However, this is because the tail of the unphysical hybrid of the nanomode and Aitken

mode happens to extend into the observable size range. Although such a tail mimics atmospheric processing, the resulting size distributions do not compare well to what was observed. Processing the particles from ternary nucleation produces a more appropriate Aitken mode. It peaks at a more realistic diameter, albeit still ~10-20 nm too small. Performance in the accumulation mode is less satisfactory and changes little from the standard Binary CMAQ case. Nighttime size distributions consistently have fewer particles in the ultrafine size range than observed. Particle number concentrations from the Ternary w/Processing case are the best of the nucleation options in some instances, but often they are little changed from the Binary case. Neither simple ternary nucleation nor ternary nucleation with processing to the Aitken mode solves the size distribution and number concentration issues for this case study.

This leads to the conclusion that including ternary nucleation and nanoparticle growth with sulfuric acid is not the complete solution. The addition of organics for nanoparticle growth would increase the growth rate and allow more particles to survive to the Aitken mode. Based on how ternary nucleation and sulfuric acid growth affected the size distributions, however, it is likely that this would further increase the overprediction in the 10-30 nm range during the middle of the day and do little to improve performance in the 30-200 nm range. Adding a complete representation of the nanomode as a h-mode in CMAQ instead of a parameterization could improve the results for particles less than 20 nm by accounting for all the interactions of the nanomode with itself and with other modes. The challenge is that the nanomode is the least likely of the common atmospheric aerosol modes to be lognormal. It is necessary to either accept this inaccuracy or include a sectional representation which would dramatically slow the model and reduce its usefulness. As our knowledge of atmospheric aerosol nucleation progresses, it will be possible to develop more advanced techniques for including the role of organics and better representing the nanomode. Until that time, the work included here is a large step forward in integrating nucleation in CMAQ and improving the aerosol size distributions, and it represents the state-of-the-art modeling for particle nucleation.

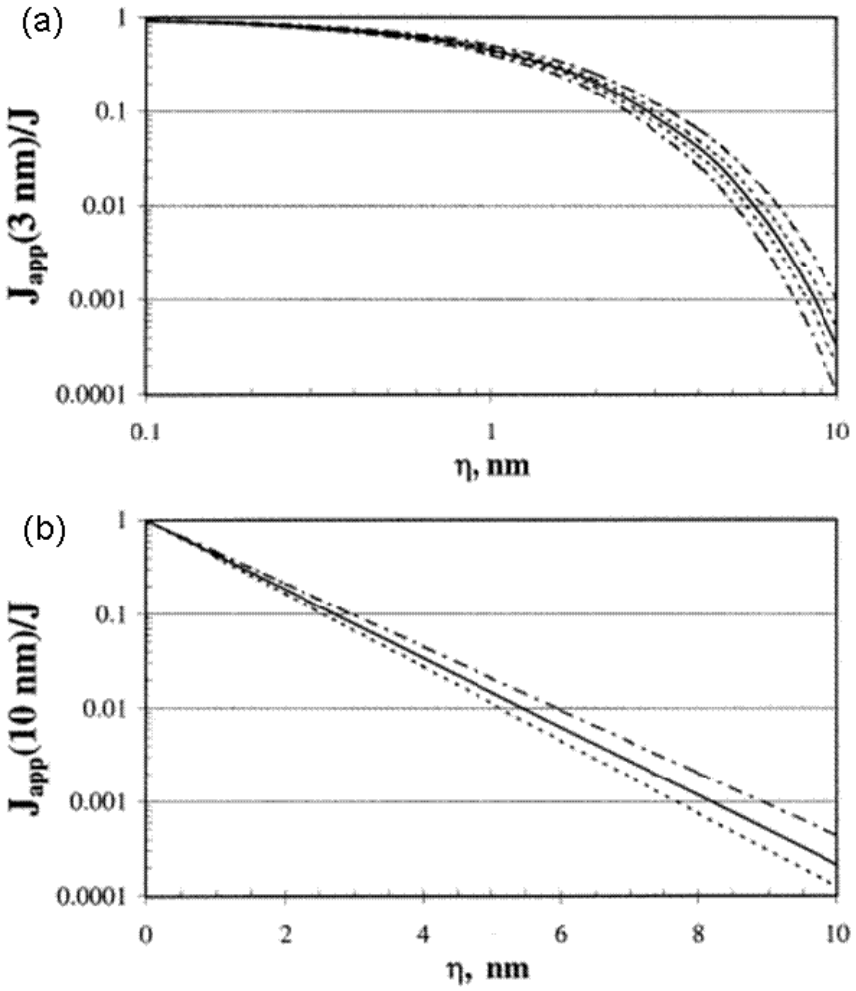

Figure 5.1 Ratio of the apparent and real nucleation rates as a function of η for (a) d_p = 3 nm and (b) d_p = 10 nm. From equation 5.4 and Kerminen and Kulmala (2002).

Table 5.1 List of Nucleation Simulations. The color corresponds to Figures 5.2-5.4 and 5.9-5.16.

Simulation	Nucleation Type	Nucleation Processing	v.4.5 Bug Fixes
None	none	none	no
Binary	binary	none	no
Ternary	ternary	none	no
Ternary w/Processing	ternary	yes, to 10 nm	no
Ternary w/Processing v4.5	ternary	yes, to 10 nm	sulfuric acid emissions, mode merging

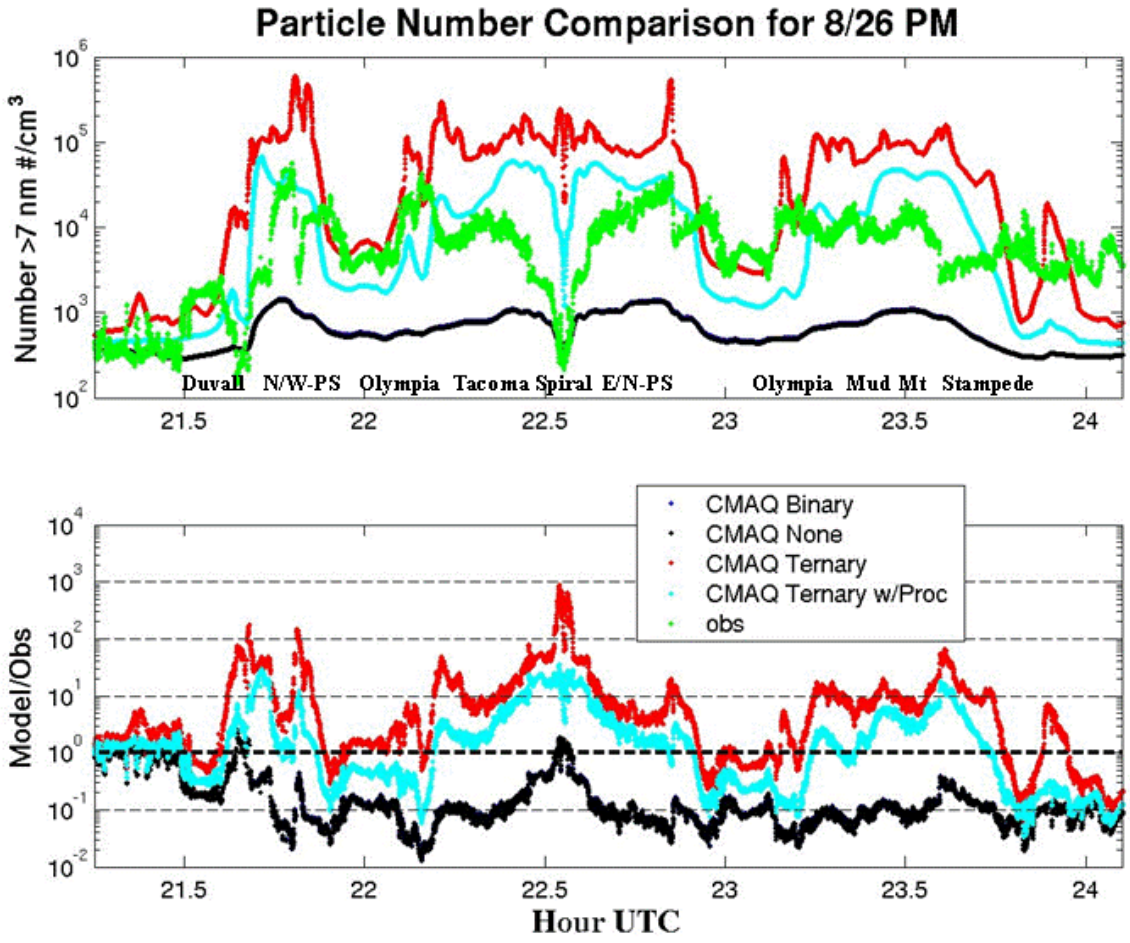

Figure 5.2 Comparison of CMAQ number concentration >7 nm (instrument lower detection limit) to observations on the afternoon of 26 August for the four nucleation options.

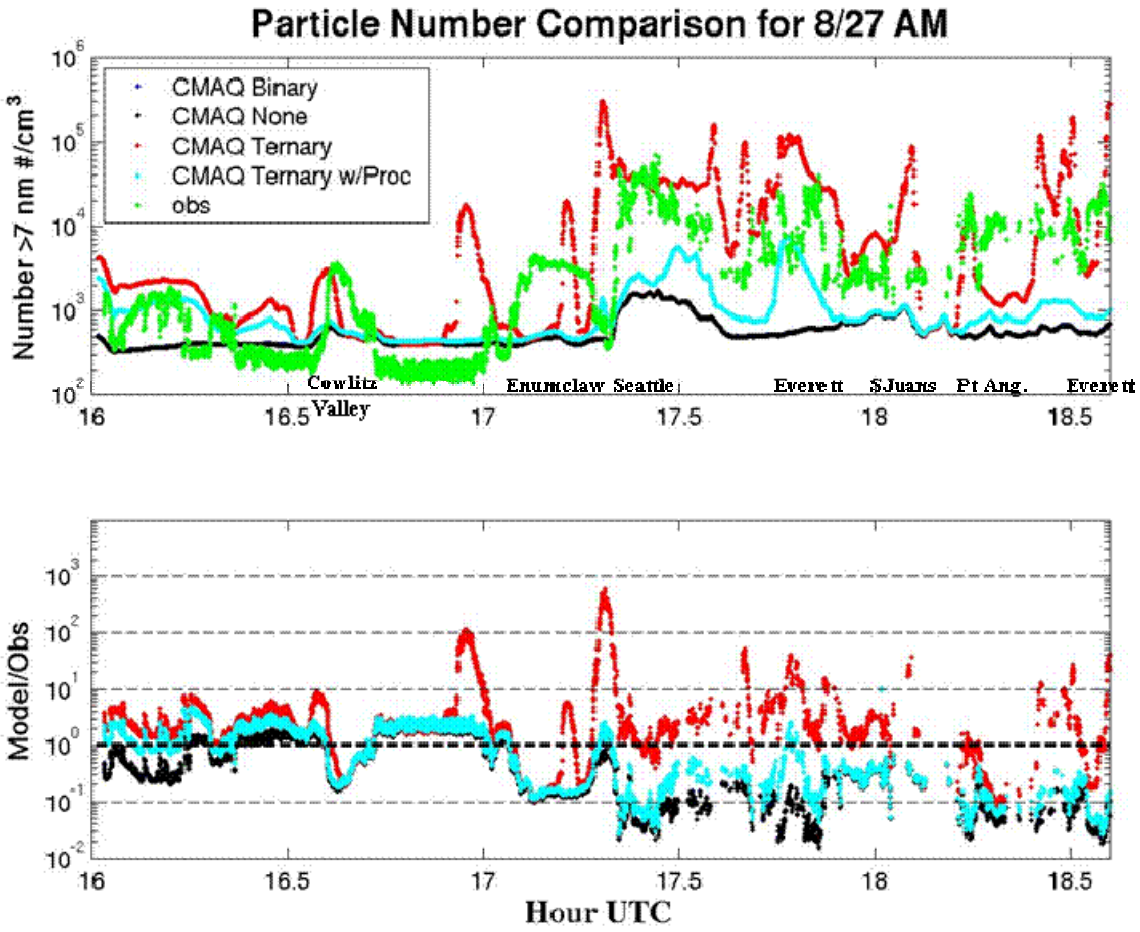

Figure 5.3 Comparison of CMAQ number concentration >7 nm (instrument lower detection limit) to observations on the morning of 27 August for the four nucleation options.

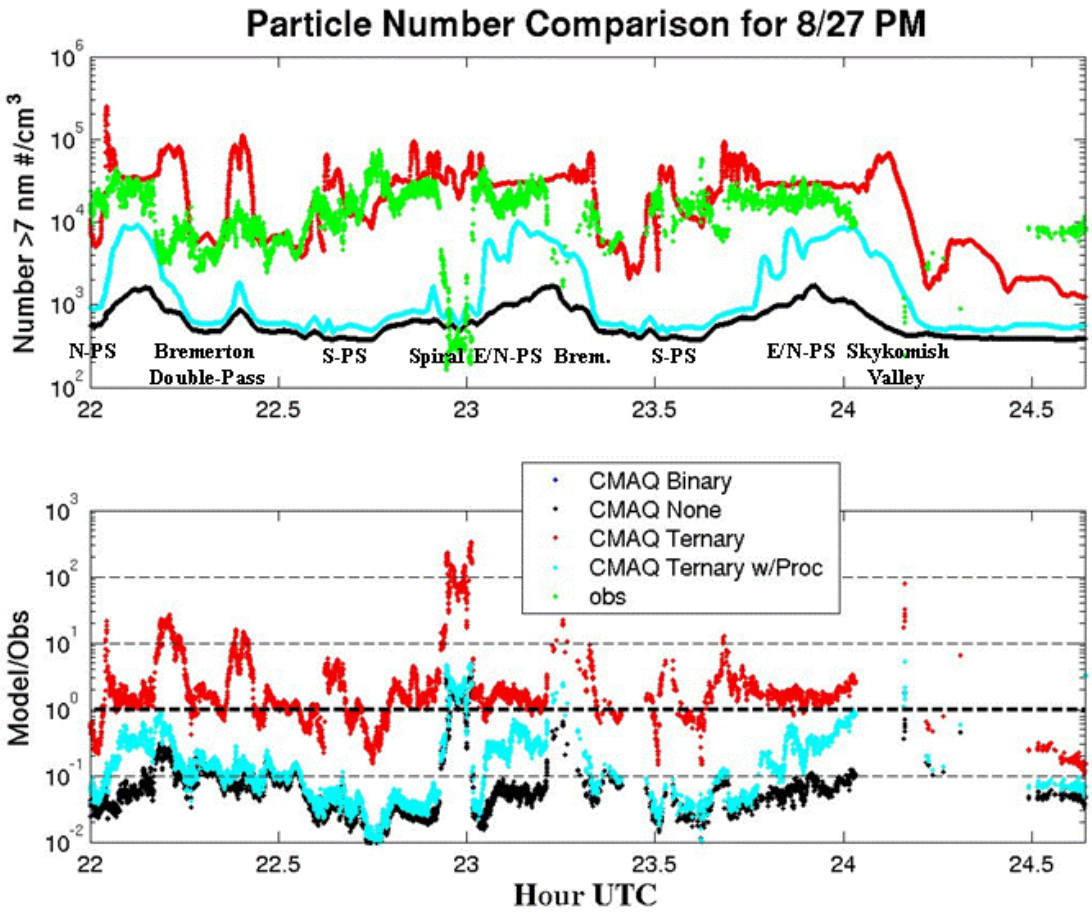

Figure 5.4 Comparison of CMAQ number concentration >7 nm (instrument lower detection limit) to observations on the afternoon of 27 August for the four nucleation options.

Table 5.2 Bias of CMAQ number concentration (1/cm^3) at observable sizes for five nucleation options and five observation periods. The Sumas average is limited to daytime hours.

	PNW2001 Aircraft			Pacific 2001	
	08/26PM	08/27AM	08/27PM	Langley	Sumas
Binary	-6,500	-4,000	-14,800	-11,700	-14,100
None	-6,500	-4,000	-14,800	-11,700	-14,100
Ternary	47,900	9,300	15,600	8,600	17,800
Ternary w/Processing	7,100	-3,500	-13,200	-9,500	-2,300
Ternary w/Processing v4.5 changes	6,400	-3,500	-13,800	-9,100	-2,000

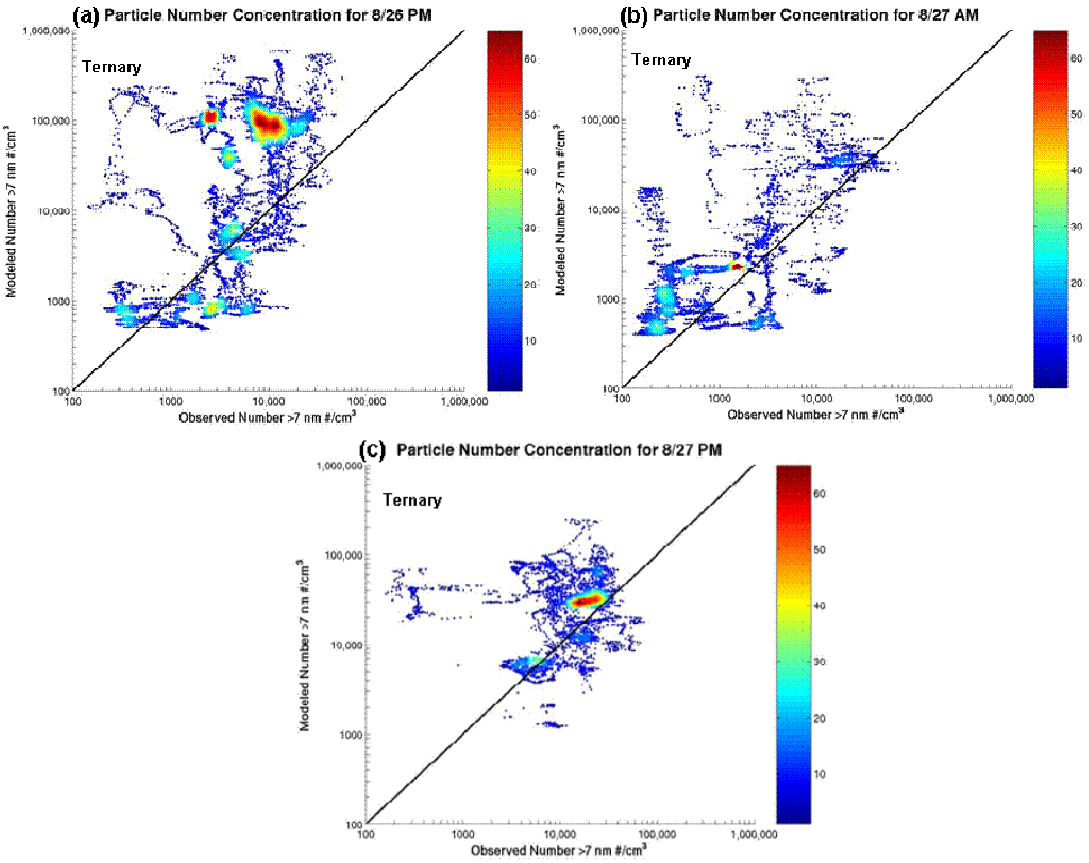

Figure 5.5 Observed number concentration versus "Ternary" modeled number concentration >7 nm (instrument lower detection limit) for: (a) afternoon of 26 August, (b) morning of 27 August, and (c) afternoon of 27 August. The color scale represents the relative density of points.

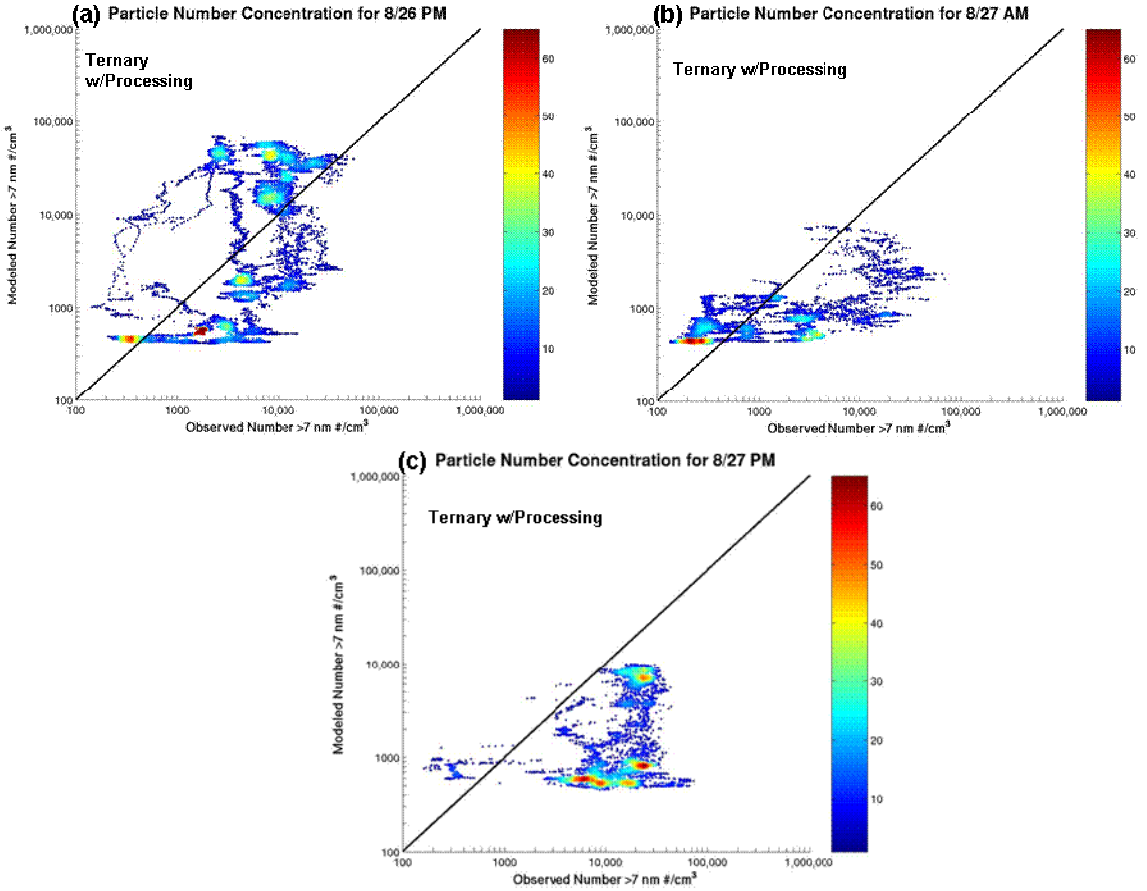

Figure 5.6 Observed number concentration versus "Ternary with Processing" modeled number concentration >7 nm (instrument lower detection limit) for: (a) afternoon of 26 August, (b) morning of 27 August, and (c) afternoon of 27 August. The color scale represents the relative density of points.

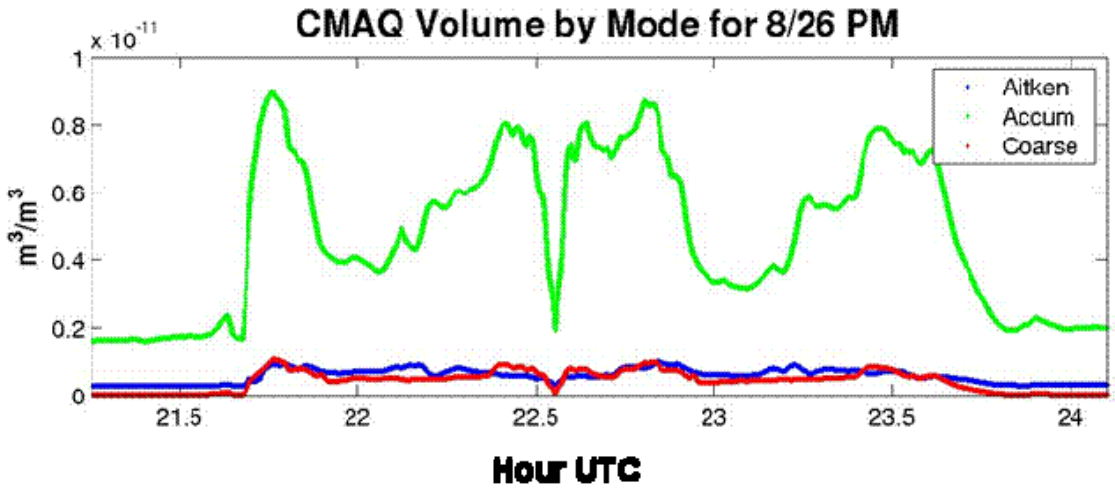

Figure 5.7 "Ternary with Processing" CMAQ volume for the PNW2001 flight on the afternoon 26 August in the Aitken, accumulation, and coarse modes.

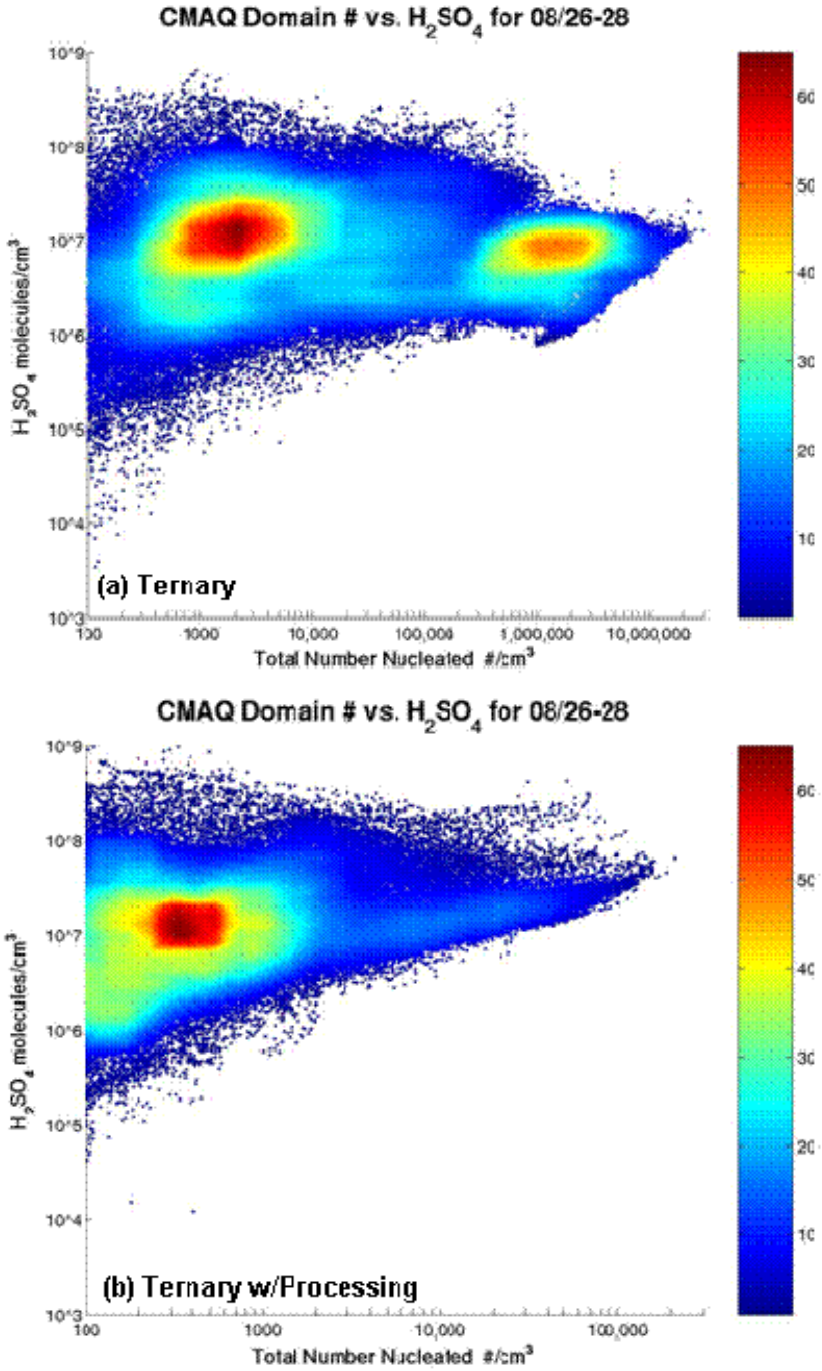

Figure 5.8 CMAQ domain-wide total number concentration of nucleated particles versus sulfuric acid concentration for the cases: (a) Ternary and (b) Ternary with Processing. The number of nucleated particles is estimated by subtracting out the Binary results. The color scale represents the relative density of points.

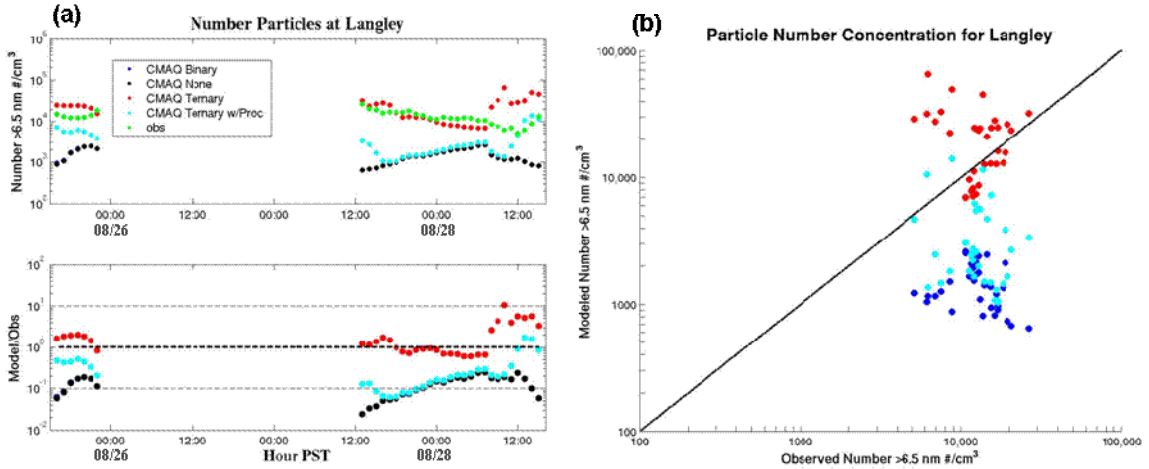

Figure 5.9 (a) Comparison of CMAQ number concentration >6.5 nm (instrument lower detection limit) to observations at Langley for the four nucleation options: (a) as a time series and (b) as a scatter plot.

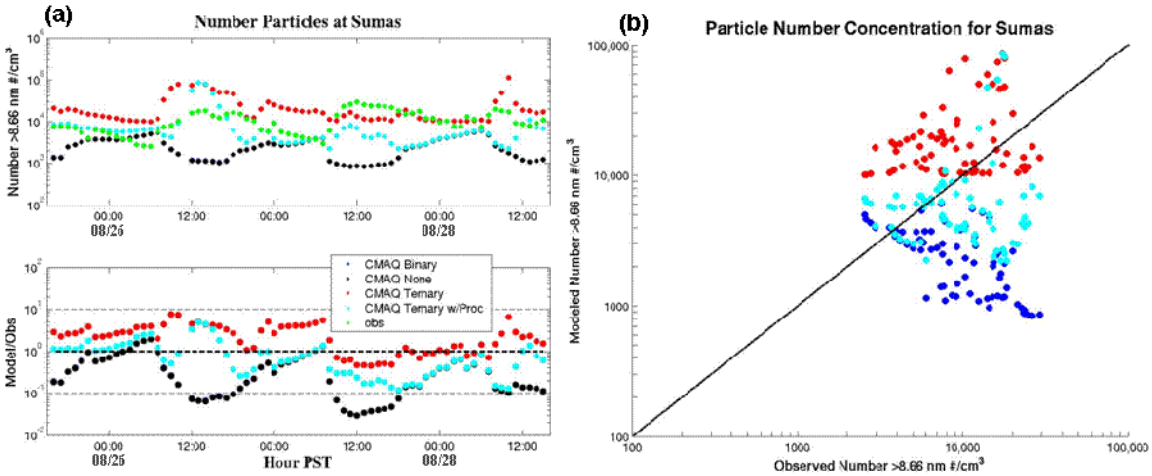

Figure 5.10 Comparison of CMAQ number concentration >8.66 nm (instrument lower detection limit) to observations at Sumas for the four nucleation options: (a) as a time series and (b) as a scatter plot.

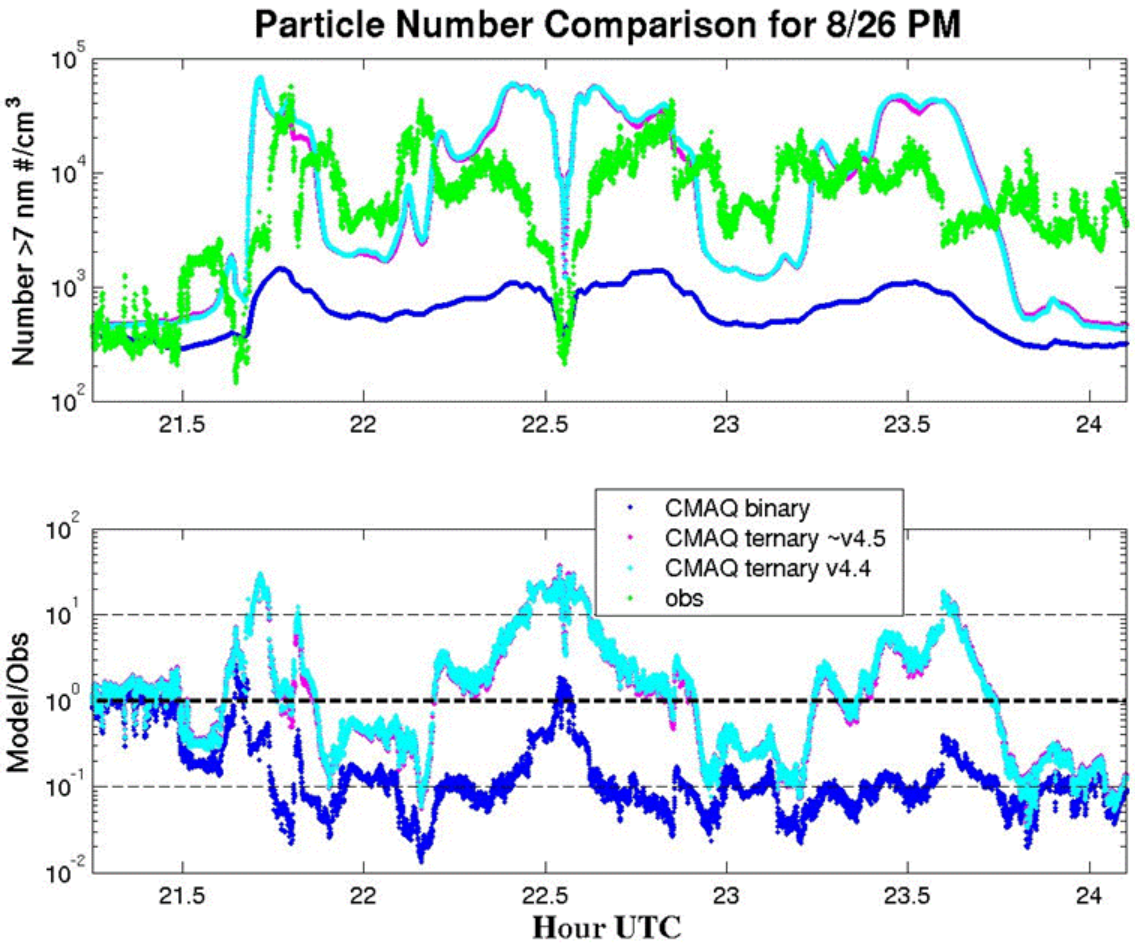

Figure 5.11 Comparison of CMAQ number concentration >7 nm (instrument lower detection limit) to observations on the afternoon of 26 August for the "Binary", "Ternary with Processing", and "Ternary with Processing v4.5" cases.

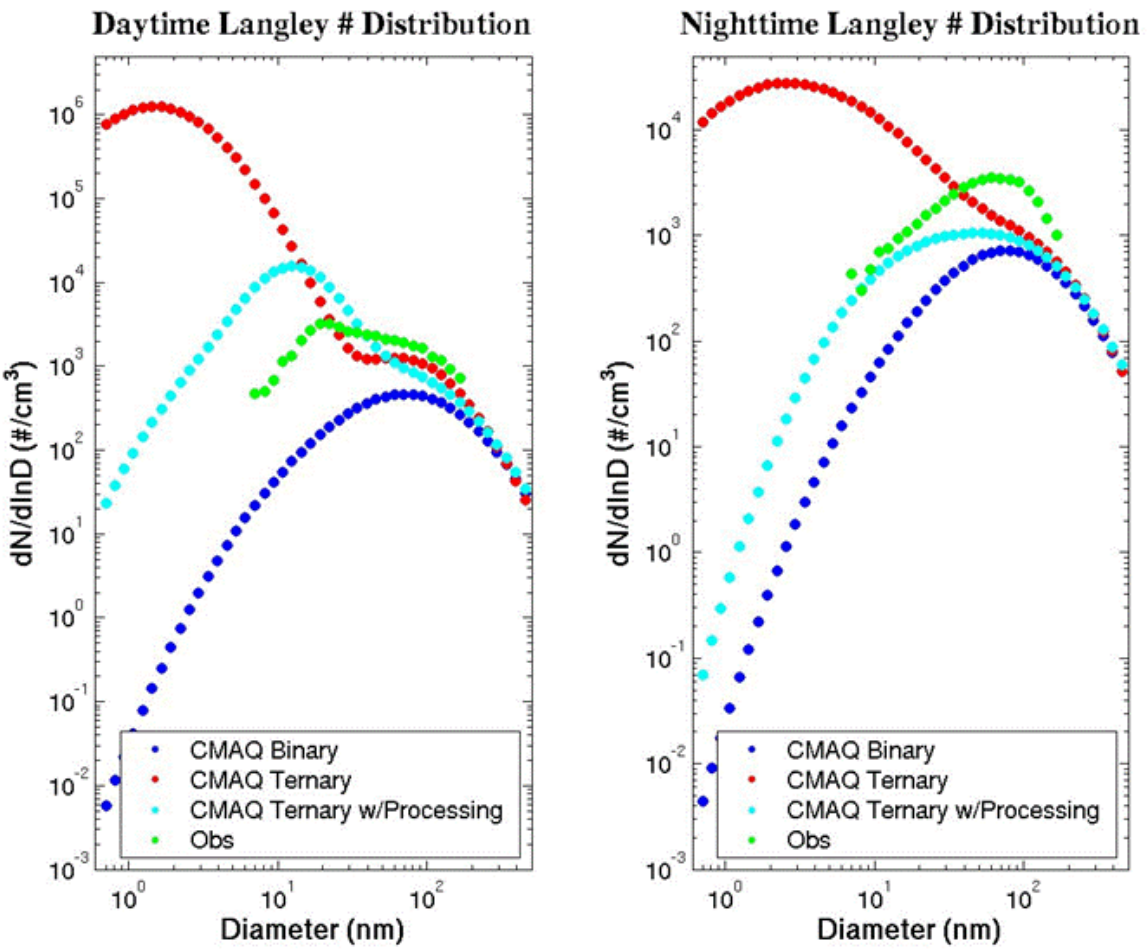

Figure 5.12 Day and night average number size distributions at Langley as observed and for the "Binary", "Ternary", and "Ternary with Processing" cases.

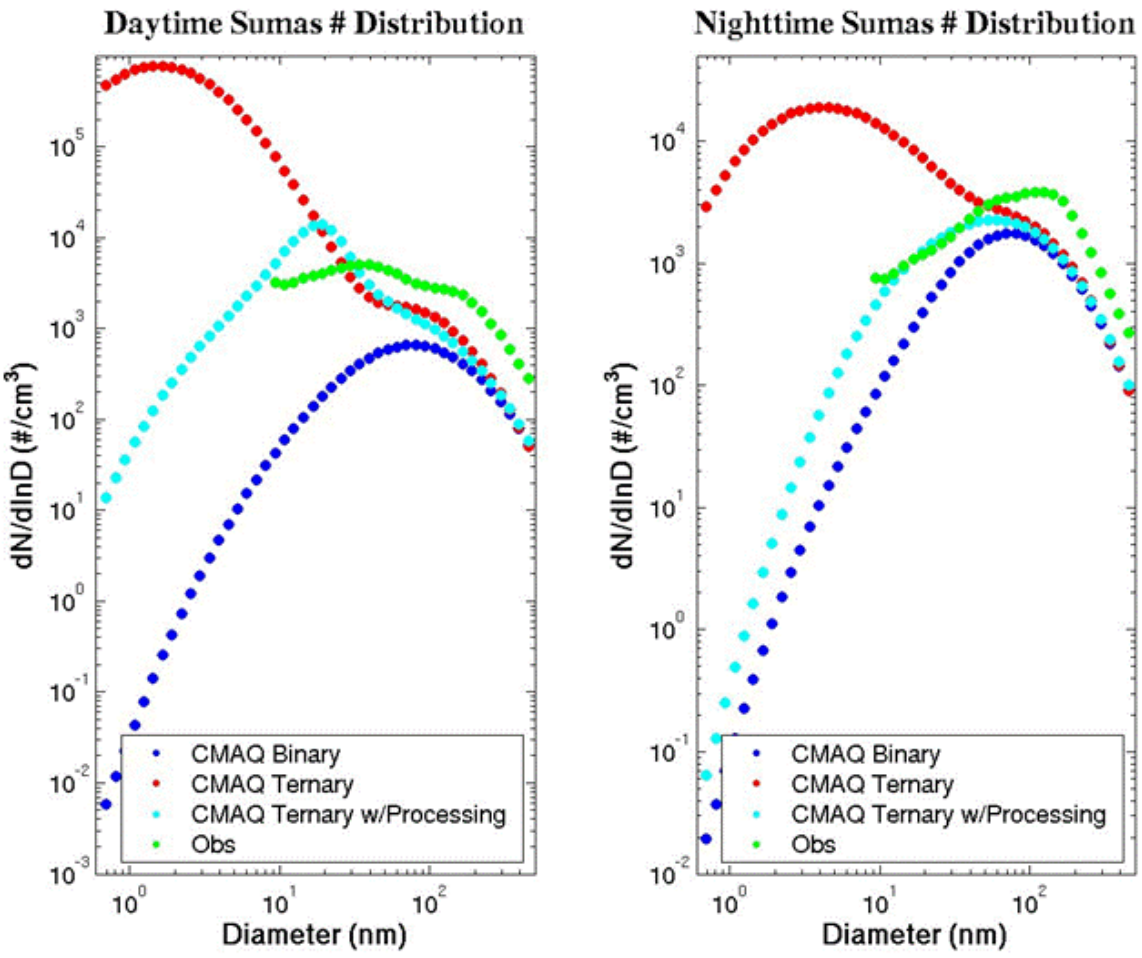

Figure 5.13 Day and night average number size distributions at Sumas as observed and for the "Binary", "Ternary", and "Ternary with Processing" cases.

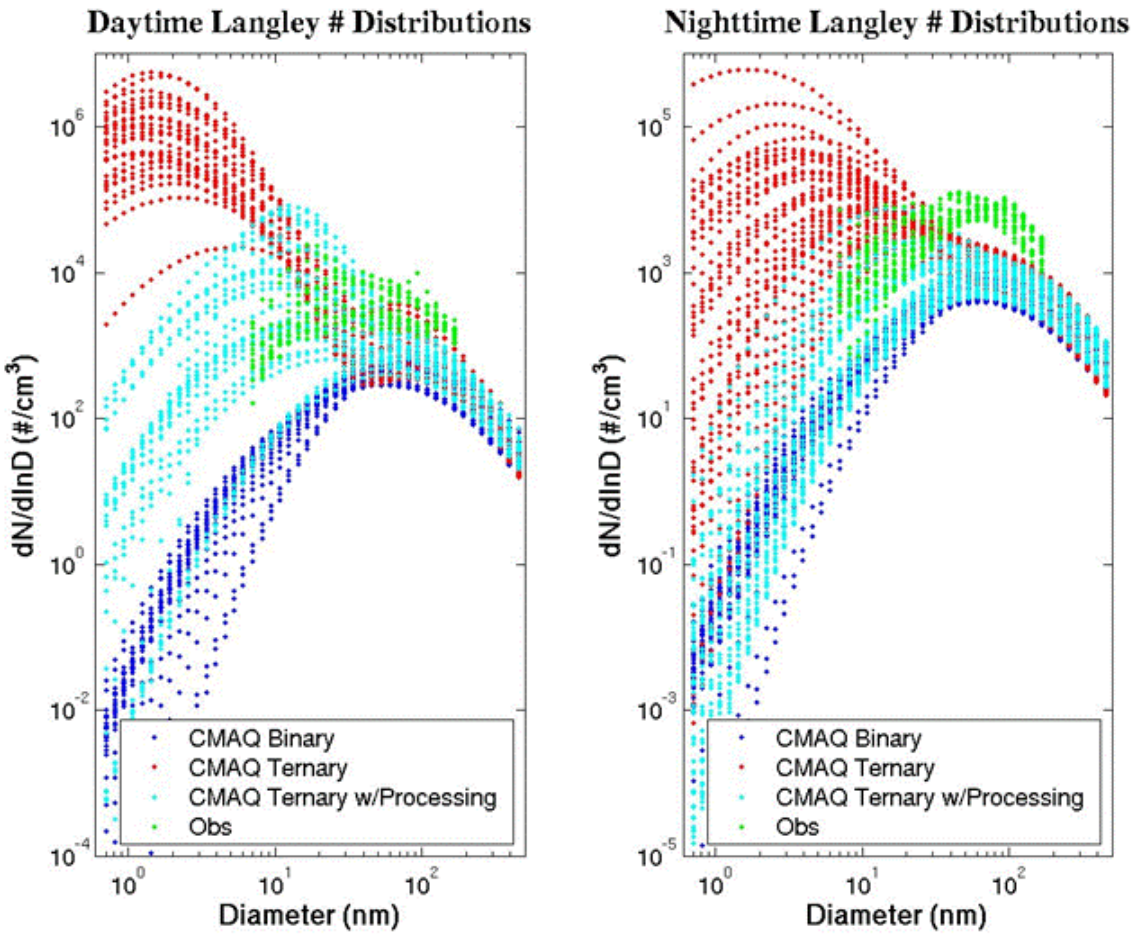

Figure 5.14 Day and night hourly number size distributions at Langley as observed and for the "Binary", "Ternary", and "Ternary with Processing" cases.

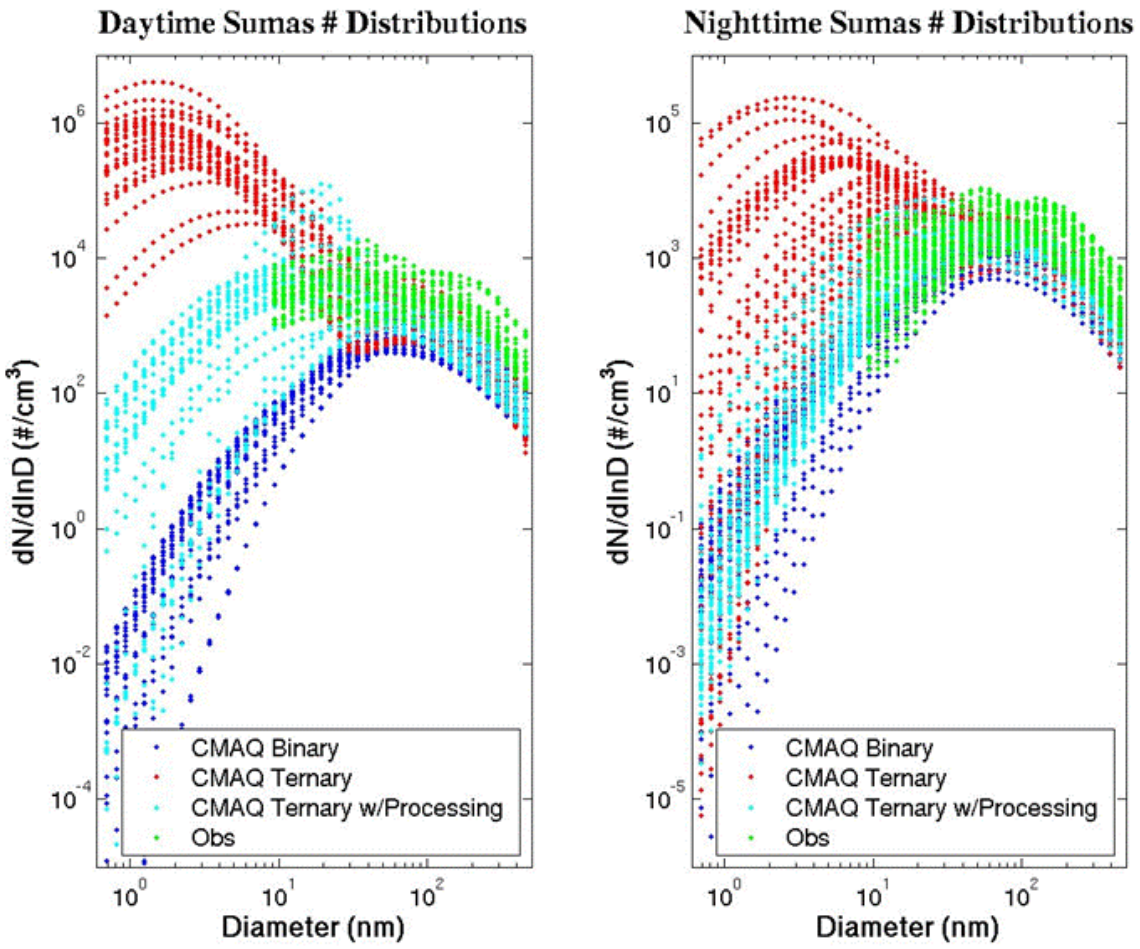

Figure 5.15 Day and night hourly number size distributions at Sumas as observed and for the "Binary", "Ternary", and "Ternary with Processing" cases.

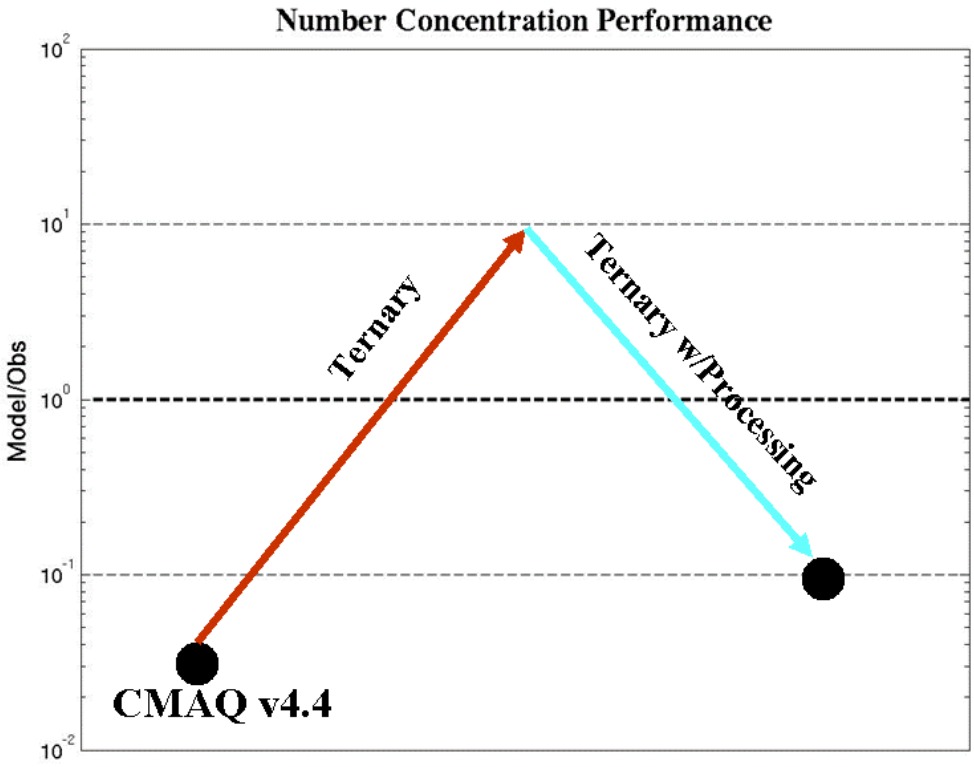

Figure 5.16 Summary of number concentration performance for the base CMAQ v4.4, CMAQ with ternary nucleation, and CMAQ with ternary nucleation and processing of the nucleated particles to the Aitken mode.

6. Emissions size distributions

6.1. Theory

Direct emission and nucleation from the gas phase are the two production pathways of ultrafine particles. An error in the emission aerosol size distribution, especially in the ultrafine range, is a potential cause for the large, consistent underprediction of aerosol ultrafine number because CMAQ uses nearly identical emission size distributions for all sources, locations, and times. Furthermore, these distributions are based on woefully outdated measurements and an inappropriate spatial scale.

CMAQ's emission size distributions come from a review by K. T. Whitby (1978) which compiled measurements from field campaigns in the 1960s and 1970s. Most, if not all, of the distributions were measured with the Whitby Aerosol Analyzer (WAA). This instrument typically measured 8 size bins less than 100 nm with centers of 8.75, 12.5, 17.5, 25.0, 35.0, 50.0, 70.0, and 90.0 nm. There is considerable uncertainty in the Aitken mode median diameter as measured by the WAA, and the WAA measured a monodisperse aerosol as having a modal standard deviation of typically 1.3. The charging and counting efficiency of the instrument became quite poor for particle diameters less than 20 nm (Whitby et al., 1972). Counter to this, modern sizing instruments such as the Scanning Mobility Particle Sizer (SMPS) typically have 30-60 size bins below 100 nm (e.g., Hogrefe et al., 2006) and accurately count particles typically down to 10 nm or as low as 2.5 nm (Heim et al., 2004). The SMPS and other modern instruments improve our understanding of the Aitken mode and the size distribution of emitted particles.

Especially because of the better counting sensitivity below 20 nm, it is likely modern instruments will estimate a much larger contribution to the overall size distribution from the Aitken mode and will, for the same emitted mass, produce more particles. Updating the emission size distribution to reflect measurements from modern instrumentation will improve the model science and potentially reduce CMAQ's number underprediction for the PNW2001 / Pacific 2001 case study.

Once the search has begun for appropriate size distributions, there is the question of what the term "emission" means for a mesoscale modeling study. K. M. Zhang et al. (2005), Ketzel and Berkowicz (2004), Gidhagen et al. (2005), and Jacobson and Seinfeld (2004) have all recognized that the term emission, especially for particulate matter, is dependent on the scale of interest. For power plants, emissions are measured at the top of the smoke stack rather than where the fuel is combusted; similarly for on-road mobile sources, emissions are typically defined with measurements taken after the exhaust exits the tailpipe. These emissions measurements have a spatial scale of meters and a time scale of a few seconds. This is a convenient scale since it lumps together all the processes that do not depend on atmospheric conditions, other than the effect of temperature on engine and catalytic converter operating efficiency.

Diesel and gasoline combustion produces a complex mixture of solid carbon, volatile unburned fuel and lube oil, metal and fuel oil ash, and sulfur in various stages of oxidation (Kittelson, 1998; Schauer et al., 1999; Kuhn et al., 2005; Kis et al., 2006). As the exhaust travels from the combustion source in the chamber through the tailpipe, catalytic converter, and muffler, the mixture of solids, liquids, and gasses undergo significant chemical and physical processes: nucleation of elemental carbon chains, cooling and condensation of semivolatile species, particle fragmentation, deposition on the walls of the exhaust system, and chemical reaction in the tailpipe and catalytic converter (Kittelson, 1998; Burtscher, 2005; Harris and Maricq, 2002). Vehicle type, fuel type, engine condition, emission control devices, and driving conditions all affect the role of these processes. Measurements after the tailpipe parameterize both combustion and

processing to the 1-10 m scale as emissions processes. Although mobile sources are used as an example here, a similar discussion applies for point combustion sources of all sizes. All transformations beyond the measurement at the mobile source tailpipe and the point source stack require consideration of the ambient air chemical composition and the meteorological conditions.

A mesoscale air quality model such as CMAQ cannot directly treat spatial scales below its grid resolution. CMAQ takes the inventory emissions in a grid cell and averages them throughout the entire cell. Hence, emissions on a spatial scale of a few meters are immediately transformed into emissions on the scale of several kilometers. Any processing that would occur to the plume as it dilutes and ages from the tens of meters to the 4 km or greater scale is ignored. This can be an important omission for the aerosol composition and aerosol mass (e.g., Volkamer et al., 2006), but it is critical for the size distribution and especially the ultrafine number concentration since multiple processes act to modify submicron particles on the these spatial scales.

For example, particle nucleation occurs when the concentrated gaseous emissions from a sulfate source produce high sulfuric acid supersaturations. Right out of the smoke stack, the plume is too concentrated in NO_x to efficiently produce the OH radical for converting SO_2 to sulfuric acid (Brock et al., 2002), and the pre-existing condensation sink may be large enough to accommodate the small amount of sulfuric acid available for condensation. Farther downwind, dilution on the edges of the plume lowers the NOx/VOC ratio, increases the OH concentration, decreases the condensation sink, and leads to new particle production. The dilution process for creating condensable vapors can take up to an hour and depends on available sunlight, atmospheric turbulence, and water vapor concentration (Wilson and McMurry, 1981; Hewitt, 2001). As the plume continues to dilute, nucleation can occur nearer the center of the plume. All of this occurs on the scale of tens of meters to 1 km and so is missed by the CMAQ mesoscale grid. Only regional nucleation will be captured on typical CMAQ scales (4 km or greater) and by the nucleation algorithm in Chapter 5.

Emissions from a tailpipe cool and dilute quickly in the turbulent road environment (Kittelson, 1998; Burtscher, 2005; Zhang and Wexler, 2004a). Since laboratory mobile emission experiments are only rarely able to reproduce typical roadway dilution ratios of 1000:1 in a few seconds, observations from vehicle chase, roadside, and tunnel experiments, along with model studies of the roadway environment, have contributed to our understanding of road processes under real conditions. Model studies suggest that turbulent mixing, dilution, and cooling result in spikes of observable new particle production especially from diesel exhaust (Zhang and Wexler, 2004a). In road tunnels and during low-wind speed conditions that preserve very high number concentrations, coagulation and deposition of nucleation mode particles play significant roles (Zhang and Wexler, 2004a; Gidhagen et al., 2003; Gidhagen et al., 2004a, 2004b). The roadside environment is difficult to measure and model but includes important stages of aerosol processing.

As the plume leaves the roadside environment, travels downwind, and mixes with the surrounding sources over the next few minutes and few hundred meters, particle concentrations decrease (Zhu et al., 2002a, 2002b; Shi et al., 1999; Gramotnev and Ristovski, 2004). Although Zhu et al. (2002a, 2002b) attributed the decrease in particle number to coagulation, modeling studies by Zhang and Wexler (2004b), Jacobson and Seinfeld (2004), Shi et al., (1999), and Gidhagen et al. (2004a) showed that the time scales of coagulation and deposition for typical roadway particle concentrations and size distributions are too short to account for the change. Instead, dilution with relatively clean ambient air accounts for the majority of the decrease in number concentration with distance from the road environment. Thus, the lifetime of nucleation mode particles is less than an hour (Bukowiecki et al., 2003).

Dilution on the scale of hundreds of meters can significantly modify aerosol size distributions. Because the fresh plume is enriched with smaller particles relative to the ambient plume, dilution can cause an apparent shifting of the nucleation and Aitken

modes to larger sizes. Also, as the plume dilutes, species that remain supersaturated continue to condense onto the existing particles, particularly those in the accumulation mode, while some species drop below saturation and begin to evaporate. The saturation vapor pressure depends on the Kelvin Effect and Raoult's Law for each particle's size and composition. Because of their greater surface to volume ratio, the diameter of smaller particles grows faster than for larger particles during condensation and also shrinks faster during evaporation. A population of particles composed of different chemicals may have some particles growing through condensation while others are evaporating, and will be experiencing a range of condensation and evaporation rates. The net effect for an externally mixed population of particles is to broaden the size distribution (Zhang and Wexler, 2004b). Evaporation of semivolatile components in 10-30 nm diameter particles has been postulated to increase the particle coagulation rate and scavenging to the accumulation mode (Jacobson et al., 2005). It has also been postulated to cause particle fragmentation of the nonvolatile carbon chains, increase the particle number, and shift the Aitken mode to smaller sizes (Gramotnev and Gramotnev, 2005a; Gramotnev and Gramotnev, 2005b). At distances farther from the road, the role of these changes slows as the concentration gradient between the plume and the entraining ambient air relaxes.

Following the changes near to the actual emission, aerosols experience significant changes to their size distributions on several additional scales still smaller than the typical mesoscale air quality model. The goal of this chapter is to develop a scientifically defensible, accurate, simple, and fast method to represent aerosol processing on these scales.

Aerosol chemistry and dynamics between the scales of meters and kilometers can be accounted for by modeling them either as part of the atmospheric processing or by including them in the emissions process. The mesoscale air quality model cannot satisfy the first option because it is unrealistic to create a nested domain with a grid resolution of meters to tens of meters for an entire urban area. In addition, parameterizations and assumptions in the atmospheric dynamics in these models are not appropriate for scales

below 1 km. Two potential modeling approaches are a plume model for one or several sources and a general spatial- and temporal- aging model. Alternatively, to fold this scale into the model emissions (as distinct from the air quality model itself), measurements of sources at 4 to 15 km distance can effectively parameterize emissions on the mesoscale, just as measurements after processing to the end of the tailpipe or to the roadside environment parameterize smaller scales. These three options are examined in more detail.

Plume models have effectively simulated near-field pollution plumes on the roadside, near-field (100 m – 1 km), and far-field (1 km – 50 km) scales. At the roadside scale, computational fluid dynamic (CFD) models use the nongeostrophic equations of motion and estimates of turbulent dispersion to calculate the flow of a plume in a complex environment at scales well below 1 km. Chemical and physical transformations for gaseous pollutants and aerosols can be calculated separately and superimposed on the modeled plume. For example, Gidhagen et al. (2003; 2004a; 2004b) used an aerosol dynamics model, MONO32 (Pirjola and Kulmala, 2000), to model ultrafine aerosol in four size sections in a Stockholm, Sweden street canyon. At the near-field scale, the U.S. EPA's Industrial Source Complex Short-Term model (ISCST3) (U.S. EPA, 1995) and it successor, the American Meteorology Society and EPA Regulatory Model (AERMOD) (Cimorelli et al., 2005), are popular dispersion models despite their neglect of aerosol dynamics. K. M. Zhang et al. (2005) partially include aerosol dynamics by linking the CALINE4 line-source roadway dispersion model (Benson, 1992) and UCD 2001 plume-source roadway dispersion model (Held et al., 2003) to a simple aerosol dilution scheme in order to investigate processing downwind of a Los Angeles freeway.

Far-field or regional models include treatments for sub-grid aerosol plumes. CMAQ, for example, contains a plume-in-grid option that includes aerosol chemistry similar to that in its Eulerian grid (Gillani and Godowitch, 1999; Godowitch, 2005), but in its current configuration, this option is more appropriate for larger plumes within a very coarse grid (36 km grid spacing or greater) rather than the meters to kilometers scale.

CAMx (ENVIRON, 2006), a regional air quality model similar to CMAQ, includes aerosols in their plume-in-grid scheme but only for the relatively simple 2-mode model. The most complex model for the sub-grid, far-field plume is CMAQ-MADRID-APT, a version of CMAQ for which the Second-order Closure Integrated puff model (SCIPUFF) with CHEMistry (SCICHEM) framework and the MADRID aerosol module have been integrated as a plume-in-grid tool into CMAQ-MADRID (Karamchandani et al., 2006).

Although tools exist for modeling the transformation of each plume from the source to the mesoscale grid, modeling each of the thousands of sources in an urban area and all of the plume interactions is infeasible. Each vehicle on a freeway produces its own plume and would need to be modeled separately until it merged with other vehicle plumes and other nearby sources. Modeling each plume in one road link and the consolidation process of all the plumes in the link could easily involve a computational demand equal to modeling the entire mesoscale Eulerian domain. Therefore it is advantageous to parameterize the roadside environment as an emissions process and treat each roadway as a plume. However, even lumping roadways within 100 m as one plume will slow the air quality model to the point of being unusable. This is just one example of the difficulty. Other major plumes from power plants, heavy industry, light industry, railroads, and ships must also be incorporated. The task quickly overwhelms current computing capabilities.

One alternative is a general spatial- and temporal- aging model. It strips out the spatial dimension from an aerosol model, models the transformation from the traditional emissions scale to the mesoscale abstractly in time, and applies characteristic changes to the sum of all the plumes in each grid cell. There are several ways to do this that represent a range from a few general atmospheric environments to the specific conditions at each grid point and time step in the case study. The most general would use an off-line model to determine how a plume from an average source (traffic, coal power plant, gas power plant, refinery, etc.) ages over the typical transition to the mesoscale for typical meteorological conditions like day/night, stagnant air, clear and sunny, cloudy and

windy, etc. Aerosol processing under various regimes could be applied to the emission sources before these emissions are input to CMAQ. The most specific application would be to run the temporal-aging model for a few different classes of sources for the specific meteorological conditions in each grid cell every hour. In this case, the advantage in speed over a full plume-in-grid model is that only a few realizations would be needed per grid cell rather than three-dimensional modeling for tens, hundreds, or thousands of plumes in each cell. These techniques would bridge the gap in scale between emissions and the mesoscale model without an unrealistic computational demand while at the same time accounting for meteorology.

While this solution treats the tailpipe or smoke stack as the point of emission and models the transformation to the mesoscale, another avenue is to parameterize every process that occurs on a scale below the resolution of the air quality model grid as "emissions" based on measurements and empirical models. This includes particle nucleation, coagulation, deposition, evaporation, condensation, and dilution. Scale parameterization concepts similar to this are used in cloud and boundary layer modeling where cloud processes and boundary layer turbulence have spatial scales much smaller than the typical model grid resolution. Moreover, such parameterization assumptions are already implicit in traditional emissions estimates for processes occurring between the combustion chamber and the end of the tailpipe or smoke stack. The task in this paradigm is to find high-quality measurements that represent 4-15 km distance from all the sources of interest. The difficulty is that a measurement from one source and one location may not represent the emissions from all sources of this kind, or even the same source at a different time under different atmospheric or operating conditions. However, one clear advantage is that these measurements exist and can be relatively easily incorporated into a modeling system now with little or no degradation in model speed, whereas even a simplified modeling solution would require significant development and testing and would make the overall modeling system less efficient. Either a modeling or measurement solution would be an improvement over the current strategy of ignoring the problem entirely. But because an overarching theme of this project is to quickly improve

size distribution modeling within the constraints of an efficient, usable model, the solution employed here is to parameterize all processes below the 4 km grid as emissions and use measurements on this scale as the size distributions of emitted primary aerosol.

6.2. Methodology

This study contains published and unpublished size distribution measurements that represent major urban sources. The focus is on improving size distribution modeling generally for industrialized, urban areas, but since the modeling for this study is centered on the Pacific Northwest, there was particular interest in characterizing the major sources in this area: (1) an urban core dominated by transportation, light industry, and residences; (2) coal-fired power plants; and (3) large, marine transport. It is not possible to separate the individual urban sources further because they will all have mixed into one plume at the 4-15 km scale. The criteria for including published results were that the data had to be measured with instruments capable of characterizing the Aitken mode and that the measurements had to represent source emissions on the 4-15 km scale, or at least had to provide an upper or lower bound on size distribution properties on this scale. Ideally, the datasets average across multiple years, seasons, and common weather patterns, but in reality this is rarely achieved since often the datasets are very limited in time. Another objective was to find a distribution of available measurements that would accurately reflect mid-latitude emissions from a developed city dominated by transportation and light industry. Most of the size distribution measurements in the past decade have been taken in North American cities with high pollution levels or in European cities with a university active in aerosol research. They are not as representative as would be desired, but they cover a range of mid-sized and large cities.

In all, 53 published studies and one unpublished study reported size distributions that meet the criteria. A summary of the datasets is given in Tables 6.1, 6.2, and 6.3. In some cases one journal article contains measurements from multiple distinct locations. Sometimes several journal articles represent data from the same site, even the same exact datasets, but either subset them differently, analyze them differently, or process different

time periods. For instance, Ketzel et al. (2003) presented distributions from the rooftop of the H. C. Ørsted Institute in Copenhagen, Denmark for 11 weeks between May and November 2001 for the purpose of separating street canyon mobile emissions from the urban background; Ketzel et al. (2004) published distributions from the same site for four weeks over 3 months in order to compare the roof-top observations to curbside and rural size distributions; and Ketzel and Berkowicz (2004) combined two years of observations at this site into one average distribution. All three reported urban background distributions from the same site but used different time periods, presented the data differently, and concluded slightly different size distribution parameters. In general, unless two articles display the same data analyzed in the same manner, the methodology here was to treat the dataset in each journal article as separate datasets as well as to treat each location within one journal article as separate datasets.

In addition to the issue of biasing toward locations where studies have been located, having multiple datasets from the same location may further bias the averaged results. However, this issue pervades many aspects of urban scale observations, and there is little that can be done to eliminate all sources of bias. Observations are already biased towards neighborhoods which have been studied rather than an adequately representative number of locations within each city. There is a wide range in how representative a dataset is for all meteorological scenarios at the site, how well a sampling site truly represents the urban background in a location, and how completely the data have been analyzed for the size distribution's characteristics. While it is tempting to make subjective and somewhat arbitrary decisions about weighing datasets, this study took the simple approach of averaging all with equal weight so long as they met the minimum criteria for a well-instrumented urban background site. Then, if the results were reasonably consistent with datasets that are very well understood and trusted (e.g., Wehner et al., 2002; Larson et al., 2006; and Brock et al., 2002), they were accepted. This has a practical justification since, as will be seen later in the analysis, the data from only a few of the highest quality datasets reproduce the entire variability in all the studies.

6.3. Results of Search for Emission Size Distributions

Thirty-seven of the qualifying journal articles contain 44 distinct urban datasets (Table 6.1). Many of these are claimed to represent traffic emissions at the kilometer scale but did not come with chemical analyses to prove this nor were statistical techniques employed to separate source-specific size distributions. Though the sampling site may in fact be dominated by traffic emissions, only three publications presented distributions segregated by sources (Larson et al., 2006; Zhou et al., 2005a; and Zhou et al., 2005b), and one publication (Zhang and Wexler, 2004b) sampled on the kilometer scale but near such a concentration of freeway traffic as to be sufficiently dominated by mobile emissions. The sample duration varied from five days (Zhou et al., 2005a) to six years (Hussein et al., 2003) with an average of 14 months, and the locations ranged from roof-top sites (e.g., Ketzel et al., 2004) to sites in city parks surrounded by a variety of streets, arterial routes, and freeways (e.g., Zhou et al., 2005a). Most datasets come from mid-latitude American and European cities that are no longer dominated by industrial emissions. Obtaining cities with these characteristics was an objective of the study and was achieved by chance. In the United States, the cities sampled were Atlanta, Baltimore, Los Angeles, Pittsburgh, Rochester, and Seattle. The European cities tend not to be the large, polluted capitals. Instead, they are Central and Northern Europe urban areas where universities have dedicated resources to aerosol sampling. Other continents are represented by Nagoya, Japan; Santiago, Chile; and Brisbane, Australia. Ideally, the total sample would include a better representation of industrialized cities, but at least there is an adequate sample size.

Few investigators have measured the aerosol size distribution, including the ultrafine range, from coal-fired power plants. One reason for this is the difficulty in sampling transient, heterogeneous plumes. The chemistry at the center and at the edges of the plume can vary dramatically. Aircraft fly through an entire plume in less than a minute, while it can take at least that long to adequately sample the size distribution. Since many sizing instruments sequentially measure the number of particles in each bin over the period of a few minutes, there is a danger that one size range of the measured distribution

represents a different aerosol environment than another size range. The problem is compounded by the challenge of drawing very small particles from the ambient plume through an aircraft inlet into the sampling system. Much of the airborne plume research effort has gone into characterizing aerosol mass and sulfate gas-to-particle conversion rates because of these complications as well as to address $PM_{2.5}$, acid deposition, and regional haze. A small minority of these studies have presented aerosol size distributions for all sizes of particles at 4-15 km processing from the source.

Thirteen studies representing 17 coal-fired power plant datasets met the needs of this study (Table 6.2). This number is higher than if the criteria for inclusion were stringently enforced. This study would normally require ambient sampling at 4-15 km distance, but only a small number of studies met this criterion. Thus, three laboratory studies (Teinemaa et al., 2002; Dekati Ltd., 2003; and Lipsky et al., 2004) were included where conditions of dilution and residence time represented the mesoscale. Two of the laboratory studies and one ambient study were conducted in Europe, while 12 ambient datasets and the remaining laboratory dataset were collected in the United States and Canada. Because a power plant's downwind effluent can depend on the type of fuel burned, on air pollution control equipment such as scrubbers, on atmospheric mixing, and on UV radiation, averaging size distributions from several power plants will average power plant conditions and fuel types. This average will represent the mix of study locations and times rather than a representative mix of power plants and fuels for a sufficient length of time.

Only five journal articles report measurements of the aerosol size distribution from large marine vessels on the scale of interest (Table 6.3). Ship traffic has not been typically viewed as a major source of air pollution in urban areas until very recently when other urban sources became dramatically cleaner and marine trade and cruise ship traffic increased dramatically. Thus far, the interest in ship emissions has mostly come from the climate community, which has been investigating the effect of SO_2, NO_x, and particulate ship emissions on global atmospheric chemistry and aerosol radiative forcing (G. Chen et

al., 2005). Early in-situ measurements of ship plumes focused on reporting the number of particles that might act as cloud condensation nuclei rather than the aerosol size distribution (e.g., Radke et al., 1989). Starting in 1994, real-world ship emissions of aerosol size distributions were measured as part of the Monterey Area Ship Track (MAST) (Frick and Hoppel, 2000; Hobbs et al., 2000), the Intercontinental Transport and Chemical Transformation (ITCT) (G. Chen et al., 2005), and the Safari 2000 (Sinha et al., 2003) aircraft campaigns. Sampling times varied from 15 seconds to several minutes. Lu et al. (2006) identified ship plumes originating in Burrard Inlet and received at the Slocan Park Pacific 2001 site in central Vancouver, BC. The aerosol size distribution displayed in their journal article represents the only known measured ship emission size distribution in an urban area and from a ground location with a long averaging time. Other datasets of marine emissions into polluted air exist (e.g., as measured from the NOAA R/V Ron Brown during the NEAQS 2004 and TEXAQS / GoMACCS 2006 experiments) but have not been analyzed to characterize the size distribution of ship emissions on the 4-15 km scale.

The appropriate emission size distributions from urban cities, coal-fired power plants, and marine vessels were compiled into one location (Tables 6.4-6.16) and applied to CMAQ to form new size distributions of emitted particles.

6.4. Application to CMAQ

The source-specific size distributions must be converted into the species-specific, lognormal modes that CMAQ expects for emissions input. First, to form lognormal modes each size distribution dataset was analyzed for the Aitken mode median diameter and standard deviation, accumulation mode median diameter and standard deviation, and the mass fraction split of $PM_{2.5}$ into Aitken and accumulation modes.

From the 44 urban size distribution datasets, some aspect of these five parameters was obtained by numerically fitting lognormal distributions to data for two datasets, recorded directly in the journal article for 17, and estimated from journal figures for 30. Parameters

for some datasets came from a combination of techniques and are counted in the tally for multiple techniques. All the values for each parameter were averaged and then subjectively adjusted to conform to a minority of datasets that are the highest quality and known to be highly applicable to this study. For instance, the average of the Aitken median diameter is 30 nm, but 25 nm was used to better conform to Larson et al. (2006) and Wehner et al. (2002). The accumulation mode standard deviation was adjusted from 1.8 to 1.7 for the same reason.

For power plants, numerical fitting, journal tables or text, and estimation from journal figures provided size distribution information for one, four and 12 datasets, respectively. With fewer datasets for each parameter than for urban areas, there is more uncertainty in the values and more opportunity for a spurious dataset to affect the average. The Aitken median diameter, Aitken standard deviation, accumulation standard deviation, and Aitken/accumulation $PM_{2.5}$ split were all adjusted towards the dataset of the highest known quality (Conesville, OH from Brock, in preparation), and in all of these cases had the same effect as down-weighting the Hobbs et al. (1983) Labadie, MO and Centralia, WA datasets.

No marine vessel datasets were fit numerically, four studies gave specific size distribution information, and parameters were estimated from 13 datasets. The information for the Aitken median diameter, accumulation median diameter, and Aitken/accumulation $PM_{2.5}$ split was simply averaged, and there was no rationale for emphasizing or de-emphasizing any datasets. None of the datasets provides an Aitken or accumulation mode standard deviation. For these two parameters, the power plant values were used since marine vessels are more similar to power plants in that they are both large, sulfate-rich combustion sources that mix with only a few (or no) other similar sources on the 4-15 km scale. It is only an approximate solution since power plants typically have pollution control devices that limit SO_2 and soot emissions while marine vessels do not.

Because most of the size distribution parameters were not explicitly recorded in publications but instead had to be estimated from figures and other information provided, there is considerable error and uncertainty in some of the derived parameters. However, the literature analysis revealed a similar level of variability in the datasets from location to location, and sometimes equivalent variability for datasets using the same fundamental data source. For example, the three journal articles from the same site in Copenhagen (Ketzel et al., 2003; Ketzel et al., 2004; Ketzel and Berkowicz, 2004) gave averaged Aitken median diameters of 28 to 39 nm. Even numerical fitting to high-quality datasets has similar variability when different fitting parameters are used. The CMAQ-specific emission size distributions for urban areas, power plants, and marine vessels on the 4-15 km scale are presented in Table 6.17 and Figure 6.1.

The source-specific size distributions on the 4-15 km scale differ substantially from the CMAQ emission size distributions (Figure 6.1b). The biggest difference is that the new distributions have a more prominent Aitken mode. CMAQ's elemental and organic carbon distribution has an Aitken mode that is only modestly larger than its accumulation mode, and CMAQ's distribution for sulfate, nitrate, and unspeciated mass has no Aitken mode at all. All of the new sources have distributions with significantly more $PM_{2.5}$ apportioned to the Aitken mode, up to 25% for marine vessels. The Aitken mode number median diameter increases from 13 nm in CMAQ to 25 nm for urban areas and power plants and to 60 nm for marine vessels, while the Aitken mode standard deviation remains unchanged. The accumulation mode median diameter also increases by 50-100%, and the mode's standard deviation decreases from 2.0 to 1.7 for urban areas and to 1.5 for power plants and marine vessels. These changes represent a large departure from what CMAQ has been using.

The second step to using the measured emission size distributions in CMAQ was to resolve the disconnect between the measured size distributions of emitted particles, the format of emission inventories, and the method CMAQ uses to import emissions and represent aerosols. Standard emissions inventories provide particle emissions as $PM_{2.5}$

and PM_{10} by major chemical species for specific sources. An emissions processor such as SMOKE maps the emissions from all the sources to the model grid and period of simulation. In the process, the sources are partitioned into chemical species and the species-specific emissions are summed for all sources in the grid cell, thereby transforming what had been a source-specific inventory into a species-specific emissions grid. CMAQ accepts emitted $PM_{2.5}$ as a function of grid cell and time step for sulfate, nitrate, organic carbon, elemental carbon, and unspeciated mass from SMOKE. Because the emission processor output comes in terms of speciated $PM_{2.5}$ or PM_{10}, the particle emissions routine in CMAQ, AERO_EMIS.F, assumes a size distribution of emitted particles for each particle species (see Chapter 2.1 for a more detailed explanation of CMAQ emissions). It is impossible to use the measurements of source-specific emissions when CMAQ uses species-specific distributions.

The proper solution is to modify SMOKE so that it applies a size distribution profile in addition to a chemical species profile when processing sources and summing them within a grid cell. This presents a coding challenge since it would require modifying two very different models – including extensive changes to SMOKE – and coordinating the output from SMOKE and the input to CMAQ. To make it useful for the modeling community, model developers for both SMOKE and CMAQ would need to coordinate releases to include size distribution capabilities. It is the best solution in the long run, but for most purposes, most of the improvement in emission size distributions can be achieved without it because the difference between these updated distributions and what is currently in CMAQ is much greater than that among the emitted size distributions for the major urban, power plant, and ship sources (Figure 6.1b).

Instead of adding a size distribution profile to SMOKE, another possibility is to take each species (elemental carbon, organic carbon, nitrate, sulfate, and unspeciated mass) and apply the emission size distribution from the source that emits the most of that species. For example, the Washington State Department of Ecology emissions inventory for regional modeling states that King County area and mobile (minus marine vessels)

$PM_{2.5}$ emissions are 7,065 tons per day, King County marine emissions are 352 tons per day, and the Pacific Power Centralia Power Plant emits 2107 tons per day (Table 6.18). Since King County contains half of the population in the five most populated counties of the Puget Sound region, the Puget Sound urban emissions are expected to be double those of King County. The $PM_{2.5}$ emissions are partitioned into emissions of organic carbon, elemental carbon, and sulfate based on emission inventory speciation profiles for marine vessels and power plants and based on the SMOKE output grids for the urban area. The urban area sources emit much more elemental carbon, organic carbon, and total $PM_{2.5}$ than do marine vessels and power plants. The urban sulfate emissions are comparable to the emissions from the Centralia Power Plant when the Centralia $PM_{2.5}$ was speciated based on the latest profile (Hodan, 2003). The Department of Ecology inventory apportions a much smaller percentage of $PM_{2.5}$ into sulfate, so the sulfate emissions in Western Washington for this simulation are clearly dominated by urban sources. Nitrate was ignored in this study since little nitrate is emitted as primary mass in the inventory. The Centralia Power Plant dominates unspeciated $PM_{2.5}$, but as the dumping ground for uncharacterized emissions, this category is highly uncertain and much of this mass is likely organic carbon. If we try to translate the source-specific size distributions into species-specific size distributions, the simplest, most defensible action is to use the urban source emitted size distribution for all emitted species. Although this conclusion is based on data from the Puget Sound region, it probably applies to a majority of urban areas.

CMAQ v4.4 was modified to use the urban emission size distribution for all $PM_{2.5}$ species: sulfate, nitrate, elemental carbon, organic carbon, and unspeciated $PM_{2.5}$. The emission size distribution for coarse mode aerosol species was not modified. The subroutine AERO_EMIS.F was expanded to handle a separate size distribution for sulfate from the other species, but this option was not used. The added functionality could be very easily modified so that two species have a separate size distribution from the other three, and only a small amount of code would need to be added so that all species have separate size distributions. Park et al. (2006) also updated the emission size distribution in CMAQ and focus on the split of emitted $PM_{2.5}$ into the Aitken and accumulation

modes. They concluded from tunnel measurements of traffic emissions (Venkataraman et al., 1994) that 15% of the emitted elemental and organic carbon should be emitted into the Aitken mode. This study arrived at a similar conclusion based on a much more extensive analysis.

Given the discussion above, two simulations of the case study were run (Table 6.19): a Best Guess scenario where all $PM_{2.5}$ emissions are emitted with the urban size distribution in Table 6.17, and an Upper Bound scenario where the emission size distribution emitted the most particles while remaining within the bounds of the studies in Table 6.1. For the Upper Bound scenario, the Aitken mode median diameter was lowered from the Best Guess value of 25 nm to 19 nm, the lower end of the range from the urban datasets. A similar rational was used to increase the percentage of $PM_{2.5}$ emissions apportioned to the Aitken mode from 10% to 20%. However in this scenario the increase was based on the standard deviation of the values from urban datasets since the upper end is diffuse and not clustered around one value. Only these two parameters of the size distribution were changed for the Upper Bound scenario because they have by far the largest effect on the number of emitted particles. The Best Guess and Upper Bound scenarios were implemented in CMAQ, run for the PNW2001 / Pacific 2001 case study, and compared to observations and to the standard CMAQ v4.4 without nucleation modifications (Base Case).

6.5. Results

Before comparing CMAQ runs with different emissions size distributions, it is possible to examine the change in emitted particles using the conversion factor from emitted $PM_{2.5}$ to emitted number:

$$M_{0,emission} = N_{fac} * M_{3,emission}, \text{ and} \tag{6.1}$$

$$N_{fac} = M_{ait} * \frac{\exp\left(4.5 * \ln \sigma_{g,ait}\right)}{D_{gv,ait}^3} + \left(1 - M_{ait}\right) * \frac{\exp\left(4.5 * \ln \sigma_{g,acc}\right)}{D_{gv,acc}^3} \tag{6.2}$$

where $M_{0,emission}$ is the number emission rate for a volume emission rate, $M_{3,emission}$, and M_{ait} is the fraction of emitted $PM_{2.5}$ apportioned to the Aitken mode. Since M_{ait} differs for organic and elemental carbon in the Base Case, the change in the number of emitted particles is different for carbon than for sulfate, nitrate, and unspeciated mass. Table 6.20 presents the factor increase (>1.0) or decrease (<1.0) of emitted particles as parameters in the emission size distribution are changed.

Starting with organic and elemental carbon, when the mass-based percentage of $PM_{2.5}$ emissions apportioned to the Aitken mode was increased from 0% (Base Case) to 10% (Best Guess) and to 20% (Upper Bound) while holding the other parameters at the Base Case values, the number of emitted particles increases by a factor of 30 and 59. When the Aitken mode median diameter was changed along with the Aitken mode apportionment (from 30 nm and 0.1% to 60 nm and 10% for Best Guess and to 50 nm and 20% for Upper Bound), the number of emitted particles increased over the Base Case by only 4.3 and 13.1. This is indicative of the range through which the full Best Guess and Upper Bound distributions increase the number of emitted particles – a factor of 3.9 and 12.8 – because the Aitken median diameter and Aitken mode apportionment have by far the biggest effect on the number of emitted particles. For the sulfate, nitrate, and unspeciated emissions, the parameters display similar sensitivity: the number of emitted particles increases by a factor of 5.6 and 18.0 for the Best Guess and Upper Bound scenarios. The change is greater for these species than for carbon since none of their emitted $PM_{2.5}$ went to the Aitken mode in the Base Case. When these emission size distribution changes were made to the mix of species emitted from the entire domain, Puget Sound, and Seattle / Bellevue (50%, 90%, and 93% OC+EC, respectively), the Best Guess and Upper Bound scenarios increase the number of emitted particles by a factor of 4 to 5 and a factor of 13 to 15 (Table 6.21).

About half of the enhancement in the number of emitted particles is preserved as an increase in number concentrations after CMAQ meteorological, dynamical, and chemical processing. The other half is combined with the surviving particles, lost to the earth's

surface through dry deposition, or advected out of the domain. Figure 6.2 shows the number of modeled particles at the lowest model layer from the Best Guess and Upper Bound scenarios divided by the number from the Base Case. The factor is above one over land, which means that the changes in emissions always increase the number of modeled particles. The Best Guess scenario produces about three times more particles in the urban areas than the Base Case, and in regions impacted by sulfate emissions, it produces up to four times more particles. Enhancements greater than a factor of four occur in the immediate vicinity of sulfate sources. The Best Guess number concentrations are correlated with the Base Case number concentrations with an $R^2 = 0.97$ domain-wide and $R^2 = 0.98$ for urban and urban-influenced areas. There are no cases where the Best Guess scenario creates high number concentrations where they did not already exist in the Base Case. The Upper Bound scenario increases the number of particles in urban, sulfate-influenced, and sulfate-dominated areas by another multiple of three over the Best Guess scenario, and it is also very highly correlated with the Base Case number concentrations. Thus, updates to the emissions size distributions increase the number of particles modeled by CMAQ by a factor of 2 to 3 downwind of urban areas, by a factor of 3 to 4 in urban areas, and up to a factor of 4 near sulfate sources. The largest though still realistic increase in the number of particles is a factor of 12 immediately next to sulfate sources such as the pulp mills near Nanaimo, BC. This is consistent with Park et al. (2006) who found an increase by a factor of 4.3 and 6.0 at an urban location for emitting 10% and 15% of the elemental and organic carbon into the Aitken mode.

The changes in CMAQ performance can be investigated through the change in number concentrations at the time and location of observations, number concentrations in particular environments along the PNW2001 flight paths, and average size distributions at the Pacific 2001 ground stations. The updated emission chemical size distributions noticeably increase the CMAQ modeled number concentrations and reduce the number underprediction relative to observations (Figure 6.3). For the PNW2001 flights where the original underprediction was 1-2 orders of magnitude when the aircraft was in the urban-influenced Puget Sound region (plotted in black), the Best Guess number concentrations

in the observable size range (plotted in blue) are generally underpredicted by 1 order of magnitude, and for the Upper Bound (plotted in cyan) they are underpredicted by about 0.5 orders of magnitude. The Pacific 2001 sites also see an increase in number concentrations by 0.5 and 1 orders of magnitude for the Best Guess and Upper Bound cases. There is now nearly no underprediction at Langley for the Upper Bound case. As with the surface domain-wide analysis, the improvement with updated emissions is more pronounced where CMAQ models higher concentrations, regardless of source, chemical aging, day, or time of day. The features along the flight path and in the time series at the ground stations remain unchanged. Such behavior indicates that these emission size distribution changes act linearly and are not large enough to appreciably affect other aerosol processes such as nucleation and coagulation, which act nonlinearly on the number of particles and depend on the pre-existing amount of aerosol.

The Best Guess emissions distribution improves the overall character of the modeled aerosol size distributions. The Base Case produced an Aitken mode at Langley (Figure 6.4) and Sumas (Figure 6.5) that appears as little more than the lower tail of the accumulation mode. The Best Guess scenario creates a more prominent Aitken mode with a lower median diameter that is closer to observations. The average daytime Langley and Sumas Aitken modes still peak at an unrealistically high diameter and are not sufficiently distinct from the accumulation mode, but the number underprediction is now uniform below 150 nm. The Best Guess averaged nighttime distribution at Langley has an Aitken mode that is more prominent than the accumulation mode. This was desirable for the daytime, but the nighttime observation has an Aitken mode that is smaller than the accumulation mode. The error is due to a weak accumulation mode in the model since the Aitken mode is well modeled. The Upper Bound distributions at Langley and Sumas accentuate the changes from the Base Case to the Best Guess scenario to such an extent that the Aitken mode dominates the accumulation mode, the two modes are visually distinct, the Aitken median diameter is close to the observed value, and the Aitken mode is now overstated, especially at night. Updating the emission size distribution resolves the under-representation of the Aitken mode relative to the accumulation mode, but it does

not distinguish the two modes unless the Upper Bound size distribution is used, it does not solve the overall number underprediction below 150 nm during the day, and it overemphasizes the importance of the Aitken mode at night.

While updates to the emission size distribution do not alter emitted aerosol mass, they do have a small effect on the amount of modeled $PM_{2.5}$. The Best Guess scenario increases $PM_{2.5}$ at Washington surface sites by on average 0.46 $\mu g/m^3$ or 4.6%. The Pacific 2001 sites experience similar increases in modeled $PM_{2.5}$ with the largest increase at the site whose air mass is the most processed, Sumas, and the smallest increase at the urban site, Slocan Park. The Upper Bound scenario produces the same pattern of $PM_{2.5}$ increase but with a 0.69 $\mu g/m^3$ increase at Washington sites and a higher Sumas-to-Slocan Park spread at the Pacific 2001 sites. The emission size distribution affects the modeled aerosol mass more when CMAQ models a stable, shallow boundary layer. This occurs on the evening of 25 and 27 August for all three Pacific 2001 sites. It occurs additionally for Slocan Park overnight on 26-27 August and on the late afternoon of 26 August when MM5 brings a sea breeze front into Vancouver (Figure 6.6). Nitrate accounts for a large amount of the mass increase because it comprises a high proportion of modeled $PM_{2.5}$ at night when boundary layers are stable.

Several aerosol processes depend on the size distribution. Condensation of sulfate and organics is proportional to the aerosol surface area which, for constant mass, increases as the distribution is weighted towards smaller particles. Both wet and dry deposition remove fewer aerosols from the atmosphere when the distribution has a more prominent Aitken mode. For wet deposition, only particles larger than a critical size will become cloud condensation nuclei and potentially end up in raindrops that remove aerosol from the atmosphere. For dry deposition, smaller particles have a higher surface area to volume ratio and thus have a lower deposition velocity. A stable boundary layer increases the importance of dry deposition by confining the aerosol close to the surface and promotes condensation through its relatively cold surface layer. Since no rain fell during the three day simulation, it is likely that emitting aerosol preferentially into smaller sizes

for the updated emission size distribution increases modeled $PM_{2.5}$ through higher condensation and lower dry deposition during stable boundary layer conditions.

If changes in the emission size distribution can have a small effect on the modeled aerosol mass through condensation and deposition, then it is also possible for them to affect the concentration of gas-phase species. Some of the higher aerosol mass in the Best Guess and Upper Bound cases is due to a transfer of gaseous sulfate and nitrate to the aerosol phase. It is possible this would modify the gas-phase concentration of sulfur and nitrogen compounds and potentially modify the entire chemical environment. However, the CMAQ concentrations of major species involved in air pollution and aerosol chemistry such as sulfur dioxide, nitrogen oxides, ozone, and ammonia, change by less than 1% for both the Best Guess and Upper Bound cases. Nitric acid increases by 1-2% for both emission scenarios, but even this change is very small. Updates to the emission size distribution have a negligible effect on the gaseous chemical environment and only a modest effect on the modeled aerosol mass.

6.6. Conclusions

In the goal to improve CMAQ modeling of the aerosol size distribution, the emission size distributions in the model were updated to reflect current measurement techniques and to address issues of spatial and temporal scale important for aerosols. The emission size distribution used for an Eulerian grid must either incorporate all processes between combustion and the smallest resolvable spatial scale or include another modeling step for the scale between the emissions measurement and the grid scale. If this is not done, then important aerosol processes such as nucleation, coagulation, deposition, and condensation/evaporation will be misrepresented. Coagulation, deposition, condensation, and evaporation are more important closer to the emission source where smoke stacks, tailpipes, and road environments create concentrated plumes. As plumes travel farther from the source and chemically age, nucleation and dilution are most important, but condensation and evaporation also play a role on a slower time scale. Modeling each plume is computational unrealistic. Box model estimates for the transformation to the

CMAQ grid are one possibility, but another is to use measurements obtained 4-15 km from major sources to characterize emissions at the smallest resolvable scale of a typical CMAQ grid.

This study culled observations of size distributions for urban areas, power plants, and marine vessels on the 4-15 km scale directly from digital datasets and from published journal articles. The datasets disproportionately favor locations where many measurements have been taken rather than provide a representative distribution of measurements appropriate for most CMAQ domains. Nonetheless, they provide a large sample for calculating average emission size distributions. The new emission size distributions for urban areas, power plants, and marine vessels apportion a much larger fraction of aerosol mass to the Aitken mode than what is currently in CMAQ. Instead of 0% or 0.1%, now 10%, 15%, and 25% of the emitted $PM_{2.5}$ go to the Aitken mode for urban areas, power plants, and marine vessels. Even when combined with the larger Aitken median diameters suggested by this study, the new distributions emit many more particles, especially in the ultrafine range, than CMAQ currently does.

The source-specific size distributions needed to be translated into the current CMAQ modeling paradigm. They were first transformed into lognormal Aitken and accumulation modes to obtain the modal median diameters, modal standard deviations, and the apportionment of mass into the Aitken and accumulation modes. CMAQ expects the emission size distributions to be species-specific instead of by source. Because the urban source dominates the emissions of organic carbon and elemental carbon and emits a roughly equal amount of sulfate as the major power plants in the Puget Sound, the simplest and most justifiable solution was to apply the urban source Aitken and accumulation mode characteristics to all emitted species.

CMAQ was run using the urban source size distribution as the Best Guess scenario and was run for an Upper Bound scenario with an emissions size distribution that emits the highest number of particles within bounds of the compiled urban size distributions. Of

all the changes from the Base Case emission distributions, the apportionment of $PM_{2.5}$ into the Aitken and accumulation modes has the biggest effect on the number of emitted particles. For the PNW2001 / Pacific 2001 domain, the Best Guess and Upper Bound emission size distributions increase the number of emitted particles by a factor of 4-5 and 13-15 respectively. For the Best Guess scenario, the modeled number of particles increases by a factor of 2-3 downwind of urban areas, a factor of 3-4 in urban areas, and up to a factor of 4 near sulfate sources. The largest change occurs in areas with high number concentrations and in sulfate-rich regions. The time and spatial pattern of number concentrations is not affected. $PM_{2.5}$ increases 5% due to higher condensation and lower dry deposition as aerosol mass is marginally shifted to smaller-sized particles. No significant change is seen in gas-phase species. While the underprediction in particle number is only moderately corrected, the size distributions in the Aitken mode better follow the Pacific 2001 observations in terms of Aitken mode prominence and Aitken mode median diameter. The mixed model performance at night either reveals additional problems with the model simulation or suggests that the emissions size distribution must be different during the day than at night. The updated emission size distributions improve the number concentration performance (Figure 6.7), more successfully model the Aitken mode particles in the ultrafine range, and represent better model science.

Table 6.1 List of datasets used to derive the emission size distribution from urban areas.

City	Reference	Period of Observation
Alkmaar	Ruuskanen et al., 2001	4 months
Atlanta	Woo et al., 2001	13 months
Atlanta	McMurry and Woo, 2002	25 months
Atlanta	Rhoads et al., 2003	3 weeks
Baltimore	Tolocka et al., 2005	9 months
Brisbane	Morawska et al., 1999	1.75 years
Brisbane	Morawska et al., 1998	1.75 years
Copenhagen	Wåhlin et al., 2001	1.5 months
Copenhagen	Ketzel et al., 2004	4 weeks over 3 months
Copenhagen	Ketzel and Berkowicz, 2004	months of data over 2 years
Copenhagen	Ketzel et al., 2003	11 weeks over 6 months
Erfurt	Ruuskanen et al., 2001	4 months
Erfurt	Tuch et al., 1997	6 months
Goteborg	Janhäll et al., 2006	2 months
Graz, Austria	Sturm et al., 2003	< 1 month
Helsinki	Ruuskanen et al., 2001	4 months
Helsinki	Hussein et al., 2003	6 years
Helsinki	Hussein et al., 2005	12 weeks in 1/99, 6/00, and 2/01
Helsinki	Laakso et al., 2003	3 years
Kuopio	Kikas et al., 1996	1-2 months
Leipzig	Wehner et al., 2002	3 months
Leipzig	Wiedensohler et al., 2002	4.5 years
Leipzig	Tuch et al., 2003	5 years
Leipzig	Wehner and Wiedensohler, 2002	4 years
Leipzig	Putaud et al., 2003	4 years
Leipzig	Wehner et al., 2002 (self-processed)	3 months
London	Putaud et al., 2003	1.5 years
Los Angeles	K. M. Zhang et al., 2005	5 months
Los Angeles	Kim et al., 2002	5 months
Los Angeles	Sardar et al., 2005	2 months
Milano-Bresso	Putaud et al., 2003	2 months
Nagoya	Minoura and Takekawa, 2005	2 months
Pittsburgh	Zhou et al., 2005b	13 months
Pittsburgh	Bein et al., 2005	1 year
Pittsburgh	Zhang et al., 2005	3 weeks
Pittsburgh	Stanier et al., 2004a	1 year
Pittsburgh	Zhou et al., 2005a	5 days
Pittsburgh	Cabada et al., 2004	1 year
Rochester, NY	Jeong et al., 2006	1 year
Santiago, Chile	Trier, 1997	2.5 years
Seattle	Larson et al., 2006	1.5 years
Stockholm	Gidhagen et al., 2005	1 month
Tallinn	Kikas et al., 1996	1-2 months
Tartu	Kikas et al., 1996	1-2 months

Table 6.2 List of datasets used to derive the emission size distribution from power plants.

Site	Reference	Period of Observation
Centralia, WA	Hobbs et al., 1983	4 plumes on 4 days
Chamber study	Lipsky et al., 2004	N/A
Chamber study	Tienemaa et al., 2002	N/A
Conesville, OH	Brock, in preparation	a few hours
Cumberland, TN	Brock et al., 2002	2 passes
Finland	Dekati Ltd., 2003	1 plume on 1 day
Four corners, NM	Hobbs et al., 1983	3 plumes on 3 days
Gallatin, TN	Brock et al., 2002	1 pass
Hong Kong	Yao et al., 2006	1 summer and 1 winter plume
Johnsonville, TN	Brock et al., 2002	3 passes
Labadie, MO	Cantrell and Whitby, 1978	1 pass
Nanticoke, ON	Cho, 2005	21 passes over 5 winter/summer flights
Navajo, AZ	McMurry et al., 1981	1 pass
Navajo, AZ	Wilson and McMurry, 1981	2 plumes on one morning
Paradise, KY	Mueller and Imhoff, 1994	N/A
Stacks of 3 pp's	Ylatalo, 2006	N/A
Thomas Hill, MO	Brock et al., 2002	1 pass

Table 6.3 List of datasets used to derive the emission size distribution from marine vessels.

Vessel	Reference	Period of Observation
Bremen Express	Frick and Hoppel, 2000	3 passes
Fremo Scorpius	Hobbs et al., 2000	1 pass
MSC Giovanna	Sinha et al., 2003	1 pass
NYK Sunrise	Hobbs et al., 2000	2 passes
Royal Sphere	Sinha et al., 2003	1 pass
Sea Pearl	Frick and Hoppel, 2000	4 passes
Slocan Park, Vancouver, BC	Lu et al., 2006	30 minute average
Star Livorno	Hobbs et al., 2000	2 passes
Tai He	Hobbs et al., 2000	1 pass
Unidentified	Frick and Hoppel, 2000	2 passes
unidentified ship #1 off CA coast	G. Chen et al., 2005	2 passes
unidentified ship #2 off CA coast	G. Chen et al., 2005	2 passes
USS Mt. Vernon	Frick and Hoppel, 2000	3 passes

Table 6.4 Summary of datasets used to derive the Aitken mode median diameter from urban areas.

Site	Aitken Median Diameter (nm)	Reference
Atlanta	20	Woo et al., 2001
Atlanta	25	McMurry and Woo, 2002
Atlanta	47	Rhoads et al., 2003
Brisbane	30	Morawska et al., 1999
Brisbane	40	Morawska et al., 1998
Copenhagen	25	Wåhlin et al., 2001
Copenhagen	35	Ketzel and Berkowicz, 2004
Copenhagen	45	Ketzel et al., 2003
Copenhagen	25	Ketzel et al., 2004
Goteborg, Sweden	35	Janhäll et al., 2006
Graz, Austria	25	Sturm et al., 2003
Helsinki	40	Hussein et al., 2003
Helsinki	34	Hussein et al., 2005
Kuopio	25	Kikas et al., 1996
Leipzig	24	Wehner and Wiedensohler, 2002
Leipzig	25	Wiedensohler et al., 2002
Leipzig	20	Tuch et al., 2003
Leipzig	22.5	Wehner et al., 2002
Leipzig	22.4	Wehner et al., 2002 (self-processed)
London	26	Putaud et al., 2003
Los Angeles	50	K. M. Zhang et al., 2005
Los Angeles	35	Kim et al., 2002
Milano-Bresso	28	Putaud et al., 2003
Nagoya	40	Minoura and Takekawa, 2005
Pittsburgh	40	Zhou et al., 2005b
Pittsburgh	32	Bein et al., 2005
Pittsburgh	30	Zhang et al., 2005
Pittsburgh	40	Stanier et al., 2004
Pittsburgh	20	Zhou et al., 2005a
Seattle	22.5	Larson et al., 2006
Stockholm	20	Gidhagen et al., 2005
Tallinn	25	Kikas et al., 1996
Tartu	25	Kikas et al., 1996
Average	30.3	
Value Used	**25**	

Table 6.5 Summary of datasets used to derive the Aitken mode standard deviation from urban areas.

Site	Aitken Standard Deviation	Reference
Atlanta	1.9	Woo et al., 2001
Helsinki	1.75	Hussein et al., 2003
Helsinki	1.85	Hussein et al., 2005
Leipzig	1.83	Wehner et al., 2002 (self-processed)
London	1.6	Putaud et al., 2003
Milano-Bresso	1.61	Putaud et al., 2003
Seattle	1.7	Larson et al., 2006
Average	1.7	
Value Used	**1.7**	

Table 6.6 Summary of datasets used to derive the accumulation mode median diameter from urban areas.

Site	Acc. Median Diameter (nm)	Reference
Baltimore	114	Tolocka et al., 2005
Brisbane	89	Morawska et al., 1999
Helsinki	151	Hussein et al., 2003
Helsinki	115	Hussein et al., 2005
Leipzig	125	Wehner and Wiedensohler, 2002
Leipzig	140	Putaud et al., 2003
Leipzig	105	Wehner et al., 2002 (self-processed)
Milano-Bresso	87	Putaud et al., 2003
Pittsburgh	106	Stanier et al., 2004a
Pittsburgh	200	Cabada et al., 2004
Santiago	100	Trier, 1997
Seattle	109	Larson et al., 2006
Average	120.1	
Value Used	**120**	

Table 6.7 Summary of datasets used to derive the accumulation mode standard deviation from urban areas.

Site	Acc. Standard Deviation	Reference
Helsinki	1.57	Hussein et al., 2003
Helsinki	1.9	Hussein et al., 2005
Leipzig	1.89	Putaud et al., 2003
Leipzig	2.07	Wehner et al., 2002 (self-processed)
London	2	Putaud et al., 2003
Milano-Bresso	1.92	Putaud et al., 2003
Santiago	1.46	Trier, 1997
Seattle	1.6	Larson et al., 2006
Average	1.8	
Value Used	**1.7**	

Table 6.8 Summary of datasets used to derive the fraction of $PM_{2.5}$ apportioned to the Aitken mode (100% minus this value for the accumulation mode) from urban areas.

Site	Aitken / Acc split	Reference
Alkmaar, Netherlands	5%	Ruuskanen et al., 2001
Bologna	4%	Putaud et al., 2003
Erfurt, Germany	4%	Ruuskanen et al., 2001
Erfurt, Germany	1%	Tuch et al., 1997 via Kittelson et al., 1998b
Gent	4%	Putaud et al., 2003
Helsinki	15%	Hussein et al., 2003
Helsinki	16%	Hussein et al., 2005
Helsinki	2%	Laakso et al., 2003
Helsinki, Finland	9%	Ruuskanen et al., 2001
Leipzig	1%	Wehner et al., 2002 (self-processed)
Los Angeles	20%	Sardar et al., 2005
Pittsburgh	40%	Bein et al., 2005
Pittsburgh	1%	Stanier et al., 2004a
Pittsburgh	5%	Cabada et al., 2004
Seattle	25%	Larson et al., 2006
Average	10.2%	
Value Used	**10**	

Table 6.9 Summary of datasets used to derive the Aitken mode median diameter from power plants.

Site	Aitken Median Diameter (nm)	Reference
Centralia, WA	17	Hobbs et al., 1983
Conesville	20	Brock, in preparation
Four Corners	15	Hobbs et al., 1983
Johnsonville, Tennessee	60	Brock et al., 2002
Laboratory	50	Lipsky et al., 2004
Laboratory	55	Tienemaa et al., 2002
Labadie, MO	8	Cantrell and Whitby, 1978
Nanticoke	34	Cho, 2005
Navajo	11	McMurry et al., 1981
Navajo	15	Wilson and McMurry, 1981
Stacks of 3 pp's	55	Ylatalo, 2006
Thomas Hill, Missouri	15	Brock et al., 2002
Average	29.6	
Value Used	**25**	

Table 6.10 Summary of datasets used to derive the Aitken mode standard deviation from power plants.

Site	Aitken Standard Deviation	Reference
Centralia, WA	1.9	Hobbs et al., 1983
Conesville	1.75	Brock, in preparation
Four Corners	2.7	Hobbs et al., 1983
Average	2.1	
Value Used	**1.7**	

Table 6.11 Summary of datasets used to derive the accumulation mode median diameter from power plants.

Site	Acc. Median Diameter (nm)	Reference
Centralia, WA	432	Hobbs et al., 1983
Conesville	115	Brock, in preparation
Cumberland, TN	107	McMurry et al., 1981
Four Corners	550	Hobbs et al., 1983
Hong Kong	344	Yao et al., 2006
Lab	130	Teinemaa et al., 2002
Lab	150	Dekati Ltd., 2003
Labadie, MO	65	Cantrell and Whitby, 1978
Thomas Hill, MO	130	Brock et al., 2002
TVA Paradise	150	Mueller and Imhoff, 1994
Average	217.3	
Value Used	**150**	

Table 6.12 Summary of datasets used to derive the accumulation mode standard deviation from power plants.

Site	Acc. Standard Deviation	Reference
Centralia, WA	1.2	Hobbs et al., 1983
Conesville	1.55	Brock, in preparation
Four Corners	1.09	Hobbs et al., 1983
Labadie, MO	1.7	Cantrell and Whitby, 1978
Average	1.4	
Value Used	**1.5**	

Table 6.13 Summary of datasets used to derive the fraction of $PM_{2.5}$ apportioned to the Aitken mode (100% minus this value for the accumulation mode) from power plants.

Site	Aitken / Acc split	Reference
Centralia, WA	85%	Hobbs et al., 1983
Conesville	8%	Brock, in preparation
Cumberland, TN	70%	Brock et al., 2002
Four Corners	75%	Hobbs et al., 1983
Gallatin	13%	Brock et al., 2002
Johnsonville, TN	34%	Brock et al., 2002
Labadie	27%	Cantrell and Whitby, 1978
Navajo	15%	McMurry et al., 1981
Navajo	12%	Wilson and McMurry, 1981
Thomas Hill, MO	5%	Brock et al., 2002
Average	34.4%	
Value Used	**15**	

Table 6.14 Summary of datasets used to derive the Aitken mode median diameter from marine vessels.

Site	Aitken Median Diameter (nm)	Reference
Bremen Express	80	Frick and Hoppel, 2000
Fremo Scorpius	60	Hobbs et al., 2000
Mt. Vernon	40	Frick and Hoppel, 2000
NYK Sunrise	90	Hobbs et al., 2000
NYK Sunrise	40	Hobbs et al., 2000
Sea Pearl	50	Frick and Hoppel, 2000
Slocan Park Organics	40	Lu et al., 2006
Slocan Park Sulfate	64	Lu et al., 2006
Star Livorno	70	Hobbs et al., 2000
Star Livorno	40	Hobbs et al., 2000
Tai He	80	Hobbs et al., 2000
Unidentified	60	Frick and Hoppel, 2000
Average	59.5	
Value Used	**60**	

Table 6.15 Summary of datasets used to derive the accumulation mode median diameter from marine vessels.

Site	Acc. Median Diameter (nm)	Reference
Slocan Park organics	150	Lu et al., 2006
Slocan Park sulfate	172	Lu et al., 2006
Average	161	
Value Used	**150**	

Table 6.16 Summary of datasets used to derive the fraction of $PM_{2.5}$ apportioned to the Aitken mode (100% minus this value for the accumulation mode) from marine vessels.

Site	Aitken / Acc split	Reference
California Coast	25%	G. Chen et al., 2005
MSC Giovanna	15%	Sinha et al., 2003
Royal Sphere	33%	Sinha et al., 2003
Slocan Park Organics	25%	Lu et al., 2006
Slocan Park Sulfate	50%	Lu et al., 2006
Average	30%	
Value Used	**25**	

Table 6.17 Lognormal parameters in CMAQ v4.4 (Base Case) compared to those for urban areas, power plant, and marine vessel sources.

Emission Species	Mode	% Mass	D_g (nm)	D_{gv} (nm)	σ_g
sulfate	i	0	13	30	1.7
	j	100	80	300	2.0
nitrate	i	0	13	30	1.7
	j	100	80	300	2.0
other fine	i	0	13	30	1.7
	j	100	80	300	2.0
organic	i	0.1	13	30	1.7
	j	99.9	80	300	2.0
elemental carbon	i	0.1	13	30	1.7
	j	99.9	80	300	2.0

Emission Species	Mode	% Mass	D_g (nm)	D_{gv} (nm)	σ_g
urban	i	10	25	60	1.7
	j	90	120	280	1.7
power plant	i	15	25	60	1.7
	j	85	150	250	1.5
marine vessel	i	25	60	140	1.7
	j	75	170	280	1.5

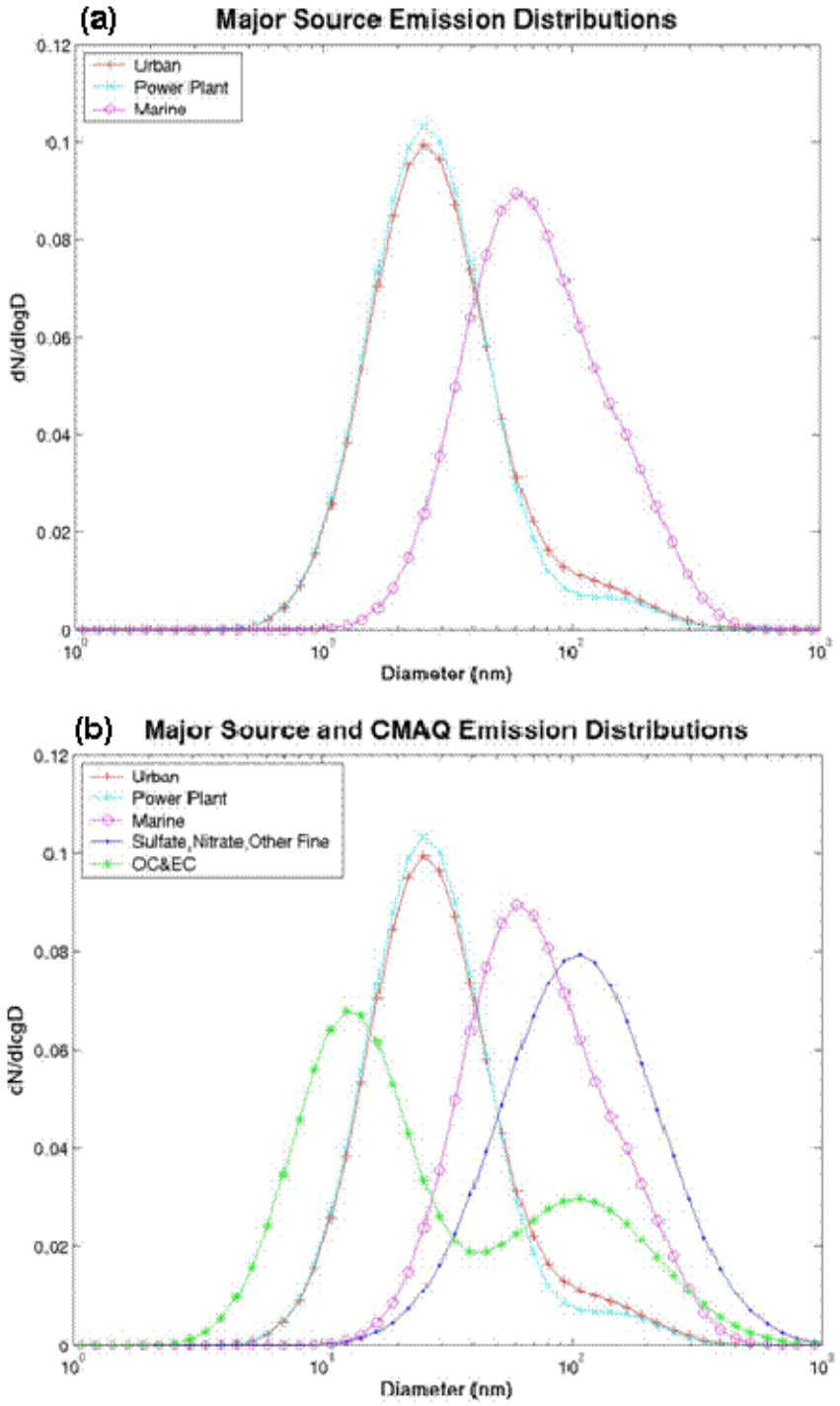

Figure 6.1 (a) Emission size distributions on 4-15 km scale for urban areas, power plants, and marine vessels, and (b) the same distributions plotted with emission size distributions in CMAQ v.4.4 (Base Case) for organic and elemental carbon and for sulfate, nitrate, and unspeciated mass.

Table 6.18 Emissions in Western Washington for major sources studies by $PM_{2.5}$ mass and by species. The power plant sulfate emissions have been updated based on Hodan (2003) and were not used in this case study. "tpy" = tons per year.

	PM2.5 emissions (tpy)	% OC	% EC	% Sulfate
King County	7065	35%	58%	3%
Puget Sound (est.)	14130	35%	58%	3%
Centralia Power Plant	2107	20%	1%	16%
King County marine	352	22%	74%	3%

		OC emissions (tpy)	EC emissions (tpy)	Sulfate Emissions (tpy)
King County		2473	4098	212
Puget Sound (est.)		4946	8195	424
Centralia Power Plant		421	21	337
King County marine		77	260	11

Table 6.19 (a) Summary of Aitken and accumulation mode parameters for Best Guess and Upper Bound scenarios in CMAQ. Coarse mode parameters remained unchanged from CMAQ v4.4. (b) comparison of Best Guess and Upper Bound to Base Case.

Emission Species	Mode or Component	% Mass	D_g (nm)	D_{gv} (nm)	σ_g
Best Guess	i	10	25	60	1.7
	j	90	120	280	1.7
Upper Bound	i	20	19	50	1.7
	j	80	120	280	1.7

	Organics	All Others	All Species			
Name	% Mass in Ait	% Mass in Ait	Aitken Dgv	Aitken σg	Acc Dgv	Acc σg
Base	0.1	0	30 nm	1.7	300 nm	2
Best Guess	10	10	60 nm	1.7	280 nm	1.7
Upper Bound	20	20	50 nm	1.7	280 nm	1.7

Table 6.20 Number of emitted particles as size distribution parameters are changed divided by the number of emitted particles for the Base Case emission size distribution. Boxes are colored dark blue when the changes relate specifically to the Best Guess emission size distribution and are colored cyan for the Upper Bound emission size distribution.

Aitken D_g to 60	Aitken D_g to 50	Acc D_g to 280	Acc σ_g to 1.7	Aitken/Acc split to 10	Ait/Acc split to 20	Organics	Others
√						0.8	1.0
	√					0.8	1.0
		√				1.2	1.2
			√			0.6	0.4
				√		30	41
					√	59	83
√				√		4.3	6.0
	√				√	13.1	18.5
√		√	√	√		3.9	5.6
	√	√	√		√	12.8	18.0

Table 6.21 Factor increase in emissions for the Best Guess and Upper Bound emissions size distributions for the domain, Puget Sound, and Seattle / Bellevue.

	Domain	Puget Sound	Seattle / Bellevue
% OC/EC	50	90	93
Best Guess	5.0	4.4	4.3
Upper Bound	15.3	13.5	13.4

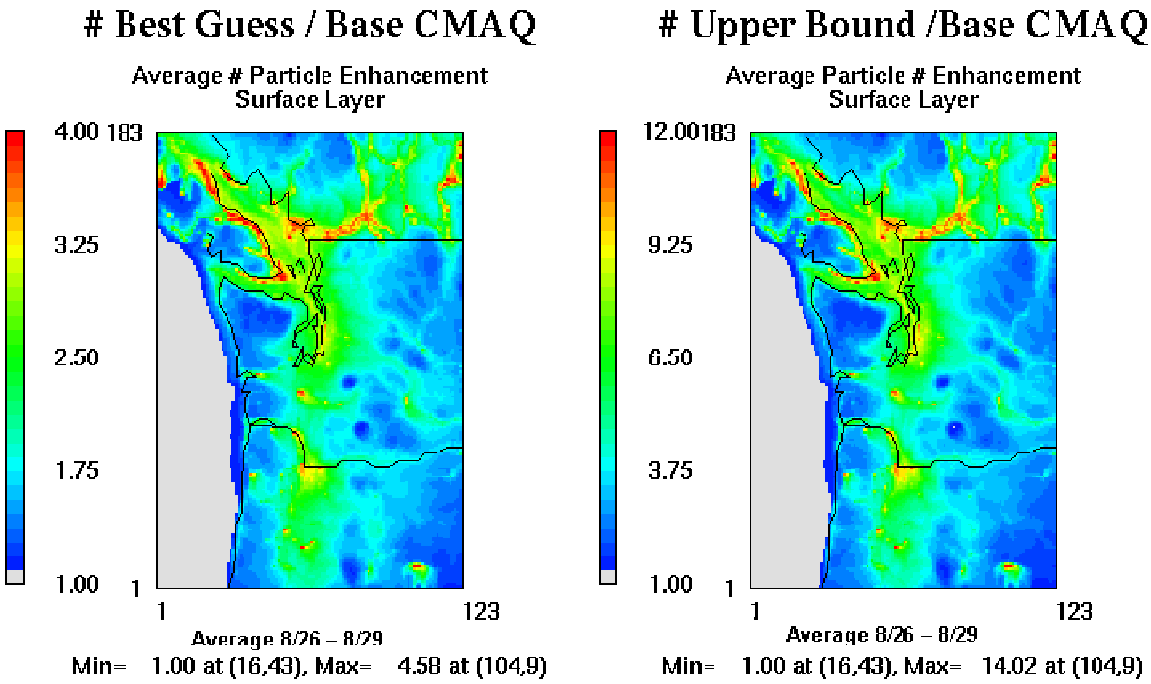

Figure 6.2 Average modeled particle number enhancement for the Best Guess and Upper Bound scenarios relative to the Base Case (Base CMAQ). Values are averaged for the 72 hour period 00 UTC 25 August to 23 UTC 28 August.

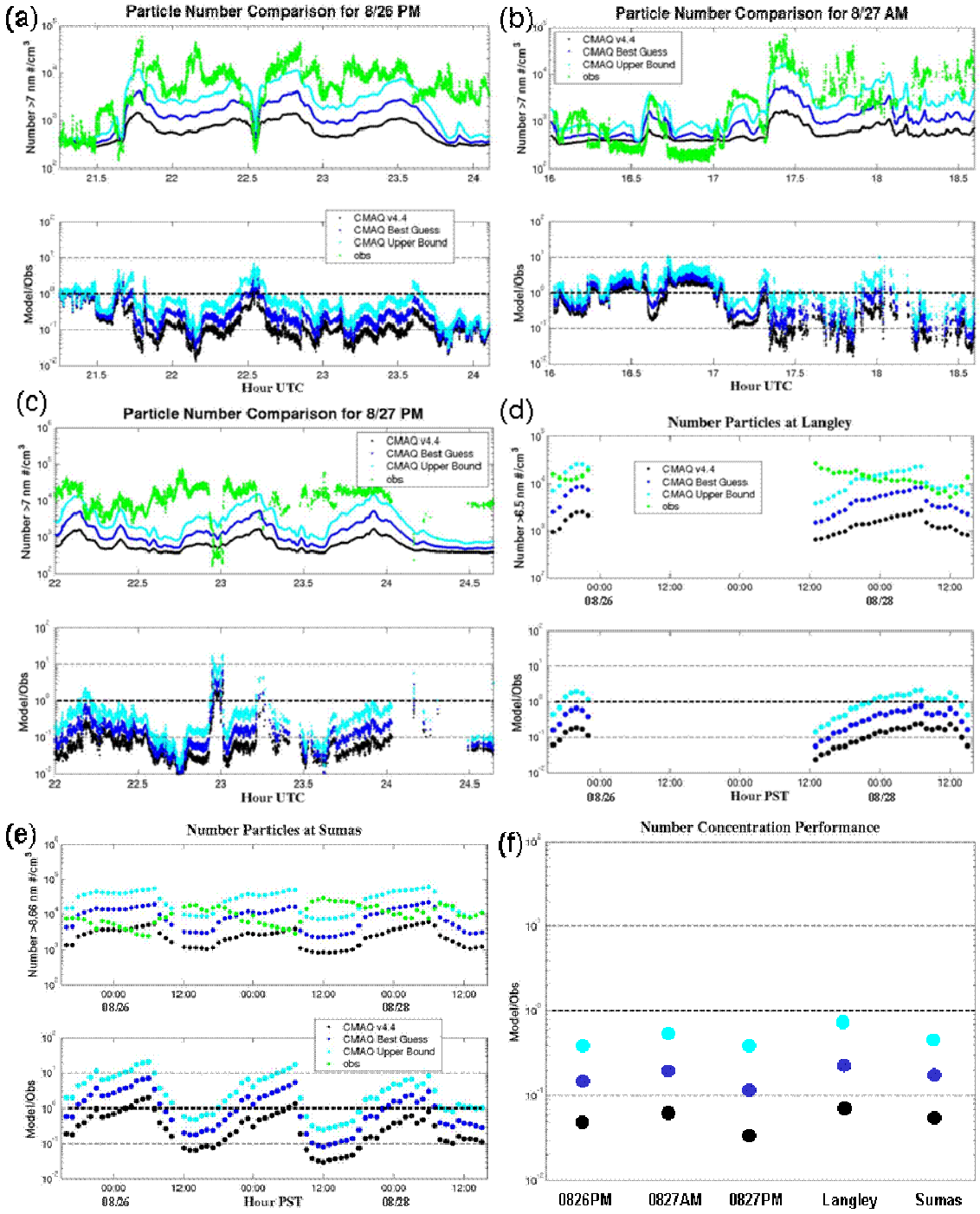

Figure 6.3 Comparison of CMAQ number concentration to observations for the PNW2001 flights on (a) the afternoon of 26 August, (b) the morning of 27 August, and (c) the afternoon of 27 August, and for the Pacific 2001 sites (d) Langley and (e) Sumas from 00 UTC 26 August to 00 UTC 29 August. (f) summarizes the performance from (a)-(e).

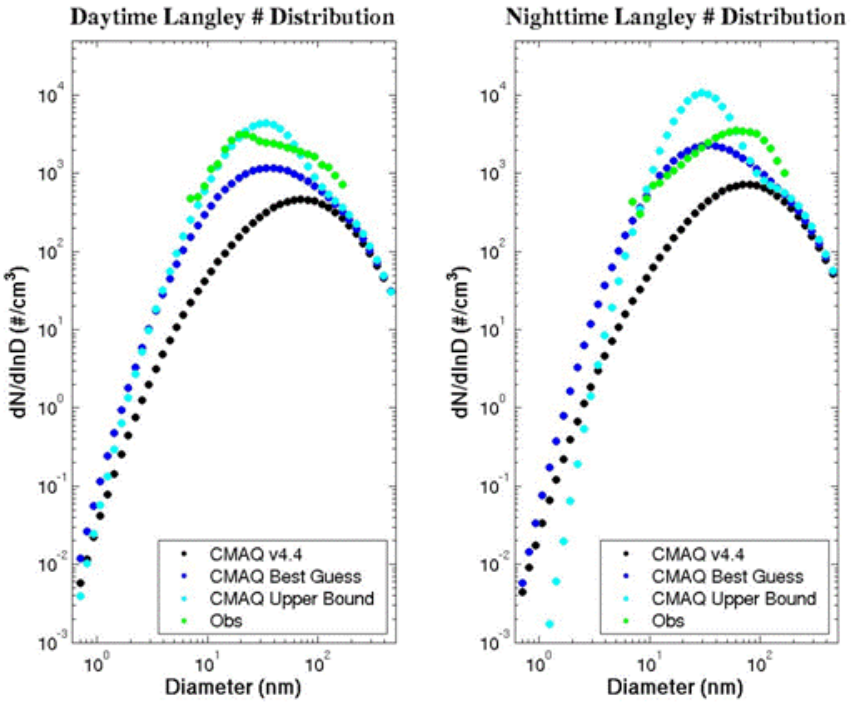

Figure 6.4 Day and night average size distributions at Langley as observed and for the Base Case (CMAQ v4.4, in black), Best Guess (blue), and Upper Bound (cyan) cases.

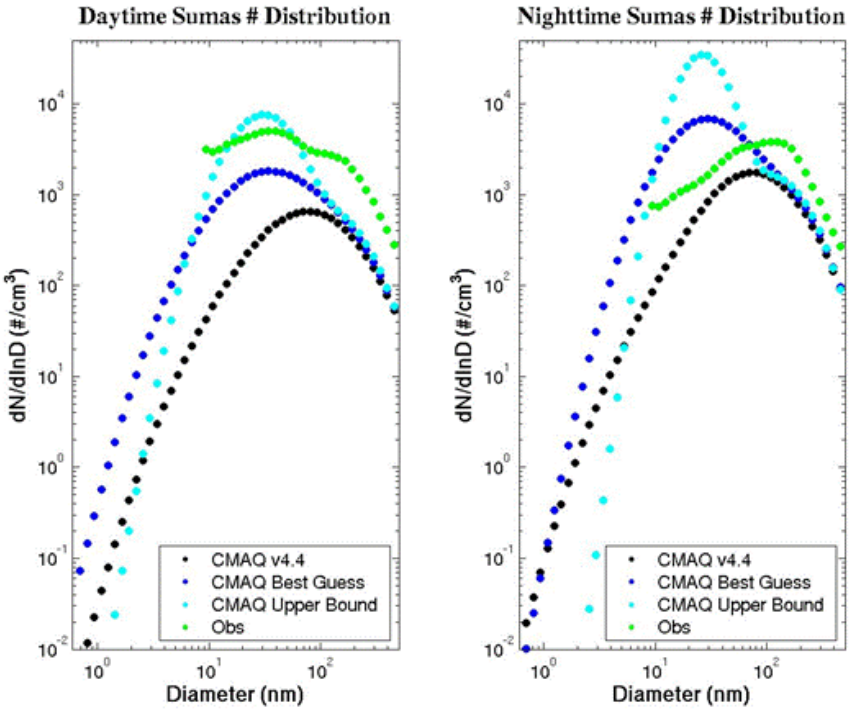

Figure 6.5 Day and night average size distributions at Sumas as observed and for the Base Case (CMAQ v4.4, in black), Best Guess (blue), and Upper Bound (cyan) cases.

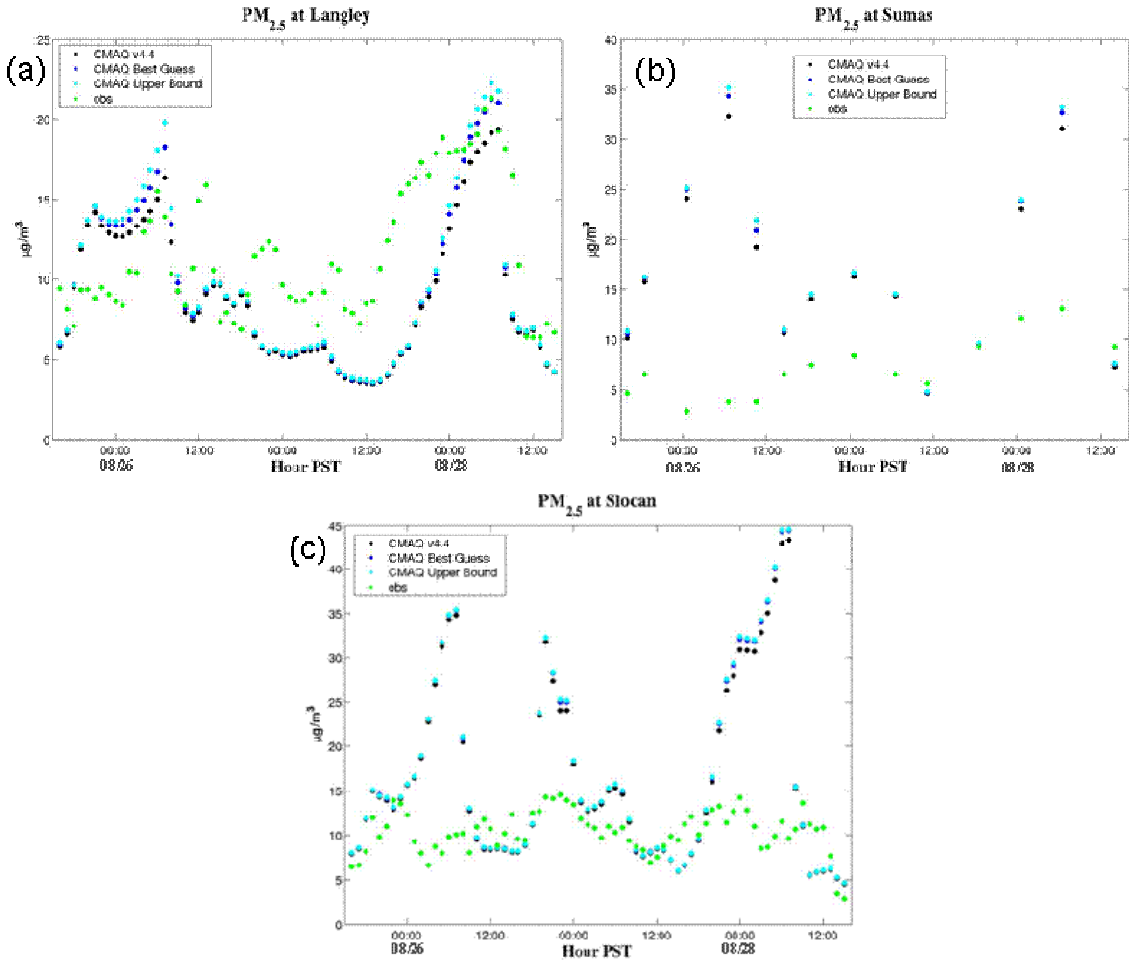

Figure 6.6 Hourly $PM_{2.5}$ from observations, Base Case (CMAQ v4.4, in black), Best Guess (blue), and Upper Bound (cyan) cases for (a) Langley, (b) Sumas, and (c) Slocan Park from 00 UTC 26 August to 00 UTC 29 August 2001.

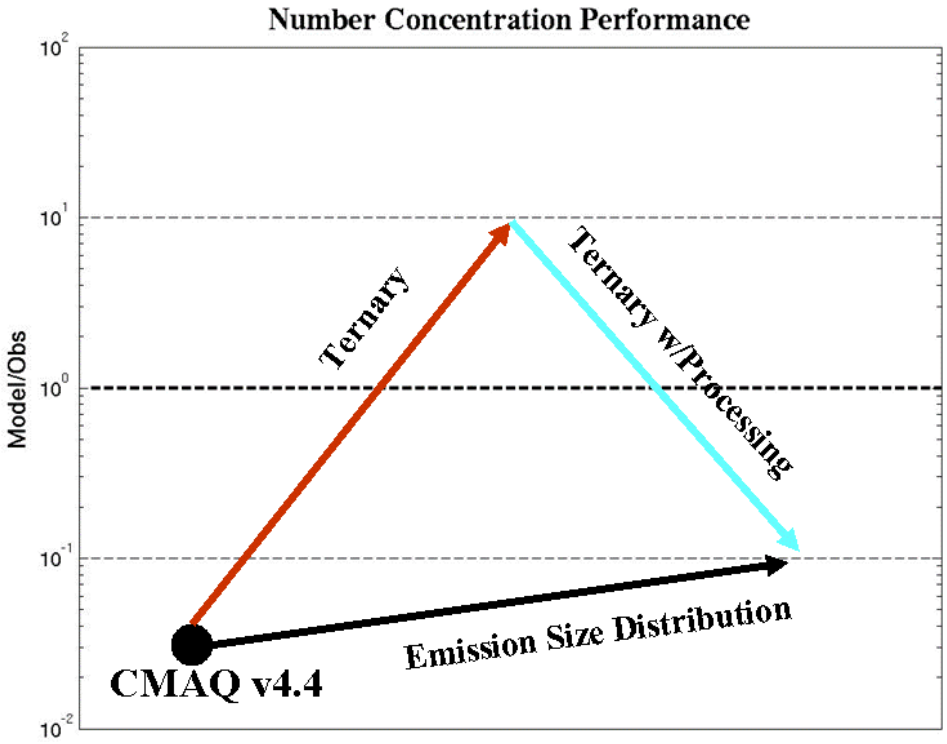

Figure 6.7 Summary of number concentration performance for the Base Case (CMAQ v4.4 with no modifications), CMAQ with ternary nucleation, CMAQ with ternary nucleation and processing of the nucleated particles to the Aitken mode, and CMAQ with the Best Guess emission size distributions.

7. Combined Updates to CMAQ Size Distributions

7.1. Theory

This chapter reports results from combining the particle nucleation and emission size distribution improvements that in previous chapters were implemented in isolation. The updates to the emission size distributions resulted in modest, consistent increases in modeled particle concentrations, while the updates to particle nucleation created large changes in number concentrations that varied greatly in time and space. Because the emissions improvements had a relatively small effect on aerosol properties in urban areas, it is possible the emissions changes would act as a linear perturbation to the ternary nucleation case when the two are combined.

However, a polluted air mass is a complicated, multidimensional chemical system that rarely responds linearly to a change in emissions or to a change in internal aerosol processes such as particle nucleation. Although updating the emissions size distributions as reported in Chapter 6 increased the number of particles fairly linearly, the situation is different with both updates because particle nucleation responds nonlinearly to the properties of existing aerosols. Nucleation and the steady-state value of condensable gases depend on the available surface area. Partitioning more emitted mass into the Aitken mode results in a higher aerosol surface area for the same emitted volume. New particle production can be quickly shut down if an increase in surface area can accommodate the supersaturated vapor. At the same time, shifting mass into smaller particles can preserve aerosol number concentrations through a decrease in dry deposition and wet deposition. Smaller particles have a lower settling velocity and are less likely to

serve as cloud condensation nuclei. The net result of changes to both nucleation and emissions may not be a simple combination of the individual changes.

7.2. Application to CMAQ

The Ternary with Processing nucleation case and Best Guess emission size distribution case were merged to create a Combined Update version of CMAQ v4.4. The Ternary with Processing case included ternary nucleation based on Napari et al. (2002b) and processing of new particles to the Aitken mode (10 nm) using Kerminen and Kulmala (2002). New particles are added to the Aitken mode if they grow fast enough to avoid coagulation with existing particles. Sulfur is conserved within the aerosol module of CMAQ for the first time. The equilibrium sulfuric acid concentration, condensing sulfuric acid mass, and nucleating sulfuric acid mass are solved for iteratively using a combination of an Approximate Newton's Method and a Linear Bisection. As the most sophisticated version of nucleation tested in CMAQ, it is called the Nucleation case for this chapter. The Best Guess case modifies the emissions size distribution so that 10% of the emitted $PM_{2.5}$ goes into the Aitken mode, the Aitken mode volume median diameter increases from 30 nm to 60 nm, the accumulation mode volume median diameter decreases from 300 nm to 280 nm, and the accumulation mode standard deviation decreases from 2.0 to 1.7. The Best Guess emission size distribution case is called the Emission case for this chapter. It reflects the best estimate of the emitted aerosol size distribution for a 4-15 km mesoscale grid. Combining the Nucleation and Emission cases was relatively straightforward and did not cause complicated coding errors since they involve separate subroutines that do not interact until the top-level aerosol driver.

7.3. Results

The Combined Update scenario increases the number concentration by an average of 4.7 for all hours and grid cells in the lowest model layer. The enhancement is a factor of 2-3 in rural areas, 10-15 in urban areas, and up to 37 near specific point sources (Figure 7.1). Both the Nucleation and Emission cases increase the number concentrations on

average, but since the increase is larger for the Nucleation case, the average spatial pattern for the Combined Update looks more like Nucleation than Emission (Figure 7.2). Although it is possible to discern areas where the Emission case contributes to the Combined Update, the increase due to emissions changes is largely reflected in Figure 7.1 as a small augmentation to the Nucleation particle enhancement factor. Figure 7.3 makes this clearer by dividing the number concentrations from the Combined Update by those from the Nucleation case and separately by those from the Emission case. The quotient of Combined Update and Nucleation reveals that the Emission scenario on average contributes to the Combined Update number concentrations along inland waterways, near Vancouver Island, along the Trans-Canadian Highway, and near a point source in southeast Oregon. Figure 7.3b highlights the areas that experience regional nucleation in the Puget Sound, Willamette Valley, Tri-Cities area, and the southern slope of the British Columbia Coast Range. The Combined Update increases the number of particles over the Base Case CMAQ v4.4 mostly in areas of nucleation and adds another small increase throughout polluted areas via updates to the emission size distribution.

One interesting example of how the nucleation and emissions improvements interact can be seen at 8 AM PST 27 August in Figures 7.4 and 7.5. Nucleation near Yakima, east of Tacoma, and in southern British Columbia has just started within the hour and is evident in both the Nucleation and Combined Update number enhancement maps (Figure 7.4a and 7.4b). Figure 7.4b shows no enhancement over western Washington because nucleation was not occurring overnight and it has not yet started there. The broad enhancement over eastern Washington is the result of particle nucleation the day before between Vancouver, BC and Portland, OR that was advected across the Cascade Mountains in overnight westerly flow. The Emission enhancement in Figure 7.4c occurs in the urban areas, along inland waterways, and at two point sources near Nanaimo on Vancouver Island. Figures 7.5a and 7.5b show clearly how the emissions and nucleation changes occur in different areas. In fact, the emission and nucleation changes are often separated either in time or in space. The Emission case has its largest effect during the morning rush hour when the boundary layer is still shallow and before nucleation has

started in the model. The second but less influential burst of emissions occurs during the late afternoon after regional nucleation has ended. Except for the interaction between nucleation and emissions in the late morning, it is easy to visualize how the Combined Update case can be a linear combination of changes made to particle nucleation and particle emissions.

The Combined Update number concentrations are underpredicted in a manner similar to that of the Nucleation case (Tables 7.1-7.2 and Figures 7.6-7.10). The additional particles for the Combined Update (magenta for this chapter) relative to the Base Case CMAQ v4.4 (black for this chapter) in Table 7.1 are approximately the sum of the additional particles from Nucleation (cyan for this chapter) and from Emission (blue for this chapter). This is evident in Figures 7.6-7.10 when the Nucleation and Emission cases are of a similar magnitude. Often during the PNW2001 flights or at the Pacific 2001 ground sites, either the Nucleation or Emission model predicts many more particles than the other. As they trade these roles, the Combined Update is driven by whichever has a higher number concentration. An example is on the afternoon of 27 August in Figure 7.8. The Nucleation case dominates the Combined Update when the model samples the air mass north and east of Seattle where ternary nucleation predicts high concentrations (hours 22.15, 23.2, and 23.85), while the Emission case dominates the Combined Update in the more diffusely polluted parts of the Puget Sound where the emissions changes create more new particles than regional nucleation does. In background boundary layer conditions, the Nucleation and Emission cases contribute particles on roughly the same order so that the Combined Update concentrations look like a sum of the two. An example is on the afternoon of 26 August in the clean background boundary layer air mass west of Olympia (hours 21.9-22.1 and 22.9-23.2 on Figure 7.6). In tropospheric background conditions such as hours 16-16.5 on Figure 7.7, the Nucleation case contributes a larger number of particles and dominates the Combined Update number concentrations. The Combined Update has less of a number underprediction than its Nucleation and Emission components, but it still underpredicts number concentrations by up to one order of magnitude.

The Combined Update size distributions at Langley and Sumas track the daytime Nucleation distributions and the nighttime Emission distributions (Figures 7.11 and 7.12). The ternary nucleation algorithm has a major effect at these sites during the day, but at night when there is no nucleation, the changes in the emission size distributions dominate the Combined Update. This is somewhat unfortunate for both daytime and nighttime performance. During the day, the Nucleation size distribution overemphasizes the Aitken mode relative to the accumulation mode. Although the Emission size distribution does not adequately separate the Aitken and accumulation modes and does not have a sufficiently low Aitken median diameter, it properly simulates the relative prominence of the two modes. At night, neither the Nucleation nor Emission cases simulate the importance of the accumulation mode, but the Nucleation case does a better job than the Emission case of simulating the Aitken mode and its importance relative to the accumulation mode. The better result would have been for the Combined Update to assume the daytime Emission and nighttime Nucleation size distributions. Despite these errors, the Combined Update size distribution retains some advantages of the individual nucleation and emission changes: the daytime Aitken mode is more prominent than the accumulation mode; the two modes are better separated during the day and the night; and the Aitken mode peaks at a lower diameter day and night. In some ways, using both the nucleation and emissions updates produces worse size distributions than either update separately, but the combination still improves the size distribution performance over the Base Case CMAQ v4.4.

The size distribution changes seen at Langley and Sumas apply more generally to the entire domain. Table 7.3 shows the Aitken and accumulation mode parameters averaged for the lowest model layer for the whole domain, the greater Puget Sound and Lower Fraser Valley, the more polluted portion of the Puget Sound (Olympia to Everett and east to the Cascade foothills), and Seattle. Domain-wide and in all urban subsets, the Combined Update Aitken and accumulation modes are more separated than the Base Case and more separated than each of the Nucleation and Emission cases independently.

Both modal standard deviations decrease slightly with any and all model improvements. Both the Nucleation and Emission cases decrease the Aitken median diameter from the Base Case value, and the Combined Update decreases it more than either the Nucleation or Emission case alone. The more separated modes, smaller modal standard deviations, and smaller Aitken median diameter are all positive changes. The combination of the nucleation and emission updates improves the aerosol size distribution parameters across the entire domain.

A close inspection revealed that the Combined Update is not the simple sum of the Nucleation and Emission cases. Figure 7.13 shows the number concentrations for each scenario averaged across the greater Puget Sound and Lower Fraser Valley urban and urban-influenced regions. It also plots the sum of the number concentrations for the Nucleation and Emission cases (Nucleation + Emission). If the Combined Update were a perfect linear sum, its number concentrations would overlie Nucleation + Emission. There are times when the two traces are close, but most of the time the difference between Nucleation + Emission and the Combined Update is as large as between the Combined Update and Nucleation.

For further investigation, the number concentration from the Base Case is removed from the number of particles for each model update. For example, the average domain-wide number in the lowest layer from the Combined Update minus the average domain-wide number in the lowest layer from the Base Case represents the influence of the Combined Update model changes. This is done to isolate the particle enhancement from each scenario. For different subsets of the domain, Figure 7.14 displays the number of particles due to the combined updates divided by sum of the particles when each nucleation and emission update is implemented in isolation. All subsets exhibit the same general behavior.

The discussion will focus on the Puget Sound and Lower Fraser Valley since it has both areas of high nucleation and high emissions. The Combined Update number

concentration ranges from as little as 83% of Nucleation + Emission to as much as 106%. The Combined Update adds more particles to the simulation than Nucleation + Emission during 17 hours and adds fewer particles during 55 hours. The average difference between the two traces is -14,000 particles. The Combined Update adds the fewest particles relative to Nucleation + Emission in the first few hours of particle nucleation, such as 10-11 AM PST 26 August and 8-10 AM PST 28 August. At those times, morning rush hour is just ending and the boundary layer is quickly breaking down. The juxtaposition of emissions during the morning rush hour and subsequent nucleation in the urban plume a few hours later is the clearest example of how the nucleation and emissions improvements interact.

The nonlinearity of the combined aerosol changes is a result of the emissions update and its Aitken mode with smaller particles and more surface area. The extra surface area in the Combined Update relative to the Nucleation case can suppress production of new Aitken mode particles either by decreasing the sulfuric acid concentration or by increasing the coagulation sink for the smaller 2-10 nm particles. In fact, at the onset of nucleation in the mornings, η (the parameter describing survival of new particles to the Aitken mode, as defined in Chapter 5.1) is larger for the Combined Update than for the Nucleation case while the sulfuric acid concentration is also higher. So, the coagulation sink of nucleation mode particles is one likely reason for why the Combined Update number concentrations are not a linear combination of the Nucleation and Emission cases. A second reason is that intermodal coagulation at all hours increases nonlinearly as the mean size of the Aitken mode decreases and the number of Aitken mode particles increases. The smaller particles have more Brownian motion and are more likely to collide and attach to larger particles. The higher number concentration increases the rate of collision and loss of Aitken mode particles. The addition of surface area, the increase in Brownian motion, and the higher number concentration increase the importance of intermodal coagulation between the nucleation, Aitken, and accumulation modes. For the most part, however, the nonlinearity between the nucleation and emission improvements in CMAQ is minor.

As with the individual Nucleation and Emission cases, the combination of the model improvements increases $PM_{2.5}$ and has little effect on gaseous species. The average increase in $PM_{2.5}$ at the Washington ground stations is 1.33 $\mu g/m^3$ or 14%. As with the number concentrations, the increase in $PM_{2.5}$ represents nearly the sum from the Nucleation and Emission cases (Table 7.4). The largest deviation occurs at Langley and other slightly downwind locations that experience the highest modeled particle nucleation rates. The combination of ternary nucleation, nucleation mode processing, and conservation of sulfur increases sulfate mass especially in the Aitken mode. Sulfate accounts for roughly 2/3 of the additional aerosol mass from the nucleation updates. The remainder is mostly nitrate and ammonia since the increases in particle surface area and particle acidity promote conversion of nitrate and ammonia to the aerosol phase (in v4.4, N_2O_5 hydrolysis depends on both acidity and particle surface area). The emissions updates do not emit more mass into the domain, but they indirectly lead to higher modeled $PM_{2.5}$ by shifting the emitted $PM_{2.5}$ mass into smaller particles with a higher surface area to volume ratio. In addition to a decrease in dry deposition, all condensable species respond to the higher surface area with a new equilibrium favoring the aerosol phase. There is little change in the concentration of gas-phase species from the Base Case. Only ammonia shows a significant difference, decreasing 4-5% at Langley and Slocan Park just as in the Nucleation case. The increase in $PM_{2.5}$ and the change in ammonia concentrations are small compared to the change in number concentrations.

7.4. Conclusions

A new version of CMAQ v4.4 with improvements to nucleation and to emission size distributions represents the current state of the science for modeling ultrafine particles. Of all the processes that create and destroy ultrafine particles, the creation of particles through nucleation and emissions are the two processes most scientifically outdated in CMAQ v4.4. Each process was updated independently in Chapters 5 and 6 to isolate their effect on model results. This chapter reports results from combining the two

improvements and provides this study's best effort at modeling the entire aerosol size distribution in the Pacific Northwest.

Even with the nucleation and emission changes, the Combined Update version of CMAQ v4.4 still underpredicts aerosol number in urban areas by up to one order of magnitude. This is an improvement over the 1-2 orders of magnitude underprediction in the Base Case CMAQ v4.4 (Figure 7.15). With the addition of an effective nucleation algorithm, the underprediction is now theoretically more sensitive to meteorological parameters such as actinic flux and temperature. It is no longer uniform across urban-influenced areas in time of day, location, or chemical environment. The modeled daytime size distributions reproduce the observed data in terms of distinct Aitken and accumulation modes, an Aitken mode that is more prominent than the accumulation mode, and an Aitken mode that peaks at a lower diameter. The modeled nighttime distributions better separate the Aitken and accumulation modes and shift the Aitken mode to smaller sizes. However, the Aitken mode is now too strong, especially during the day, and the entire accumulation mode needs to be increased by 0.5 orders of magnitude at all hours. Although the model changes do not specifically add aerosol mass and only shift it to smaller particles, they add 10-15% more $PM_{2.5}$ by altering aerosol processes that depend on the surface area to volume ratio such as coagulation, condensation, dry deposition, and cloud processing. Despite the residual number underprediction and size distribution errors, the science improvements to CMAQ's particle nucleation and emissions generally improve performance for the full aerosol size distribution. This applies specifically to the PNW2001 / Pacific 2001 case study, but likely also for other modeling domains and scenarios.

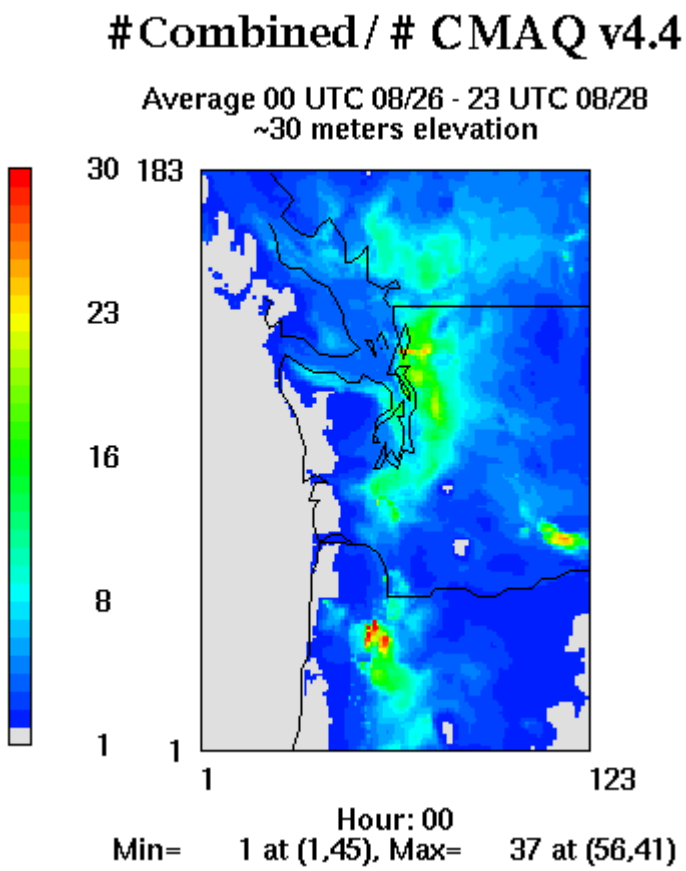

Figure 7.1 Average particle number enhancement for the Combined Update scenario relative to the Base Case (CMAQ v4.4). Values are averaged for the 72 hour period 00 UTC 26 August to 23 UTC 28 August.

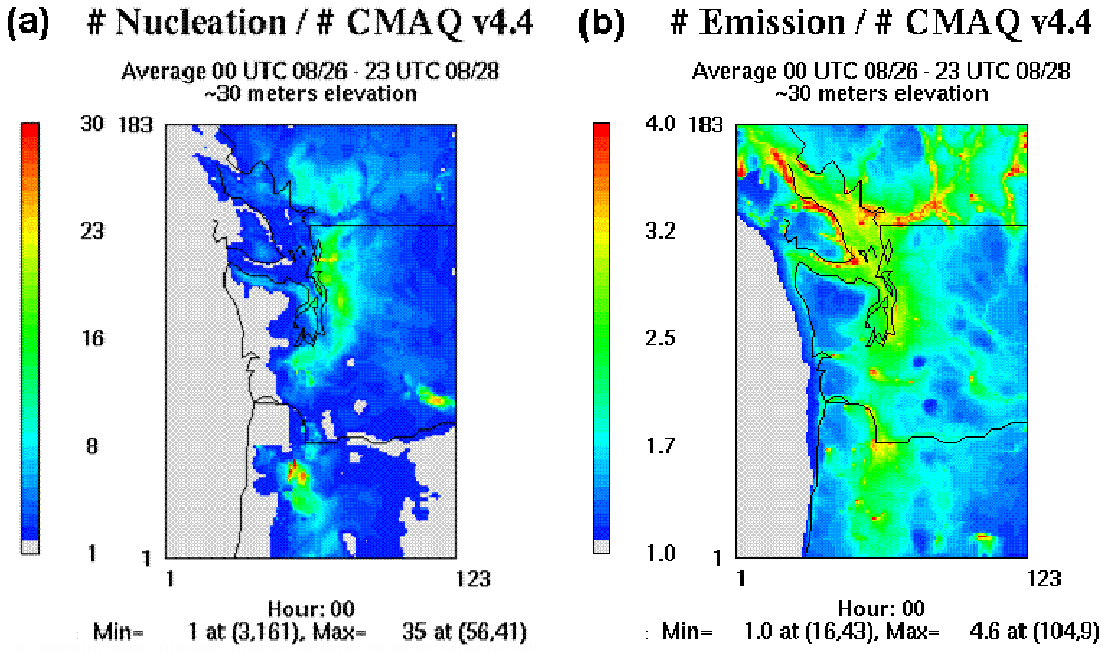

Figure 7.2 Average particle number enhancement for the (a) Nucleation and (b) Emission scenarios relative to the Base Case (CMAQ v4.4). Values are averaged for the 72 hour period 00 UTC 26 August to 23 UTC 28 August. Color scales differ for the two maps. Nucleation and Emission refer to the Ternary with Processing and Best Guess scenarios from Chapters 5 and 6.

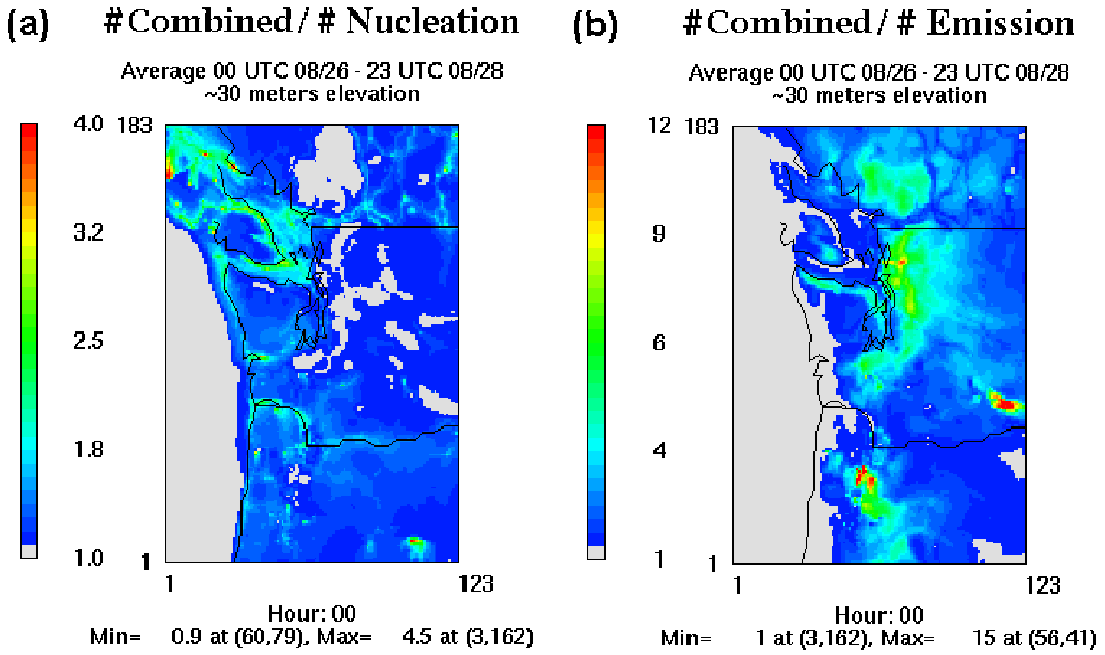

Figure 7.3 Average particle number enhancement for the Combined Update scenario relative to (a) Nucleation and (b) Emission. Values are averaged for the 72 hour period 00 UTC 26 August to 23 UTC 28 August. Color scales differ for the two maps.

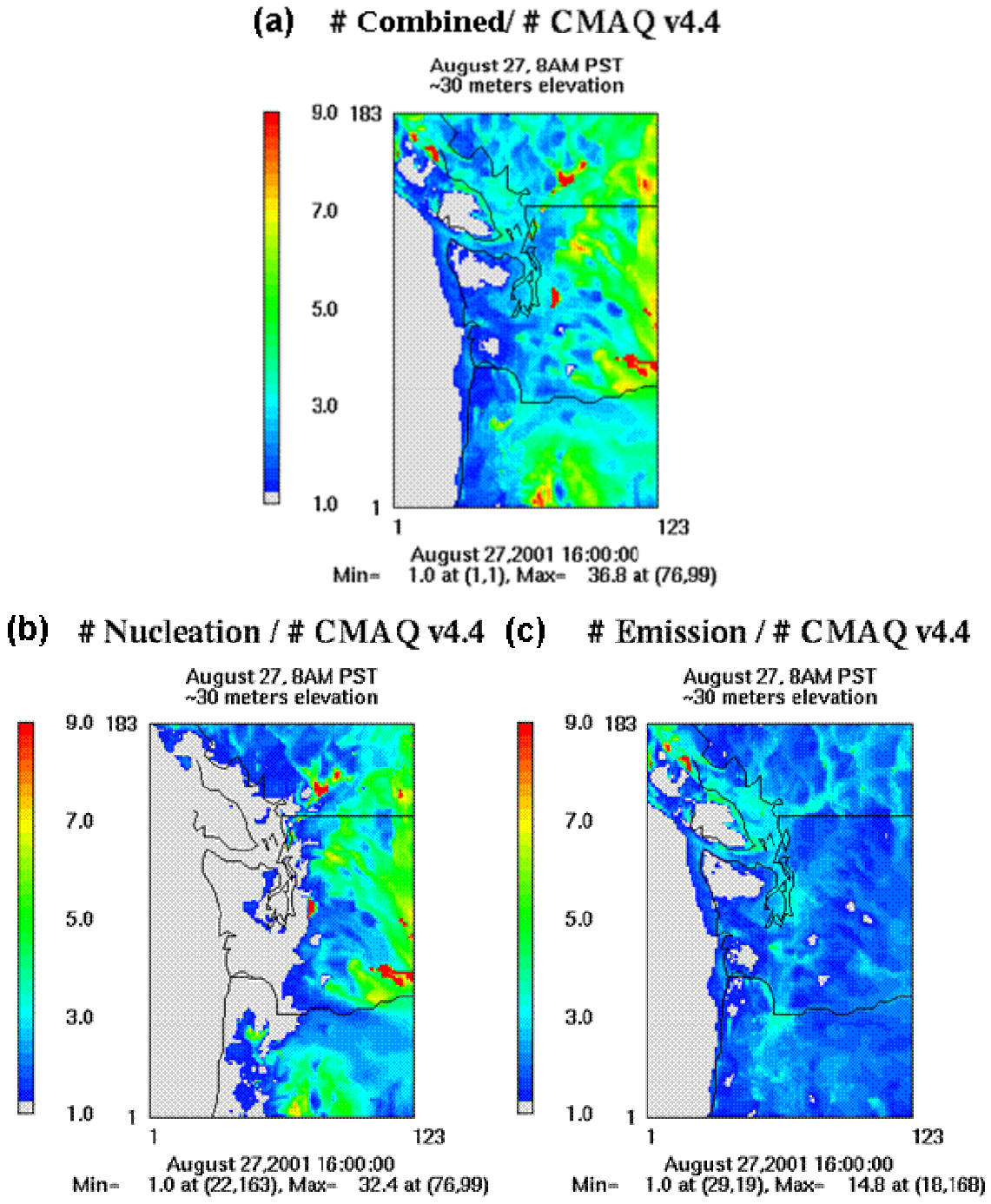

Figure 7.4 Particle number enhancement for the (a) Combined Update, (b) Nucleation, and (c) Emission scenarios relative to the Base Case (CMAQ v4.4) at 8 AM PST 27 August.

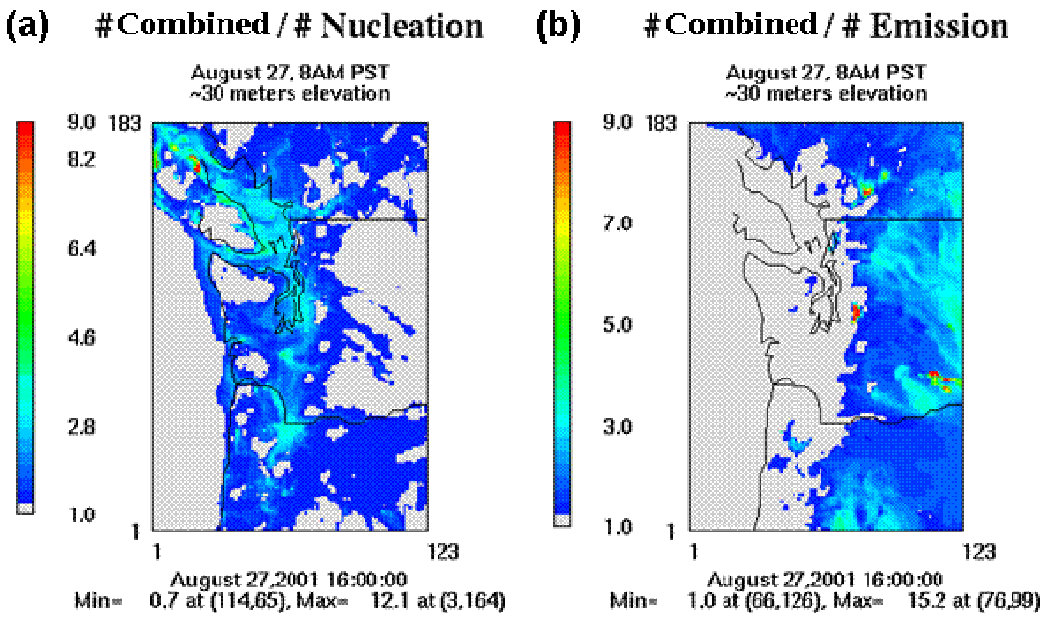

Figure 7.5 Particle number enhancement for the Combined Update scenario relative to (a) Nucleation and (b) Emission at 8 AM PST 27 August.

Table 7.1 Average observable number bias relative to observations for the PNW2001 flights and for the two Pacific 2001 sites where aerosol number observations are available. The Sumas number concentrations are limited to daytime hours.

Number Error Relative to Observations						
	0826PM	0827AM	0827PM	Langley	Sumas (daytime)	Average
CMAQ v.4.4	-6,469	-3,961	-14,782	-11,696	-14,147	-10,211
Nucleation	7,111	-3,514	-13,193	-9,506	-2,329	-4,286
Emission	-5,761	-3,416	-13,802	-8,576	-11,047	-8,520
Combined Update	7,893	-3,036	-12,484	-6,537	733	-2,686

Table 7.2 Difference in the number of observable particles between each scenario and the Base Case CMAQ v4.4 for the PNW2001 flights and for the two Pacific 2001 sites where aerosol number observations are available. The Sumas number concentrations are limited to daytime hours.

	Number Difference from CMAQ v4.4					
	0826PM	0827AM	0827PM	Langley	Sumas (daytime)	Average
CMAQ v.4.4	Ø	Ø	Ø	Ø	Ø	
Nucleation	13,580	447	1,589	2,190	11,818	5,925
Emission	708	545	980	3,120	3,100	1,691
Combined Update	14,362	925	2,298	5,159	14,880	7,525

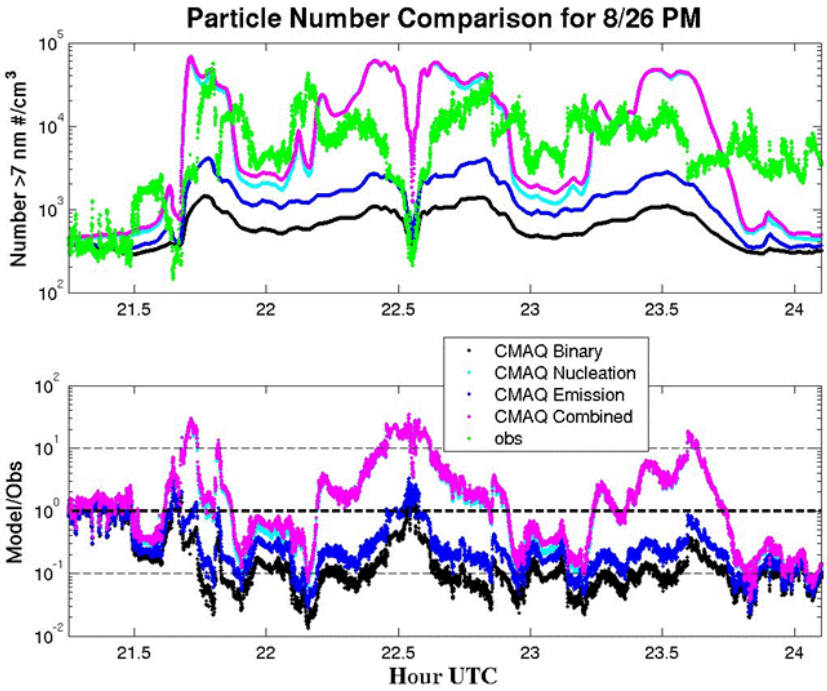

Figure 7.6 Comparison of CMAQ number concentration > 7 nm (instrument lower detection limit) to observations for the PNW2001 flight on the afternoon of 26 August.

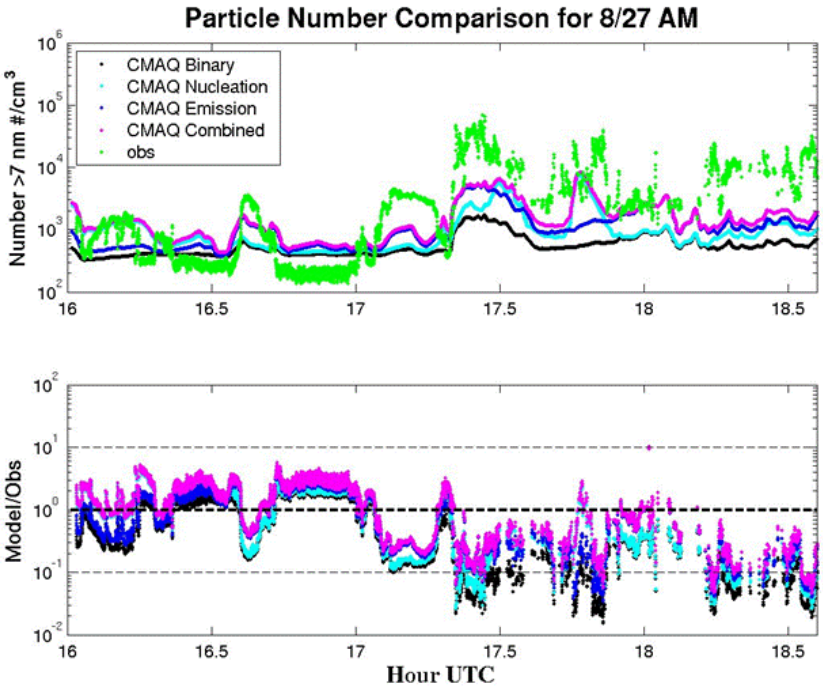

Figure 7.7 Comparison of CMAQ number concentration > 7 nm (instrument lower detection limit) to observations for the PNW2001 flight on the morning of 27 August.

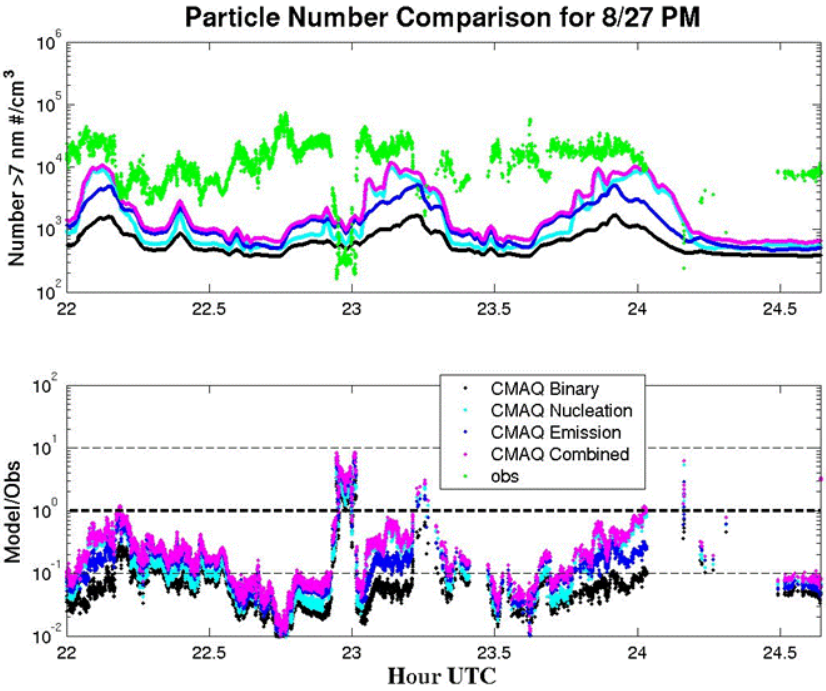

Figure 7.8 Comparison of CMAQ number concentration > 7 nm (instrument lower detection limit) to observations for the PNW2001 flight on the afternoon of 27 August.

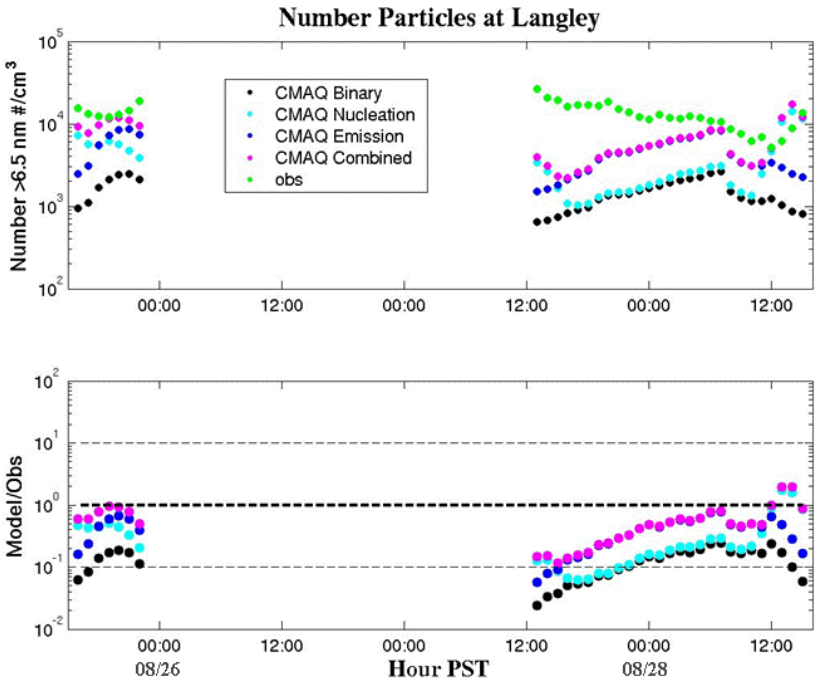

Figure 7.9 Comparison of CMAQ number concentration > 6.5 nm (instrument lower detection limit) to observations at Langley during 00 UTC 26 August to 23 UTC 28 August.

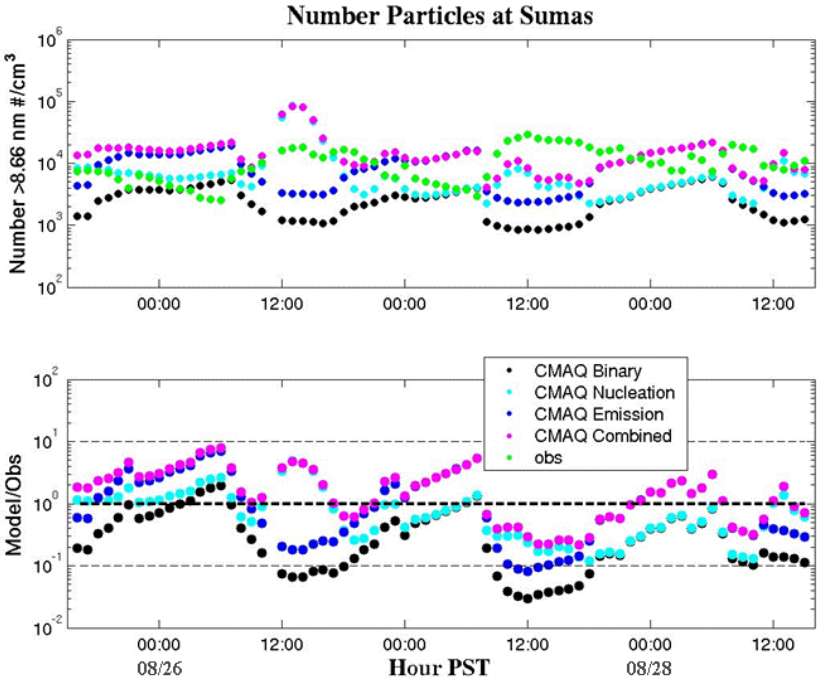

Figure 7.10 Comparison of CMAQ number concentration > 8.66 nm (instrument lower detection limit) to observations at Sumas during 00 UTC 26 August to 23 UTC 28 August.

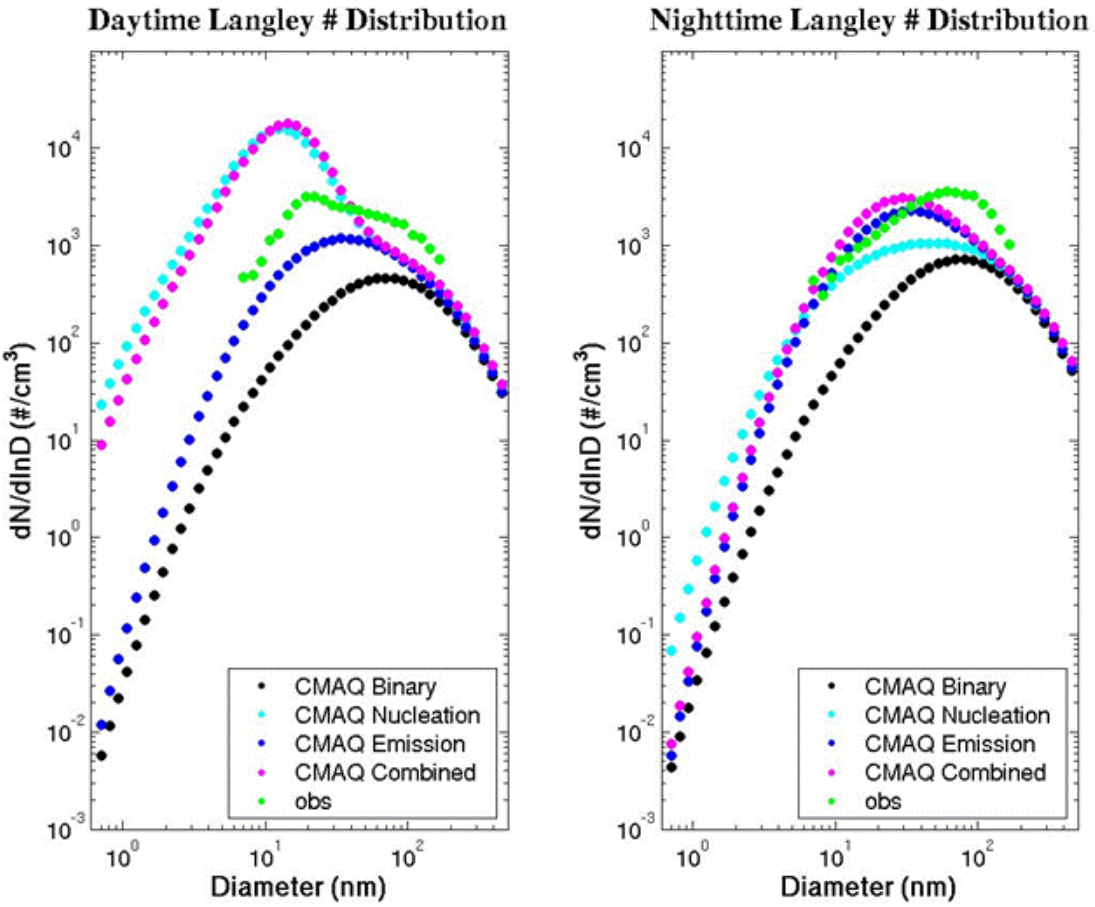

Figure 7.11 Day and night average size distributions at Langley as observed and for the Base Case (CMAQ Binary), Nucleation, Emission, and Combined Update cases.

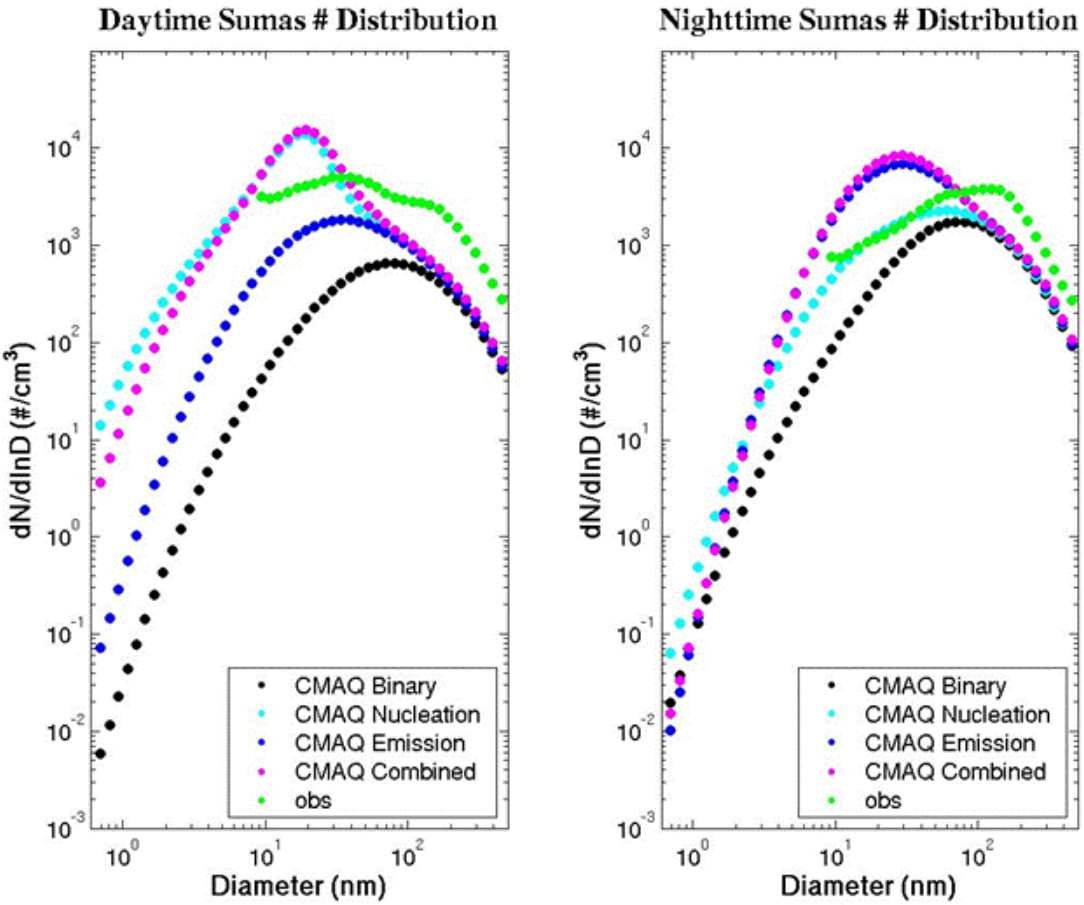

Figure 7.12 Day and night average size distributions at Sumas as observed and for the Base Case (CMAQ Binary), Nucleation, Emission, and Combined Update cases.

Table 7.3 Lowest layer Aitken and accumulation mode parameters regionally-averaged from 00 UTC 26 August to 23 UTC 28 August.

Domain

	$D_{g,ait}$ (nm)	$D_{g,acc}$ (nm)	$\sigma_{g,ait}$	$\sigma_{g,acc}$
CMAQ v.4.4	41	78	2.3	2.3
Nucleation	42	88	2.1	2.2
Emission	36	95	2.2	2.2
Combined Update	38	104	2.1	2.1

Puget Sound / LFV

	$D_{g,ait}$ (nm)	$D_{g,acc}$ (nm)	$\sigma_{g,ait}$	$\sigma_{g,acc}$
CMAQ v.4.4	45	81	2.3	2.2
Nucleation	35	85	2.1	2.1
Emission	36	111	2.1	2.0
Combined Update	30	111	2.0	2.0

Puget Sound

	$D_{g,ait}$ (nm)	$D_{g,acc}$ (nm)	$\sigma_{g,ait}$	$\sigma_{g,acc}$
CMAQ v.4.4	46	82	2.3	2.2
Nucleation	38	86	2.1	2.1
Emission	38	110	2.1	2.0
Combined Update	32	109	2.0	2.0

Seattle

	$D_{g,ait}$ (nm)	$D_{g,acc}$ (nm)	$\sigma_{g,ait}$	$\sigma_{g,acc}$
CMAQ v.4.4	43	81	2.3	2.1
Nucleation	30	81	2.1	2.1
Emission	34	117	2.1	1.9
Combined Update	26	109	2.0	2.0

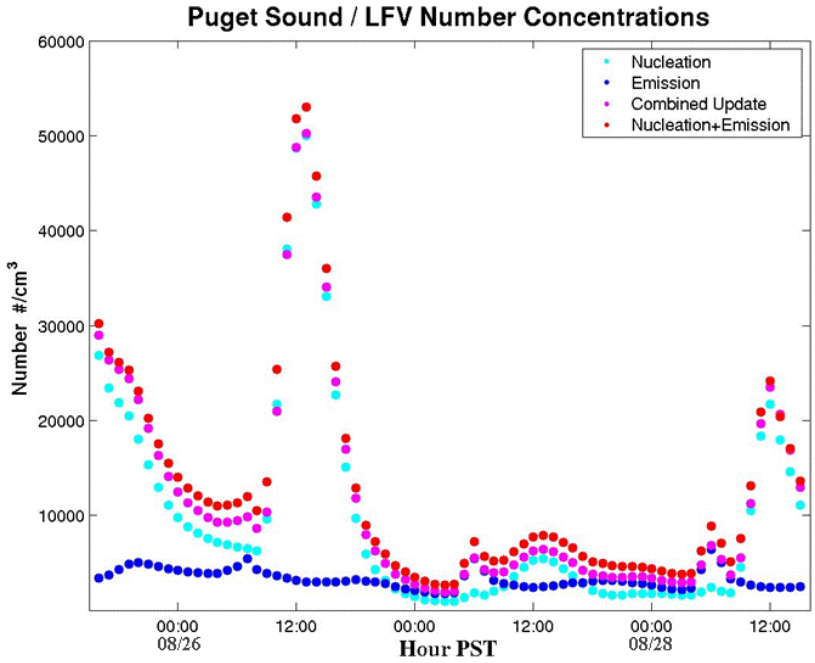

Figure 7.13 Lowest-layer average number concentration in the Puget Sound and Lower Fraser Valley as a function of time for 00 UTC 26 August to 23 UTC 28 August.

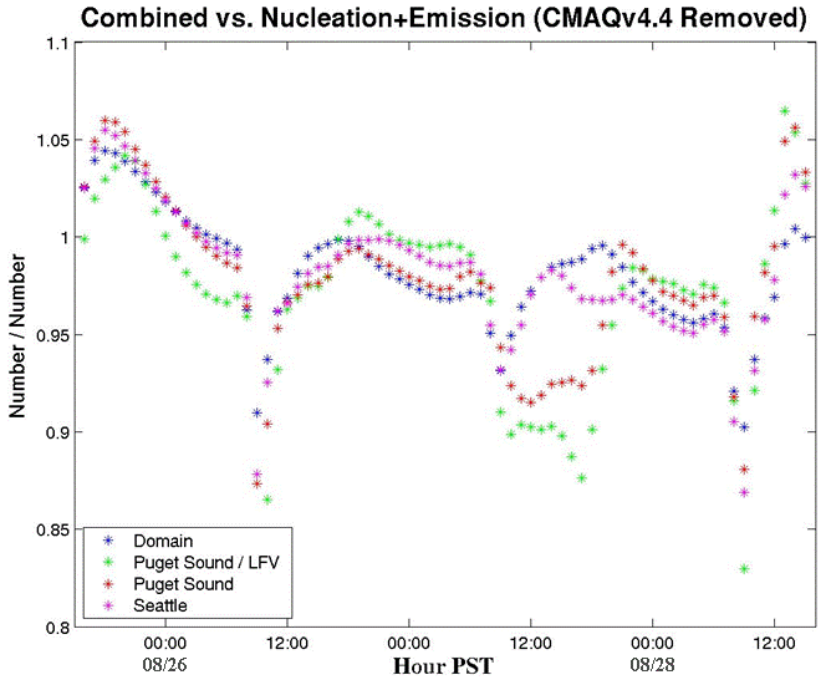

Figure 7.14 Lowest-layer Combined Update divided by the sum of the Nucleation and Emission cases for four regions: domain-wide, the Puget Sound / Lower Fraser Valley, Puget Sound, and Seattle. Each scenario has the Base Case CMAQ v4.4 number concentration removed.

Table 7.4 Surface $PM_{2.5}$ averaged for Washington observation locations. The difference for each case from the Base Case CMAQ v4.4 is shown in the four columns to the right for the Washington stations and for each Pacific 2001 site.

	$PM_{2.5}$				
		difference from CMAQ v4.4			
	WA obs	WA obs	Lnel	Sumas	Slocan Park
CMAQ v.4.4	9.79	Ø	Ø	Ø	Ø
Nucleation	10.84	1.05	1.16	1.29	1.12
Emission	10.25	0.46	0.47	0.67	0.39
Combined Update	11.12	1.33	1.59	1.87	1.52
Observations	10.46	Ø	Ø	Ø	Ø

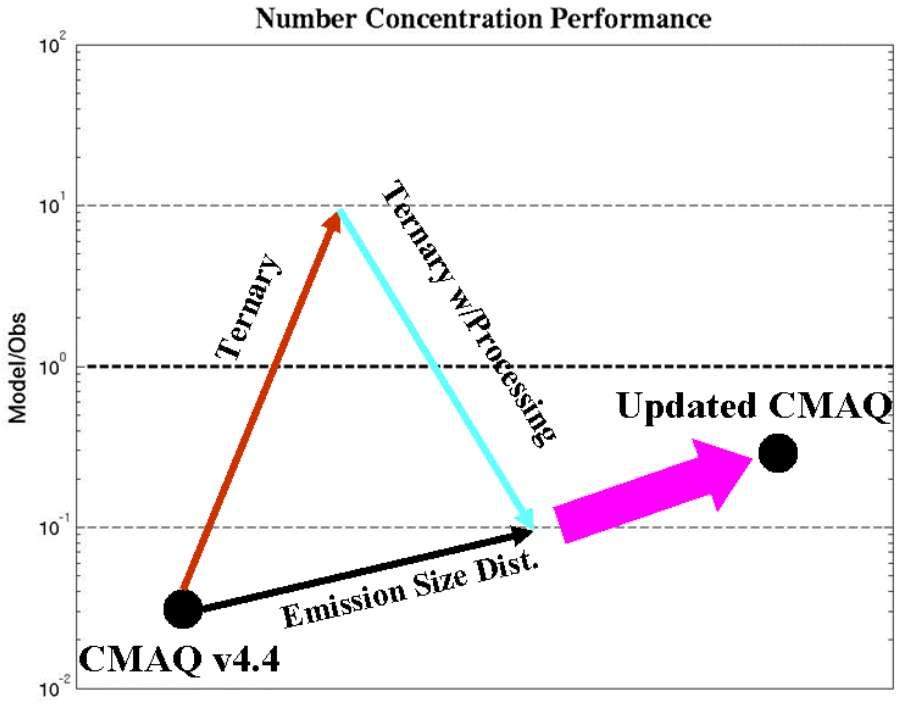

Figure 7.15 Total, lowest-layer modeled surface area in the Puget Sound / Lower Fraser Valley between 00 UTC 26 August and 23 UTC August for Base Case CMAQ v4.4, Nucleation, Emission, and Combined Update.

8. Conclusion

CMAQ v.4.4 was run for a short period of August 2001 in the Pacific Northwest when specialized air quality data from aircraft and surface sites were available. The focus was performance of the modeled aerosol size distributions and especially the ultrafine particles with diameters less than 100 nm. Based on results from the initial comparison, modifications were made to CMAQ to better represent ultrafine particles. The nucleation routine was changed to include ammonia in the nucleation process and to treat freshly nucleated particles within the existing three-mode lognormal structure. The size distribution of emitted particles was updated to reflect the smallest resolvable scale in a typical CMAQ grid and to fully include emissions of ultrafine particles. The objectives were to model the entire aerosol size distribution as accurately as possible and to update the science in CMAQ for ultrafine particles.

The unmodified CMAQ v4.4 underpredicts total particle number concentrations by 1-2 orders of magnitude. The bias is consistent throughout the day and across the urban-influenced region. It becomes progressively worse for smaller particle sizes, is not associated with any one chemical species, and is not correlated with a particular source or air mass aging fraction. The number of particles could have been underpredicted due to a poor representation of aerosol in general, but performance for total and speciated $PM_{2.5}$ is in line with other CMAQ simulations, is slightly overpredicted on average, and exhibits a time-series bias uncorrelated with the number underprediction. Errors in the meteorological simulation and in gaseous concentrations (precursors to aerosol) do not show a pattern consistent with the number underprediction. Of all the aerosol processes that create and destroy particles in an urban environment, the particle formation

mechanisms in CMAQ v4.4 for regional nucleation and direct source emissions are outdated scientifically and are most likely to cause a consistent underprediction in time, space, and chemical species that is more pronounced at smaller sizes.

The addition of the most recent process mechanisms for ternary nucleation, conservation of sulfur, and nucleation mode scavenging and growth produces number concentrations and size distributions closer to observed values in the Pacific Northwest in 2001. In CMAQ v4.4, few particles are produced through regional nucleation and there is no structural method for modeling them separately from the Aitken mode. Adding ternary nucleation and processing of the nucleation mode to the Aitken mode results in improvement but with a residual number underprediction of up to 1 order of magnitude. The model's performance is now much less consistent in space and time because ternary nucleation and nucleation mode processes are extremely sensitive to the input parameters and to the pre-existing aerosol properties. The modeled number size distributions have the three major qualities of urban aerosol, which are a distinct Aitken and accumulation mode, an Aitken mode that is more prominent than the accumulation mode during the day, and an Aitken mode whose number peaks below 50 nm. Despite the better performance, there are remaining issues such as a daytime Aitken mode that is too narrow and overpredicted in general, an accumulation mode that is too weak below 200 nm, and number concentrations that are higher on average but not always enhanced over the unmodified CMAQ v.4.4.

Updating the emission aerosol size distribution to reflect modern mesoscale measurements refines the modeled aerosol size distributions. The most important change is the increased apportionment of emitted $PM_{2.5}$ into the Aitken mode from 0 or 0.1% to 10%. The number of modeled particles increases by a factor of 2-3 downwind of urban areas, a factor of 3-4 in urban areas, and up to a factor of 4 near sulfate sources. If the emissions are driven by the size distributions that produce the most number of particles while remaining scientifically realistic, the number of modeled particles increases by typically a factor of 5-10. The enhancement is only a partial step towards solving the

underprediction by 1-2 orders of magnitude, but the new emission size distributions produce better modeled size distributions. The daytime distributions have fairly distinct Aitken and accumulation modes, and the overall shape is reasonable despite being uniformly underpredicted by a factor of 5 below 200 nm. Nighttime distributions at Langley are well modeled in the Aitken mode but negatively biased in the accumulation mode. The updated emissions size distributions modestly improve the number concentration performance and better model the Aitken mode particles in the ultrafine range.

When the nucleation and emission changes are made together, the resulting simulation shows characteristics of each major model upgrade, depending on which one is playing a larger role at the time and location. The effect of the nucleation changes is most obvious during the daytime in urban-influenced regions when regional nucleation produces large concentrations of particles. The emissions changes have a larger effect at night and on 27 August when daytime regional nucleation is muted. Even with both improvements in tandem, the total number of particles is underpredicted by up to 1 order of magnitude. Despite residual errors, the size distributions are better modeled in terms of separate Aitken and accumulation modes, an Aitken mode that is more prominent than the accumulation mode, and an Aitken mode that peaks below 50 nm. The changes to model nucleation and emission processes improve overall model performance and scientific integrity.

The fact that these changes make a noticeable improvement in results adds weight to this study's premise that regional nucleation occurs regularly during the Puget Sound summer and that emissions of Aitken mode particles are an important component to the ambient aerosol size distribution. Yet, the underprediction in particle concentrations is only reduced and not eliminated entirely, and the modeled size distributions using both the nucleation and emissions changes together assume some negative aspects of the individual cases. It is very likely that our understanding of aerosol pollution, especially in the ultrafine range, is not yet complete. Certainly the role of organic compounds in

growing nucleation mode particles to 10-20 nm is an unresolved scientific question and the focus of intense research. Mesoscale emissions of particles below the common instrument detection limit of 3-10 nm may be a substantial source of aerosol. Since the accumulation mode number below 250 nm is consistently underpredicted while $PM_{2.5}$ mass is well modeled, CMAQ's mode merging, competing gas phase condensation, or particle coagulation could be removing particles from the Aitken mode and low end of the accumulation mode and stacking them in the high end of the accumulation mode. A modeling technique for representing aerosol processing on the neighborhood scale is a necessary step beyond the observation-based parameterization in this study. Regardless of these open research questions, this study shows that after model improvements CMAQ is able to reproduce number concentrations to within one order of magnitude and produce size distributions with the appropriate major features. The updated science that makes this possible was chosen to improve the model in the Pacific Northwest but applies generally to simulations in all mid-latitude regions influenced by urban emissions.

Bibliography

Alam, A., J. P. Shi, and R. M. Harrison, 2003: Observations of new particle formation in urban air. *J. Geophys. Res.*, **108**, 4093, doi:10.1029/2001JD001417.

Alfarra, M. R., H. Coe, J. D. Allan, K. N. Bower, H. Boudries, M. R. Canagaratna, J. L. Jimenez, J. T. Jayne, A. A. Garforth, S.-M. Li, and D. R. Worsnop, 2004: Characterization of urban and rural organic particulate in the Lower Fraser Valley using two Aerodyne Aerosol Mass Spectrometers. *Atmos. Environ*., **38**, 5745-5758.

Aklilu, Y.-A., and M. Mozurkewich, 2004: Determination of external and internal mixing of organic and inorganic aerosol components from hygroscopic properties of submicrometer particles during a field study in the Lower Fraser Valley. *Aerosol Sci. Technol.*, **38**, 140-154.

Anderson, T. L., D. S. Covert, J. D. Wheeler, J. M. Harris, K. D. Perry, B. E. Trost, and D. A. Jaffe, 1999: Aerosol backscatter fraction and single scattering albedo: Measured values and uncertainties at a coastal station in the Pacific Northwest. *J. Geophys. Res*., **104**, 26,793–26,807.

Anlauf, K., S.-M. Li, R. Leaitch, J. Brook, K. Hayden, D. Toom-Sauntry, and A. Wiebe, 2006: Ionic composition and size characteristics of particles in the Lower Fraser Valley: Pacific 2001 field study. *Atmos. Environ*., **40**, 2662-2675.

Anttila, T., and V.-M. Kerminen, 2003: Condensational growth of atmospheric nuclei by organic vapours. *J. Aerosol. Sci*., **34**, 41-61.

Asmi, A., 2005: Modal modelling of aerosol dynamics and formation in regional scale. *Proc. 2005 European Aerosol Conference*, European Aerosol Assemby, Ghent, Belgium.

——, B. Schell, I. A. Ackermann, H. Hass, and M. Kulmala, 2001: Development of nucleation scheme for modal regional model. Abstracts of the European Aerosol Conference, 2001.

Ball, S. M., D. R. Hanson, F. L. Eisele, and P. H. McMurry, 1999: Laboratory studies of particle nucleation: Initial results for H_2SO_4, H_2O, and NH_3 vapors. *J. Geophys. Res.*, **104**, 23,709-23,718.

Barna, M., and B. Lamb, 2000: Improving ozone modeling in regions of complex terrain using observational nudging in a prognostic meteorological model. *Atmos. Environ*., **34**, 4889-4906.

Bein, K. J., Y. Zhao, A. S. Wexler, and M. V. Johnston, 2005: Speciation of size-resolved individual ultrafine particles in Pittsburgh, Pennsylvania. *J. Geophys. Res*., **110**, D07S05, doi:10.1029/2004JD004708.

Benson, P. E., 1992: A review of the development and application of the CALINE3 and CALINE4 models. *Atmos. Environ*., **26**, 379-390.

Bey, I., D. J. Jacob, R. M. Yantosca, J. A. Logan, B. D. Field, A. M. Fiore, Q. Li, H. Y. Liu, L. J. Mickley, M. G. Schultz, 2001: Global modeling of tropospehric chemistry with assimilated meteorology: Model description and evaluation. *J. Geophys. Res.*, **106**, 23,073-23,095.

Bhave, P., C. Nolte, J. Pleim, D. Schwede, and S. Roselle, 2005: Recent developments in the CMAQ aerosol module. *Proc. Models-3 Users' Workshop*, Research Triangle Park, N.C. [Available from http://www.cmascenter.org/conference/2005/ppt/p17.pdf.]

——, G. Sarwar, W. Appel, and R. Dennis, 2006: Revised treatment of N2O5 hydrolysis in CMAQ. *Proc. 5th Models-3 Users' Workshop*, Research Triangle Park, N.C. [Available from http://www.cmascenter.org/conference/2006/agenda.cfm.]

Binkowski, F. S., and U. Shankar, 1995: The Regional Particulate Matter model. 1. Model description and preliminary results. *J. Geophys. Res.*, **100**, 26,191-26,209.

——, and S. J. Roselle, 2003: Models-3 Community Multiscale Air Quality (CMAQ) model aerosol component. 1. Model description. *J. Geophys. Res.*, **108**, 4183, doi:10.1029/2001JD001409.

Birmili, W., A. Wiedensohler, C. Plass-Dülmer, and H. Berresheim, 2000: Evolution of newly formed aerosol particles in the continental boundary layer: a case study including OH and H_2SO_4 measurements. *Geophys Res Lett*., **27**, 2205-2208.

Boudries, H., M. R. Canagaratna, J. T. Jayne, M. R. Alfarra, J. Allan, K. N. Bower, H. Coe, S. C. Pryor, J. L. Jimenez, J. R. Brook., S. Li, and D. R. Worsnop, 2004: Chemical and physical processes controlling the distribution of aerosols in the Lower

Fraser Valley, Canada, during the Pacific 2001 field campaign, *Atmos. Environ.*, **38**, 5759-5774.

Brock, C. A., R. A. Washenfelder, M. Trainer, T. B. Ryerson, J. C. Wilson, J. M. Reeves, L. G. Huey, J. S. Holloway, D. D. Parrish, G. Hübler, and F. C. Fehsenfeld, 2002: Particle growth in the plumes of coal-fired power plants. *J. Geophys. Res.*, **107**, 10.1029/2001JD001062.

Brook, J. R., K. B. Strawbridge, B. J. Snyder, H. Boudries, D. Worsnop, S. Sharma, K. Anlauf, G. Lu, and K. Hayden, 2004: Towards an understanding of the fine particle variations in the LFV: integration of chemical, physical and meteorological observations. *Atmos. Environ.*, **38**, 5775-5788.

Bukowiecki, N., J. Dommen, A. S. H. Prévôt, E. Weingartner, and U. Baltensperger, 2003: Fine and ultrafine particles in the Zürich (Switzerland) area measured with a mobile laboratory: an assessment of the seasonal and regional variation throughout a year. *Atmos. Chem. Phys.*, **3**, 1477-1494.

Burtscher, H., 2005: Physical characterization of particulate emissions from diesel engines: A review. *J. Aerosol. Sci.*, **36**, 896-932.

Byun, D. W., 1999a: Dynamically consistent formulations in meteorological and air quality models for multiscale atmospheric studies. Part II: Mass Conservation Issues. *J. Atmos. Sci.*, **56**, 3808-3820.

——, 1999b: Fundamental of one-atmosphere dynamics for multiscale air quality modeling. *Science Algorithms of the EPA Models-3 Community Multi-scale Air Quality (CMAQ) Modeling System*, D. W. Byun and J. K. S. Ching, Eds., NERL, Research Triangle Park, NC, Chapter 5.

——, and J. K. S. Ching, 1999: Science Algorithms of the EPA Models-3 Community Multiscale Air Quality (CMAQ) Modeling System. EPA/600/R-99/030, Off. of Res. and Dev., U.S. Environ. Prot. Agency, Washington, D.C.

——, and K. L. Schere, 2006: Review of the governing equations, computational algorithms, and other components of the Models-3 Community Multiscale Air Quality (CMAQ) modeling system. *Appl. Mech. Rev.*, **59**, 51-77.

——, J. Pleim, R. T. Tang, and A. Bourgeois, 1999a: Meteorology-Chemistry Interface Processor (MCIP) for Models-3 Community Multiscale Air Quality (CMAQ) modeling system. *Science Algorithms of the EPA Models-3 Community Multi-scale Air Quality (CMAQ) Modeling System*, D. W. Byun and J. K. S. Ching, Eds., NERL,

Research Triangle Park, NC, Chapter 12.

——, J. Young, J. Pleim, M. T. Odman, and K. Alapaty, 1999b: Numerical transport algorithms for the Community Multiscale Air Quality (CMAQ) chemical transport model in generalized coordinates. *Science Algorithms of the EPA Models-3 Community Multi-scale Air Quality (CMAQ) Modeling System*, D. W. Byun and J. K. S. Ching, Eds., NERL, Research Triangle Park, NC, Chapter 7.

——, C.-K. Song, P. B. Percell, J. Pleim, T. Otte, J. Young, and R. Mathur, 2006: Linkage between WRF/NMM and CMAQ models. *Proc. 5th Models-3 Users' Workshop*, Research Triangle Park, N.C. [Available from http://www.cmascenter.org/conference/2006/agenda.cfm.]

Cabada, J. C., S. Rees, S. Takahama, A. Khlystov, S. N. Pandis, C. I. Davidson, and A. L. Robinson, 2004: Mass size distribution and size resolved chemical composition of fine particulate matter at the Pittsburgh supersite. *Atmos. Environ.*, **38**, 3127-3141.

Cantrell, B. K., and K. T. Whitby, 1978: Aerosol size distributions and aerosol volume formation for a coal-fired power plant plume. *Atmos. Environ.*, **12**, 323-333.

Capaldo, K. P., C. Pilinis, and S. N. Pandis, 2000: A computationally efficient hybrid approach for dynamic gas/aerosol transfer in air quality models. *Atmos. Environ.*, **34**, 3617-3627.

Carter, W. P. L., 2000: Documentation of the SAPRC-99 chemical mechanism for VOC reactivity assessment. Final Report to California Air Resources Board, Contract 92-329 and 95-308, SARC, University of California, Riverside, CA.

Chen, G., and coauthors, 2005: An investigation of the chemistry of ship emission plumes during ITCT 2002. *J. Geophys. Res.*, **110**, D10S90, doi:10.1029/2004JD005236.

Chen, J., H. Mao, R. W. Talbot, and R. J. Griffin, 2006: Application of the CACM and MPMPO modules using the CMAQ model for the eastern United States. *J. Geophys. Res.*, **111**, D23S25, doi:10.1029/2006JD007603.

Cheng, Y., S.-M. Li, A. Leithead, and J. R. Brook, 2006: Spatial and diurnal distributions of *n*-alkanes and *n*-alkan-2-ones on PM2.5 aerosols in the Lower Fraser Valley, Canada. *Atmos. Environ.*, **40**, 2706-2720.

Cho, S.-H., 2005: Detailed Microphysical Modeling Study of Particle Size Distributions in an Industrial Plume. Ph.D. Dissertation, York University, Canada. [Available from

http:// www.yorku.ca/dvm/DianePublications.htm.]

Cimorelli, A. J., S. G. Perry, A. Venkatram, J. C. Weil, R. J. Paine, R. B. Wilson, R. F. Lee, W. D. Peters, and R. W. Brode, 2005: AERMOD: A dispersion model for industrial source applications. Part I: General model formulation and boundary layer characterization. *J. Appl. Meteo*., **44**, 682-693.

Clarke, A.D., V. N. Kapustin, F. L. Eisele, R. J. Weber, and P. H. McMurry, 1999: Particle production near marine clouds: sulfuric acid and predictions from classical binary nucleation. *Geophys. Res. Lett*., **26**, 2425-2428.

CMAS, cited 2006: AEROSOL_NOTES – 15 Mar 2006. [Available online at http://www.cmascenter.org/help/model_docs/cmaq/4.5.1/AEROSOL_NOTES.txt.]

Coffman, D. J., and D. A. Hegg, 1995: A preliminary study of the effect of ammonia on particle nucleation in the marine boundary layer. *J. Geophys. Res.,* **100** (D4), 7147-7160.

Covert. D. S., V. N. Kapustin, T. S. Bates, and P. K. Quinn, 1992: New particle formation in the marine boundary layer. *J. Geophys. Res.,* **97**, 20,581-20,589.

Dal Maso, M. M. Kulmala, K. E. J. Lehtinen, J. M. Mkel, P. Aalto, and C. D. O'Dowd, 2002: Condensation and coagulation sinks and formation of nucleation mode particles in coastal and boreal forest boundary layers. *J. Geophys. Res*., **107**, D198097, doi:10.1029/2001JD001053.

Davidson, P. M., N. Seaman, K. Schere, C. Wayland, and K. Carey, 2003: National air quality forecasting capability: First steps toward implementation. *Proc. Models-3 Users' Workshop*, Research Triangle Park, N.C. [Available from http://www.cmascenter.org/2003_workshop/downloads.html.]

Davidson, C. I., R. F. Phalen, and P. A. Solomon, 2005: Airborne particulate matter and human health: A review. *Aerosol Sci. Technol*., **39**, 737-749.

Dekati Ltd., 2003: Applying a fine particle sampler for combustion studies. Dekati Ltd. Technical note. [Available from www.dekati.com/technicalnotes/FPS_technical_note.pdf.]

Delfino, R. J. A. M. Murphy-Moulton, R. T. Burnett, J .R. Brook, and M. R. Becklake, 1997: Effects of air pollution on emergency room visits for respiratory illnesses in Montreal, Quebec. *Am. J. Respir. Crit. Care Med*., **155**, 568-576.

DieselNet, 2002: Diesel exhaust particle size. DieselNet Technology Guide. [Available from http://www.dieselnet.com/tech/dpm_size.html].

Dockery, D. W., and coauthors, 1993: An association between air pollution and mortality in six US cities. *N. Engl. J. Med.*, **329**, 1753-1759.

Dudhia, J., D. Gill, Y-R Guo, K Manning, J Michalakes, and A. Bourgeois, 2001: PSU/NCAR mesoscale modeling system tutorial class notes and user's guide: MM5 modeling system version 3. [Available from http://www.mmm.ucar.edu/mm5/documents/tutoral-v3-notes.pdf.]

Eder, B., and S. Yu, 2006: A performance evaluation of the 2004 release of Models-3 CMAQ. *Atmos. Environ.*, **40**, 4811-4824.

——, and coauthors, 2003: Evaluation of Models-3 CMAQ. *Proc. Models-3 Users' Workshop*, Research Triangle Park, N.C. [Available from http://www.cmascenter.org/2003_workshop/downloads.html.]

Eisele, F. L., E. R. Lovejoy, E. Kosciuch, K. F. Moore, R. L. Mauldin III, J. N. Smith, P. H. McMurry, and K. Iida, 2006: Negative atmospheric ions and their potential role in ion-induced nucleation. *J. Geophys. Res.*, **111**, D04305, doi:10.1029/2005JD006568.

ENVIRON, 2006: CAMx User's Guide, Version 4.40 (pp. 1-261), Novato, CA: ENVIRON International Corporation. [Available from http://www.camx.com/files/CAMxUsersGuide_v4.40.pdf].

Environment Canada, cited 2002: Pacific 2001 Air Quality Study. [Available online at http://www.msc.ec.gc.ca/projects/pacific2001/index_e.html.]

Fan, J., R. Zhang, D. Collins, and G. Li, 2006: Contribution of secondary condensable organics to new particle formation: A case study in Houston, Texas. *Geophys. Res. Lett.*, **33**, L15802, doi:10.1029/2006GL026295.

Fan, X., J. R. Brook, and S. A. Mabury, 2004: Measurement of organic and elemental carbon associated with $PM_{2.5}$ during Pacific 2001 study using an integrated organic gas and particle sampler. *Atmos. Environ.*, **38**, 5801-5810.

Freiman, M. T., N. Hirshel, and D. M. Broday, 2006: Urban-scale variability of ambient particulate matter attributes. *Atmos. Environ.*, **40**, 5670-5684.

Frick, G. M., and W. A. Hoppel, 2000: Airship measurements of ship's exhaust plumes and their effect on marine boundary layer clouds. *J. Atmos. Sci.*, **57**, 2625-2648.

Gauderman, W. J., and coauthors, 2004: The effect of air pollution on lung development from 10 to 18 years of age. *N. Engl. J. Med*., **351**, 1057-1067.

Gery, M. W., G. Z. Whitten, J. E. Killus, and M. C. Dodge, 1989: A photochemical kinetics mechanism for urban and regional scale computer modeling. *J. Geophys. Res*., **94**, 12925-12956.

Gidhagen, L., C. Johansson, J. Strm, A. Kristensson, E. Swietlicki, L. Pirjola, and H.-C. Hansson, 2003: Model simulation of ultrafine particles inside a road tunnel. *Atmos. Environ*., **37**, 2023-2036.

——, ——, J. Langner, and G. Olivares, 2004a: Simulation of NO_x and ultrafine particles in a street canyon in Stockholm, Sweden. *Atmos. Environ*., **38**, 2029-2044.

——, ——, G. Omstedt, J. Langner, and G. Olivares, 2004b: Model simulations of NO_x and ultrafine particles close to a Swedish highway. *Environ. Sci. Technol*., **38**, 6730-6740.

——, ——, J. Langner, and V. L. Foltescu, 2005: Urban scale modeling of particle number concentration in Stockholm. *Atmos. Environ*., **39**, 1711-1725.

Gillani, N. V., and J. M. Godowitch, 1999: Plume-in-grid treatment of major point source emissions. *Science Algorithms of the EPA Models-3 Community Multi-scale Air Quality (CMAQ) Modeling System*, D. W. Byun and J. K. S. Ching, Eds., NERL, Research Triangle Park, NC, Chapter 9.

Godowitch, J. M., 2005: Development and application of the CMAQ plume-in-grid-model. *4th Annual CMAS Models-3 Users' Conference*, Chapel Hill, NC. 26-28 Sept., 2005.

Gramotnev, D. K., and G. Gramotnev, 2005a: Modeling of aerosol dispersion from a busy road in the presence of nanoparticle fragmentation. *J. Appl. Meteo*., **44**, 888-899.

——, and ——, 2005b: A new mechanism of aerosol evolution ner a busy road: fragmentation of nanoparticles. *J. Aerosol. Sci*., **36**, 323-340.

Gramotnev, G., and Z. Ristovski, 2004: Experimental investigation of ultra-fine particle size distribution near a busy road. *Atmos. Environ*., **38**, 1767-1776.

Grell, G. A., S. E. Peckham, R. Schmitz, S. A. McKeen, G. Frost, W. C. Skamarock, and B. Eder, 2005: Fully coupled "online" chemistry within the WRF model. *Atmos. Environ.*, **39**, 6957-6975.

Harris, S. J., and M. M. Maricq, 2002: The role of fragmentation in defining the signature size distribution of diesel soot. *J. Aerosol Sci.*, **33**, 935-942.

Hayden, K. L., K. G. Anlauf, S.-M. Li, A. M. Macdonald, J. W. Bottenheim, J. R. Brook, and H. A. Wiebe, 2004: Characterization of gaseous nitrogen oxides in the Lower Fraser Valley during Pacific 2001. *Atmos. Environ.*, **38**, 5811-5823.

Heim, M., G. Kasper, G. P. Reischl, and C. Gerhart, 2004: Performance of a new commercial electrical mobility spectrometer. *Aerosol Sci. Technol.*, **38(S2)**, 3-14.

Held, T., D. P. Y. Chang, and D. A. Niemeier, 2003: UCD 2001: An improved model to simulate pollutant dispersion from roadways. *Atmos. Environ.*, **37**, 5325-5336.

Hewitt, C. N., 2001: The atmospheric chemistry of sulphur and nitrogen in power station plumes. *Atmos. Environ.*, **35**, 1155-1170.

Hobbs, P. V., M. W. Eltgroth, D. A. Hegg, and L. F. Radke, 1983: Particle formation and growth in power plant plumes. Volume 1: field observations and theoretical studies of the evolution of particles in the plumes from coal-fired electric power plants. Final Report to the Electric Power Research Institute, EA-3105, Volume 1 Research Project 330-1.

——, and coauthors, 2000: Emissions from ships with respect to their effects on clouds. *J. Atmos. Sci.*, **57**, 2570-2590.

Hodan, W., 2003: Recommendations for the update and improvement of existing PM2.5 split factors. Report to the Environmental Protection Agency, Pacific Environmental Services, Contract 68-D-02-104 / WA1-05.

Hogrefe, O., G. G. Lala, B. P. Frank, J. J. Schwab, and K. L. Demerjian, 2006: Field evaluation of a TSI 3034 Scanning Mobility Particle Sizer in New York City: Winter 2004 intensive campaign. *Aerosol Sci. Technol.*, **40**, 753-762.

Hong, S.- Y., and H.- L. Pan, 1996: Nonlocal boundary layer vertical diffusion in a medium-range forecast model. *Mon. Wea. Rev.*, **124**, 2322-2339.

Houghton, J. T., Y. Ding, D. J. Griggs, M. Noguer, P. J. van der Linden, X. Dai, K. Maskell, C. A. Johnson, 2001: *Climate Change 2001: The Scientific Basis*. Cambridge University Press, 881 pp.

Houyoux, M., J. Vukovich, and J. E. Brandmeyer, 2002: Sparse Matrix Operator Kernel Emissions modeling system--SMOKE user manual. Research Triangle Park, N.C.

[Available from http://www.cleanairinfo.com/PMModelPerformanceWorkshop2.]

Huang, L., J. R. Brook, W. Zhang, S. M. Li, L. Graham, D. Ernst, A. Chivulescu, and G. Lu, 2006: Stable isotope measurements of carbon fractions (OC/EC) in airborne particulate: A new dimension for source characterization and apportionment. *Atmos. Environ.*, **40**, 2690-2705.

Hussein, T., A. Puustinen, P. P. Aalto, J. M. Mäkelä, K. Hämeri, and M. Kulmala, 2003: Urban aerosol number size distributions. *Atmos. Chem. Phys. Discuss.*, **3**, 5139-5184.

——, K. Hämeri, P. P. Aalto, P. Paatero, and M. Kulmala, 2005: Modal structure and spatial-temporal variations of urban and suburban aerosols in Helsinki—Finland. *Atmos. Environ.*, **39**, 1655-1668.

Jacobson, M. Z., 1997a: Development and application of a new air pollution modeling system. Part II: Aerosol module structure and design. *Atmos. Environ.*, **31A**, 131-144.

——, 1997b: Development and application of a new air pollution modeling system. Part III: Aerosol-phase simulations. *Atmos. Environ.*, **31A**, 587-608.

——, and J. H. Seinfeld, 2004: Evolution of nanoparticle size and mixing state near the point of emission. *Atmos. Environ.*, **38**, 1839-1850.

——, D. B. Kittelson, and W. F. Watts, 2005: Enhanced coagulation due to evaporation and its effect on nanoparticle evolution. *Environ. Sci. Technol.*, **39**, 9486-9492.

Jang, M., N. M. Czoschke, S. Lee, and R. M. Kamens, 2002: Heterogeneous atmospheric aerosol production by acid-catalyzed particle-phase reactions. *Science*, **298**, 814-817.

Janhäll, K. F. G. Olofson, P. U. Andersson, J. B. C. Pettersson, and M. Hallquist, 2006: Evolution of the urban aerosol during winter temperature inversion episodes. *Atmos. Environ.*, **40**, 5355-5366.

Jeong, C.-H., G. J. Evans, P. K. Hopke, D. Chalupa, and M. J. Uteli, 2006: Influence of atmospheric dispersion and new particle formation events on ambient particle number concentration in Rochester, United States, and Toronto, Canada. *J. Air & Waste Manage. Assoc.*, **56**, 431-443.

Jiang, W., 2003: Instantaneous secondary organic aerosol yields and their comparison with overall aerosol yields for aromatic and biogenic hydrocarbons. *Atmos. Environ.*, **37**, 5439-5444.

——, and H. Roth, 2003: A detailed review and analysis of science, algorithms, and code in the aerosol components of Models-3/CMAQ: I. Kinetic and thermodynamic processes in the AERO2 module. Report Number PET-1534-03S, Institute for Chemical Process and Environmental Technology, National Research Council Canada, Ottawa, Ontario, Canada, 2003/03.

——, E. Giroux, D. Yin, and H. Roth, 2003: Comparison of three secondary organic aerosol algorithms implemented in CMAQ. *Proc. Models-3 Users' Workshop*, Research Triangle Park, N.C. [Available from http://www.cmascenter.org/2003_workshop/downloads.html.]

——, S. Smyth, É. Giroux, H. Roth, and D. Yin, 2006: Differences between CMAQ fine mode particle and $PM_{2.5}$ concentrations and their impact on model performance evaluation in the lower Fraser valley. *Atmos. Environ.*, **40**, 4973-4985.

Jobson, T., and coauthors, 2002: Airborne measurements of hydrocarbons and aerosols in the Puget Sound airshed. *Eos Trans. AGU*, **83** (47), Fall Meet. Suppl., Abstract A71A-0062.

Karamchandani, P., C. Seigneur, K. Vijayaraghavan, and S.-Y. Wu, 2002: Development and application of a state-of-the-science plume-in-grid model. *J. Geophys. Res.*, **107**, 4403, doi:10.1029/2002JD002123.

——, K. Vijayaraghavan, S.-Y. Chen, C. Seigneur, and E. S. Edgerton, 2006: Plume-in-grid modeling for particulate matter. *Atmos. Environ.*, **40**, 7280-7297.

Kerminen, V.-M., and M. Kulmala, 2002: Analytical formulae connecting the "real" and the "apparent" nucleation rate and the nuclei number concentration for atmospheric nucleation events. *J. Aerosol. Sci.*, **33**, 609-622.

——, T. Anttila, K. E. J. Lehtinen, and M. Kulmala, 2004a: Parameterization for atmospheric new-particle formation: application to a system involving sulfuric acid and condensable water-soluble organic vapors. *Aerosol Sci. Technol.*, **38**, 1001-1008.

——, K. J. Lehtinen, T. Anttila, and M. Kulmala, 2004b: Dynamics of atmospheric nucleation mode particles: A timescale analysis. *Tellus*, **56B**, 135-146.

Ketzel, M., and R. Berkowicz, 2004: Modelling the fate of ultrafine particles from exhaust pipe to rural background: an analysis of time scales for dilution, coagulation, and deposition. *Atmos. Environ.*, **38**, 2639-2652.

——, P. Wåhlin, A. Kristensson, E. Swietlicki, R. Berkowicz, and F. Palmgren, 2003:

Particle and trace gas emission factors under urban driving conditions in Copenhagen based on street and roof-level observations. *Atmos. Environ*., **37**, 2735-2749.

——, ——, ——, ——, ——, O. J. Nielsen, and F. Palmgren, 2004: Particle size distribution and particle mass measurements at urban, near-city and rural level in the Copenahgen area and Southern Sweden. *Atmos. Chem. Phys*., **4**, 281-292.

Kikas, Ü, A. Mirme, E. Tamm, and T. Raunemaa, 1996: Statistical characteristics of aerosol in Baltic Sea region. *J. Geophys. Res*., **101**, 19319-19327.

Kim, S., S. Shen, C. Sioutas, Y. Zhu, and W. C. Hinds, 2002: Size distribution and diurnal and seasonal trends of ultrafine particles in source and receptor sites of the Los Angeles Basin. *J. Air & Waste Manage. Assoc*., **52**, 297-307.

Kis, V. K., M. Pósfai, and J. L. Lábár, 2006: Nanostructure of atmospheric soot particles. *Atmos. Environ*., **40**, 5533-5542.

Kittelson, D. B., 1998: Engines and nanoparticles: A review. *J. Aerosol Sci*., **29**, 575-588.

——, W. F. Watts, Jr., and M. Arnold, 1998a: Review of diesel particulate matter sampling methods final report. [Available from http://www.me.umn.edu/centers/cdr/reports/EPAreport3.pdf]

——, ——, and ——,1998b: Review of diesel particulate matter sampling methods supplemental report #2: aerosol dynamics laboratory and on-road studies. [Available from http://www.me.umn.edu/centers/cdr/reports/EPAreport2.pdf]

Knipping, E. M., 2005: Roadmap for development of CMAQ-MADRID. *Proc. 4th Models-3 Users' Workshop*, Research Triangle Park, N.C. [Available from http://www.cmascenter.org/conference/2005/archive.cfm.]

Korhonen, P., M. Kulmala, A. Laaksonen, Y. Visanen, R. McGraw, and J. H. Seinfeld, 1999: Ternary nucleation of H_2SO_4, NH_3, and H_2O in the atmosphere. *J. Geophys. Res.*, **104**, 26,349-26,353.

——, K. E. J. Lehtinen, L. Pirjola, I. Napari, H. Vehkamäki, M. Noppel, and M. Kulmala, 2003: Simulation of atmospheric nucleation mode: A comparison of nucleation models and size distribution representations. *J. Geophys. Res.*, **108**, 4471, doi:10.1029/2002JD003305.

Ku, M., C. Hogrefe, K. Civerolo, and G. Sistla, 2004: An assessment of CMAQ with TEOM measurements over the eastern US. *Proc. PM Model Performance Workshop*,

Research Triangle Park, N.C. [Available from http://www.cleanairinfo.com/PMModelPerformanceWorkshop2004/agenda.htm.]

Kuhn, T., S. Biswas, P. M. Fine, M. Geller, C. Sioutas, 2005: Physical and chemical characteristics and volatility of PM in the proximity of a light-duty vehicle freeway. *Aerosol Sci. Technol*., **39**, 347-357.

Kulmala, M., A. Laaksonen, and L. Pirjola, 1998: Parameterizations for sulfuric acid/water nucleation rates. *J. Geophys. Res.*, **103**, 8301-8307.

——, L. Pirjola, and J. M. Mäkelä, 2000: Stable sulphate clusters as a source of new atmospheric particles. *Nature*, **404**, 66-69.

——, M. Dal Maso, J. Mäkelä, L. Pirjola, M. Väkevä, P. Aalto, P. Mikkulainen, K. Hämeri, and C. O'Dowd, 2001: On the formation, growth and composition of nucleation mode particles. *Tellus Ser. B.*, **53**, 479-490.

——, V.-M. Kerminen, T. Anttila, A. Laaksonen, and C. D. O'Dowd, 2004a: Organic aerosol formation via sulphate cluster activation. *J. Geophys. Res.*, **109** , D04205, doi:10.1029/2003JD003961.

——, L. Laakso, K. E. J. Lehtinen, I. Riipinen, M. Dal Maso, T. Anttila, V.-M. Kerminen, U. Hõrrak, M. Vana, and H. Tammet, 2004b: Initial steps of aerosol growth. *Atmos. Chem. Phys.*, **4**, 2553-2560.

——, H. Vehkamäki, T. Petäjä, M. Dal Maso, A. Lauri, V.-M. Kerminen, W. Birmili, and P. H. McMurry, 2004c: Formation and growth rates of ultrafine atmospheric particles: A review of observations. *J. Aerosol Sci.*, **35**, 143-176.

——, M. T. Petäjä, P. Mönkkönen, I. K. Koponen, M. Dal Maso, P. P. Aalto, K. E. J. Lehtinen, and V.-M. Kerminen, 2005: On the growth of nucleation mode particles: source rates of condensable vapor in polluted and clean environments. *Atmos. Chem. Phys*., **5**, 409-416.

Laakso, L., T. Hussein, P. Aarnio, M. Komppula, V. Hiltunen, Y. Viisanen, and M. Kulmala, 2003: Diurnal and annual characteristics of particle mass and number concentrations in urban, rural and Arctic environments in Finland. *Atmos. Environ*., **37**, 2629-2641.

——, T. Anttila, K. E. J. Lehtinen, P. P. Aalto, M. Kulmala, U. Hõrrak, J. Paatero, M. Hanke, and F. Arnold, 2004: Kinetic nucleation and ions in boreal particle formation events. *Atmos Chem. Phys*., **4**, 2353-2366.

Laaksonen, A., A. Amed, J. Joutsensaari, L. Hiltunen, F. Cavalli, W. Junkermann, A. Asmi, S. Fuzzi, and M. C. Facchini, 2005: Cloud condensation nucleus production from nucleation events at a highly polluted region. *Geophys. Res. Lett*., **32**, L06812, doi:10.1029/2004GL022092.

Laden, F., J. Schwartz, F. E. Speizer, and D. W. Dockery, 2006: Reduction in fine particulate air pollution and mortality: Extended follow-up of the Harvard six cities study. *Am. J. Respir. Crit. Care Med*., **173**, 667-672.

Larson, T. V., D. S. Covert, E. Kim, R. Elleman, A. B. Schreuder, and T. Lumley, 2006: Combining size distribution and chemical species measurements into a multivariate receptor model of $PM_{2.5}$. *J. Geophys. Res*., **111**, D10S09, doi:10.1029/2005JD006285.

Lehtinen, K. E. J., and M. Kulmala, 2003: A model for particle formation and growth in the atmosphere with molecular resolution in size. *Atmos. Chem. Phys*., **3**, 251-257.

Leithead, A., S.-M. Li, R. Hoff, Y. Cheng, and J. Brook, 2006: Levoglucosan and dehydroabietic acid: Evidence of biomass burning impact on aerosols in the Lower Fraser Valley. *Atmos Environ*., **40**, 2721-2734.

Li, S.-M., 2004: A concerted effort to understand the ambient particulate matter in the Lower Fraser Valley: the Pacific 2001 Air Quality Study. *Atmos. Environ.*, **38**, 5719-5731.

Lipsky, E. M., N. J. Pekney, G. F. Walbert, W. J. O'Dowd, M. C. Freeman, and A. Robinson, 2004: Effects of dilution sampling on fine particle emissions from pulverized coal combustion. *Aerosol Sci. Technol*., **38**, 574-587.

Lu, G., J. R. Brook, M. R. Alfarra, K. Anlauf, W. R. Leaitch, S. Sharma, D. Wang, D. R. Worsnop, and L. Phinney, 2006: Identification and characterization of inland ship plumes over Vancouver, BC. *Atmos. Environ*., **40**, 2767-2782.

Lyyränen, J. Jokiniemi, E. I. Kauppinen, and J. Joutsensaari, 1999: Aerosol characterization in medium-speed diesel engines operating with heavy fuel oils. *J. Aerosol. Sci*., **30**, 771-784.

Mäkelä, J. M., and coauthors, 2001: Chemical composition of aerosol during particle formation events in boreal forest. *Tellus Ser. B*, **53**, 380-393.

Malm, W. C., J. F. Sisler, D. Huffman, R. A. Edlred, and T. A. Cahill, 1994: Spatial and seasonal trends in particle concentration and optical extinction in the United States. *J. Geophys. Res.,* **99**, 1347-1370.

——, B. A. Schichtel, M. L. Pitchford, L. L. Ashbaugh, and R. A. Eldred, 2004: Spatial and monthly trends in speciated fine particle concentration in the United States. *J. Geophys. Res.*, **109**, D03306, doi:10.1029/2003JD003739.

Marti, J. J., A. Jefferson, X. P. Cai, C. Richert, P. H. McMurry, and F. Eisele, 1997: H2SO4 vapor pressure of sulfuric acid and ammonium sulfate solutions. *J. Geophys. Res.*, **102**, 3725-3735.

Maykut, N. J. Lewtas, E. Kim, and T. V. Larson, 2003: Source apportionment of $PM_{2.5}$ at an urban IMPROVE site in Seattle, Washington. *Environ. Sci. Technol*., **37**, 5135-5142.

McMurry, P. H., and S. K. Friedlander, 1979: New particle formation in the presence of an aerosol. *Atmos. Environ.*, **13**, 1635-1651.

——, and K. S. Woo, 2002: Size distributions of 3-100-nm urban Atlanta aerosols: measurement and observations. *J. Aerosol. Med*., **15**, 169-178.

——, and F. L. Eisele, 2005: Preface to topical collection on new particle formation in Atlanta. *J. Geophys. Res*., **110**, D22S01, doi:10.1029/2005JD006644.

——, D. J. Rader, and J. L. Stith, 1981: Studies of aerosol formation in power plant plumes—I. Growth laws for secondary aerosols in power plant plumes: implications for chemical conversion mechanisms. *Atmos. Environ*., **15**, 2315-2327.

——, and coauthors, 2005: A criterion for new particle formation in the sulfur-rich Atlanta atmosphere, *J. Geophys. Res*., **110**, D22S02, doi:10.1029/2005JD005901.

Mebust, M. R., B. K. Eder, F .S. Binkowski, and S. J. Roselle, 2003: Models-3 Community Multiscale Air Quality (CMAQ) model aerosol component. 2. Model evaluation. *J. Geophys. Res.*, **108**, 4184, doi:10.1029/2001JD001410.

Miller, K. A., D. S. Siscovick, L. Sheppard, K. Shepherd, J. H. Sullivan, G. L. Anderson, and J. D. Kaufman, 2007: Long-term exposure to air pollution and incidents of cardiovascular events in women. *N. Engl. J. Med*., **356**, 447-458.

Minoura, H., and H. Takekawa, 2005: Observation of number concentrations of atmospheric aerosols and analysis of nanoparticle behavior at an urban background area in Japan. *Atmos. Environ*., **39**, 5806-5816.

Mohr, M. S. Ylatalo, N. Klippel, E. I. Kauppinen, O. Riccius, and H. Burtscher, 1996: Submicron fly ash penetration through electrostatic precipitators at two coal power

plants. *Aerosol. Sci. Technol*., **24**, 191-204.

Morawska, L., S. Thomas, N. Bofinger, D. Wainwright, and D. Neale, 1998: Comprehensive characterization of aerosols in a subtropical urban atmosphere: particle size distribution and correlation with gaseous pollutants. *Atmos. Environ*., **32**, 2467-2478.

——, ——, M. Jamriska, and G. Johnson, 1999: The modality of particle size distributions of environmental aerosols. *Atmos. Environ*., **33**, 4401-4411.

Mozurkewich, M. T.-W. Chan, Y.-A. Aklilu, and B. Verheggen, 2004: Aerosol particle size distributions in the lower Fraser Valley: Evidence for particle nucleation and growth. *Atmos. Chem. Phys. Discuss*., **4**, 1623-1663.

Mueller, S. F., and R. E. Imhoff, 1994: Estimates of particle formation and growth in coal-fired boiler exhaust—I. Observations. *Atmos. Environ.*, **28**, 595-602.

Mueller, S. F., E. M. Bailey, T. M. Cook, and Q. Mao, 2006: Treatment of clouds and the associated response of atmospheric sulfur in the Community Multiscale Air Quality (CMAQ) modeling system. *Atmos. Environ*., **40**, 6804-6820.

Napari, I., M. Noppel, H. Vehkamäki, and M. Kulmala, 2002a: An improved model for ternary nucleation of sulfuric acid-ammonia-water. *J. Chem. Phys*., **116**, 4221-4227.

——, ——, ——, and ——, 2002b: Parameterization of ternary nucleation rates for H_2SO_4-NH_3-H_2O vapors. *J. Geophys. Res.*, **107**, 4381, doi:10.1029/2002JD002132.

Nenes, A., S. N. Pandis, and C. Pilinis, 1998: ISORROPIA: A new thermodynamic equilibrium model for multiphase multicomponent inorganic aerosols. *Aquat. Geochem.*, **4**, 123-152.

——, ——, and ——, 1999: Continued development and testing of a new thermodynamic aerosol module for urban and regional air quality models. *Atmos. Environ.*, **33**, 1553-1560.

Norman, A.-L., K. Anlauf, K. Hayden, B. Thompson, J. R. Brook, S.-M. Li, and J. Bottenheim, 2006: Aerosol sulphate and its oxidation on the Pacific NW coast: S and O isotopes in PM2.5. *Atmos. Environ*., **40**, 2676-2689.

Oberdörster, G., 2001: Pulmonary effects of inhaled ultrafine particles. *Int. Arch. Occup. Environ.Health*, **74**, 1-8.

——, E. Oberdörster, and J. Oberdörster, 2005: Nanotoxicology: An emerging discipline evolving from studies of ultrafine particles. *Environ. Health Perspect*., **113**, 823-839.

O'Dowd and coauthors, 1999: On the photochemical production of new particles in the coastal boundary layer. *Geophys. Res. Lett*., **26**, 1707-1710.

——, P. Aalto, K. Hameri, M. Kulmala, and T. Hoffmann, 2002: Aerosol formation – atmospheric particles from organic vapors. *Nature*, **416**, 497-498

Odum, J. R., T. Hoffmann, T. Bowman, D. Collins, R. C. Flagen, and J. H. Seinfeld, 1996: Gas/particle partitioning and secondary organic aerosol yields. *Environ. Sci. Technol*., **30**, 2580-2585.

O'Neill, S. M., and B. K. Lamb, 2005: Intercomparison of the Community Multiscale Air Quality Model and CALGRID using process analysis. *Environ. Sci. Technol*., **39**, 5742-5753.

——, and coauthors, 2006: Modeling ozone and aerosol formation and transport in the Pacific Northwest with the Community Multi-scale Air Quality (CMAQ) modeling system. *Environ. Sci. Technol*., **40**, 1286-1299.

Otte, T. L., and J. E. Pleim, 2005: MCIPv3: Using WRF-EM output with CMAQ. *Proc. 4th Models-3 Users' Workshop*, Research Triangle Park, N.C. [Available from http://www.cmascenter.org/conference/2005/archive.cfm.]

——, and coauthors, 2005: Linking the Eta model with the Community Multiscale Air Quality (CMAQ) modeling system to build a national air quality forecasting system. *Wea. Forecasting*, **20**, 367-384.

Pankow, J. F., 1994: An absorption model of gas/particle partitioning of organic compounds in the atmosphere. *Atmos. Environ*., **28**, 185-188.

Park., S.-K., A. Marmur, S. B. Kim, D. Tian, Y. Hu, P. H. McMurry, and A. G. Russell, 2006: Evaluation of fine particle number concentrations in CMAQ. *Aerosol Sci. Technol*., **40**, 985-996.

Parker, J. D., T. J. Woodruff, R. Basu, and K. C. Schoendorf, 2005: Air pollution and birth weight among term infants in California. *Pediatrics*, **115**, 121-128.

Phares, D. J., K. P. Rhoads, M. V. Johnston, and A. S. Wexler, 2003: Size-resolved ultrafine particle composition analysis. 2. Houston. *J. Geophys. Res.*, **108**, 8420, doi:10.1029/2001JD001212.

Pirjola, L., and M. Kulmala, 2000. Aerosol dynamical model Multimono. *Boreal Environ. Res.*, **5**, 361-374.

Pleim, J. E., 2006: A New Combined Local and Non-Local PBL Model For Meteorology and Air Quality Modeling. *Proc. 5th Models-3 Users' Workshop*, Research Triangle Park, N.C. [Available from http://www.cmascenter.org/conference/2006/agenda.cfm.]

——, and J. S. Chang, 1992: A non-local closure model for vertical mixing in the convective boundary layer. *Atmos. Environ.*, **26A**, 965-981.

——, and D. W. Byun, 2001: Application of a new land-surface, dry deposition, and PBL model in the Models-3 Community Multi-Scale Air Quality (CMAQ) Model System. *Air Pollution Modeling and Its Application, XIV*, S.-E. Gryning and F. Schiermeier, Eds., Plenum Press, 297-305.

——, G. Gipson, S. Roselle, and J. Young, 2003: New features of the 2003 release of the CMAQ model. *Proc. 2nd Models-3 Users' Workshop*, Research Triangle Park, N.C. [Available from http://www.cmascenter.org/conference/2003/archive.html.]

——, S. Roselle, J. Young, G. Gipson, and R. Mathur, 2004: New developments in the Community Multiscale Air Quality (CMAQ) model. *Proc. 3rd Models-3 Users' Workshop*, Research Triangle Park, N.C. [Available from http://www.cmascenter.org/conference/2004/archive.html.]

——, S. Roselle, J. Young, D. Schwede, R. Mathur, and P. Bhave, 2005: New developments in CMAQ model physics. *Proc. 4th Models-3 Users' Workshop*, Research Triangle Park, N.C. [Available from http://www.cmascenter.org/conference/2005/archive.cfm.]

——, and coauthors, 2006: The 2006 CMAQ release and plans for 2007. *Proc. 5th Models-3 Users' Workshop*, Research Triangle Park, N.C. [Available from http://www.cmascenter.org/conference/2006/agenda.cfm.]

Pope, C. A. III, 2004: Air pollution and health – Good news and bad. *N. Engl. J. Med.*, **351**, 1132-1134.

——, M. J. Thun, M. M. Namboodiri, D. W. Dockery, J.S. Evans, F. E. Speizer, and C. W. Heath, Jr., 1995: Particulate air pollution as a predictor of mortality in a prospective study of US adults. *Am. J. Respir. Crit. Care Med.*, **151**, 669-674.

——, R. T. Burnett, M. J. Thun, E. E. Calle, D. Krewski, K. Ito, and G. D. Thurston, 2002: Lung cancer, cardiopulmonary mortality, and long-term exposure to fine

particulate air pollution. *J. Amer. Med. Assoc*., **287**, 1132-1141.

——, R. T. Burnett, G. D. Thurston, M. J. Thun, E. E. Calle, D. Krewski, and J. J. Godleski, 2004: Cardiovascular mortality and long-term exposure to particulate air pollution. *Circulation*, **109**, 71-77.

Pryor, S. C., K. Anlauf, H. Boudries, K. Hayden, C. L. Schiller, and A. Wiebe, 2004: Spatial and temporal variability of high resolution reduced nitrogen concentrations in the Fraser Valley. *Atmos. Environ.*, **38**, 5825-5836

Pun, B., C. Seigneur, and S-Y. Wu, 2002a: Modeling regional haze in Big Bend National Park with CMAQ. *Proc. Models-3 Users' Workshop*, Research Triangle Park, N.C. [Available from http://www.cmascenter.org/workshop/2002wspresent.html.]

——, S-Y. Wu, and C. Seigneur, 2002b: Contribution of biogenic emissions to the formation of ozone and particulate matter in the eastern United States. *Environ. Sci. Technol*., **36**, 2586-3596.

——, ——, ——, J. H. Seinfeld, R. J. Griffin, and S. N. Pandis, 2003: Uncertainties in modeling secondary organic aerosols: Three-dimensional modeling studies in Nashville/western Tennessee. *Environ. Sci. Technol*., **37** (16), 3647-3661.

——, and coauthors, 2006: Modeling regional haze in the BRAVO study using CMAQ-MADRID: 1. Model evaluation. *J. Geophys. Res*., **111**, D06302, doi:10.1029/2004JD005608.

Putaud, J.-P., and coauthors, 2003: A European aerosol phenomenology: physical and chemical characteristics of particulate matter at kerbside, urban, rural, and background sites in Europe. European Commission, report nr. 20411EN, (http://ies.jrc.cec.eu.int/Download/cc).

——, and coauthors, 2004a: A European aerosol phenomenology—2: chemical characteristics of particulate matter at kerbside, urban, rural, and background sites in Europe. *Atmos. Environ*., **38**, 2579-2595.

——, R. Van Dingenen, A. Dell'Acqua, F. Raes, E. Matta, S. Decesari, M. C. Facchini, and S. Fuzzi, 2004b: A European Aerosol Phenomenology - 1: physical characteristics of particulate matter at kerbside, urban, rural and background sites in Europe. *Atmos. Chem. Phys*., **4**, 889-902.

Radke, L. F., J. A. Coakley, Jr., and M. D. King, 1989: Direct and remote sensing observations of the effects of ships on clouds. *Science*, **246**, 1146-1149.

Ramanathan, V., P. J. Crutzen, J. T. Kiehl, and D. Rosenfeld, 2001: Aerosol, climate, and the hydrological cycle. *Science*, **294**, 2119-2124.

Rhoads, K. P., D. J. Phares, A. S. Wexler, and M. V. Johnston, 2003: Size-resolved ultrafine particle composition analysis. 1. Atlanta. *J. Geophys. Res.*, **108**, 8418, doi:10.1029/2001JD001211.

Roselle, S. J., and F. S. Binkowski, 1999: Cloud Dynamics and Chemistry. *Science Algorithms of the EPA Models-3 Community Multi-scale Air Quality (CMAQ) Modeling System*, D. W. Byun and J. K. S. Ching, Eds., NERL, Research Triangle Park, NC, Chapter 11.

Roth, H., W. Jiang, D. Yin, and E. Giroux, 2003: CMAQ nucleation algorithms and their impact on PM modeling results in the Lower Fraser Valley. *Proc. Models-3 Users' Workshop*, Research Triangle Park, N.C. [Available from http://www.cmascenter.org/2003_workshop/downloads.html.]

Rothen-Rutishauser, B. M., S. Schurch, B. Haenni, N. Happ, and P. Gehr, 2006: Interaction of fine particles and nanoparticles with red blood cells visualized with advanced microscopic techniques. *Environ. Sci Technol.*, **40**, 4353-4359.

Russell, A. and R. Dennis, 2000: NARSTO critical review of photochemical models and modeling. *Atmos. Environ.*, **34**, 2283-2324.

Ruuskanen, J. Th. Tuch, H. Ten Brink, A. Peters, A. Khlystov, A. Mirme, G. P. A. Kos, B. Brunekreef, H. E. Wichmann, G. Buzorius, M. Vallius, W. G. Kreyling, and J. Pekkanen, 2001: Concentrations of ultrafine, fine, and $PM_{2.5}$ particles in three European cities. *Atmos. Environ.*, **35**, 3729-3738.

Sakurai, H., M. A. Fink, P. H. McMurry, L. Mauldin, K. F. Moore, J. N. Smith, and F. L. Eisele, 2005: Hygroscopicity and volatility of 4-10 nm particles during summertime atmospheric nucleation events in urban Atlanta. *J. Geophys. Res.*, **110**, D22S04, doi:10.1029/2005JD005918.

Salma, I. M. Dal Maso, M. Kulmala, and G. Záray, 2002: Modal characteristics of particulate matter in urban atmospheric aerosols. *Microchem. J.*, **73**, 19-26.

Samet, J. M., D. M. DeMarini, and H. V. Malling, 2004: Do airborne particles induce heritable mutations? *Science*, **304**, 971-972.

Sardar, S. B., P. M. Fine, C. Sioutas, 2005: Seasonal and spatial variability of the size-resolved chemical composition of particulate matter (PM_{10}) in the Los Angeles Basin.

J. Geophys. Res., **110**, D07S08, doi:10.1029/2004JD004627.

Schauer, J. J., M. J. Kleeman, G. R. Cass, and B. R. T. Simoneit, 1999: Measurement of emissions from air pollution sources. 2. C1 through C30 organic compounds from medium duty diesel trucks. *Environ. Sci. Technol*., **33**, 1578-1587.

Schell, B., I. J. Ackermann, H. Hass, F. S. Binkowski, and A. Ebel, 2001: Modeling the formation of secondary organic aerosol within a comprehensive air quality model system. *J. Geophys. Res.*, **106**, 28,275-28,293.

Schere, K., 2002: The Models-3/CMAQ Model: 2002 release – new features. *Proc. Models-3 Users' Workshop*, Research Triangle Park, N.C. [Available from http://www.cmascenter.org/workshop/2002wspresent.html.]

Schroeder, W., and J. Munthe, 1998: Atmospheric Mercury – An overview. *Atmos. Environ*., **32**, 809-822.

Schwartz, J., D. Slater, T. V. Larson, W. E. Pierson, and J. Q. Koenig, 1993: Particulate air pollution and hospital emergency room visits for asthma in Seattle. *Am. Rev. Respir. Dis*., **147**, 826-831.

Seaman, N. L., 2000: Meteorological modeling for air-quality assessments. *Atmos. Environ*., **34**, 2231-2259.

——, D. R. Stauffer, and A. M. Lario-Gibbs, 1995: A multiscale four-dimensional data assimilation system applied in the San Joaquin Valley during SARMAP. Part I: modeling design and basic performance characteristics. *J. Appl. Meteor*., **34**, 1739-1761.

Seigneur, C., B. Pun, K. Lohman, and S-Y. Wu, 2003: Regional modeling of the atmospheric fate and transport of benzene and diesel particles. *Environ. Sci. Technol*., **37**, 5236-5246.

Seinfeld, J. H., and S. N. Pandis, 1998: Atmospheric Chemistry and Physics From Air Pollution to Climate Change. John Wiley, 1326 pp.

Sheppard, L., D. Levy, G. Norris, T. V. Larson, and J. Q. Koenig, 1999: Effects of ambient air pollution on nonelderly asthma hospital admissions in Seattle, Washington, 1987-1994. *Epidemiology*, **10**, 23-30.

Shi, J. P., A. A. Khan, and R. M. Harrison, 1999: Measurements of ultrafine particle concentration and size distribution in the urban atmosphere. *Sci. Total Environ*., **235**,

51-64.

Sinha, P., P. V. Hobbs, R. J. Yokelson, T. J. Christian, T. W. Kirchstetter, and R. Bruintjes, 2003: Emissions of trace gases and particles from two ships in the southern Atlantic Ocean. *Atmos. Environ*., **37**, 2139-2148.

Smith, J. N., K. F. Moore, F. L. Eisele, D. Voisin, A. K. Ghimire, H. Sakruai, and P. H. McMurry, 2005: Chemical composition of atmospheric nanoparticles during nucleation events in Atlanta. *J. Geophys. Res*., **110**, D22S03, doi:10.1029/2005JD005912.

Smyth, S. C., W. Jiang, D. Yin, H. Roth, and É. Giroux, 2006: Evaluation of CMAQ O_3 and $PM_{2.5}$ performance using Pacific 2001 measurement data. *Atmos. Environ*., **40**, 2735-2749.

Snow, J. A., J. B. Dennison, D. A. Jaffe, H. U. Price, J. K. Vaughan, and B. Lamb, 2002: Aircraft and surface observations of air quality in Puget Sound and a comparison to a regional model. *Atmos. Environ*., **37**, 4019-4032.

Snyder, B. J., and K. B. Strawbridge, 2004: Meteorological analysis of the Pacific 2001 air quality field study. *Atmos. Environ*., **38**, 5733-5743.

Stanier, C. O., A. Y. Khlystov, and S. N. Pandis, 2004a: Ambient aerosol size distributions and number concentrations measured during the Pittsburgh Air Quality Study (PAQS). *Atmos. Environ*., **38**, 3275-3284.

——, ——, and ——, 2004b: Nucleation events during the Pittsburgh air quality study: Description and relation to key meteorological, gas phase, and aerosol parameters. *Aerosol Sci. Technol*., **38 (S1)**, 253-264.

Stauffer, D. R., and N. L. Seaman, 1990: Use of four-dimensional assimilation in a limited-area mesoscale model. Part I: experiments with synoptic-scale data. *Mon. Wea. Rev.*, **118**, 1250-1277.

Stokes, R. H., and R. A. Robinson, 1966: Interactions in aqueous nonelectrolyte solutions. I. Solute-solvent equilibria. J. Phys. Chem., 70, 2126–2131.

Stockwell, W. R., P. Middleton, J. S. Chang, and X. Tang, 1990: The second generation Regional Acid Deposition Model chemical mechanism for regional air quality modeling. *J. Geophys. Res*., **95**, 16343-16367.

Stolzenburg, M., and P. McMurry, 1991: An ultrafine aerosol condensation nucleus

counter. *Aerosol Sci. Technol*., **14**, 48-65.

——, ——, H. Sakurai, J. N. Smith, R. L. Mauldin III, and F. L. Eisele, 2005: Growth rates of freshly nucleated atmospheric particles in Atlanta. *J. Geophys. Res*., **110**, D22S05, doi:10.1029/2005JD005935.

Strawbridge, K. B., and B. J. Snyder, 2004a: Daytime and nighttime aircraft lidar measurements showing evidence of particulate matter transport into the Northeastern valleys of the Lower Fraser Valley, BC. *Atmos. Environ*., **38**, 5873-5886.

——, and ——, 2004b: Planetary boundary layer height determination during Pacific 2001 using the advantage of a scanning lidar instrument, *Atmos. Environ*., **38**, 5861-5871.

Sturm, P. J., U. Baltensperger, M. Bacher, B. Lechner, S. Hausberger, B. Heiden, D. Imhof, E. Weingartner, A. S. H. Prevot, R. Kurtenbach, and P. Wiesen, 2003: Roadside measurements of particulate matter size distribution. *Atmos. Environ*., **37**, 5273-5281.

Svensmark H., and E. Friis-Christensen, 1997: Variation of cosmic ray flux and global cloud coverage - A missing link in solar-climate relationships. *J. Atmos. Sol.-Terr. Phy*., **9**, 1225-1232.

Teinemaa, E., U. Kirso, M. R. Strommen, and R. M. Kamens, 2002: Atmospheric behavior of oil-shale combustion fly ash in a chamber study. *Atmos. Environ*., **36**, 813-824.

Tolocka, M. P., D. A. Lake, and M. V. Johnston, 2005: Size-resolved fine and ultrafine particle compostion in Baltimore, Maryland. *J. Geophys. Res*., **110**, D07S04, doi:10.1029/2004JD004573.

Trier, A., 1997: Submicron particles in an urban atmosphere: a study of optical size distributions—I. *Atmos. Environ*., **31**, 909-914.

Tuch, Th., P. Brand, H. E. Wichmann, and J. Heyder, 1997: Variation of particle number and mass concentration in various size ranges of ambient aerosols in Eastern Germany. *Atmos. Environ*., **31**, 4193-4197.

——, B. Wehner, M. Pitz, J. Cyrys, J. Heinrich, W. G. Kreyling, H. E. Wichmann, and A. Wiedensohler, 2003: Long-term measurements of size-segregated ambient aerosol in two German cities located 100 km apart. *Atmos. Environ*., **37**, 4687-4700.

U.S. EPA, 1995: User instructions. Vol. I, User's Guide for the Industrial Source Complex (ISC3) Dispersion Models (revised). U.S. Environmental Protection Agency, EPA-454/b-95-003a.

U.S. EPA, 1999: Regional haze regulations; Final rule. Federal Register, Vol. 64, No. 126, 40 CFR Part 51, 35713- 35774.

U.S. EPA, 2003. User's guide to MOBILE6.1 and MOBILE6.2: Mobile source emission factor model. [Available online at http://www.epa.gov/otaq/models/mobile6/420r03010.pdf.]

U.S. EPA, 2005: Standards of performance for new and existing stationary sources: Electric utility steam generation units. Federal Register, Vol. 70, No. 95, 40 CFR Parts 60, 72, and 75, 28605-28700.

U.S. EPA, cited 2007a: Clean Air Act. [Available online at http://www.epa.gov/air/caa/.]

U.S. EPA, cited 2007b: Biogenic Emissions Inventory System (BEIS) Modeling. [Available online at http://www.epa.gov/asmdnerl/biogen.html].

van de Hulst, H. C., 1981: *Light scattering by small particles*. Dover Publications, 470 pp.

Van Dingenen, R., and coauthors, 2004: A European Aerosol Phenomenology - 1: physical characteristics of particulate matter at kerbside, urban, rural and background sites in Europe. *Atmos. Environ.*, **38**, 2561-2577.

Vana, M., M. Kulmala, M. Dal Maso, U. Hõrrak, and E. Tamm, 2004: Comparative study of nucleation mode aerosol particles and intermediate air ions formation events at three sites. *J. Geophys. Res.*, **109**, D17201, doi:10.1029/2003JD004413.

Vaughan, J., and coauthors, 2004: A numerical daily air quality forecast system for the Pacific Northwest. *Bull. Am. Meteorol. Soc*., **85**, 549-561.

Vehkamäki, H. M. Kulmala, I. Napari, K. E. J. Lehtinen, C. Timmreck, M. Noppel, and A. Laaksonen, 2002: An improved parameterization for sulfuric acid—water nucleation rates for tropospheric and stratospheric conditions. *J. Geophys. Res.*, **107**, 4622, doi:10.1029/2002JD002184.

Venkataraman, C., J. M. Lyons, and S. K. Friedlander, 1994: Size distributions of polycyclic aromatic hydrocarbons and elemental carbon. 1. Sampling, measurement methods, and source characterization. *Environ. Sci. Technol*., **28**, 555-562.

Vingarzan, R., and S.-M. Li, 2006: The Pacific 2001 Air Quality Study – synthesis of findings and policy implications. *Atmos Environ*., **40**, 2637-2649.

Volkamer, R., J. L. Jimenez, F. San Martini, K. Dzepina, Q. Zhang, D. Salcedo, L. T. Molina, D. R. Worsnop, and M. J. Molina, 2006: Secondary organic aerosol from anthropogenic air pollution: Rapid and higher than expected. *Geophys. Res. Lett*., **33**, L17811, doi:10.1029/2006GL026899.

Wåhlin, P., F. Palmgren, and R. Van Dingenen, 2001: Experimental studies of ultrafine particles in streets and the relationship to traffic. *Atmos. Environ*., **35 (S1)**, S63-S69.

Washington Department of Ecology, 2004: Air Quality Data Summary: 1999-2002. Air Quality Program, Publication Number 04-02-002.

Watson, J. G., 2002: Visibility: science and regulation. *J. Air & Waste Manage. Assoc*., **52**, 628-713.

Weber, R. J., J. J. Marti, R. H. McMurry, F. L. Eisele, D. J. Tanner, and A. Jefferson, 1997: Measurements of new particle formation and ultrafine particle growth rates at a clean continental site. *J. Geophys. Res.*, **102**, 4375-4385.

——, R. H. McMurry, L. Mauldin, D. J. Tanner, F. L. Eisele, F. J. Brechtel, S. M. Kreidenweis, G. L. Kok, R. D. Schillawski, and D. Gaumgardner, 1998: A study of new particle formation and growth involving biogenic and trace gas species measured during ACE 1. *J. Geophys. Res.*, **103**, 16,385-16,396.

——, and coauthors, 2003: New particle formation in anthropogenic plumes advecting from Asia observed during TRACE-P. *J. Geophys. Res.*, **108**, 8814, doi:10.1029/2002JD003112.

Wehner, B., and A. Wiedensohler, 2002: Long term measurements of submicrometer urban aerosols: statistical analysis for correlations with meteorological conditions and trace gases. *Atmos. Chem. Phys*., **2**, 1699-1733.

——, W. Birmili, T. Gnauk, and A. Wiedensohler, 2002: Particle number size distributions in a street canyon and their transformation into the urban-air background: measurements and a simple model study. *Atmos. Environ*., **36**, 2215-2223.

Whitby, K. T., 1978: The physical characteristics of sulfur aerosols. *Atmos. Environ.*, **12**, 135-159.

——, B. Y. H. Liu, R. B. Husar, and N. J. Barsic, 1972: The Minnesota Aerosol-Analyzing System used in the Los Angeles Smog Project. *Aerosols and Atmospheric Chemistry*, G. M. Hidy, Ed., Academic Press, 189-217.

Wiedensohler, A., B. Wehner, and W. Birmili, 2002: Aerosol number concentrations and size distributions at mountain-rural, urban-influenced rural, and urban-background sites in Germany. *J. Aerosol. Med*., **15**, 237-243.

Wilson, J. C., and P. H. McMurry, 1981: Studies of aerosol formation in power plant plumes – II. Secondary aerosol formation in the Navajo Generating Station plume. *Atmos. Environ*., **15**, 2329-2339.

Woo, K. S., D. R. Chen, D. Y. H. Pui, and P. H. McMurry, 2001: Measurement of Atlanta aerosol size distributions: Observations of ultrafine particle events. *Aerosol Sci. Technol*., **34**, 75-87.

Xiu, A., and J. E. Pleim, 2001: Development of a land surface model. Part I: application in a mesoscale meteorological model. *J. Appl. Meteor*., **40**, 192-209.

Yao, X., N. T. Lau, M. Fang, and C. K. Chan, 2006: Use of stationary and mobile measurements to study power plant emissions. *J. Air & Waste Manage. Assoc.*, **56**, 144-151.

Yin, D., W. Jiang, H. Roth, and É. Giroux, 2004: Improvement of biogenic emissions estimation in the Canadian Lower Fraser Valley and its impact on particulate matter modeling results. *Atmos. Environ*., **38**, 507-521.

Ylatalo, S., 2006: Studies on aerosol particle emission, sampling, and authenticity. Ph.D. Thesis, University of Helsinki, 69 pp. [Available from http://ethesis.helsinki.fi/julkaisut/mat/fysik/vk/ylatalo/studieso.pdf.]

Yu, F., and R. P. Turco, 2000: Ultrafine aerosol formation via ion-mediated nucleation. *Geophys. Res. Lett*., **27**, 883-886.

——, and ——, 2001: From molecular clusters to nanoparticles: Role of ambient ionization in tropospheric aerosol formation. *J. Geophys. Res*., **106**, 4797-4814.

——, C. Cai, and K. L. Demerjian, 2004: Regional scale modeling of particle nucleation in the lower atmosphere over the Eastern United States, *Eos Trans. AGU*, **85(47)**, Fall Meet. Suppl., Abstract A44B-01.

Yu, S., and coauthors, 2003: Simulation of primary and secondary (biogenic and

anthropogenic) organic aerosols over the United States by US EPA Models-3/CMAQ: Evaluation and regional analysis. *Proc. Models-3 Users' Workshop*, Research Triangle Park, N.C. [Available from http://www.cmascenter.org/2003_workshop/downloads.html.]

Zhang, K. M., 2005: Development of the CMAQ-UCD sectional aerosol model. *Proc. Models-3 Users' Workshop*, Research Triangle Park, N.C. [Available from http://www.cmascenter.org/conference/2005/archive.cfm.]

——, and A. S. Wexler, 2002a: Modeling the number distributions of urban and regional aerosols: theoretical foundations. *Atmos. Environ.*, **36**, 1863-1874.

——, and ——, 2002b: A hypothesis for growth of fresh atmospheric nuclei. *J. Geophys. Res.*, **107**, 4577, doi:10.1029/2002JD002180.

——, and ——, 2004a: Evolution of particle number distribution near roadways – Part I: analysis of aerosol dynamics and its implications for engine emission measurement. *Atmos. Environ.*, **38**, 6643-6653.

——, and ——, 2004b: Evolution of particle number distribution near roadways – Part II: the 'Road-to-Ambient' process. *Atmos. Environ.*, **38**, 6655-6665.

——, ——, D. A. Niemeier, Y. F. Zhu, W. C. Hinds, and C. Sioutas, 2005: Evolution of particle number distribution near roadways. Part III: Traffic analysis and on-road size resolved particulate emission factors. *Atmos. Environ.*, **39**, 4155-4166.

Zhang, Q., C. O. Stanier, M. R. Canagaratna, J. T. Jayne, D. R. Worsnop, S. N. Pandis, and J. L. Jimenez, 2004: Insights into the chemistry of new particle formation and growth events in Pittsburgh based on aerosol mass spectrometry. *Environ. Sci. Technol.*, **38**, 4797-4809.

——, M. R. Canagaratna, J. T. Jayne, D. R. Worsnop, and J-L. Jimenez, 2005: Time- and size-resolved chemical composition of submicron particles in Pittsburgh: Implications for aerosol sources and processes. *J. Geophys. Res.*, **110**, D07S09, doi:10.1029/2004JD004649.

Zhang, R., I. Suh, J. Zhao, D. Zhang, E. C. Fortner, X. Tie, L. T. Molina, and M. J. Molina, 2004: Atmospheric new particle formation enhanced by organic acids. *Science*, **304**, 1487-1490.

Zhang, Y., B. Pun, K. Vijayaraghavan, S-Y. Wu, C. Seigneur, S. N. Pandis, M. Z.

Jacobson, A. Nenes, and J. H. Seinfeld, 2004: Development and application of the Model of Aerosol Dynamics, Reaction, Ionization, and Dissolution (MADRID). *J. Geophys. Res.,* **109**, D01202, doi:10.1029/2003JD003501.

——, P. Liu, M. Z. Jacobson, P. Bhave, S.-C. Yu, S. Roselle, and K. Schere, 2006a: A comparative study of homogeneous nucleation parameterizations, part II. 3-D model simulations. *J. Geophys. Res*., submitted.

——, ——, B. Pun, and C. Seigneur, 2006b: A comprehensive performance evaluation of MM5-CMAQ for the summer 1999 southern oxidants study episode, Part III: Diagnostic and mechanistic evaluations. *Atmos. Environ.*, **40**, 4856-4873.

Zhou, L., E. Kim, P. K. Hopke., C. O. Stanier, and S. Pandis, 2004: Advanced factor analysis on Pittsburgh particle size-distribution data. *Aerosol Sci. Technol*., **38 (S1)**, 118-132.

——, P. K. Hopke, C. O. Stanier, S. N. Pandis, J. M. Ondov, and J. P. Pancras, 2005a: Investigation of the relationship between chemical composition and size distribution of airborne particles by partial least squares and positive matrix factorization. *J. Geophys. Res*., **110**, D07S18, doi:10.1029/2004JD005050.

——, E. Kim, and P. K. Hopke, 2005b: Mining airborned particulate size distribution data by positive matrix factorization. *J. Geophys. Res*., **110**, D07S19, doi:10.1029/2004JD004707.

Zhu, Y., W. C. Hinds, S. Kim, S. Shen, and S. Sioutas, 2002a: Study of ultrafine particles near a major highway with heavy-duty diesel traffic. *Atmos. Environ*., **36**, 4323-4335.

——, ——, ——, and C. Sioutas, 2002b: Concentration and size distribution of ultrafine particles near a major highway. *J. Air & Waste Manage. Assoc*., **52**, 1032-1042.

Vita

Robert Elleman was born on Tax Day, 1975. He grew up in Cincinnati, Ohio with exciting weather and poor visibility from aerosol pollution. Armed with a desire to understand the natural world, he majored in Geological Sciences at Brown University and earned his Bachelor of Science, Magna Cum Laude in 1997. While a remote sensing consultant in the Washington, DC beltway, Robert decided that a Ph.D. in Atmospheric Sciences sounded like a good idea. He moved to Seattle in 2000, enrolled in the program at the University of Washington, and emerged with a newly minted doctorate in 2007.